IntechOpen

Geospatial Technology
Environmental and Social Applications

Edited by Pasquale Imperatore and Antonio Pepe

GEOSPATIAL TECHNOLOGY - ENVIRONMENTAL AND SOCIAL APPLICATIONS

Edited by **Pasquale Imperatore** and **Antonio Pepe**

Geospatial Technology - Environmental and Social Applications
http://dx.doi.org/10.5772/61680
Edited by Pasquale Imperatore and Antonio Pepe

Contributors

Dayong Shen, Suarau Oshunsanya, OrevaOghene Aliku, Serge Olivier Kotchi, Nathalie Barrette, Alain A. Viau, Jae-Dong Jang, Valery Gond, Mir Abolfazl Mostafavi, Christine Barbeau, Don Cowan, Yuanzhi Zhang, Megan Sheremata, William A. Gough, Leonard J. S. Tsuji, Giuseppe Solaro, Pasquale Imperatore, Antonio Pepe, Chun-Chih Tsui, Xiao-Nan Liu, Horng-Yuh Guo, Zueng-Sang Chen, José Luis Silván-Cárdenas, Pablo López-Ramírez, Adriana Allen, Rita Lambert

Notice

First published in Croatia, 2016 by INTECH d.o.o.
eBook (PDF) Published by IN TECH d.o.o.
Place and year of publication of eBook (PDF): Rijeka, 2019.
IntechOpen is the global imprint of IN TECH d.o.o.
Printed in Croatia

Legal deposit, Croatia: National and University Library in Zagreb

Additional hard and PDF copies can be obtained from orders@intechopen.com

Geospatial Technology - Environmental and Social Applications
Edited by Pasquale Imperatore and Antonio Pepe
p. cm.
Print ISBN 978-953-51-2626-3
Online ISBN 978-953-51-2627-0
eBook (PDF) ISBN 978-953-51-6674-0

Meet the editors

Pasquale Imperatore received the Laurea degree (cum laude) in electronic engineering and the PhD degree in electronic and telecommunication engineering, both from the University of Naples Federico II, Italy. Currently he is a research fellow at the Institute of Electromagnetic Environmental Sensing (IREA), Italian National Research Council (CNR), Naples, Italy. His research interests include microwave remote sensing and electromagnetics, with emphasis on scattering in random layered media, perturbation methods, SAR data modeling and processing, SAR interferometry, parallel computing, radio localization, as well as electromagnetic propagation modeling, simulation, and channel measurement. Dr. Imperatore is an IEEE member and is a member of InTech's Editorial Advisory Board. He acts as a reviewer for several peer-reviewed journals.

Antonio Pepe received the Laurea degree in electronic engineering and the PhD degree in electronic and telecommunication engineering from the University of Napoli Federico II, Napoli, Italy, in 2000 and 2007, respectively. In 2001, he joined the IREA-CNR where he is a permanent researcher. He was a visiting scientist at the University of Texas in 2005, the JPL in 2009, and the ECNU, Shanghai, in 2014 and 2015. Since 2012, he has been an adjunct professor of Signal Theory at the University of Basilicataa. He was the recipient of the 2014 Best Reviewer mention of the IEEE Geoscience and Remote Sensing Letters. His research interests include the development of advanced InSAR algorithms with a particular interest toward phase unwrapping problems.

Contents

Preface

The world we live in is subject to global environmental change, natural hazards, growth of human population, and increasing urbanization, with significant impacts on social community and Earth's ecosystems, thus posing great challenges for the scientific community. Nowadays, Earth observation information is acquired at increasingly finer (spatial, temporal, and spectral) scales, thus continuously providing a significant amount of geospatial data to be processed and utilized. Within this context, the pervasive relevance of geospatial information and the development of emerging geospatial technologies offer new opportunity for bridging the gap between remote sensing scientific know-how and end users of products and services.

Geospatial technology (also referred to as geomatics or geomatics engineering) comprises tools and techniques dealing with the use of spatially referenced information, for the description and modeling of spatial and dynamic phenomena related to the Earth's environment. Therefore, geospatial technology is an emerging area of research arising from the convergence and integration of different tools and techniques used for the acquisition and analysis of geospatial data in various research fields (including remote sensing, geographic information systems (GIS), geo-informatics, navigation systems, geography, statistics, geophysics, and environmental science).

According to the development of integrated approaches and tools, a variety of location-specific data types derived from multiple sources (e.g. radar and optical sensors, GPS, wireless networks, etc.) can profitably be used, for instance, in decision making, problem solving, and collaboration in the areas of emergency and sustainable management of environmental resources, with important implications both on regional and global development.

This book addresses environmental and social applications of geospatial technologies, thus also providing a multidisciplinary perspective on emerging geospatial techniques and tools. It consists of ten chapters offering insight into geospatial technology progress and trends. Authors present several application-oriented studies from various parts of the world, including applications in collaborative geomatics, geospatial statistics, GIS, agriculture, and natural hazard monitoring.

Dr. Pasquale Imperatore
Institute of Electromagnetic Environmental Sensing (IREA),
Italian National Research Council (CNR),
Naples, Italy

Dr. Antonio Pepe
Institute for Electromagnetic Sensing of the Environment (IREA),
Italian National Research Council (CNR),
Italy

Chapter 1

Geomatics Applications to Contemporary Social and Environmental Problems in Mexico

Jose Luis Silván-Cárdenas, Rodrigo Tapia-McClung,
Camilo Caudillo-Cos, Pablo López-Ramírez,
Oscar Sanchez-Sórdia and
Daniela Moctezuma-Ochoa

Additional information is available at the end of the chapter

http://dx.doi.org/10.5772/64355

Abstract

Trends in geospatial technologies have led to the development of new powerful analysis and representation techniques that involve processing of massive datasets, some unstructured, some acquired from ubiquitous sources, and some others from remotely located sensors of different kinds, all of which complement the structured information produced on a regular basis by governmental and international agencies. In this chapter, we provide both an extensive revision of such techniques and an insight of the applications of some of these techniques in various study cases in Mexico for various scales of analysis: from regional migration flows of highly qualified people at the country level and the spatio-temporal analysis of unstructured information in geotagged tweets for sentiment assessment, to more local applications of participatory cartography for policy definitions jointly between local authorities and citizens, and an automated method for three dimensional (3D) modelling and visualisation of forest inventorying with laser scanner technology.

Keywords: crowdsourcing, airborne laser scanner, crime analysis, migration, volunteered geographic information

1. Introduction

The term geomatics was originally conceived by Michel Paradis, a French-Canadian surveyor, as the discipline of gathering, storing, processing and delivering spatially referenced

information [1]; as such, geomatics has been tied to the development of geospatial technology since its birth. The Encyclopaedia of Geographic Information Science by Karen Kemp defines geomatics as the 'science of building efficient Earth related data production workflow' [2]. According to this definition, the discipline of geomatics 'truly highlights the necessary shift from a technology-oriented silo approach to a data-flow-oriented system approach geared toward a result in a given context' [2]. It is the result-oriented mode that stresses the need for a transdisciplinary approach, which has been adopted by researchers at the Geography and Geomatics Research Centre in Mexico (CentroGeo).

As the technology evolves, the research field of geomatics has to necessarily expand along its entire workflow, from data acquisition to geospatial information dissemination. For instance, the georeferencing capability of mobile devices and their extensive use in social networking are producing unprecedented amounts of information that can be of high relevance for many important topics such as security, marketing, mental health, disaster management, etc. Consequently, social media analysis is becoming a very important research topic within geomatics and its related fields.

In Section 2, we provide a brief review of major steps within the geomatics approach, from data acquisition processes and processing techniques to the analysis and visualisation methods used for information extraction and representation. Then, in Section 3 we provide illustrative examples of applied geomatics research to contemporary social and environmental problems in Mexico. Section 4 ends this chapter by providing some concluding remarks.

2. The geomatics approach

In this section, we discuss the general steps involved in addressing social or environmental issues from geomatics. The goal is to make a general review of data acquisition, processing, analysis, visualisation and interpretation, providing examples from different fields such as remote sensing, crime analysis or social media.

2.1. Data acquisition processes

2.1.1. Remote sensing

Since Gaspard-Félix Tournachon took the first aerial photograph in 1858 from a tethered balloon over Paris, the interest for observing the Earth from afar has grown to the point that cameras are put on board of any sort of flying devices including kites, balloons, airplanes, rockets, satellites, spatial stations and unmanned aerial vehicles (drones). Indeed, aerial photography has been the most common, versatile and economical form of remote sensing, but other types of sensors besides cameras have also been developed [3].

In this sense, remote sensing is a continuously evolving field that is devoted to the design and development of new and effective techniques for data acquisition of the Earth's surface from remote locations, typically from space and aircrafts. All these techniques share a common

http://dx.doi.org/10.5772/64355

principle: to record the energy, typically the electromagnetic radiation, that has interacted with the Earth's surface in order to retrieve some information about it.

The range of frequencies (or wavelengths) of the electromagnetic radiation that the sensor is sensitive to is of prime importance because it determines which materials can be detected. It also influences whether to use the natural illumination of the sun or to use an artificial energy source. Sensors are active or passive depending on whether they include an artificial source of energy or not. Thus, for instance, infrared and thermal cameras are considered passive sensors because they sense the reflected near-infrared light and the emitted thermal infrared from hot bodies, respectively, whereas radar and lidar systems are considered active sensors because they send microwave and laser beams, respectively, and detect the backscattered energy.

The ability to measure quantities of radiant energy (radiance/reflectance, emittance, backscattering, etc.) would have not been as useful as it is, except because the sensors are coupled with global positioning systems (GPSs) and inertial measuring units (IMUs) for measuring location and orientation, thus enabling the production of digital representations of surface features that can be integrated into geodatabases.

Furthermore, a substantial body of knowledge from related fields, such as radiative transfer theory, imaging spectroscopy, image/signal processing and computer vision, has been advanced that allows deriving ready-to-use information in the form of data layers that can be overlaid within a geographic information system (GIS). These layers include vegetation indices, digital elevation models, surface temperature, soil moisture, rainfall, snow cover, night light, impervious surface, mineral abundance and land-cover types, to name just a few. These surface features are specified by the various resolutions and dynamic ranges of the sensor (spatial, temporal, spectral and radiometric). The former refers to the smallest spatial, temporal, spectral and radiometric difference, which the sensor can resolve, whereas the latter refers to the largest differences that can be resolved. Hence, depending on the resolution/dynamic-range characteristics of sensors, they have distinct uses.

2.1.2. In situ data collection

In situ data collection refers to the collection of georeferenced data (mainly points and areas) measured on the ground for a number of reasons, such as validating cartographic or remotely-sensed products, producing data layers, model calibration and/or validation, or simply gaining some understanding of the study area, amongst other reasons.

Regarding the methods for in situ data collection, one can guess that there are as many as the fields involved. One fundamental question to answer before anything is done is: What do we need to know from the ground? Then, we can decide the variables to be measured, the sampling scheme and personnel and instrumentation needed. Among the many decisions to make is whether to perform a random or systematic sampling; whilst the former is preferred for accuracy assessment purposes, the latter is desirable for spatial analysis, for example, spatial interpolation.

Today, there is a growing number of affordable digital technologies that enable the collection and real-time analysis of georeferenced field data. Not only is the increase in performance, resolution and portability of measuring devices but also the functionality that enables on-site analysis and visualisation that is making the in situ data collection more efficient with reduced uncertainty [4]. Laser-based technology (e.g. range finders, dendrometers, terrain profilers, terrestrial laser scanners, etc.) has enabled the measurement of inaccessible locations and generation of coloured point clouds that capture the three dimensional (3D) structure of the sampled site. On the other hand, modern communication protocols, mobile device network coverage and cloud storage capabilities are also facilitating field data management and sharing in unprecedented ways.

2.1.3. Crowdsourcing

The ubiquitous use of mobile devices and Internet access has fostered the ability of citizens to collect their own data for varied purposes. Many apps and platforms have been developed that allow citizens to collect data. GeoKey is a backend platform that allows the creation of customised projects [5]. One still needs to programme a frontend, but it is quite versatile in the types of data it can handle. GeoCitizen is a platform developed for community-based spatial planning. Its goal is to provide means and information for citizens to access data and get involved in every step of the planning process [6]. Ushahidi is a well-known platform used for crisis mapping [7]. It gained momentum during and after the massive earthquake that hit Haiti in 2010 [8]. OpenTreeMap allows users to collaborate in creating a massive inventory of trees that are useful for ecosystem management and urban forestry [9]. iNaturalist focuses on users collecting data about observations of the natural world [10]. Waze has also become a very common platform that allows real-time communication with other users reporting traffic conditions whilst driving [11]. NoiseTube has also been used for participatory noise pollution mapping and monitoring [12].

Without necessarily challenging the existence of official records, it is increasingly common to compare what the official figures tell with what the citizenry observes and experiences on its everyday life.

Crowdsourcing and volunteered geographic information (VGI) are two terms that have been more pervasive in the academic literature. But what, if any, is the difference between them? Crowdsourcing can be found in many different topics, not just geographical information and 'implies a coordinated bottom-up grassroots effort to contribute information' [13]. For some, VGI represents an 'unprecedented shift in the content, characteristics, and modes of geographic information, creation, sharing, dissemination and use' [14]. Others, such as Harvey, propose that not all crowdsourced data are volunteer data. He suggests making a distinction when data are collected with an 'opt-in' or an 'opt-out' agreement [15].

Nonetheless, both ideas—crowdsourcing and VGI—rely on data being contributed by many users. In a sense, they are strong advocates of the 'wisdom of the crowds' and collective intelligence: the idea of whether a product created collectively is better than the best individual product [16, 17].

http://dx.doi.org/10.5772/64355

The deluge of mobile apps makes it possible to crowdsource data practically anywhere. In Mexico, however, strong biases can be introduced with this form of data collection, as it may be far more popular in urban settings with the added issue that not all regions in the country have the same mobile network coverage [18].

2.2. Processing techniques

Data-processing techniques refer to techniques for data preparation prior to any information extraction. These techniques include data reformatting, cleaning, rectification, denoising, enhancement, etc. Although a thorough review of such techniques is beyond the scope of this chapter, it is worth noting that most techniques that operate in raster formats come from the digital image-processing field, where theoretical developments have been around filtering techniques in both the space and frequency domains. Additionally, techniques such as principal components analysis (PCA) and minimum noise fraction (MNF) are applied as spectral transformations of multispectral and hyperspectral images, whilst some spatial, multiscale representations, for example, wavelets, are used for image denoising or spatial enhancement (pansharpening).

In fields such as crowdsourcing or social media analysis, the preprocessing can be even more important (since there is no adequate way to calibrate the 'instruments' used to acquire data), but, opposed to remote sensing, there is no sound theoretical framework from where to draw techniques. This situation requires, in the best case, the use of some form of ground truthing to discard spurious data. Wherever reliable data are not available, the researcher must resort to his/her domain knowledge or heuristic algorithms to preprocess the data.

2.3. Analysis and interpretation

The increasing production of spatial data from both official and non-official sources and with unstructured formats has placed a larger complexity in its management and analysis. On the one side, information granularity has incremented both spatially and temporally, thus making it necessary to develop analytical tools that simultaneously take into account space and time for decision-making. On the other side, the great diversity of sources of information that share the spatial component has triggered the efforts for interoperability, which implies the possibility of combining multidimensional information that can provide potential knowledge. In this section, we describe some of the most pervasive methods of analysis used by geospatial technologies.

2.3.1. Cluster analysis

Generally speaking, cluster analysis refers to the process of grouping objects into classes by some measure of similarity. These objects can be either abstract, as the companies in the stock market, or physical as the states within a country. The similarity measures used on cluster analysis depend on the kind of objects and the characteristics being analysed. If the interest is in grouping earthquake occurrences, then the Euclidian distance is a reasonable similarity

measure, but if we are grouping counties around some measurement of its economic performance, the Mahalanobis metric could be a reasonable choice.

Cluster analysis has been successfully used in many applications: market research uses segmentation to target products; in biology, it is used for taxonomy and DNA sequencing; in image recognition, it is used in image segmentation.

Certainly, cluster analysis is not new within the field of geographic data analysis; ISODATA has been in use for over 40 years in multispectral image classification [19]; the famous John Snow map of the cholera outbreak in London is also a case of cluster analysis, and the concept of regionalisation, when approached from a spatial analysis perspective, can be interpreted as a case of geographically constrained clustering, that is, clusters in which observations are grouped together by their similarity in the feature space but restricted to their neighbourhood relations in the geographical space [20].

Recently, the increase in the quantity of data collected every day from a great number of disparate sources has stemmed a new interest in the techniques derived from cluster analysis. One of the reasons of this recent interest lies in the flexibility of the similarity measures that can be used. This is especially important when working with what has been labelled as unmodelled data, that is, data that are not structured for analysis, such as natural language. This kind of information has become more frequent as technologies such as social media and the pervasiveness of sensors are becoming commonplace.

Although there are cluster analysis techniques that clearly come from the statistical modelling tradition, such as the work of Kulldorf on epidemics or ISODATA [21], the recent increase in clustering methods comes from the algorithmic culture. Applications such as handwritten recognition or image segmenting make extensive use of clustering methods from the algorithmic culture [22–25].

In the field of geographic data analysis, there are also some important developments. In particular, the field of geographic knowledge discovery (GKD) is gaining recognition as is evident from the amount of conferences and special issues devoted to the topic ([26, 27], amongst others).

On the subject of cluster analysis as a mean for extracting geographic knowledge from unmodelled data, there have been some interesting recent developments. Frias-Martinez et al. proposed a technique for extracting land-use information from geolocated Twitter feed and used spectral clustering for the extraction of regular activity zones [28]. Lee et al. used *k*-means clustering to detect unusual crowds also using geolocated tweets. These works rely solely on the spatio-temporal properties of the data, which is interesting because the techniques developed could be easily translated to work with different datasets, such as mobile telephone records [29].

There are also some interesting examples that combine the spatio-temporal properties with the semantic content of the messages. Amongst these, we find the work of Gabrielli et al. who deduced trajectories from the geolocated Twitter feed and enriched these trajectories with semantic information from the users (e.g. whether the user is a tourist) and the surroundings

http://dx.doi.org/10.5772/64355

(the types of venues located around the user at a given moment) [30]. Also, the works of Boetcher and Lee or Kim et al. present techniques for the detection of local clusters of activity around specific topics of interest [31, 32].

This development in the GKD field, from an academic perspective, has happened in parallel with the development of the data-mining field in the application-driven environment of start-ups and technology corporations. Currently, as the academic field matures, it is beginning to catch up with the technology side developed in the commercial world. The shift of focus towards real-time analysis [33] stresses the need to not only develop better algorithms but also develop them on top of a technological stack that allows the scaling up needed to solve the problems associated with real- or near-real-time analysis.

In the GIS field, the recent development of the CyberGIS paradigm attempts to build a bridge between traditional GIS and new advances on distributed data stores, parallel computing and collaborative workflows [34–36]. Research on the parallelisation of *k*-means and the application of the map-reduce programming paradigm to cluster analysis in general are examples of the direction of technology research within the field of cluster analysis in a GKD framework [37, 38].

2.3.2. Network analysis

Network analysis in the geospatial community generally refers to analysis techniques associated with the optimisation of transportation routes. In this section, we investigate techniques that originated in the field of graph theory to analyse social networks, applied to geographical phenomena—particularly, migration flows.

Migration between metropolitan areas can be conceived as a weighted graph in which nodes (n) are the cities and the edges (m) are the flows between them. In transport analysis literature, there are several techniques to deal with networks; one of the most frequently cited is the nodal region approach [39]. This method is used for quantifying the degree of association between pairs of cities in a way that allows the identification of the strongest association of the network. The result is a graph with a maximum of $(n - 1)$ edges. Further modifications were introduced by Graizbord [40] and Suárez and Delgado [41] in order to provide more flexibility in the hierarchy of the nodes and the size of the filtered graph, as well as some restrictions in the definition of salient flows, such as the comparison from a gravitational model or previous data on migration flows.

Bender-deMoll mentions in his network analysis and mapping report that characterisation of flows of goods and people is a classic field of application of social network [42]. Networks are used to represent flow patterns between sets of entities and constitute a useful analysis of movement structures. Results of some studies on trade flows have shown to provide more knowledge and have helped predict global resources flow between countries. By analysing data on both forced and voluntary migrations, a strong correlation has been found between the geography and the relationships shown by aggregate flows. In the same way, these flows reflect the social links of migrants, that is, they usually move to places where relatives and/or

friends are located, or to places that information networks have detected to be viable for development.

One way to characterise flows is to detect communities, an exercise similar to cluster analysis. With a binary network, this type of analysis can only be performed if the difference between the number of edges (m) and nodes (n) is not too large. If $m \gg n$, edge distribution is so homogeneous that communities do not make any sense. However, community detection is possible if the network is weighted and weights have a heterogeneous distribution [43].

The community detection problem requires partitioning a network in groups of densely connected nodes, where nodes belonging to different communities have disperse links. The quality of resulting partitions is usually measured with the so-called modularity of the partition. The modularity of a partition (Q) is a scalar value between −1 and 1 that measures the density of links inside communities as compared to links between communities. In the particular case of weighted networks,

$$Q = \frac{1}{2m}\sum_{ij}\left[A_{ij} - \frac{k_i k_j}{2m}\right]\delta\left(c_i, c_j\right) \tag{1}$$

where A_{ij} represents the weight of the edge between i and j, $k_i = \Sigma_j A_{ij}$ is the sum of the weights of the edges attached to node i, c_i is the community to which node i is assigned, $\delta(c_i c_j)$ equals 1 if c_i and c_j are in the same community and 0 otherwise, and $m = \frac{1}{2}\sum_{ij} A_{ij}$.

The Louvain method to optimise the modularity function finds high modularity partitions on large networks in short time and unfolds complete hierarchical community structures for the network. In the final solution, the output partition contains communities of the most densely linked nodes [44].

2.4. Visualisation and interpretation

Starting around the mid-1990s, geovisualisation—the use of visual representations in order to employ vision to solve spatial problems—entered the GIScience arena. MacEachren et al. provided tools for dynamic exploration of data to help discover relationships and patterns by means of exploratory spatial data analysis (ESDA) [45]. At the turn of the century, the term geovisual analytics started to be heard. It deals with analytical reasoning and decision-making whilst using interactive visual interfaces (e.g. maps and other graphic representations) linked to computational methods and the human capacity of knowledge construction and representation [46]. This section presents some of the most popular visual analytics techniques.

2.4.1. Kernel density

One of the most commonly used hotspot detection methods is kernel density estimation. Its advantages reside in the simple interpretation and its availability in almost any geographical information system [47]. One of this method's weaknesses is the need to accumulate observations in a wide temporal window and unfortunately, as many other hotspot detection methods,

http://dx.doi.org/10.5772/64355

it treats spatial and temporal aspects as separate entities, thus ignoring the spatio-temporal interactions.

2.4.2. Knox's index

Halfway through the twentieth century, Knox proposed a statistical test to detect epidemics [48]. Essentially, it was a statistical independence test for contingency tables classifying individual events that were registered by their location close in time and space. A more robust implementation goes beyond the simple independence test, testing for randomness of the spatial pattern [49]. The null hypothesis is as follows: the occurrence of an event is randomly distributed between the locations. That is, distances in time between pairs of observations are independent to the distances in space. The statistics is as follows:

$$x = \sum_{i=1}^{N} \sum_{j=1}^{i-1} a_{ij}^{\delta} a_{ij}^{\tau} \tag{2}$$

With the following restrictions:

$$a_{ij}^{\delta} = \begin{cases} 1, \text{if the distance between cases } i \text{ and } j < \delta \\ 0, \text{if the distance between cases } i \text{ and } j > \delta \end{cases}$$

$$a_{ij}^{\tau} = \begin{cases} 1, \text{if the distance between cases } i \text{ and } j < \tau \\ 0, \text{if the distance between cases } i \text{ and } j > \tau \end{cases}$$

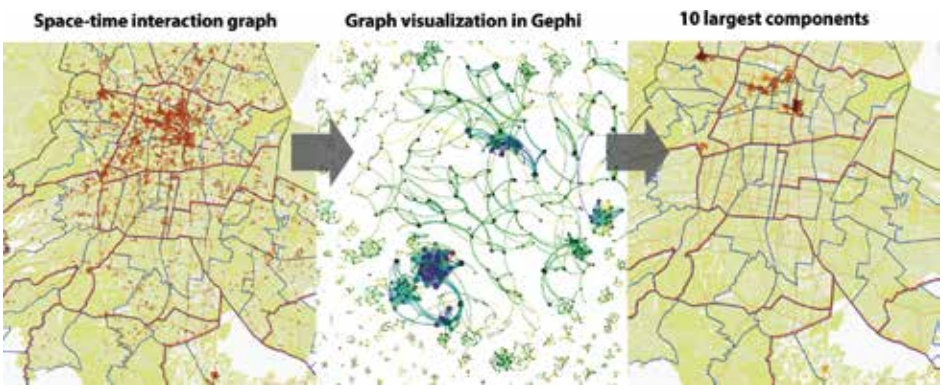

Figure 1. Space-time interaction graph representation and simplification of larceny theft cases in 2009 in Mexico City.

The randomisation technique for the assessment of space-time significance consists on shuffling the temporal distances between cases or events whilst holding the spatial distances constant, and compare the observed and the expected values from Monte Carlo simulations.

The Knox test was originally designed to account for latency periods: time between exposure and the manifestation of symptoms [49].

The added value given to Knox's index by means of a graphic output was to characterise the graph with some simple metrics from network analysis. The only transformation performed on the graph was to invert the role of nodes and edges. The degree of each node and the size of each connected component are useful for detecting significant spatio-temporal events through graph pruning. **Figure 1** illustrates how the application of this index metrics is useful for detecting critical areas in order to design police operations that would align different material and human resources (surveillance cameras, street policemen, police cars, etc.).

2.4.3. Heat maps

Originally designed for displaying financial information that would allow stockbrokers to detect anomalistic behaviours, heat maps were patented, trademarked and made their way into geographical data. Heat maps have been associated to choropleth maps and have become very useful to represent point, line or area density data. Heat maps are also known as density surfaces. They are useful for identifying those areas of a map that have high-density counts within a spatial context [50].

It is probable that after Google released the ability to include heat maps as separate layers using the Maps Javascript API in 2012, the use of heat maps for geospatial data experienced a boom [51]. Since then, many more options have become available.

2.4.4. Flows representation

One of the most often used representations of entities moving between geographical locations is a flow map, in which locations are represented as lines or arrows with their width proportional to the flow magnitudes.

The origin-destination (OD) matrix is an alternative non-geographic visualisation of this kind of data; the magnitudes are represented by the cell colours in a heat map with the rows corresponding to the origins and the columns with the destinations.

A kriskogram is created using a two-step procedure. Firstly, all related geographical units are projected as a set of evenly spaced dots on a straight line called the location line. The order of locations can be arranged using geographical criteria such as the overall orientation of the spatial units, or demographic criteria, such as gross migration or population. In the second step, the migration flow between two places is represented as a half-circle drawn from the origin to the destination in a clockwise direction with the circle's centre located on the middle point between the two corresponding dots on the location line [52].

Flowstrates is an interactive visualisation approach in which the origins and destinations are displayed in two separate maps, and the changes over time of the flow magnitudes are represented in a separate heat map view in the middle [53].

Figure 2 shows examples of the three types of visualisations mentioned in the text. It is evident the kriskogram has two disadvantages: firstly, it loses all spatial reference and secondly it is

http://dx.doi.org/10.5772/64355

impossible to identify the direction of the flow. It facilitates, however, the identification of magnitudes. Heat maps have certain strengths when the network disperses, with few flows. As the network becomes denser, reading it becomes more complex. The method by Boyandin et al. is very interesting since it proposes an interactive exploration tool [53]. Incorporating the heat map allows the identification of trends in migratory flows between pairs of places and avoids information redundancy present in matrix representations by transforming an array of data into one of minimal information in which each flow occupies one row in the heat map. One inconvenience is that as more regions are selected as origins or destinations, the length of the array can grow substantially.

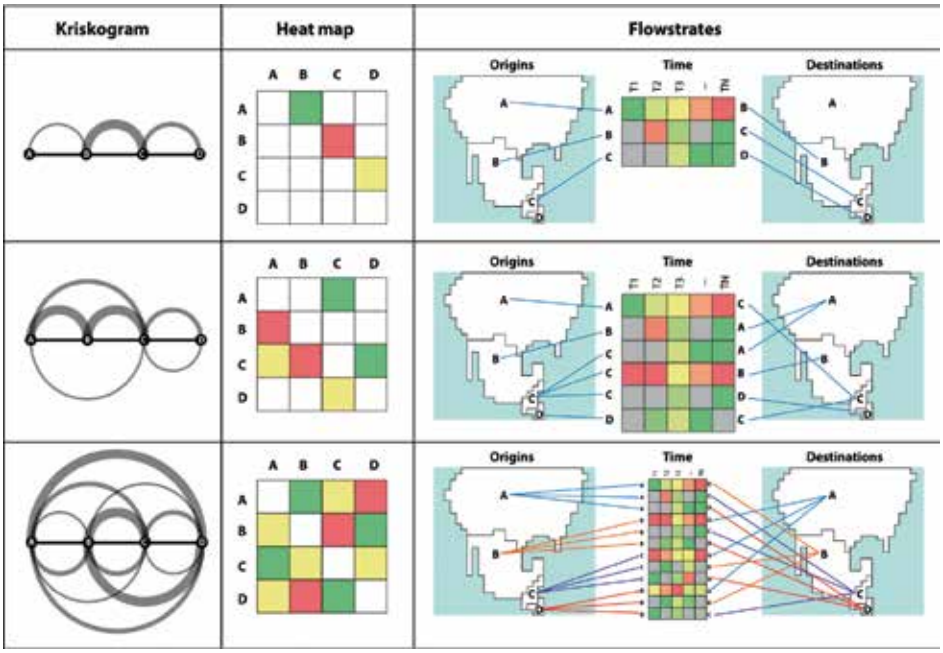

Figure 2. Flow visualisations comparison. Adapted from [52–54].

For our case studies, kriskograms were ruled out because they lose all spatial references. However, we use arcs that avoid overlapping flows. We move away from heat maps in their traditional matrix form and instead use a heat map layer on top of a geographical base. Flowstrates' potential lies in the explicit incorporation of temporal trends. Unfortunately in our case, we lack time series to profit from this representation.

2.4.5. 3D modelling

The development of 3D modelling can be traced back to the 1970s, when efforts of several industries in developing computer-aided design software started. Today, 3D modelling techniques have become an indispensable tool for inventorying and visualisation of objects through digital platforms, but also for producing models with 3D printing devices.

There are several ways for producing 3D scenes. Traditionally, 3D models have been generated manually and algorithmically, especially in the realm of industrial and architectural design. Commercial 3D GIS software, such as ESRI's ArcScene and City Engine, can convert two-dimensional (2D) features into 3D features by applying an extrusion operation (**Figure 3**) and provide extensive libraries of 3D models of vegetation and urban infrastructure [55, 56]. Alternatively, models of actual vegetation and buildings can be generated through remote sensing and computer vision techniques.

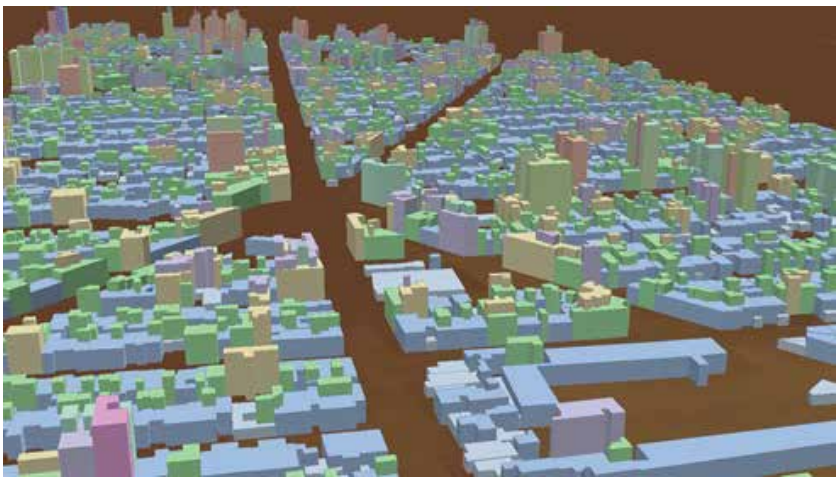

Figure 3. Extruded building footprint from a 2D database.

With the development of laser scanners and advances in photogrammetric techniques, the interest of 3D modelling in the geospatial industry and science has shifted towards the development of new automated or semiautomatic methods for generating photorealistic scenes of the landscape. Close-range data acquisition, such as terrestrial laser scanners (TLSs) and multiple oblique photographs taken with drones, allows the detailed reconstruction of buildings and trees, whereas large-scale projects require the integration of airborne laser scanners (ALSs), aerial photography and satellite-based data acquisitions.

Tree reconstruction and modelling from ALS data have been developed using the voxel approach [36], simple geometrical models such as paraboloids and ellipsoids [57], wrapped surfaces derived by radial basis functions and isosurfaces [58], whereas detailed modelling of trees has been carried out using mobile laser scanners (MLSs), where tree trunk and branches are detected and reconstructed [59]. Buildings are also reconstructed from both laser scanner data [60] and photogrammetric techniques using multiple oblique photographs [61]. These methods are, however, not fully integrated within the 3D GIS platforms but rather are components of remote sensing and photogrammetric-processing systems.

There has also been an increasing demand to use 3D models in virtual reality (VR) and augmented reality (AR) environments, in which virtual and immersive scenes are generated in real time for several applications such as education, training, manufacturing, remote

http://dx.doi.org/10.5772/64355

operations, entertainment, collaborative work, and so on. The key idea is the interaction of humans with 3D models (in place of real objects) that are immersed in a background scene and may include ambient stimuli. Although VR and AR have evolved separately, efforts have been made to integrate these techniques with 3D GIS [62].

The adoption of these technologies has been proved successfully for urban planning, cadastral information updating and for archaeological cultural heritage documentation and visualisation.

2.4.6. Space-time data representations

In the early stages of geographic information sciences, most analyses and representations were focused on static data and models. This is, as Goodchild argues, a consequence of the close relationship that existed within digital data and hard-copy maps [63]. The former was produced by a digitisation of the latter, which implies that digital data had to accommodate to the lengthy and costly procedure of updating, for example, the general topographic maps.

As the field and its associated technology evolved, we have seen an ever-increasing amount of spatio-temporal information gathered: satellite images, GPS traces, climate data, etc. In order to make sense of these data and to fully realise its potential in helping unveil the dynamics of the processes that produce the 'static' patterns observed, we need better tools to digitally represent and analyse spatio-temporal data.

In terms of the digital representation of spatio-temporal data, the early work of Langram and Chrisman on spatio-temporal topology clearly represents a departing point for the evolution of the field [64]. From a theoretical perspective, the work of Hagerstrand on spatial diffusion and space-time geography represents an equally important starting point for space-time modelling from a spatial analysis perspective [65, 66].

Although the field has seen great advances from these early examples, the main issues involving the establishment of the temporal dimension in the GIS field were already present: geographical models need to be explicitly temporal (as Hagerstrand's innovation diffusion [65]), the need of theoretical foundations that explain the way in which the modelled subjects interact in space and time (when studying human populations, this lies within space-time geography, but when we deal with different problems, e.g. ecology, the theories will certainly arise from different fields), and, finally, the need for data structures that allow storing and processing spatio-temporal data in ways that are meaningful to the problems at hand.

3. Case studies

This section presents examples drawn from the experience of the authors working in social and environmental issues, which will help clarify the concepts exposed in the previous sections. Although not always explicit, all of the examples presented here include the steps of data processing, analysis and visualisation as well as results interpretation. The intent is not

to provide a complete explanation of each example but to provide a general application context to complement the general approach presented in the previous sections.

3.1. Social media analysis of subjective well-being

A proposed technique for global polarity classification in short texts, specifically Twitter, is described. The main objective was to obtain a map of subjective well-being for conterminous Mexico; this map will allow us to see the differences in regional perceptions about general well-being. Although this kind of maps can be obtained by traditional methods, such as polls, it is important to note that the amount of resources, human and economic, involved in such exercises, makes it impossible to measure well-being on finer spatio-temporal resolutions. On the other hand, validating a methodology based on social media analysis allows us a very fine-grain analysis, certainly, losing some of the robustness obtained with traditional polling.

For this, we classified the polarity (or sentiment) for each short text (in this case, a tweet). Sentiment analysis is one of the most important tasks in text mining. Nevertheless, this kind of analysis has several challenges related to the complexity of human language, that is, multitude of styles, informal writing, language mixing, short contexts, orthographic and grammatical errors, an always-growing vocabulary, etc. The sentiment classification attempts to determine if one document has a positive, negative or neutral opinion or any level of them (e.g. positive+, negative+, etc.). Determining whether a text document has a positive or a negative opinion is becoming an essential tool for both public and private companies [67]. This tool is useful in knowing 'what people think', which can be important information to help in any decision-making process (for governments, marketing companies, etc.) [68].

3.1.1. Related work

Nowadays, several methods have been proposed in the community of opinion mining and sentiment analysis. Most of these works employ Twitter as a principal input of data and they aim at classifying entire documents as overall positive- or negative-polarity levels (sentiment). Such is the work presented by da Silva et al., which proposes an approach to classify sentiment of tweets by using classifier ensembles and lexicons; tweets are classified as positive or negative. As a result, it is concluded that classifier ensembles formed by several and diverse components are promising for tweet sentiment classification [69]. Moreover, several state-of-the-art techniques were compared in four databases. The best accuracy result reported was around 75%.

Another method for sentiment extraction and classification of unstructured text is proposed by Shahbaz et al. who used five classes: strongly positive, positive, neutral, negative and strongly negative [70]. The proposed solution combines techniques of natural language processing (NLP) at sentence level and algorithms of opinion mining. The accuracy result was 61% for five levels and 75% by reducing to three levels (positive, negative and neutral).

An approach of multi-label sentiment classification was proposed by Liu et al., which has three main components: text segmentation, feature extraction and multi-label classification [71]. The features used included raw segmented words and sentiment features based on three sentiment

http://dx.doi.org/10.5772/64355

dictionaries: DUTSD, NTUSD and HD. Moreover, here, a detailed study of several multi-label classification methods is conducted, in total, 11 state-of-the-art methods have been considered: BR, CC, CLR, HOMER, RAkEL, ECC, MLkNN, and RF-PCT, BRkNN, BRkNN-a and BRkNN-b. These methods were compared in two microblog datasets, and the reported results of all methods are around 0.50 of *F*-measure.

In general, most of the analysed works classify the documents mainly in three polarities: positive, neutral and negative. Moreover, most works analyse social media (mainly Twitter) documents. In this section, we describe a method to classify sentiment in tweets. The sentiment of the messages will be classified into three polarity levels: P (positive), neutral and N (negative). The proposed method is based on several standard techniques such as LDA (Latent Dirichlet Allocation), LSI (Latent Semantic Indexing), term frequency-inverse document frequency (TF-IDF) matrix in combination with the well-known SVM (Support Vector Machine) classifier.

3.1.2. Proposed solution

The overall workflow can be summarised as follows. A preprocessing step is first carried out, then a pseudo-phonetic transformation is applied and, finally, the *q*-gram expansion is generated.

The preprocessing focused on the task of finding a good representation for tweets. Since tweets are full of slang and misspellings, the tweet text is normalised using procedures such as error correction, usage of special tags, part of speech (POS) tagging and negation processing. Error correction consists on reducing words-tokens with invalid duplicate vowels and consonants to valid-standard Spanish words (ruidoooo → ruido; jajajaaa → ja; jijijji → ja). Error correction uses an approach based on a Spanish dictionary, a statistical model for common double letters and heuristic rules for common interjections. In the case of the usage of special tags, twitter's users (i.e. @user) and URLs, they are removed using regular expressions; in addition, 512 popular emoticons were classified into four classes (P, N, NEU, NONE), which are replaced by a polarity tag in the text, for example, positive emoticons such as :), :D are replaced by _POS, and negative emoticons such as :(, :S are replaced by _NEG. Emoticons without any polarity charge are discarded.

In the POS-tagging step, all words are tagged and lemmatised using the Freeling tool for the Spanish language stop words are removed, and only content words (nouns, verbs, adjectives and adverbs), interjections, hashtags and polarity tags are used for data representation [72]. In the negation step, Spanish negation markers are attached to the nearest content word, for example, 'no seguir' is replaced by 'no_seguir', 'no es bueno' is replaced by 'no_bueno', 'sin comida' is replaced by 'no_comida'; a set of heuristic rules for negations are used in this case. Finally, all diacritic and punctuation symbols are also removed.

In a second step, and with the purpose of reducing typos and slangs, a semi-phonetic transformation was applied. Firstly, the following transformations (with precedence from top to bottom) as shown in **Table 1** were carried out.

In this transformation notation, square brackets do not consume symbols and means for any valid symbols. The idea is not to produce a pure phonetic transformation as in Soundex-like algorithms, but try to reduce the number of possible errors in the text. Notice that the last two transformation rules are partially covered by the statistical modelling used for correcting words (explained in the preprocessing step). Nonetheless, this pseudo-phonetic transformation does not follow the statistical rules of the previous preprocessing step.

$cx \mid xc \rightarrow x$	$ll \rightarrow y$	$w \rightarrow u$
$qu \rightarrow k$	$z \rightarrow s$	$v \rightarrow b$
$gue \mid ge \rightarrow je$	$h \rightarrow \in$	$\Psi\Psi \rightarrow \Psi$
$gui \mid gi \rightarrow ji$	$c[a \mid o \mid u] \rightarrow k$	$\Psi\Delta\Psi\Delta \rightarrow \Psi\Delta$
$sh \mid ch \rightarrow x$	$c[e \mid i] \rightarrow s$	

* i denotes the imaginary unit number.

Table 1. List of transformations applied to geotagged tweets.

Finally, along with the bag of words representation (of the normalised text), the four- and five-gram characters of the normalised text were added. Blank spaces were normalised and taken into account to the q-gram expansion; so, some q-grams will be over one word. In addition to these previous steps, several transformations (LSI, LDA and TF-IDF matrix) were conducted to generate several data models for the testing phase.

3.1.3. Results and analysis

For the experiments, a total of 7218 tweets, with six polarity levels were split into two sets from the TASS challenge, were used [73]. Firstly, the tweets provided were shuffled and then the first set, hereafter the training set, was created with the first 6496 tweets (approximately 90% of the dataset), and the second set, hereafter the validation set, was composed of the rest 722 tweets (approximately 10% of the dataset). The training set was used to fit a Support Vector Machine (SVM) using a linear kernel with $C = 1$, weights inversely proportional to the class frequencies, and using the one-against-rest multiclass strategy. The validation set was used to select the best classifier using as performance the score $F1$- or F-measure. This measure considers both the precision and the recall. The $F1$-score can be interpreted as a weighted average of the precision and recall, where an $F1$-score reaches its best value at 1 and worst at 0.

The first step was to model the data using different transformations, namely Latent Dirichlet Allocation (LDA) using an online learning proposed by Hoffman in [74], Latent Semantic Indexing (LSI), and TF-IDF. **Figure 4** presents the score F1, in the validation set, of an SVM using either LSI or LDA with normalised text, different levels of q-gram (4 and 5 g), and the number of topics is varied from 10 to 500 as well. It is observed that LSI outperformed LDA in all the configurations tested.

http://dx.doi.org/10.5772/64355

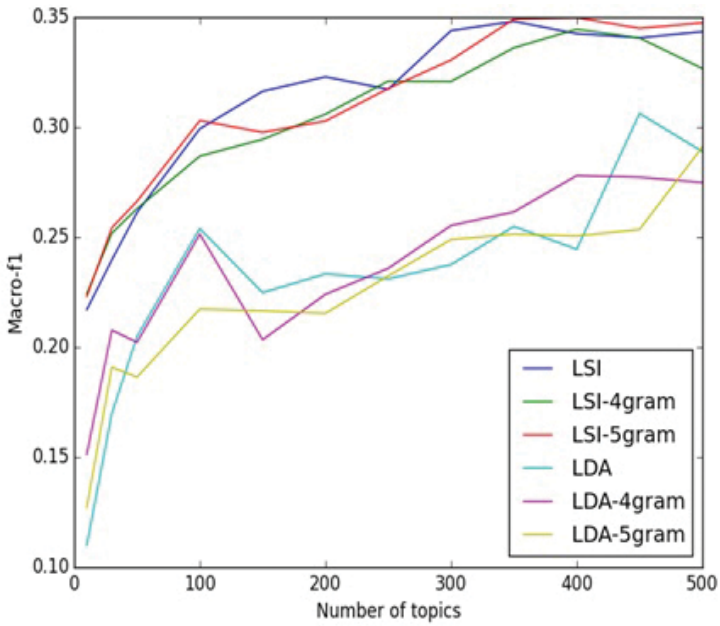

Figure 4. Performance of the various text transformations tested.

An equivalent performance was also observed when comparing the performance of normalised text, 4 and 5 g (**Figure 4**). Given that the implemented LSI depends on the order of the documents, more experiments are needed to know whether any particular configuration is statistically better than other. **Table 1** complements the information presented in **Figure 1**. **Table 1** presents the score F1 per polarity and the average (Macro-F1) for different configurations.

Table 1 is divided into five blocks, the first and second correspond to an SVM with LSI and TF-IDF, respectively. It is observed that TF-IDF outperformed LSI; within LSI and TF-IDF, it can be seen that 5 and 4 g got the best performance in LSI and TF-IDF, respectively. The third row block presents the performance when the features are a direct addition of LSI and TF-IDF; here, it is observed that the best performance is with 4 g. The fourth row block complements the previous results by presenting the best performance of LSI and TF-IDF, that is, LSI with 5 g and TF-IDF with 4 g. It is observed that this configuration has the best overall performance in P+, N, none and average (Macro-F1). Finally, the last row block gives an indication of whether the phonetic transformation is making any improvement. One major conclusion of this work is that the phonetic transformation is making a small difference.

As a final contribution, a set of experimental statistics were generated for the National Institute of Geography and Statistics (or INEGI from its Spanish name), yielding a map of subjective well-being for conterminous Mexico (**Figure 5**). This map reflects the importance of geospatial information, harvested from social media, because it allows us to measure subjective well-being on finer spatial and temporal resolutions than traditional methods.

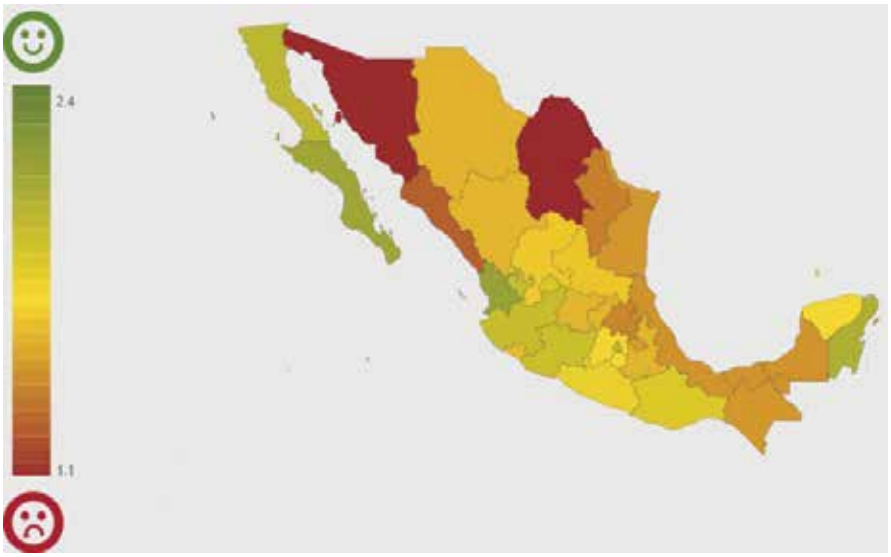

Figure 5. Subjective well-being map of Mexico based on the sentiment analysis of tweet messages.

3.2. Characterisation of migratory flow patterns of highly qualified people in Mexico

Many real systems—social, technological, biological and information—can be described as networks. We have only found few studies that treat migration from this perspective in the literature: one focusing on multiscale mobility in the United Kingdom [75], another dealing with internal migration in the United States [76], a global migration study stressing the flows between the OECD countries [77] and global flows [78, 79].

This case study treats the characterisation of migration flows of highly qualified human resources (defined by means of academic achievement—people with undergraduate degrees and those with graduate degrees—and people in knowledge-intensive occupations) in 59 Mexican metropolitan areas [80]. Data refer to the change of residence in the last 5 years, that is, recent migration was obtained from the 2010 General Population Census [81]. A common practice in migration studies is to aggregate data according to the analysis unit. In this case, starting with the origin-destination matrix, networks are built and then characterised. Furthermore, the square matrix is transformed into an array of minimum information that avoids redundancy and also allows for the dynamic exploration of flows between metropolitan areas.

Even though non-spatial visualisations reveal important properties of networks, it is interesting to try and shed some light on whether migration flows exhibit behaviour with strong geographical components.

Figure 6 shows the 'graduates' network. This network is partitioned in five communities and has the highest Q-value (0.66), implying a reasonable quality of the partition. It is worth noting

that the three largest metropolitan areas belong to different communities. Also, Mexico City encompasses almost half (23) of the metropolitan areas and its community is spread out throughout the whole country. By contrast, there is one community that consists of only one member and another one of only two members, both located in the centre of the country.

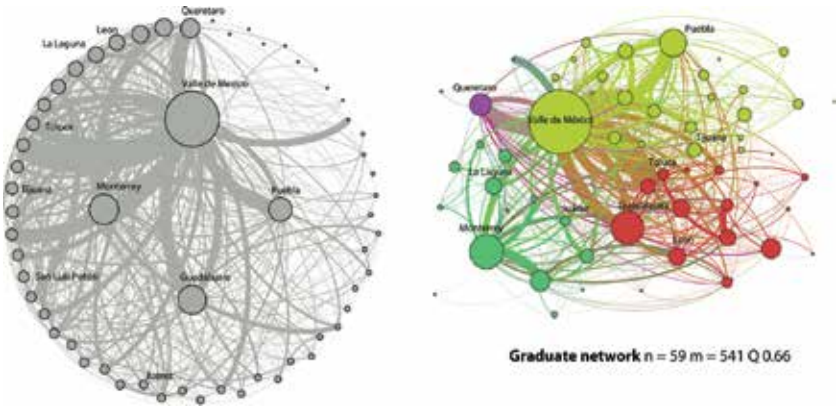

Figure 6. Graduates' migration network. Left: circular layout, showing labels for the 10 largest metropolitan areas; size is relative to the betweenness centrality parameter of the network. Right: nodes are coloured according to their community and the edges according to the source node.

An important characteristic of this study is network visualisation. By means of geographical visualisation, some network features can be highlighted according to node parameters. It also allows the identification of special structures in flow patterns.

Given the difficulty to explore flows and contextual elements related to the metropolitan areas, two separate interactive visualisations were prepared for this case. One uses Tableau Public and contains the analysis for community and role detection [82]. It also contains contextual data for each metropolitan area. The second is a geographic visualisation with special filters and functionality to explore the flows.

Tableau allows seeing the geographical arrangement of communities and the roles each metropolitan area plays (**Figure 4**). For the more dense networks—'undergraduates' and 'knowledge-intensive occupations'—there is an evident geographical component: communities tend to group regionally. The 'graduates' network instead exhibits a much smaller geographical distance than its functional one. This trend has been verified in other studies of high-quality human resources migration [83, 84]. It is important to note that concentrated or disperse functional distances cannot be highlighted using conventional network visualisations.

The interactive edges were a custom-made solution using open-source software. The frontend was built with jQuery [85] and LeafletJS [86]. The intensity of the inward and outward flows for each metropolitan area is represented with different colours and the number of migrants with relative widths. This interactive tool allows the comparison between origins and destinations for the different groups considered. Clicking on a metropolitan area simplifies

available information in the visualisation by only showing flows corresponding to that metropolitan area (**Figures 7** and **8**).

Figure 7. Communities for 'undergraduate' and 'graduate' migrations.

Figure 8. Flow visualisation for the metropolitan area of Cancun.

3.3. Volunteered geographic information for citizen empowerment

The case study presented in this section is set in a central neighbourhood in Mexico City: The Roma. The neighbourhood has experienced different stages throughout the years. At the

http://dx.doi.org/10.5772/64355

beginning of the twentieth century, it was considered to be high-class, rich people settled in the areas and several businesses experienced a florescence for several years. After a massive earthquake hit the city in 1985, many fled and the neighbourhood was partially abandoned for quite some time. Eventually, people who had lost their homes started to settle again in the neighbourhood, but by then it was not considered to be high class anymore. However, much of the architecture of the mid-1950s still remains even though many of these buildings have been occupied or have been used for different purposes other than residential. During the last decade, a gentrification process has been occurring in the neighbourhood, provoking poor people to be gradually expelled and richer people coming in. Because of the strong drastic changes that have occurred in it, the citizenry has started to notice many situations they consider to be harmful for their local environment. As a reaction, they have organised themselves and established an effective and fluent communication channel with their local authorities. After realising that they represent only a small portion of their municipality, they deemed it reasonable to explore the capabilities that crowdsourcing, VGI and participatory cartography could provide them.

For this, workshops were set up in order to find out about their needs and ideas. In an iterative process, the citizen part together with the scientific counterpart from CentroGeo converged on a list of variables to be collected on the field. This list represented the most pressing issues they could tackle for the moment and that were expected to be well received by the authorities in order to act and help ameliorate their situation. A list of six categories with several categories was agreed. A digital geospatial platform suitable for data collection on the web was set up. Due to time and budget constraints, it was not possible to provide them with native mobile apps. This platform consisted of purely free and open-source software: PostgreSQL/PostGIS [87, 88] for the backend, Bootstrap [89], jQuery and LeafletJS for the frontend and PHP [90] for the communication between both parts.

Citizens were in charge of data collection and quality assurance. The platform has the possibility to quickly get an idea about the spatial distribution of issues on the neighbourhood by means of a typical clustering strategy of collected data points. This is a very useful way for citizens to get an overall impression of what situations are persistent and, most importantly, where. Additionally, it is possible to create heat maps on the fly for the selected variables. This is useful for citizens to explore the possible existence of spatial correlation in the data they collected for different variables in their neighbourhood (**Figure 9**).

Overall, the case study was very successful in terms of allowing citizens to get more involved in noticing more details about everyday situations they face. It also helped them define possible courses of action to improve those situations in the neighbourhood. As of now, citizens are analysing all of the information they collected and establishing a plan to negotiate with their authorities. The process has helped them become more empowered because now they find themselves with data they did not think was possible to obtain. They thought they had to solely rely on what their local authorities could provide them and they have also found how they can come together for a greater good.

Also, it is worth mentioning that the maps that were obtained have been extremely useful to show where things are happening. This has been very helpful in increasing the citizenry's spatial awareness of their neighbourhood.

Figure 9. Citizen-mapping platform for the Roma neighbourhood showing clusters and categories.

3.4. Crime data analysis to support public safety in Mexico City

CentroGeo participated in the development of a geointelligence platform for Mexico City's Public Safety Ministry [91]. Back in 2004, this institution started georeferencing crime reports; in 2010, they already had enough experience in this task, but analytical capabilities were still short in order to extract useful information for decision-making. In this section, we present the implementation of a crime hotspot detection method that uses a spatio-temporal interaction graph.

The method mentioned in Section 2.4.2 was implemented in the context of Compstat-style planning and decision-making meetings that took place every week. A team of analysts would prepare comparative statistics and maps to establish police operations to focalised problems. Due to resource scarcity, it is imperative for public safety tasks to be prioritised. Hotspot detection for specific crime types was a first relevant criterion for decision-making.

As mentioned before, a first part of the process in mapping spatio-temporal hotspots consisted in the calculation of Knox's index together with the creation of the spatio-temporal interaction graph. Afterwards, the graph was characterised to identify the largest connected components, corresponding to priority areas (**Figure 1**).

http://dx.doi.org/10.5772/64355

Once these priority areas had been identified, human and material resources available to attack the problem were mapped. According to the detailed temporal patterns of incidents, it was possible to establish priority schedule tables for operating surveillance cameras in Mexico City (**Figure 10**).

Figure 10. Tactical planning map for the crime analysis study showing a hot area for larceny theft in Mexico City.

Implementing a geointelligence process in Mexico City's Public Safety Ministry was influenced both by the concept of geointelligence and by the institutional will to introduce a more fitting policing model for public safety in Mexico City. However, this has not been a linear process; instead, it has proven to be a complex, changing process entangling research and technical development results with daily demands emerging from the dynamics of the police institution.

3.5. Use of 3D vegetation modelling for forest inventorying Mexico City's Conservation Land

We present a case study of semiautomatic 3D forest generation through airborne laser scanner data over the Mexico City's Conservation Land (MCCL). Located in the southern fringe of Mexico City, the MCCL delivers important environmental services such as carbon sequestration, oxygen production, catchment, human recreation, among others, to the inhabitants of the city. However, its permanence has been threatened by urban sprawl during the past three decades generating several problems such as clandestine logging, illegal settlements and pollution [92]. The continuous monitoring and inventoring of this forested area will help authorities to preserve and improve this area. In this study, a 3D scene for an area of around 50 m^2 was generated using ALS data. Since the generation procedure and the accuracy assessment have been reported elsewhere [93, 94], here we only highlight the major processing steps and provide some theoretical insights of the 3D models.

3.5.1. ALS data processing

Point clouds acquired with the ALS50-II sensor flown by INEGI between November and December 2007 over the entire Basin of Mexico were employed in this study.

Basic processing prior to modelling surfaces with ALS data is the ground filtering and segmentation of the point cloud. The former refers to the segregation of ground points from the entire point cloud. Since feature heights are measured with respect to the ground, a bare-terrain surface must be first generated through interpolation of ground points. Then off-ground feature heights are normalised by subtracting the terrain elevation from the point cloud, and detection of objects of interest is conducted on the terrain-normalised dataset. For tree canopy detection, a fruitful approach is the watershed segmentation algorithm of the normalised digital height model with reversed z-coordinate. The segmentation procedure delineates watersheds that correspond, approximately, to tree crowns. Then, the segmentation is simply transferred to the points for the purpose of point selection.

3.5.2. Tree crown modelling

Points of individual trees were automatically selected using the segmentation information and best fit models were selected for each segment. A library of crown models was constructed from a generic revolution model of the form of Eq. (3), where (x, y, z) denotes a generic 3D point, and (u, θ) are the independent variables in the ranges [0,1] and [0,π), respectively,

$$\begin{aligned} x &= C(u)\, r \cos\theta \\ y &= C(u)\, r \sin\theta \\ z &= h + (h - b)\, S(u) \end{aligned} \tag{3}$$

In this model, the crown size is represented by tree parameters, namely the maximum crown radius (r), the bottom crown height (b), and the top crown height (h), whereas the shape is represented by functions $C(u)$ and $S(u)$ defined in Eq. (4), where $c_1,\ldots,c_7$ denote the shape parameters

$$\begin{aligned} C(u) &= \left(c_1 - \left(c_2 + c_3 S(u)\right)^{c_4}\right)^{\frac{1}{c_5}} \\ S(u) &= 1 - (1 - u^{c_6})^{c_7} \end{aligned} \tag{4}$$

In order to simplify the model selection procedure, we computed the structure and location parameters from point statistics, and optimised shape parameters through a simplified least-squares orthogonal distance-fitting procedure. The orthogonal distance was computed only for a limited set of shape parameter combinations as given in **Table 2**, and then the least orthogonal distance model was selected as the best fit model. For visualisation purposes, the tree trunk was modelled as a cylinder of radius $0.1r$ and height b (**Figure 11**).

Model name	c_1	c_2	c_3*	c_4	c_5	c_6	c_7
Ellipsoid	1	1	2	2	2	2	2.4
Cylinder	2	0	1	0	2	1	1
Paraboloid	0	0	1	1	2	1	2
Hyperboloid	−1	i	−0.4142i	2	2	0.95	1.95
Cone	0	0	−i	2	2	1	1
Zparaboloid	0	0	−i	2	1	1	0.5

Table 2. Parameter combinations used for the crown shape model Eq. (4).

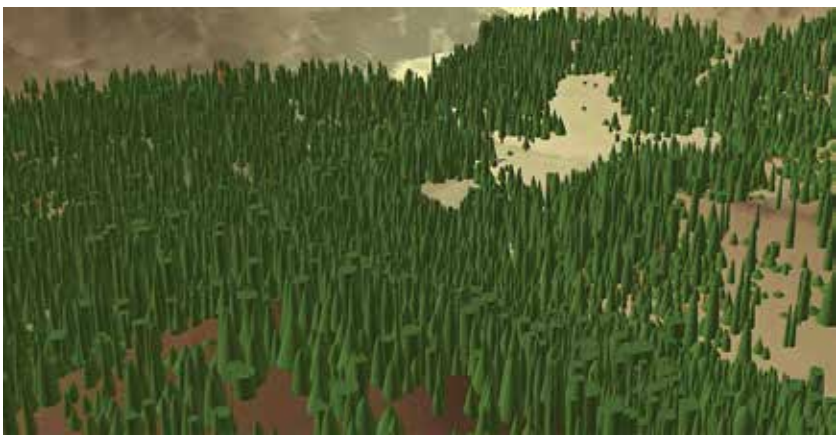

Figure 11. 3D visualisation of modelled forest from ALS data in the Mexico City Conservation Land.

The assessment of this product with ground truth data has shown the potential of ALS [93], especially for species communities exhibiting sparse distribution (such as *Pinus hartwegii* sp.), since limitations due to occlusion problems along dense species communities (such as *Abies religiosa* sp.) have also been reported suggesting the need to incorporate complementary TLS acquisitions. In any case, the utility of these techniques for large-scale inventorying is yet to be seen.

4. Concluding remarks

Geographic data collection has experienced a paradigm shift in terms of users being not only consumers but also generators. Traditionally, government agencies were in charge of collecting relevant information for different uses: cadastral, population and business censuses, vehicle registrars, natural resources, etc. However, it has become increasingly popular to be able to generate geographical data that do not necessarily adhere to governmental standards. Furthermore, it has become trending not only to collect but also to share these data in what

constitutes one of the pillars of neogeography: 'sharing location information with friends and visitors, help shape context, and conveying understanding through knowledge of place' [95], especially with all the mapping technologies available on the web [96].

This qualitative shift in the quantity and diversity of data that are gathered and examined has come with a shift in the techniques and technologies used to process and analyse information. In a seminal paper, Breiman talked about two cultures in data analysis: the 'classical' one, where data are modelled around a theoretical statistical distribution which, implicitly, assumes the kinds of processes producing the observations, and inferences are drawn from the distribution properties; and the 'algorithmic' one, where the focus is on extracting meaningful patterns and insights through the use of algorithmic models, without any assumptions about the mechanisms producing the observations [97]. This latter culture, stemming from the more empirical or applied fields, such as market research, electoral polling or computational biology, has gained momentum as the data we gather and analyse come, more often than not, from sources we cannot control (in a statistical sense), such as news outlets or social media feeds.

Author details

Jose Luis Silván-Cárdenas*, Rodrigo Tapia-McClung, Camilo Caudillo-Cos,
Pablo López-Ramírez, Oscar Sanchez-Sórdia and Daniela Moctezuma-Ochoa

*Address all correspondence to: jlsilvan@centrogeo.org.mx

Geography and Geomatics Research Centre – CentroGeo, Mexico City, Mexico

References

[1] Paradis, M. De l'arpentage à la géomatique (From surveying to geomatics). Can Surveyor. 1981;35(3):262–268.

[2] Kemp, K. Encyclopedia of Geographic Information Science. Sage; LA, USA 2008.

[3] Lillesand, TM, Kiefer, RW, Chipman, JW. Remote Sensing and Image Interpretation. 6th ed. USA: John Wiley & Sons, Inc.; NJ, USA 2008. 756p.

[4] McCaffrey, KJW, Jones, RR, Holdsworth, RE, Wilson, RW, Clegg, P, Imber, J, Holliman, N, Trinks, I. Unlocking the spatial dimension: digital technologies and the future of geoscience fieldwork. J Geol Soc. 2005;162(6):927–938.

[5] University College London. GeoKey [Internet]. 2015 [Updated: Nov 9 2015]. Available from: http://geokey.org.uk/. [Accessed: Jan 15 2016].

[6] Atzmanstorfer K, Resl R, Eitzinger A, Izurieta X. The GeoCitizen-approach: community-based spatial planning – an Ecuadorian case study. Cartogr Geogr Inf Sci. 2014;41(3): 1–12.

[7] Usahidi. Usahidi [Internet]. 2015 [Updated: Sep 15 2015]. Available from: https://www.ushahidi.com/

[8] Zook M, Graham M, Shelton T, Gorman S. Volunteered geographic information and crowdsourcing disaster relief: a case study of the Haitian earthquake. World Med Health Policy. 2010;2(2):6–32.

[9] OpenTreeMap. OpenTreeMap [Internet]. 2015. Available from: https://www.opentreemap.org/. [Accessed: Nov 9 2015]

[10] California Academy of Sciences. iNaturalist [Internet]. 2015. Available from: http://www.inaturalist.org/. [Accessed: Nov 9 2015]

[11] Waze. Waze Live Map [Internet]. 2015. Available from: https://www.waze.com/livemap. [Accessed: Sep 9 2015]

[12] Sony Computer Science Laboratory Paris. Software Languages Lab VUB. NoiseTube [Internet]. 2015. Available from: http://www.noisetube.net/. [Accessed: Feb 17 2015]

[13] Crooks A, Pfoser D, Jenkins A, Croitoru A, Stefanidis A, Smith D, et al. Crowdsourcing urban form and function. Int J Geogr Inf Sci. 2015;29(5):720–741.

[14] Sui D, Goodchild M, Elwood S. Volunteered geographic information, the exaflood, and the growing digital divide. In: MF Goodchild, editor. Crowdsourcing Geographic Knowledge: Volunteered Geographic Information (VGI) in Theory and Practice. Netherlands: Springer Science & Business Media; Netherlands 2013. pp. 1–12.

[15] Harvey F. To volunteer or to contribute locational information? Towards truth in labeling for crowdsourced geographic information. In: MF Goodchild, editor. Crowdsourcing Geographic Knowledge: Volunteered Geographic Information (VGI) in Theory and Practice. Springer Netherlands; Netherlands 2013. pp. 31–42.

[16] Surowiecki J. The Wisdom of Crowds: Why the Many are Smarter Than the Few and How Collective Wisdom Shapes Business Economies Societies and Nations. New York: Doubleday; 2004. 296p.

[17] Spielman SE. Spatial collective intelligence? credibility, accuracy, and volunteered geographic information. Cartogr Geogr Inf Sci. Taylor & Francis; 2014;41(2):115–124.

[18] OpenSignal. Mexico's cell phone coverage [Internet]. 2015 [cited 2016 Feb 4]. Available from: http://opensignal.com/?lat=23.2897&lng=-101.8675&initZoom=6&isHeatMap=1

[19] Ball, GH, Hall, DJ, Stanford Research Institute, United States, Office of Naval Research, Information Sciences Branch. Isodata, a novel method of data analysis and pattern classification. Stanford Research Institute, Menlo Park, Calif, 1965.

[20] Duque, JC, Ramos, R, Suriñach, J. Supervised regionalization methods: a survey. Int Reg Sci Rev. 2007; 30:195–220. doi:10.1177/0160017607301605

[21] Kulldorff, M. Prospective time periodic geographical disease surveillance using a scan statistic. J R Stat Soc Ser A Stat Soc. 2001; 164:61–72. doi:10.1111/1467-985X.00186

[22] Chen, Y-K, Wang, J-F. Segmentation of single- or multiple-touching handwritten numeral string using background and foreground analysis. IEEE Trans Pattern Anal Mach Intell. 2000; 22:1304–1317. doi:10.1109/34.888715

[23] Chuang, K-S, Tzeng, H-L, Chen, S, Wu, J, Chen, T-J. Fuzzy c-means clustering with spatial information for image segmentation. Comput Med Imaging Graph. 2006;30:9–15. doi:10.1016/j.compmedimag.2005.10.001

[24] Ng, HP, Ong, SH, Foong, KWC, Goh, PS, Nowinski, WL. Medical image segmentation using K-means clustering and improved watershed algorithm. In: 2006 IEEE Southwest Symposium on Image Analysis and Interpretation. Presented at the 2006 IEEE Southwest Symposium on Image Analysis and Interpretation; 2006. pp. 61–65. doi: 10.1109/SSIAI.2006.1633722

[25] Wang, S, Anselin, L, Bhaduri, B, Crosby, C, Goodchild, MF, Liu, Y, Nyerges, TL. CyberGIS software: a synthetic review and integration roadmap. Int J Geogr Inf Sci. 2013;27:2122–2145. doi:10.1080/13658816.2013.776049

[26] Huang, R, Yang, Q, Pei, J, Gama, J, Meng, X, Li, X (Eds.). Advanced Data Mining and Applications, Lecture Notes in Computer Science. Berlin, Heidelberg: Springer Berlin Heidelberg; 2009.

[27] Miller, HJ, Han, J (Eds.). Geographic Data Mining and Knowledge Discovery, 2nd ed. Boca Raton, FL: CRC Press; 2009.

[28] Frias-Martinez, V, Frias-Martinez, E. Spectral clustering for sensing urban land use using Twitter activity. Eng Appl Artif Intell. 2014;35:237–245. doi: 10.1016/j.engappai.2014.06.019

[29] Lee, R, Wakamiya, S, Sumiya, K. Discovery of unusual regional social activities using geo-tagged microblogs. World Wide Web. 2011;14:321–349. doi: 10.1007/s11280-011-0120-x

[30] Gabrielli, L, Rinzivillo, S, Ronzano, F, Villatoro, D. From tweets to semantic trajectories: mining anomalous urban mobility patterns. In: J Nin, D Villatoro, editors. Citizen in Sensor Networks, Lecture Notes in Computer Science. Springer International Publishing; Switzerland 2014. pp. 26–35.

[31] Boettcher, A, Lee, D. EventRadar: a real-time local event detection scheme using twitter stream. IEEE. 2012;358–367. doi:10.1109/GreenCom.2012.59

[32] Kim, T, Huerta-Canepa, G, Park, J, Hyun, SJ, Lee, D. What's happening: finding spontaneous user clusters nearby using twitter. In: 2011 IEEE Third International Conference on Privacy, Security, Risk and Trust (PASSAT) and 2011 IEEE Third

International Conference on Social Computing (SocialCom). Presented at the 2011 IEEE Third International Conference on Privacy, Security, Risk and Trust (PASSAT) and 2011 IEEE Third International Conference on Social Computing (SocialCom); 2011. pp. 806–809. doi: 10.1109/PASSAT/SocialCom.2011.135

[33] Kim, T., Huerta-Canepa, G., Park, J., Hyun, S.J., Lee, D., 2011. What's Happening: Finding Spontaneous User Clusters Nearby Using Twitter, in: 2011 IEEE Third International Conference on Privacy, Security, Risk and Trust (PASSAT) and 2011 IEEE Third Inernational Conference on Social Computing (SocialCom). Presented at the 2011 IEEE Third International Conference on Privacy, Security, Risk and Trust (PASSAT) and 2011 IEEE Third Inernational Conference on Social Computing (SocialCom), IEEE, Boston, MA, pp. 806–809. doi:10.1109/PASSAT/SocialCom.2011.135

[34] Padmanabhan, A, Wang, S, Cao, G, Hwang, M, Zhang, Z, Gao, Y, Soltani, K, Liu, Y. FluMapper: a cyberGIS application for interactive analysis of massive location-based social media. Concurr Comput Pract Exp. 2014;26:2253–2265. doi:10.1002/cpe.3287

[35] Wang, S, Hu, H, Lin, T, Liu, Y, Padmanabhan, A, Soltani, K. CyberGIS for data-intensive knowledge discovery. SIGSPATIAL Spec. 2015;6:26–33.

[36] Wang, Y, Weinacker, H, Koch, B. A lidar point cloud based procedure for vertical canopy structure analysis and 3D single tree modeling in forest. Sensors. 2008;8. 3938-3951

[37] Li, L., Xi, Y., 2011. Research on Clustering Algorithm and Its Parallelization Strategy, in: 2011 International Conference on Computational and Information Sciences (ICCIS). Presented at the 2011 International Conference on Computational and Information Sciences (ICCIS), IEEE, Chengdu, China, pp. 325–328. doi:10.1109/ICCIS.2011.223

[38] Marozzo, F, Talia, D, Trunfio, P. P2P-MapReduce: parallel data processing in dynamic cloud environments.., J Comput Syst Sci. JCSS Special Issue: Cloud Computing. 2012;78:1382–1402. doi: 10.1016/j.jcss.2011.12.021

[39] Nystuen, JD, Dacey, MF. A graph theory interpretation of nodal regions. Pap Reg Sci. 2005;7(1):29–42.

[40] Graizbord, B. Geografía del transporte en el area metropolitana de la Ciudad de México. Mexico, AC: El Colegio de; 2008. 386p.

[41] Súarez-Lastra, M, Delgado-Campos, J. Urban structure and efficiency. Job accessibility, residential location and income to Mexico City's metropolitan area. Econ Soc y Territ. 33 2007;6(23):693–724.

[42] Bender-deMoll, S. Potential human rights uses of network analysis and mapping. A report to the Science and Human Rights Program of the American Association for the Advancement of Science. 2008. Available at http://skyeome.net/wordpress/wp-content/uploads/2008/05/Net_Mapping_Report.pdf Accessed Feb 12 2016.

[43] Fortunato, S. Community detection in graphs. Phys Rep 2008;486(3–5):75–174.

[44] Blondel, VD, Guillaume, J-L, Lambiotte, R, Lefebvre, E. Fast unfolding of communities in large networks. J Stat Mech Theory Exp. 2008;2008(10):P10008.

[45] MacEachren, AM, Gahegan, M, Pike, W, Brewer, I, Cai, G, Lengerich, E, et al. Geovisualisation for knowledge construction and decision support. IEEE Comput Graph Appl. 2004;24(1):13–17.

[46] Andrienko, G, Andrienko, N, Jankowski, P, Keim, D, Kraak, M-J, MacEachren, A, et al. Geovisual analytics for spatial decision support: Setting the research agenda. Int J Geogr Inf Sci. 2007;21(8):839–857.

[47] Smith, S, Bruce, C. CrimeStat III. Workbook. Washington, D.C.: National Institute of Justice; Washington, DC, USA 2008. 113p.

[48] Knox, EG, Bartlett, MS. The detection of space-time interactions. J R Stat Soc Ser C (Appl Stat). 1964;13(1):25–30.

[49] Jacquez, GM, Greiling, DA, Durbeck, H, Estberg, L, Do, E, Long, A, Rommel B. ClusterSeer User Guide 2: Software for identifying disease clusters. Ann Arbor, MI: TerraSeer Press 2002.

[50] Pettit, C, Widjaja, I, Russo, P, Sinnott, R, Stimson, R, Tomko, M. Visualisation support for exploring urban space and place. ISPRS Ann Photogramm Remote Sens Spat Inf Sci 2012;I–2(1):153–158.

[51] Google. Google Geo Developers Blog [Internet]. 2012 [cited 2016 Feb 15]. Available from: http://googlegeodevelopers.blogspot.mx/2012/06/powerful-data-visualisation-with.html

[52] Xiao, N, Chun, Y. Visualizing migration flows using kriskograms. Cartogr Geogr Inf Sci. 2009;36(2):183–191.

[53] Boyandin, I, Bertini, E, Bak, P, Lalanne, D. Flowstrates: an approach for visual exploration of temporal origin-destination data. Comput Graph Forum. 2011;30(3):971–980.

[54] Tobler, W. Experiments in migration mapping by computer. Am Cartogr. 1987;14(2): 155–163.

[55] ESRI. ArcGIS 3D Analyst [Internet]. 2011 [Updated: 2016]. Available from: http://www.esri.com/software/arcgis/extensions/3danalyst/. [Accessed: 12/03/2016]

[56] ESRI. Esri CityEngine [Internet]. 2011 [Updated: 2016]. Available from: http://www.esri.com/software/cityengine. [Accessed: 12/03/2016]

[57] Morsdorf, F, Meier, E, Kötz, B, Itten, KI, Dobbertin, M, Allgöwer, B. LIDAR-based geometric reconstruction of boreal type forest stands at single tree level for forest and wildland fire management. Remote Sens Environ. 2004;92:353–362.

[58] Kato, A, Moskal, LM, Schiess, P, Swanson, ME, Calhoun, D, Stuetzle, W. Capturing tree crown formation through implicit surface reconstruction using airborne lidar data. Remote Sens Environ. 2009;113:1148–1162.

[59] Rutzinger, M, Pratihast, AK, Oude Elberink, S, Vosselman, G. Detection and modelling of 3D trees from mobile laser scanning data. Int Arch Photogramm Remote Sens Spat Inf Sci. 2010;38:520–525.

[60] Sampath, A, Shan, J. Segmentation and reconstruction of polyhedral building roofs from aerial lidar point clouds. IEEE Trans Geosci Remote Sens. 2010;48(3):1554–1567.

[61] Faugeras, O, Robert, L, Laveau, S, Csurka, G, Zeller, C, Gauclin, C, Zoghlami, I. 3-d reconstruction of urban scenes from image sequences. Comput Vis Image Understand. 1998;69(3):292–309.

[62] Verbree, E, Maren, GV, Germs, R, Jansen, F, Kraak, M-J. Interaction in virtual world views-linking 3D GIS with VR. Int J Geogr Inf Sci. 1999;13(4):385–396.

[63] Goodchild, M. Time, space, and GIS. Past Place: Newsl Hist Geogr Spec Group Assoc Am Geogr. 2006;14(2):8–9.

[64] Langran G, Chrisman NR. A framework for temporal geographic information. Cartogr Int J Geogr Inf Geovisualisation. 1988;25(3):1–14.

[65] Hagerstrand T. Innovation diffusion as a spatial process. Chicago, USA: Univerity of Chicago Press; 1968.

[66] Hagerstrand T. Diorama, path and project. Tijdschrift voor economische en sociale geografie. Swedish 1982;73(6):323–339.

[67] Peng, T, Zuo, W, He, F. SVM based adaptive learning method for text classification from positive and unlabeled documents. Knowl Inf Syst. 2008;16(3):281–301.

[68] Pang, B, Lee, L. Opinion mining and sentiment analysis. Found Trends Inf Retr. 2008;2(1–2):1–135.

[69] da Silva, NFF, Hruschka, ER, Hruschka, ER. Tweet sentiment analysis with classifier ensembles. Decis Supp Syst. 2014;66:170–179.

[70] Shahbaz, M, Guergachi, A. Sentiment miner: a prototype for sentiment analysis of unstructured data and text. In: 2014 IEEE 27th Canadian Conference on Electrical and Computer Engineering (CCECE); 2014; Canada. IEEE; pp. 1–7.

[71] Liu, SM, Chen, J-H. A multi-label classification based approach for sentiment classification. Expert Syst Appl. 2015;42(3):1083–1093.

[72] Padró, L, Stanilovsky, E. Freeling 3.0: towards wider multilinguality. In: Nicoletta C. et al., editors. Eighth International Conference on Language Resources and Evaluation; Istanbul, Turkey; 2012.

[73] Martínez-Cámara, E, Martín-Valdivia, MT, Urena-López, LA, Montejo-Ráez, AR. Sentiment analysis in twitter. Nat Lang Eng. 2014;20(1):1–28.

[74] Hoffman, M, Bach, FR, Blei, DM. Online learning for latent Dirichlet allocation. In: Lafferty JD, Williams CKI, Shawe-Taylor J, Zemel RS, Culotta A, editors. Advances in Neural Information Processing Systems; Curran Associates, Inc.; NY, USA 2010. pp. 856–864.

[75] Askar, D, House, T. Complex patterns of multiscale human mobility in United Kingdom methodology data. Warwick, UK; 2010. Accessed February 12 2015. Available at https://www2.warwick.ac.uk/fac/cross_fac/complexity/study/emmcs/outcomes/studentprojects/askar_m2.pdf

[76] Maier, G, Vyborny, M. Internal migration between US States – a social network analysis. European Regional Science Association; Vienna, Austria 2005.

[77] Tranos, E, Gheasi, M, Nijkamp, P. International migration: a global complex network. Environ Plan B Plan Des. 2015;42(1):4–22.

[78] Fagiolo, G, Mastrorillo, M. International migration network: topology and modeling. Phys Rev E Stat Nonlin Soft Matter Phys. 2013; 88(1):012812.

[79] Porat, I, Benguigui, L. World migration degree. Global migration flows in directed networks. 2015. Available from http://arxiv.org/abs/1511.05338. Accessed February 8 2016.

[80] CONAPO (Consejo Nacional de Población), INEGI (Instituto Nacional de Estadística y Geografía). Delimitation of Mexico's metropolitan areas 2010. Mexico, 2013.

[81] INEGI (Instituto Nacional de Estadílstica y Geografía). Censo de Población y Vivienda 2010: Interactive data query [Internet]. 2011 [cited 2015 Feb 1]. Available from: http://www.inegi.org.mx/lib/olap/consulta/general_ver4/MDXQueryDatos.asp?#Regreso&c=27770

[82] Tableau Foudation. Tableau [Internet]. 2003 [Updated: 2016]. Available from: http://www.tableau.com/. [Accessed: Nov 2015]

[83] Zelinsky, W. The hypothesis of the mobility transition. Geogr Rev. 1971;61(2):219–249.

[84] Abel, JR, Deitz, R. Do colleges and universities increase their region's human capital? J Econ Geogr. 2012;12(August 2011):667–691.

[85] jQuery Foundation. jQuery [Internet]. 2016 [Updated: 2016]. Available from: https://jquery.com/. [Accessed: Jan 2016]

[86] Vladimir Agafonkin. Leaflet [Internet]. 2015 [Updated: 2016]. Available from: http://leafletjs.com/. [Accessed: Feb 2016]

[87] PosgreSQL. PosgreSQL [Internet]. 2009 [Updated: 2013]. Available from: http://www.postgresql.org.es/. [Accessed: Jan 2016]

[88] OSGeo. PostGIS [Internet]. 2016 [Updated: 2016]. Available from: http://postgis.net/. [Accessed: Feb 2016]

[89] @mdo and @fat. BootStrap [Internet]. 2015 [Updated: 2016]. Available from: http://getbootstrap.com. [Accessed: Jan 2015]

[90] The PHP Group. PHP [Internet]. 2001 [Updated: 2016]. Available from: http://php.net. [Accessed: Jan 2016]

[91] Martínez-Viveros, E, Chapela, J, Morales-Gamas, A, Caudillo-Cos, C, Tapia-McClung, R, Ledesma, M, et al. Construction of a web-based crime geointelligence platform for Mexico city's public safety. In: Leitner M, editor. Crime Modeling and Mapping Using Geospatial Technologies SE-18. Springer Netherlands; Netherlands 2013. pp. 415–439.

[92] Aguilar, GA, Ward, MP. Globalization, regional development, and mega-city expansion in Latin America: analyzing Mexico City´s peri-urban hinterland. Cities. 2003;20(1):3–21.

[93] Silván-Cárdenas, JL. A segmentation method for tree crown detection and modelling from LiDAR measurements. Pattern Recognition. LNCS. 2012;7329:65–74.

[94] Silván-Cárdenas, JL, Corona-Romero, N, Galeana-Pizaña, JM, Nuñez-Hernández, JM, Madrigal Gómez, JM. Geospatial technologies to support coniferous forests research and conservation efforts in Mexico. In: Weber RP, editor. Old-Growth Forests and Coniferous Forests: Ecology, Habitat and Conservation. New York: Nova Science Publishers; pp. 67–123.

[95] Turner, A. Introduction to neogeography. O'Reilly Media, Inc.; CA, USA 2006. 54p.

[96] Haklay, M, Singleton, A, Parker, C. Web mapping 2.0: the neogeography of the GeoWeb. Geogr Compass. 2008;2(6):2011–2039.

[97] Breiman, L. Statistical modeling: the two cultures. Stat Sci. 2001;16:199–215.

Chapter 2

Effect of Sampling Density on Estimation of Regional Soil Organic Carbon Stock for Rural Soils in Taiwan

Chun-Chih Tsui, Xiao-Nan Liu, Horng-Yuh Guo and Zueng-Sang Chen

Additional information is available at the end of the chapter

http://dx.doi.org/10.5772/64210

Abstract

Accurately quantifying soil organic carbon (SOC) stocks in soils is considered necessary and important for studying the soil quality and productivity, modeling the global carbon cycle, and assessing the global climate change. The objectives of this chapter are (1) to evaluate the effects of sampling density and interpolation methods on spatial distribution of SOC density (SOCD) and (2) to estimate the SOC stocks in 0–30, 0–50, and 0–100 cm layer of Tainan rural soils (2192 km^2), Taiwan. Ordinary kriging (OK), empirical Bayesian kriging (EBK), and inverse distance weighting (IDW) methods and four sampling densities (n = 7388, 1168, 370, or 77) were used for spatial interpolation. The results indicated that different sampling densities had significant effects on predicting the spatial patterns of SOCD, but no significant difference was found among three interpolation methods. Spatial pattern of SOCD obtained from the highest sampling density appeared to be the most detailed distribution, and the prediction accuracy showed a reducing trend with decreasing sampling density. At least 1 sample per 2 km × 2 km area was suggested. The estimates of SOC stocks in different layers of Tainan soils ranged from 8.03 to 8.08 million tons in 0–30 cm, 11.92 to 12.04 million tons in 0–50 cm, and 20.38 to 20.65 million tons in 0–100 cm.

Keywords: soil organic carbon (SOC) stock, soil organic carbon density (SOCD), sampling density, interpolation method, agricultural land

1. Introduction

Soil organic carbon (SOC) is one of the largest carbon reservoirs of the earth's surface and plays an important role in the global carbon cycle [1, 2]. As the Kyoto Protocol was adopted

in the annual Conference of Parties (COPs) of the UNFCCC in 1997, soil organic carbon and its potential to become a managed sink for atmospheric CO_2 have received much attention. Accurately quantifying soil organic carbon (SOC) stocks in soils is considered necessary for studying the soil quality, modeling the global carbon cycle, and assessing the global climate change. In recent years, many countries and local government have attempted to assess the C stock in their regions, including the soil organic carbon density (SOCD) and storage at global level [3–5], especially in some European countries, the United States of America, Indonesia [6], South Korea, New Zealand [7], and Australia [8].

In Taiwan, accurate estimation of SOC stocks based on detailed soil investigation is still absent at the national scale or regional scale. There have been several soil survey projects on agricultural soils for various purposes by Taiwan Agricultural Research Institute (TARI), Council of Agriculture, Taiwan. By calculating the SOC content of soil pedons and the distribution area of different soil orders, Chen and Hseu [9] first attempted to estimate the SOC stocks in rural lands of Taiwan. They indicated that 81 Tg (million tons) and 162 Tg of SOC were stored in the 0–30 and 0–100 cm of agricultural soils within an area of 1.68 million ha. Chen et al. [10] reported that SOC stocks in the 0–20 cm soil layer of cultivated lands (~0.85 million ha) were 21.7 and 27.5 Tg, which were calculated based on two legacy database obtained from detail soil surveys conducted by TARI in 1960s and 1980s, respectively. Taking the cultivated lands into account, the estimates of SOC stocks in the upper 20 cm soils of both studies mentioned earlier were similar (27.5 and 27.3 Tg), indicating that legacy soil survey data are our best resource to monitor the dynamics of soil C [6].

SOC stocks have strong spatial heterogeneity and dependence. Geostatistics have proven to be a useful tool in predicting the spatial distribution of soil properties that are very spatially dependent. Several spatial interpolation methods have been used to explore the spatial distribution characteristics of SOC. For example, ordinary kriging (OK) interpolation estimation, which provides the best linear unbiased prediction at unsampled locations, has been widely used to describe the structure of spatial dependence and quantify SOC stocks in relatively large areas [11]. At present, there are dozens of spatial interpolation methods described in the literature; however, many factors such as sample size and the nature of the data are possible to affect the estimation of a spatial interpolator, and until now, there are no consistent findings regarding what is the best interpolation method. Many studies had focused on comparing different estimation methods to reduce uncertainty of regional SOC prediction. However, studies assessing the effect of sampling density on spatial variability of SOC estimation were relatively few [12], and issues of sampling density and interpolation method are both important to our understanding of SOC variability [13].

Chien et al. [14] and Liu et al. [15] have compared the performance of some spatial interpolation methods at regional scale in Taiwan; however, estimating the SOC stocks of the whole city by different interpolation methods has never been previously studied in Taiwan. The objectives of this chapter are (1) to estimate the soil organic carbon density (SOCD) and SOC stocks in 0–30, 0–50, and 0–100 cm soils and its spatial distribution at four sampling densities at regional scale, (2) to evaluate the effects of sampling density on estimation of SOCD and SOC stocks, and (3) to compare the difference of SOC stocks among three geostatistical

http://dx.doi.org/10.5772/64210

techniques. The estimation will be an important reference for predicting the SOC stock in the humid subtropical region.

2. Materials and methods

2.1. Basic environmental and soil conditions of Tainan city

Tainan city is located in the southwest of Taiwan with a total area of 2192 km^2. The mean air temperature is 28.7°C in summer and 18.4°C in winter. The mean annual rainfall is 1698 mm. Except for the raining season beginning from May to September, especially the monthly rainfall is less than the evaporation and transpiration during the summer (June to August). The soil temperature regime of the study area is hyperthermic (>22°C), and soil moisture regime of most area is ustic (drying in summer from June to August). About one-third of area is occupied by hill land (30–50 m asl) in the eastern part of Tainan city, and the other two-thirds of area is calcareous alluvial plain. About 57 and 34% of the soils of Tainan city are Entisols and Inceptisols based on USDA soil classification, respectively. The most soils are sandy loam to silt loam soil texture, neutral to basic reaction, and well-drained soils. Both geographical features and soil conditions favor the growth of most vegetables, fruits, and rice production; thus, Tainan city is an important agricultural production area in Taiwan in the last five decades. Soils in the coastal alluvial area are saline soils and are used for fish farming.

2.2. Soil database of soil pedons

Dataset for estimating the SOC stock in agricultural soils of Tainan was obtained from a detailed soil survey project, which was conducted from 1992 to 2010 by TARI. Soil pedons were sampled by auger along a 250 m × 250 m cell-sized grid in the field, meaning that every 6.25 ha of the arable land has a representative soil pedon. The upper 150 cm soils were collected by dividing into six depth intervals, and soil organic matter (SOM), pH, CEC, P, K, Ca, and Mg extracted by Mehlich-III extractant were analyzed for each soil sample by TARI. Here, we converted the content of SOM to SOC by dividing a Van Bemmelen factor of 1.724 on the assumption that SOM contains 58% of organic C averagely. From these data, SOC stocks were computed for 0–30, 0–50, and 0–100 cm soil layers. The soil organic carbon density (SOCD, kg m^{-2}) for a certain soil depth (h) was calculated as follows:

$$\mathrm{SOCD}_h = \sum_{i=1}^{\mathrm{n}} \left(\mathrm{SOC}_i \times \mathrm{Bd}_i \times \mathrm{d}_i \right) \div 100$$

where SOC_i (g kg^{-1}) is the soil organic carbon content of a certain layer, Bd_i is the bulk density (g cm^{-3}), and d_i is the depth (cm). As Bd determination was not included in TARI's soil dataset, we adopted the following pedotransfer function for estimating the bulk density [16] to evaluate the SOC stock:

$$\mathrm{Bd} = 1.3026 + 0.169\log(\mathrm{d}) - 0.256\left[\ln(\mathrm{SOC})\right]^2$$

After removing the outliers and missing data, the extracted database contains the information of 7388 soil pedons.

2.3. Soil sampling design

The initial soil sampling scheme was based on a regular grid with cell sizes of 250 m × 250 m across the whole cultivated land of Tainan city. In this study, all samples were used in four subsequent estimations of SOC stocks based on regular grids of 250 m × 250 m (n = 7388), 1 km × 1 km (n = 1168), 2 km × 2 km (n = 370), and 5 km × 5 km (n = 77), respectively. One point (soil pedon) was selected near each center of the four sampling grids, and the SOCD of selected point was taken for the observed SOCD of its corresponding grid. The patterns of four scales of sampling density are shown in **Figure 1**. Seventy percent of the points were randomly

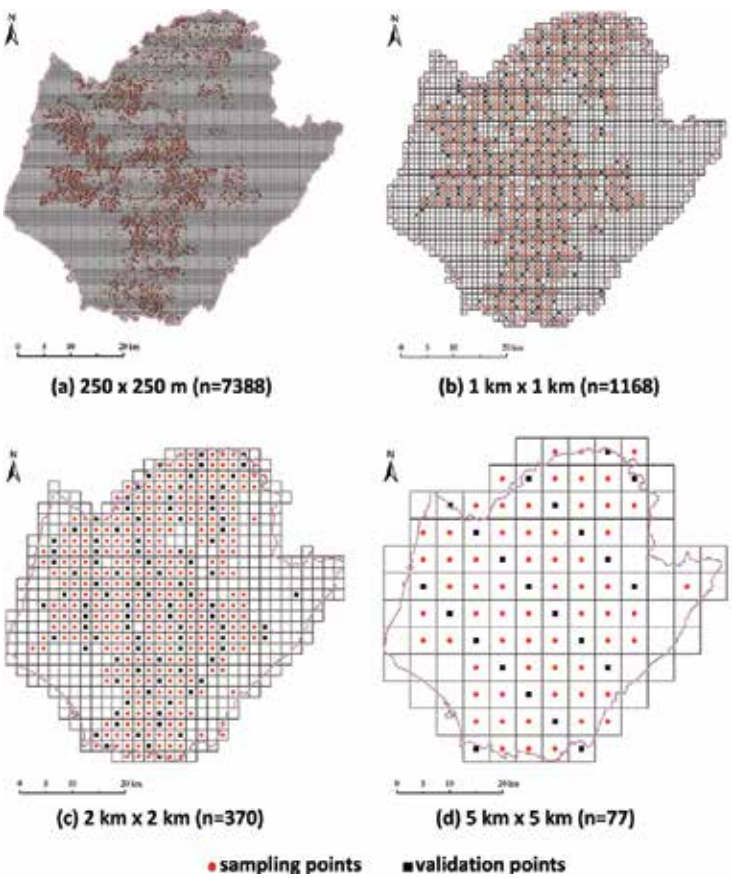

Figure 1. Grid-based sampling design patterns for soil organic carbon density (SOCD) at four sampling scales in Tainan, Taiwan.

http://dx.doi.org/10.5772/64210

selected as test data for spatial interpolation, and the rest (30%) were used for validation. The grid numbers, total sample numbers, sample number for spatial interpolation, and sample number for validation under different sampling densities are listed in **Table 1**.

Sampling density	Grid size of sampling	Grid numbers	Total sample points	Points for test (70%)	Points for validation (30%)
1 per 6.25 ha	250 m × 250 m	36,715	7388	5553	1836
1 per 1 km^2	1 km × 1 km	2407	1168	875	293
1 per 4 km^2	2 km × 2 km	633	370	279	92
1 per 25 km^2	5 km × 5 km	114	77	58	19

Table 1. Description of the test set and validation set by using different sampling densities.

2.4. Comparison of three spatial interpolation methods (IDW, OK, and EBK)

All interpolation methods have been developed based on the theory that points closer to each other have more correlations and similarities than those farther. In this study, the spatial interpolation was conducted using three different interpolation methods, which are available in the ArcGIS 10.1, to compare their estimation of SOC stocks of Tainan city soils under different sampling densities: (1) the inverse distance weighting (IDW), (2) ordinary kriging (OK), and (3) empirical Bayesian kriging (EBK). The former two methods (IDW and OK) are commonly used to spatially interpolate soil properties, while the third one (EBK) is a new probabilistic data interpolation method that is included in ArcGIS 10.1 Geostatistical Analyst.

2.4.1. Inverse distance weighting (IDW)

Inverse distance weighting (IDW) method is assumed that the rate of correlations and similarities between neighbors is proportional to the distance between them that can be defined as a distance reverse function of every point from neighboring points. The interpolating function is listed as follows:

$$Z(x) = \frac{\sum_{i=1}^{n} w_i z_i}{\sum_{i=1}^{n} w_i}$$

$$w_i = d_i^{-u}$$

where $Z(x)$ is the predicted value at an interpolated point, Z_i is the amount at a known point, n is the total number of known points used in interpolation, d_i is the distance between point i and the prediction point, and w_i is the weight assigned to point i. Higher weighting values are assigned to those points, which are closer to the interpolated points. As the distance increases,

the weight decreases, and u is the weighting power that imposes the amount of weight decreases with respect to the increase in distance [17, 18].

2.4.2. Ordinary kriging (OK)

Ordinary kriging (OK) is the most common type of kriging in practice. Kriging is a linear estimator that the estimate of the unknown value is a linear combination of the known data values [18]. The aim of kriging is to estimate the value of a random function, z, at one or more unsampled points or over larger blocks, from more or less sparse sample data on a given support, say $z(x_1)$, $z(x_2)$, … $z(x_n)$, at x_1, x_2, … x_n. This can be shown as follows:

$$z^*\left(x_0\right) = \sum_{i=1}^{n} w_i Z\left(x_j\right)$$

where w_j is the weight assigned to the known value of $z(x_j)$, and $z^*(x_0)$ is the estimated value. To ensure that the estimate is unbiased, weights are made to sum to 1 [17, 18].

2.4.3. Empirical Bayesian kriging (EBK)

Empirical Bayesian kriging (EBK) is a geostatistical interpolation method that automates the most difficult aspects of building a valid kriging model. Other kriging methods in Geostatistical Analyst are required to manually adjust parameters to receive accurate results, but EBK automatically calculates these parameters through a process of subsetting and simulation, which is implemented by estimating a lot of semivariogram models instead of a single semivariogram. The prediction in unknown locations in common kriging methods is done through calculation of semivariogram with respect to the known data locations, resulting in the underestimation of the standard error of the prediction due to overlooking the uncertainty of semivariogram. On the contrary, EBK uses an intrinsic random function as the kriging model despite the other kriging methods. The other main difference of EBK with that of the other kriging model is that EBK does not assume a tendency toward an overall mean; thus, there is the same chance for large deviations to get larger or smaller [17].

The following steps are followed in EBK. (1) Using the available data, a semivariogram model is estimated. (2) Given this semivariogram, a new value is simulated at each of the input data location. (3) With respect to the simulated data, a new semivariogram model is estimated accordingly. The calculation of a weight for the latest semivariogram according to Bayes' rule is the next step in this field. The semivariogram estimated in Step 1 is used to simulate a new set of values at the input location during the repetition of Steps 2 and 3. A new semivariogram model and its weight are produced given the simulated data. During this step, the predictions and their respective standard errors are produced at the unsampled locations. This step finally creates a spectrum of semivariograms [17].

http://dx.doi.org/10.5772/64210

2.4.4. Calculation of the SOC stocks

After spatial interpolation, a SOCD surface was created to cover the entire area of Tainan city soils. This surface was exported as a raster layer with the defined resolution (250 m × 250 m, 1 km × 1 km, 2 km × 2 km, and 5 km × 5 km), in which every grid square was assigned both a SOCD value and an area value. The next step was to accumulate as follows:

$$\text{SOC stock}_h = \sum_{i=1}^{n} \text{SOCD}_{ih} \times \text{Area}_{\text{grid}}$$

where SOC stock_h is the total amount of soil organic carbon stock at depth h in Tainan soils, n is the total grid number of the raster, i is the ith grid square, SOCD_{ih} is the soil organic carbon density for the ith grid square calculated to depth h, and $\text{Area}_{\text{grid}}$ is the area of each grid square, set by the defined resolution. The performance of IDW, OK, and EBK in mapping the spatial distribution of SOCD was evaluated by using samples from the validation set (**Table 1**).

2.5. Evaluation of the accuracy of three interpolation methods

Mean error (ME), mean absolute error (MAE), mean relative error (MRE), and root mean square error (RMSE) were calculated as follows:

$$\text{ME} = \frac{1}{n}\sum_{i=1}^{n}\left(S_{oi} - S_{vi}\right)$$

$$\text{MAE} = \frac{1}{n}\sum_{i=1}^{n}\left|S_{oi} - S_{vi}\right|$$

$$\text{MRE} = \frac{1}{n}\sum_{i=1}^{n}\frac{\left|S_{oi} - S_{vi}\right|}{S_{oi}}$$

$$\text{RMSE} = \sqrt{\frac{1}{n}\sum_{i=1}^{n}\left(S_{oi-}S_{vi}\right)^2}$$

where S_{oi} is the estimated SOCD at location i, S_{vi} is the observed SOCD at location i, and n is the total number of sample observations. The MAE and RMSE provide a measure of interpolation precision with lower values indicating more precise methods, while the ME and MRE measure the bias. Smaller ME, MRE, and RMSE values indicate less error. The coefficient of determination R^2 of linear regression line between the predicted and the measured values was also used as a measure of performance for each method.

$$R^2 = 1 - \frac{\sum_{i=1}^{n}\left(S_{vi} - S_{oi}\right)^2}{\sum_{i=1}^{n}\left(S_{vi} - \overline{S_{vi}}\right)^2}$$

where $\overline{S_{vi}}$ is the mean of observed value.

3. Results and discussion

3.1. Accuracy of different interpolation methods

The ME, MAE, MRE, RMSE, and R^2 values of cross-validation obtained from EBK, OK, and IDW methods are listed in **Table 2**. The results showed the trend that ME, MAE, MRE, and RMSE increased while R^2 decreased with reducing sampling density for a certain depth as it was expected. At the highest sampling density (1 sample per 6.25 ha), IDW method performed best with the lowest MAE, MRE, and RMSE values in 0–30 cm layer, while EBK method performed best in 0–50 cm (R^2 = 0.663) and 0–100 cm (R^2 = 0.740) layers. At the density of 1 sample per 1 km^2, the best performance was obtained by IDW method in 0–30 cm layer and by OK method in the upper 50 and 100 cm soils. At the sampling scale of 1 sample per 4 km^2, EBK and IDW methods performed best in 0–30 and 0–50 cm layers, respectively. In 0–100 cm layer, ME, MAE, and MRE obtained from EBK were the smallest, and R^2 obtained from OK was the highest. At the scale of 1 sample per 25 km^2, the prediction accuracy was low based on the R^2 value. The validation result revealed that sampling density should be more than 1 sample per 4 km^2 at least in the study area.

Considering the SOC stored at different depths, the best performance for estimating SOCD in 0–30 cm layer was obtained by IDW method at the scale of 1 sample per 6.25 ha and per 1 km^2. In 0–50 and 0–100 cm layers, EBK and OK methods performed best at the highest sampling scale and the scale of 1 sample per 1 km^2, respectively. EBK method was hypothesized as the best interpolation method, but we found that OK and IDW interpolation methods performed nearly as well as EBK in this study, and all three interpolation methods performed approximately well. Additionally, when the sampling scales were 1 sample per 6.25 ha and per 1 km^2, the R^2 value increased with soil depth; in other words, the prediction accuracy of three interpolation methods was relatively poor for estimating the SOCD in 0–30 cm layer. It indicated that soil organic carbon is affected by other related factors, and the regulating processes are complicated and vary spatially, especially in the upper soil [19].

The effect of sampling density on prediction accuracies in our study was consistent with other researches. Zhang et al. [13] conducted a research of similar sampling schemes with ours (from 0.5 km × 0.5 km to 2 km × 2 km), and they found prediction accuracies of SOC content obtained from OK and LUK (kriging combined with land use information) increased with decreased grid size. Sun et al. [12] also reported that sampling density significantly affected the estimation of regional SOC concentration, but trends do not increase regularly with the sampling density, primarily due to the complicated factors on the spatial variation in SOC. In contrast, Chien et

al. [14] evaluated the sampling scale (approximately 1 sample per 7.7–20 ha) in a 10-km^2 area and indicated that sufficient spatial information about the soil properties could still be retained even when the original sampling densities were reduced to nearly half. The best sampling design depends on the reasonable costs and acceptable extent of estimation error, for example, Sun et al. [12] found that increasing 18% of prediction accuracy had to increase the sampling density for almost 15 times. In our case, at a depth of 100 cm layer, the increases in prediction accuracy (RMSE) were 16–37% as soil samples became six times, whereas the increases in accuracy were 28–46% as soil samples increased 20 times. Therefore, sampling density should be evaluated more comprehensively in the future work.

Soil layer	Sampling density	Interpolation method	ME	MAE	MRE	RMSE	R^2
0–30 cm	1 sample per 6.25 ha	EBK	0.021	0.689	0.239	0.882	0.446
		OK	0.012	0.705	0.243	0.897	0.426
		IDW	0.013	0.686	0.236	0.882	0.445
	1 sample per 1 km^2	EBK	0.072	0.827	0.306	1.091	0.293
		OK	0.075	0.816	0.300	1.082	0.297
		IDW	0.075	0.816	0.300	1.057	0.314
	1 sample per 4 km^2	EBK	−0.027	0.678	0.213	0.827	0.528
		OK	−0.057	0.728	0.224	0.893	0.411
		IDW	−0.054	0.840	0.262	1.031	0.215
	1 sample per 25 km^2	EBK	0.404	0.943	0.416	1.166	0.039
		OK	0.349	0.862	0.375	1.076	0.151
		IDW	0.453	0.908	0.397	1.126	0.130
0–50 cm	1 sample per 6.25 ha	EBK	0.009	0.795	0.219	1.127	0.663
		OK	−0.006	1.025	0.270	1.331	0.519
		IDW	−0.031	1.059	0.274	1.397	0.466
	1 sample per 1 km^2	EBK	−0.029	1.256	0.351	1.593	0.317
		OK	−0.023	1.214	0.336	1.537	0.338
		IDW	−0.024	1.212	0.340	1.566	0.321
	1 sample per 4 km^2	EBK	−0.083	1.627	0.373	1.943	0.181
		OK	−0.019	1.569	0.364	1.887	0.247
		IDW	−0.070	1.394	0.335	1.747	0.188
	1 sample per 25 km^2	EBK	0.061	1.522	0.524	1.893	0.013
		OK	−0.010	1.499	0.505	1.883	0.034
		IDW	0.119	1.452	0.503	1.858	0.044
0–100 cm	1 sample per 6.25 ha	EBK	0.013	1.370	0.293	1.973	0.740
		OK	−0.006	1.927	0.404	2.571	0.541
		IDW	−0.052	1.951	0.394	2.630	0.519

Soil layer	Sampling density	Interpolation method	ME	MAE	MRE	RMSE	R^2
	1 sample per 1 km^2	EBK	−0.068	2.403	0.539	3.126	0.304
		OK	−0.039	2.383	0.524	3.096	0.365
		IDW	−0.046	2.383	0.533	3.145	0.340
	1 sample per 4 km^2	EBK	0.082	2.904	0.521	3.638	0.273
		OK	0.242	2.907	0.534	3.601	0.309
		IDW	0.121	2.918	0.536	3.640	0.273
	1 sample per 25 km^2	EBK	0.123	3.200	1.014	4.001	0.002
		OK	0.066	3.289	1.011	4.061	0.005
		IDW	0.224	3.213	1.015	4.076	0.002

Table 2. Prediction accuracy of soil organic carbon distribution (SOCD) estimation for cultivated soils in Tainan at various sampling density.

3.2. Spatial distribution of SOCD from different interpolation methods and sampling designs

At a depth of 0–30 cm, the spatial pattern of SOCD that generated from OK method at different sampling densities has a similar distribution, but the spatial heterogeneity and resolution of the patterns varied among different sampling densities (**Figure 2**). The spatial pattern obtained from 7388 samples (grid size = 250 m × 250 m) appeared the most detailed SOCD spatial distribution. In general, high SOCD (>3.8 kg m^{-2}) was found from the north to the northwest region and in the east by south part, and lower SOCD (<2.6 kg m^{-2}) was found in the middle and southeast by south part of Tainan (**Figures 2a**, **3a**, and **4a**). The spatial variation and local differences became less evident with decreasing the sampling density, especially at the scale of 1 sample per 25 km^2 (5 km × 5 km grid size) (**Figure 2d**). A similar trend appeared in the spatial patterns of SOCD that generated from EBK and IDW methods among different sampling scales (**Figures 3d** and **4d**). As a whole, the spatial heterogeneity and resolution of the distribution patterns varied between IDW and two kriging methods. IDW is an exact interpolator that predicts a value which is identical to the measured value at a sample location [18]. Therefore, the local maxima and local minima are reserved in estimating the spatial distribution of SOCD. There were some minor differences in the spatial patterns between OK and EBK methods at the same sampling scale. The distribution area of the highest (>5.0 kg m^{-2}) and lowest (<2.6 kg m^{-2}) SOCD estimated by EBK method was smaller than those estimated by OK method, indicating that the EBK method has a higher degree of smoothing effect when sampling grid size was larger than 1 km × 1 km. At a depth of 0–50 (**Figure 5**) and 0–100 cm (**Figure 6**), the effects of interpolation method and sampling density on the SOCD distribution pattern were similar with those in 0–30 cm layer, so we only present those obtained from EBK methods here. In general, the effect of sampling density on the result of regional SOCD estimation is very obvious. The SOCD interpolation contours, which were compiled from three methods, described SOCD spatial variability with more accuracy and detail as the sampling density increases.

http://dx.doi.org/10.5772/64210

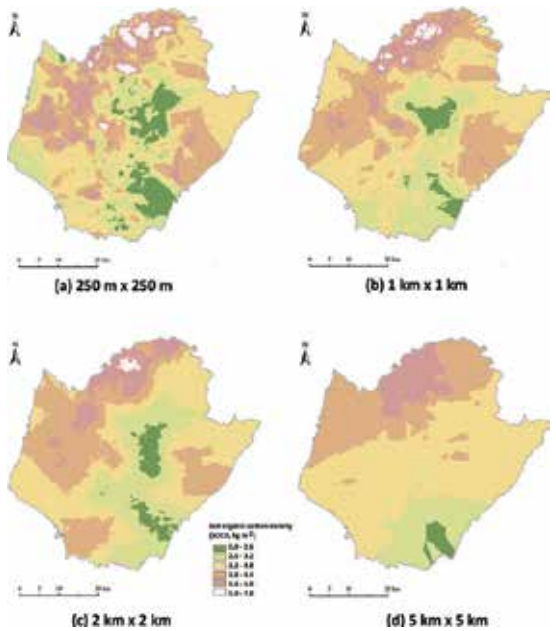

Figure 2. Distribution of soil organic carbon density (SOCD) interpolated by OK method in 0–30 cm soil layer at four sampling scales.

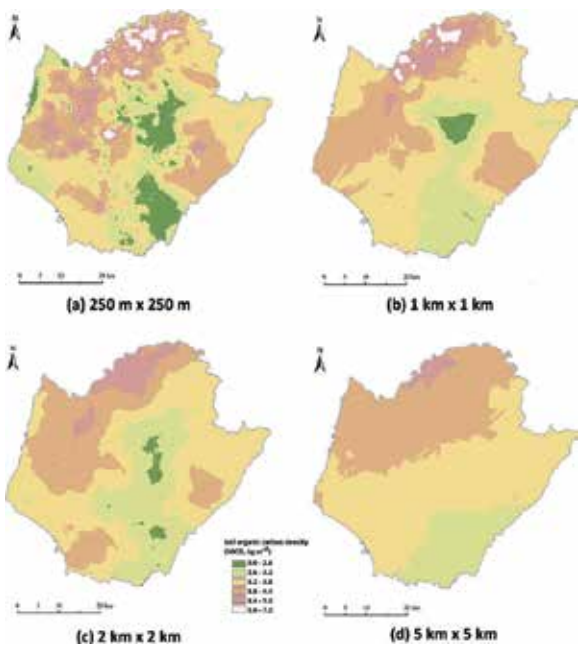

Figure 3. Distribution of soil organic carbon density (SOCD) interpolated by EBK method in 0–30 cm soil layer at four sampling scales.

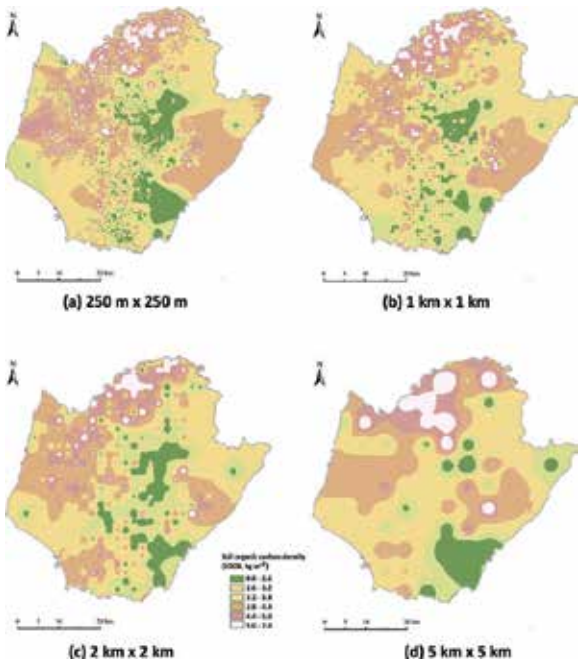

Figure 4. Distribution of soil organic carbon density (SOCD) interpolated by IDW method in 0–30 cm soil layer at four sampling scales.

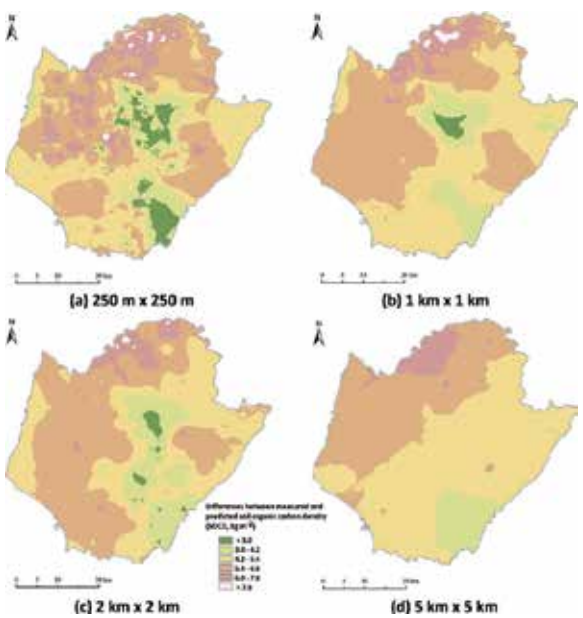

Figure 5. Distribution of soil organic carbon density (SOCD) interpolated by EBK method in 0–50 cm soil layer at four sampling scales.

http://dx.doi.org/10.5772/64210

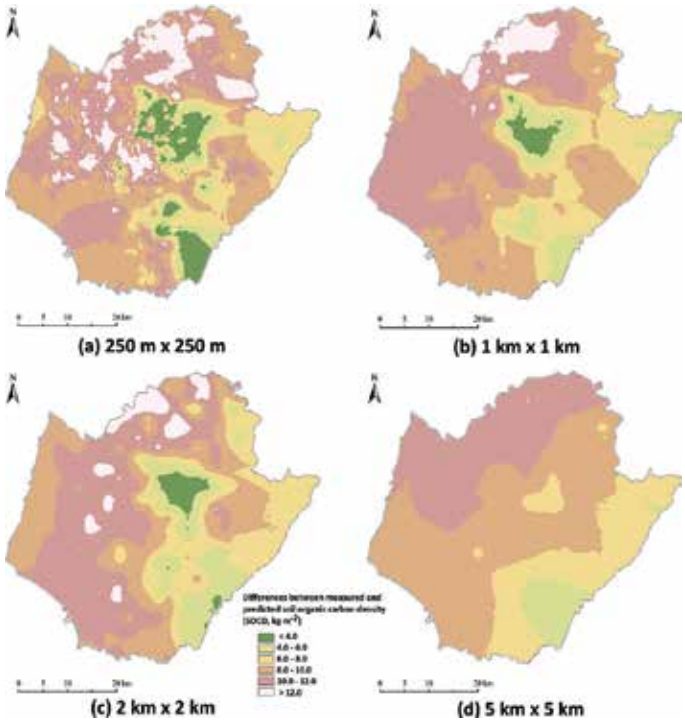

Figure 6. Distribution of soil organic carbon density (SOCD) interpolated by EBK method in 0–100 cm soil layer at four sampling scales.

Figure 7 showed the differences between the measured and the predicted values of SOCD of OK interpolation method in each 250 m × 250 m grid at different sampling scales in 0–30 cm layer. As the sampling density reduced with larger grid sizes, much more points turned to be dark purple (underestimated) and dark green (overestimated), indicating an increasing difference between the measured and the predicted values of SOCD. Most of the dark green points were added to the central region, while the dark purple points were added to the western region. The spatial distribution pattern of differences between the measured and the predicted values of SOCD in 0–30 cm by EBK and IDW was shown in **Figures 8** and **9**. At the highest sampling density (1 sample per 6.25 ha), difference plot that generated by EBK method (**Figure 8a**) had more yellow points than those generated by OK method (**Figure 7a**), indicating that EBK has a smaller interpolation error than OK at this sampling scale. The distribution of differences generated by IDW was almost appeared by yellow points at the highest sampling density (**Figure 9a**), meaning that the differences between the observed and the predicted values of SOCD were less than 0.5 kg m^{-2}. It also indicated that the IDW method had the smallest interpolation error among three methods. Generally, the spatial pattern of estimation error obtained from three interpolation methods had similar distribution pattern between the sampling scale of 1 sample per 1 km^2 and per 4 km^2 in 0–30 cm soil layer of Tainan. The patterns of interpolation error in 0–50 and 0–100 cm layers were similar with those in 0–30 cm layer, so we omitted them in the text. With the decrease in sampling density, the differences between

the measured and the predicted values of SOCD became larger, and high uncertainty was distributed around the local maxima and minima sites [18].

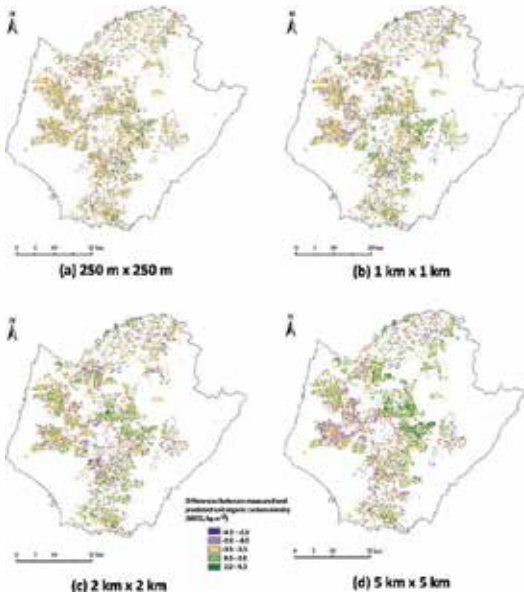

Figure 7. Differences between the measured and the predicted values of soil organic carbon density (SOCD) by OK method in 0–30 cm layer.

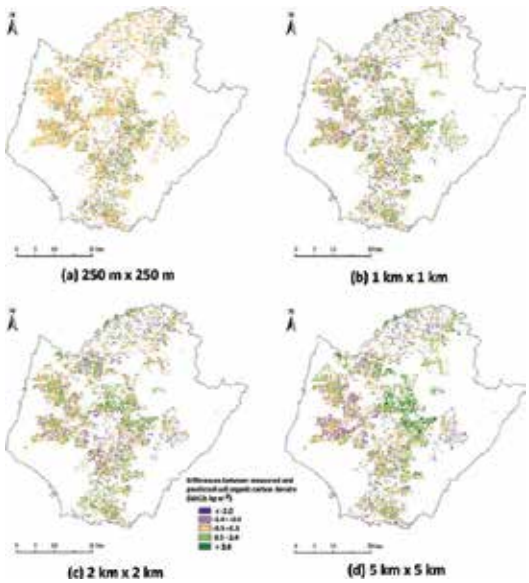

Figure 8. Differences between the measured and the predicted values of soil organic carbon density (SOCD) by EBK method in 0–30 cm layer.

http://dx.doi.org/10.5772/64210

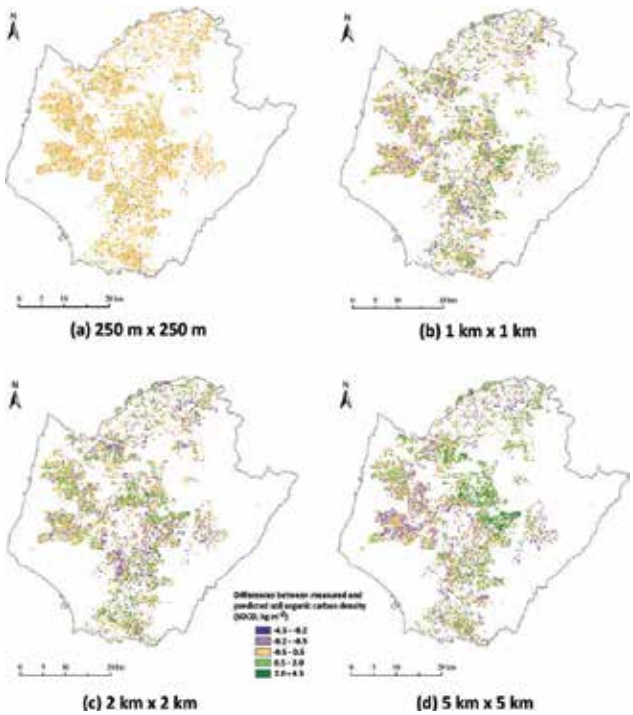

Figure 9. Differences between the measured and the predicted values of soil organic carbon density (SOCD) by IDW method in 0–30 cm layer.

3.3. Estimation of SOC stocks

The SOC stocks in soil layers of 0–30, 0–50, and 0–100 cm were listed in **Table 3**. At the highest sampling density (1 sample per 6.25 ha), the estimates of SOC stocks in 0–30 cm soil layer of Tainan were similar among three interpolation methods, which ranged from 8.03 to 8.08 million tons, while SOC stocks in 0–50 cm layer ranged from 11.92 to 12.04 million tons and in 0–100 cm layer ranged from 20.38 to 20.65 million tons. The SOC stocks at a depth of 0–30 cm increased with decreasing sampling density but decreased at a depth of 0–100 cm. On the basis of estimates at the highest sampling density, the effect of sampling scale on SOC stocks generally had less than 4% of differences under the same soil layer and interpolation method. Although the effect of sampling scale on the result of regional SOCD estimation is obvious, there was no significant effect on the estimation of total SOC stocks in Tainan in this study.

According to our estimation, around 40% of the total SOC stock in the upper 100 cm was held in 0–30 cm layer and 58% in 0–50 cm layer of agricultural soils. The ratios were slightly lower than those estimated by previous studies, which reported that 46–66% (with an average of 50%) of the total organic carbon in the upper 100 cm was stored in 0–30 m layer and 65–81% (with an average of 70%) in 0–50 cm layer of cultivated soils in Taiwan [9, 20]. For forest lands of Tainan, 40–49% of the total SOC stock in the upper 100 cm was held in 0–30 cm layer and 61–65% in 0–50 cm layer in this study. This is in accordance with the estimates of Tsai et al. [21],

which reported that 41–84% (with an average of 59%) of the total organic carbon in the upper 100 cm was stored in 0–30 m layer and 67–98% (with an average of 78%) in 0–50 cm layer of forest soils in Taiwan.

	EBK		OK		IDW	
Sampling density	**SOC stock (million ton)**	**Percentage[a] (%)**	**SOC stock (million ton)**	**Percentage (%)**	**SOC stock (million ton)**	**Percentage (%)**
0–30 cm layer						
1 sample per 6.25 ha	8.03	100	8.05	100	8.08	100
1 sample per 1 km^2	8.15	102	8.21	102	8.19	101
1 sample per 4 km^2	8.08	101	8.21	102	8.09	100
1 sample per 25 km^2	8.24	103	8.26	103	8.28	102
0–50 cm layer						
1 sample per 6.25 ha	11.92	100	11.95	100	12.04	100
1 sample per 1 km^2	12.01	101	12.24	102	12.12	101
1 sample per 4 km^2	11.89	100	12.13	102	11.95	99
1 sample per 25 km^2	11.92	100	11.95	100	11.98	99
0–100 cm layer						
1 sample per 6.25 ha	20.38	100	20.76	100	20.65	100
1 sample per 1 km^2	20.36	100	20.98	101	20.70	100
1 sample per 4 km^2	20.05	98	20.75	100	20.37	99
1 sample per 25 km^2	19.92	98	20.00	96	20.03	97

[a]The SOC stocks estimated at the highest sampling density as a standard for comparing.

Table 3. The estimates of SOC stocks in 0–30, 0–50, and 0–100 cm layers of Tainan by three interpolation methods at different sampling densities.

3.4. Land use effect on SOC stocks and SOCD

Soil organic carbon (SOC) stocks in different soil layers under different land uses were listed in **Table 4**. Generally, agricultural lands, forests, and lands for other uses occupy 49.1, 21.4, and 29.5% of the total area of Tainan, respectively. The SOC stocks in the agricultural lands, which were estimated by different interpolation methods and sampling densities, ranged from 4.10 to 4.26 million tons in 0–30 cm layer, 6.05 to 6.21 million tons in 0–50 cm layer, and 10.22 to 10.71 million tons in 0–100 cm layer. The SOC stocks in the forest lands varied between 1.55 and 1.67 million tons in 0–30 cm layer, 2.15 and 2.41 million tons in 0–50 cm layer, and 3.35 and 3.97 million tons in 0–100 cm layer. Lands for other uses stored 2.38–2.47 million tons of SOC in 0–30 cm layer, 3.56–3.65 million tons in 0–50 cm layer, and 6.06–6.37 million tons in 0–100 cm layer. Regardless of the soil layer, interpolation method, and sampling density, 50.3–

http://dx.doi.org/10.5772/64210

52.2% of the total SOC stocks stored in the agricultural lands, while forests stored 16.7–20.2% and lands for other uses stored 29.4–31.0%.

Sampling density	Grid size	Agriculture lands			Forest lands			Lands for other uses		
		EBK	OK	IDW	EBK	OK	IDW	EBK	OK	IDW
0–30 cm layer										
1 per 6.25 ha	250 m × 250 m	4.10	4.10	4.11	1.55	1.56	1.58	2.38	2.39	2.39
1 per 1 km^2	1 km × 1 km	4.14	4.16	4.16	1.61	1.64	1.62	2.41	2.41	2.41
1 per 4 km^2	2 km × 2 km	4.10	4.16	4.12	1.58	1.64	1.55	2.41	2.41	2.41
1 per 25 km^2	5 km × 5 km	4.14	4.18	4.25	1.67	1.64	1.56	2.43	2.44	2.47
0–50 cm layer										
1 per 6.25 ha	250 m × 250 m	6.13	6.14	6.13	2.24	2.33	2.25	3.55	3.58	3.57
1 per 1 km^2	1 km × 1 km	6.14	6.19	6.21	2.28	2.33	2.41	3.59	3.60	3.62
1 per 4 km^2	2 km × 2 km	6.05	6.08	6.12	2.26	2.26	2.36	3.58	3.60	3.65
1 per 25 km^2	5 km × 5 km	6.06	6.21	6.07	2.30	2.15	2.32	3.56	3.62	3.56
0–100 cm layer										
1 per 6.25 ha	250 m × 250 m	10.61	10.62	10.62	3.56	3.79	3.86	6.21	6.24	6.27
1 per 1 km^2	1 km × 1 km	10.53	10.67	10.71	3.58	3.77	3.97	6.24	6.26	6.31
1 per 4 km^2	2 km × 2 km	10.36	10.47	10.54	3.46	3.60	3.84	6.23	6.30	6.37
1 per 25 km^2	5 km × 5 km	10.22	10.46	10.26	3.63	3.35	3.68	6.07	6.21	6.06

Table 4. The estimates of SOC stocks (million tons) in different land uses of Tainan by three interpolation methods at different sampling densities.

As agriculture is the major land use in Tainan, the SOCDs of different cropping soils in the agricultural lands were further estimated by EBK interpolation method and listed in **Table 5**. In Tainan, lands for rice cropping, upland, orchard, and fallow uses were 18.2, 41.8, 37.0, and 3.0% of the total agricultural lands, respectively. The mean SOCD of different cropping soils decreased in the following order in all soil layers: rice cropping land > upland > abandoned or fallow land > orchard.

Tainan has a humid subtropical climate, which is favorable to the degradation of soil organic matter. Main parent materials of Tainan soil are calcareous sandstone, shale, and mudstone [22]. Thus, majority of the cultivated lands is calcareous alluvial soil with neutral to basic soil reaction as well as higher buffering capacity to resist changes in pH caused by chemical fertilizer. Therefore, SOC storage of agricultural soil in Tainan is not greatly affected by management or cropping system, except for rice cropping. Long-term rice cultivation has been reported to increase the SOC storage in surface soils of Taiwan [10]. In our study, however, the mean SOCD of rice cropping land was slightly, but not significantly, higher than other cropping system (**Table 5**).

Land use	Percentage of area (%)	1 sample per 6.25 ha	1 sample per 1 km^2	1 sample per 4 km^2	1 sample per 25 km^2
0–30 cm layer					
Rice cropping land	18.2	3.99 ± 0.83	3.94 ± 0.70	3.95 ± 0.60	4.00 ± 0.38
Upland	41.8	3.85 ± 0.71	3.81 ± 0.55	3.82 ± 0.53	3.77 ± 0.42
Orchard	37.0	3.53 ± 0.65	3.55 ± 0.47	3.42 ± 0.43	3.54 ± 0.32
Abandoned or fallow land	3.0	3.67 ± 0.66	3.62 ± 0.50	3.71 ± 0.47	3.70 ± 0.46
0–50 cm layer					
Rice cropping land	18.2	5.87 ± 1.46	5.86 ± 1.30	5.84 ± 1.12	5.92 ± 0.71
Upland	41.8	5.74 ± 1.11	5.71 ± 0.86	5.73 ± 0.84	5.56 ± 0.74
Orchard	37.0	5.23 ± 1.13	5.13 ± 0.82	4.97 ± 0.88	5.06 ± 0.57
Abandoned or fallow land	3.0	5.50 ± 1.08	5.43 ± 0.80	5.55 ± 0.76	5.50 ± 0.75
0–100 cm layer					
Rice cropping land	18.2	10.04 ± 3.00	9.96 ± 2.68	10.00 ± 2.49	10.05 ± 1.22
Upland	41.8	10.16 ± 2.16	10.10 ± 1.73	10.17 ± 1.69	9.55 ± 1.35
Orchard	37.0	8.52 ± 2.46	8.28 ± 1.81	7.84 ± 2.08	8.16 ± 1.29
Abandoned or fallow land	3.0	9.59 ± 2.25	9.52 ± 1.80	9.80 ± 1.69	9.40 ± 1.34

Table 5. Soil organic carbon density (kg m^{-2}, mean ± standard deviation) for different cropping soils in the agricultural land of Tainan (estimated by EBK interpolation method).

3.5. Uncertainty (improvement of the estimation of SOC stock)

The number of soil samples, the distance between sampling locations, and the choice of interpolation are factors that affect the prediction of spatial distribution for soil properties [18, 23]. Generally, the larger the number of soil samples, the more accurate the kriging maps of soil properties [18, 24]. The original database (7388 soil samples) that we used in this study was obtained from a detailed soil survey in Tainan; thus, the sample number for spatial interpolation at the highest sampling density should be large enough to provide valuable information when comparing with other researches. The distance between sampling locations is another factor that influences the spatial patterns of SOCD. Despite large sample number, the sample locations are not evenly distributed over the whole area (**Figure 1**), and it probably results in a higher uncertainty of estimation in the region with sparsely or no located observations. OK is one of the most commonly used spatial interpolation methods that only consider the spatial autocorrelation and heterogeneity of SOC but overlooks the influence of environmental variables (and so as EBK). However, SOC status is influenced by many soil characteristics and environmental factors; those overlooked factors may also contribute to the interpolation error in this study, especially in the surface soils. In addition, land use is very

http://dx.doi.org/10.5772/64210

intensive in Taiwan. The smallest sampling grid in our study (250 m × 250 m) may still be divided by different land uses and managements, which is possibly to result in high spatial variation in SOC. In the future, better techniques or models should be developed for a better understanding of the spatial distribution of SOCD and relationships between environment variables and SOCD, which are important to predict SOC stocks.

4. Conclusion

In this study, OK, EBK, and IDW methods and four scales of sampling density (1 sample per 6.25 ha, 1 km^2, 4 km^2, and 25 km^2) were used for spatial interpolation of SOCD in Tainan. The results indicated that sampling density has significant effect on the prediction for spatial patterns of SOCD. The spatial pattern obtained from the highest sampling density appeared the most detailed SOCD spatial distribution, and all indices of prediction accuracy showed a reducing trend with decreasing sampling density for a certain depth. We suggested that sampling density should be more than 1 sample per 4 km^2 at least in this study area.

All three interpolation methods performed on SOCD and SOC stocks approximately well; however, OK and EBK methods had a smoothing effect, while IDW method reserved the local maxima and local minima in estimating the spatial distribution of SOCD. Although the sampling density had a significant effect on spatial prediction of SOCD, the estimates of SOC stocks in Tainan were not significantly influenced by the sampling density and interpolation methods. The estimates of SOC stocks in 0–30 cm soil layer of Tainan ranged from 8.03 to 8.08 million tons, while SOC stocks in 0–50 cm ranged from 11.92 to 12.04 million tons and in 0–100 cm ranged from 20.38 to 20.65 million tons. In terms of agricultural land uses, the mean SOCD was slightly influenced by rice cropping system with little increase in SOCD.

Author details

Chun-Chih Tsui[1], Xiao-Nan Liu[1,2], Horng-Yuh Guo[3] and Zueng-Sang Chen[1*]

*Address all correspondence to: soilchen@ntu.edu.tw

1 Department of Agricultural Chemistry, National Taiwan University, Taipei, Taiwan

2 Guangdong Key Laboratory of Agricultural Environment Pollution Integrated Control, Guangdong Institute of Eco-Environment and Soil Sciences, Guangzhou, China

3 Division of Agricultural Chemistry, Taiwan Agricultural Research Institute, Council of Agriculture, Taichung, Taiwan

References

[1] Guo LB, Gifford RM. Soil carbon stocks and land use change: a meta analysis. Global Change Biology. 2002;8(4):345–360. DOI: 10.1046/j.1354-1013.2002.00486.x

[2] Lal R. Soil carbon sequestration impacts on global climate change and food security. Science. 2004;304(5677):1623–1627. DOI: 10.1126/science.1097396

[3] Bajtes NH. Total carbon and nitrogen in the soils of world. European Journal of Soil Science. 1996;47(2):151–163. DOI: 10.1111/j.1365-2389.1996.tb01386.x

[4] Eswaran H, Van Den Berg E, Reich P. Organic carbon in soils of the world. Soil Science Society of America Journal. 1993;57(1):192–194. DOI: 10.2136/sssaj1993.03615995005700010034x

[5] Stockmann U, Padarian J, McBratney A, Minasny B, de Brogniez D, Montanarella L, Hong SY, Rawlins BG. Global soil organic carbon assessment. Global Food Security. 2015;6(1):9–16. DOI: 10.1016/j.gfs.2015.07.001

[6] Minasny B, Sulaeman Y, McBratney A. Is soil carbon disappearing? The dynamics of soil organic carbon in Java. Global Change Biology. 2011;17(5):1917–1924. DOI: 10.1111/j.1365-2486.2010.02324.x

[7] Scott NA, Tate KR, Giltrap DJ, Tattersall Smith C, Wilde HR, Newsome PJF, Davis MR. Monitoring land-use change effects on soil carbon in New Zealand: quantifying baseline soil carbon stocks. Environmental Pollution. 2002;116(S1):S167–S186. DOI: 10.1016/S0269-7491(01)00249-4

[8] Bui E, Henderson B, Viergever K. Using knowledge discovery with data mining from the Australian Soil Resource Information System database to inform soil carbon mapping in Australia. Global Biogeochemical Cycles. 2009;23:GB4033. DOI: 10.1029/2009GB003506

[9] Chen ZS, Hseu ZY. Total organic carbon pool in soils of Taiwan. Proceedings of the National Science Council, Republic of China. Part B, Life Sciences. 1997;21:120–127.

[10] Chen CL, Lin ML, Guo HY, Chiang CF, Liu TS, Chu CL. Impact assessment of shifts of land use on soil organic carbon storage of cultivated land in Taiwan. Soil and Environment. 2000;3(4):363–378.

[11] Goovaerts P. Geostatistics in soil science: state-of-the-art and perspectives. Geoderma. 1999;89(1–2):1–45. DOI: 10.1016/S0016-7061(98)00078-0

[12] Sun WX, Zhao YC, Huang B, Shi XZ, Darilek JL, Yang JS, Wang ZG, Zhang B. Effect of sampling density on regional soil organic carbon estimation for cultivated soils. Journal of Plant Nutrition and Soil Science. 2012;175(5):671–680. DOI: 10.1002/jpln.201100181

[13] Zhang ZQ, YuDS, Shi XZ, Wang N, Zhang GX. Priority selection rating of sampling density and interpolation method for detecting the spatial variability of soil organic

carbon in China. Environmental Earth Sciences. 2015;73(5):2287–2297. DOI: 10.1007/s12665-014-3580-3

[14] Chien YJ, LeeDY, Guo HY, Houng KH. Geostatistical analysis of soil properties of mid-west Taiwan soils. Soil Science. 1997;162(4):291–298.

[15] Liu TL, Juang KW, Lee DY. Interpolating soil properties using kriging combined with categorical information of soil maps. Soil Science Society of America Journal. 2006;70(4): 1200–1209. DOI: 10.2136/sssaj2005.0126

[16] Tsui CC, Guo HY, Chen ZS. Estimation of soil carbon stocks in Taiwan arable soils by using legacy database and digital soil mapping. In: Hernandez-Soriano MC, editor. Soil Processes and Current Trends in Quality Assessment. Croatia: InTech; 2013. p. 311–335. DOI: 10.5772/53211

[17] Mirzaei R, Sakizadeh M. Comparison of interpolation methods for the estimation of groundwater contamination in Andimeshk-Shush Plain, Southwest of Iran. Environmental Science and Pollution Research. 2016;23(3):2758–2769. DOI: 10.1007/s11356-015-5507-2

[18] Xie YF, Chen TB, Lei M, Yang J, Guo QJ, Song B, Zhou XY. Spatial distribution of soil heavy metal pollution estimated by different interpolation methods: accuracy and uncertainty analysis. Chemosphere. 2011;82(3):468–476. DOI: 10.1016/j.chemosphere.2010.09.053

[19] Liu ZP, Shao M, Wang YQ. Effect of environmental factors on regional soil organic carbon stocks across the Loess Plateau region, China. Agriculture, Ecosystems and Environment. 2011;142(3–4):184–194. DOI: 10.1016/j.agee.2011.05.002

[20] Jien SH, Hseu ZY, Guo HY, Tsai CC, Chen ZS. Organic carbon storage and management strategies of the rural soils on the basis of Soil Information system in Taiwan. In: Chen ZS, Agus F, editors. Proceedings of International Workshop on Evaluation and Sustainable Management of Soil Carbon Sequestration in Asian Countries; 28–29 September 2010; IPB International Conference Center, Bogor, Indonesia. Food and Fertilizer Technology Center (FFTC) for the Asian and Pacific Region; 2010. p. 125–137.

[21] Tsai CC, Chen ZS, Hseu ZY, Duh CT, Guo HY. Organic carbon storage and management strategies of the forest soils based on the Forest Soil Survey Database in Taiwan. In: Chen ZS, Agus F, editors. Proceedings of International Workshop on Evaluation and Sustainable Management of Soil Carbon Sequestration in Asian Countries; 28–29 September 2010; IPB International Conference Center, Bogor, Indonesia. Food and Fertilizer Technology Center (FFTC) for the Asian and Pacific Region; 2010. p. 85–102.

[22] Taiwan Agricultural Research Institute (TARI). Soil Survey Report of Tainan, Taiwan. Taiwan: Taiwan Agricultural Research Institute (TARI), Council of Agriculture, Taiwan; 1969. p. 140.

[23] Kravchenko AN. Influence of spatial structure on accuracy of interpolation methods. Soil Science Society of America Journal. 2003;67(5):1564–1571. DOI: 10.2136/sssaj2003.1564

[24] Mueller TG, Pierce FJ, Schabenberger O, Warncke DD. Map quality for site-specific fertility management. Soil Science Society of America Journal. 2001;65(5):1547–1558. DOI: 10.2136/sssaj2001.6551547x

Chapter 3

Monitoring of the 2008 Chaitén Eruption Cloud Using MODIS Data and its Impacts

Yuanzhi Zhang, Jin Yeu Tsou, Zhaojun Huang,
Jinrong Hu and Wyss W.-S. Yim

Additional information is available at the end of the chapter

http://dx.doi.org/10.5772/00000

Abstract

This chapter presents the monitoring of the 2008 Chaitén eruption cloud using Moderate Resolution Imaging Spectroradiometer (MODIS) data and its impacts. The 8-day MODIS data from 3 to 10 May 2008 were used to track the movement and dispersion of the eruption cloud of the Chaitén volcano in Chile following the eruption on 2 May 2008. For detecting volcanic particulates, the procedure is adopted based on the brightness temperature difference (BTD) algorithm, by which the thermal infrared channels were centered on 11–12 μm of multispectral satellite sensors. The BTD is generally negative for volcanic ash but positive for ice and water vapor. The eruption cloud was found to drift northeastward, eastward, and southeastward crossing the central and northern part of Argentina and over the Atlantic Ocean. The timing of heavy rainfall in South Africa during May–June, in central Australia during June 2008 and in Hong Kong during June (the wettest since record began in 1884), was considered to have been connected to the dispersion of the particulates from this Chaitén eruption to further impact downstream.

Keywords: volcanic cloud dispersion, MODIS data, Chaitén eruption, heavy rainfall

1. Introduction

Volcanic eruption clouds are potentially hazardous to aircrafts in the air. The ash clouds may persist for many hours or perhaps days and have been known to produce en route flight diversions in regions thousands of kilometers from their source in [1]. As volcanic eruptions are variable in intensity and composition, the tracking of the eruption cloud is particularly

relevant to aviation safety. Additionally, the spread of eruption clouds may have possible climatic effects including precipitation changes. Due to the isolated locations of many volcanoes, remote sensing plays an important role in tracking ash clouds as they drift away from an erupting volcano. In this paper, Moderate Resolution Imaging Spectroradiometer (MODIS) data were downloaded from 3 to 10 May to monitor and retrieve the volcanic ash cloud from the 2 May eruption of Chaitén volcano in Chile and to analyze its impacts on rainfall.

Figure 1. Map of southern South America showing the location of the Chaitén Volcano.

The Chaitén volcano, a southern Andean arc volcano in Chile located at latitude 42.833°S and longitude 72.646°W (**Figure 1**), began erupting explosively in the early morning around 08:00 coordinated universal time (UT) on 2 May 2008 in [2], without warning in [3]. Ash columns

http://dx.doi.org/10.5772/00000

abruptly jetted from the volcano into the stratosphere reaching an altitude of more than 21 km followed by lava dome effusion and continuous low-altitude close space ash plumes in [4]. This eruption was the largest eruption in Chile since Cerro Hudson in 1991 in [5] and the largest explosive rhyolitic eruption since Novarupta, Alaska in 1912. Prior to this, the volcano comprised a rhyolitic lava dome within a 2.5 km diameter caldera was last thought to have erupted at 9370 ^{14}C years B.P. in [6]. The eruption had immediate and serious social and economic consequences across southern Chile and Argentina. Floods and lahars inundated the town of Chaitén and its 4625 residents were evacuated. Widespread ashfall and drifting ash clouds closed regional airports and led to the cancellation of numerous domestic and international flights in Argentina and Chile in [7]. Furthermore, the aquaculture industry in the nearby Gulf of Corcovado was badly affected, while ecotourism was curtailed and the regional nature reserves were forced to close.

2. Data and methodology

2.1. Data

In this study, the 8-day data of (from 3 to 10 May 2008) NASA-MODIS Level-1B Calibrated Geolocation Data Set (MOD02) in [8] with 1 km resolution were applied to track the movement and dispersion of the eruption cloud of the Chaitén volcano in Chile following the eruption on 2 May 2008. About 30-year average rainfall distribution image and June 2008 rainfall image were used to compare with the drought information, which was downloaded from the website of Australian Bureau of Meteorology. And the rainfall images for South Africa and annual rainfall data for Hong Kong were downloaded from the websites of South Africa Weather Service and Hong Kong Observatory, respectively.

2.2. Methods

2.2.1. Methodology for volcanic ash tracking

The most widely used approach to detect volcanic ash is based on the brightness temperature difference (BTD) procedure applied to the channels centered at around 11 and 12 μm in [9]. The BTD technique has been applied either to polar satellite instruments such as the Advanced Very High Resolution Radiometer (AVHRR) [10–11], the Moderate Resolution Imaging Spectroradiometer (MODIS) [12–17], rather than to geostationary satellite instruments as the Geostationary Operational Environmental Satellite (GOES) in [18], and the Spin Enhanced Visible and Infrared Imager (SEVIRI) measurements in [19]. In this study, the volcanic ash detection procedure adopted is based on the BTD algorithm using the thermal infrared channels centered on 11 μm and 12 μm of a multispectral satellite sensor. This is because volcanic ash contains large amounts of silicates that scatter and absorb infrared radiation in a different way than meteorological water and ice clouds in [20]. A BTD of 11–12 μm is generally negative for volcanic ash and dust and positive for ice and water clouds [11, 20, 21]. Bands 31

(11 μm) and 32 (12 μm) of MODIS data were used for volcanic ash monitoring in this study. Before BTD calculation, there are two steps. Firstly, Digital Number (DN) values need to be transferred into radiant intensity to calculate the brightness temperature since MODIS images are expressed with DN values. Secondly, brightness temperature was calculated using the Planck function.

The formulae used for Radiant Intensity calculation of bands 31 and 32 of MODIS data were used as in [22]:

$$\mathrm{Rad}\,31 = \mathrm{scale}\,31(\mathrm{band}\,31 - \mathrm{offset}\,31) \tag{1}$$

$$\mathrm{Rad}\,32 = \mathrm{scale}\,32(\mathrm{band}\,32 - \mathrm{offset}\,32) \tag{2}$$

(where rad 31 and rad 32 are the Heat Radiant Intensity ($Wm^{-2}.sr^{-1}(m^{-1})$) of bands 31 and 32 of MODIS data, respectively; while band 31 and band 32 are the DN values of band 31 and 32 of MODIS data, respectively; scale 31 and offset 31 are the radiometric calibration constant of band 31 of MODIS data, and, scale 32 and offset 32 are the radiometric calibration constant of band 32 of MODIS data).

After determination of the Heat Radiant Intensity, the brightness temperature can be calculated based on Plank function. The formulae used were used as in [22]:

$$T\,31 = K\,31,2 / \ln(1 + K\,31,1 / \mathrm{rad}\,31) \tag{3}$$

$$T\,32 = K\,32,2 / \ln(1 + K\,32,1 / \mathrm{rad}\,32) \tag{4}$$

(where K 31,1 = 729.541636 $W.m^{-2}.sr^{-1}.\mu m^{-1}$; K 31,2 = 1304.413871K; K 32, 1 = 474.684780 $W.m^{-2}.sr^{-1}.\ \mu m^{-1}$, and, K 32, 2 = 1196.978785K).

2.2.2. Methodology for rainfall study

In this study, Australian, South Africa, and Hong Kong history observation rainfall data were downloaded to study the impacts of Chaitén volcano eruption cloud on rainfall. For Australia, the average rainfall in June from 1961 to 1990 and rainfall in June 2008 were obtained as shown in **Figure 2** and **Figure 3**. For South Africa, the rainfall data of May and June were downloaded to compare the rainfall change caused by Chaitén volcanic ash migration as shown in **Figure 4** and **Figure 5**. For Hong Kong, the historical rainfall data used in this study is the annual rainfall data between 1947 and 2009 obtained from Hong Kong Observatory as shown in **Figure 6**. The figure also listed out the significant annual rainfall change of Hong Kong caused by volcanic eruptions or nuclear tests.

http://dx.doi.org/10.5772/00000

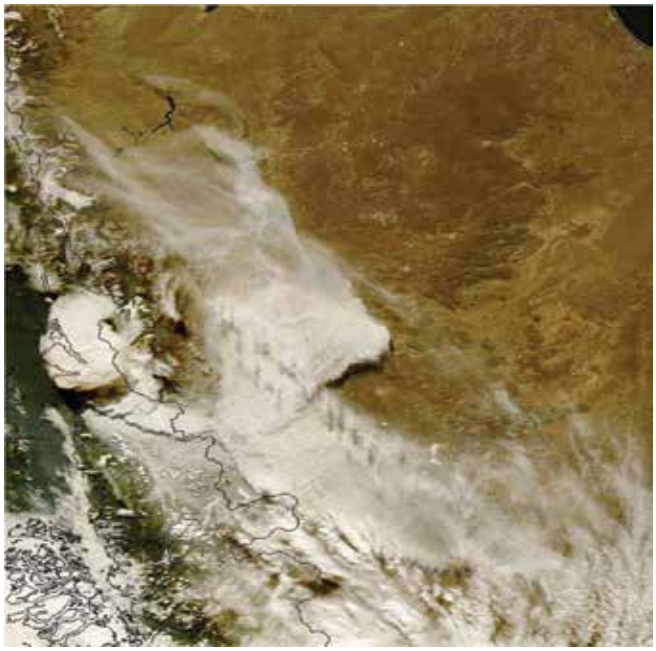

Figure 2. Average rainfall in June over the Australian continent from 1961 to 1990 (Courtesy of Australian Bureau of Meteorology).

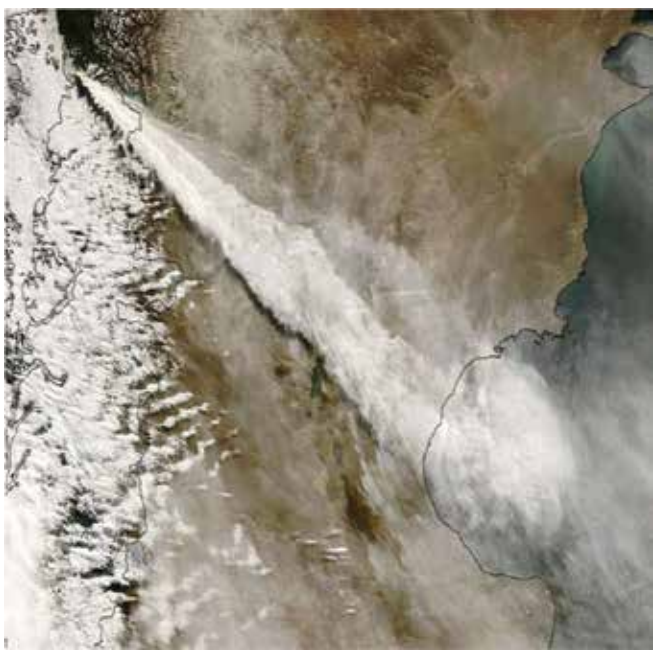

Figure 3. Heavy rainfall in June 2008 in Australia (Courtesy of Australian Bureau Meteorology).

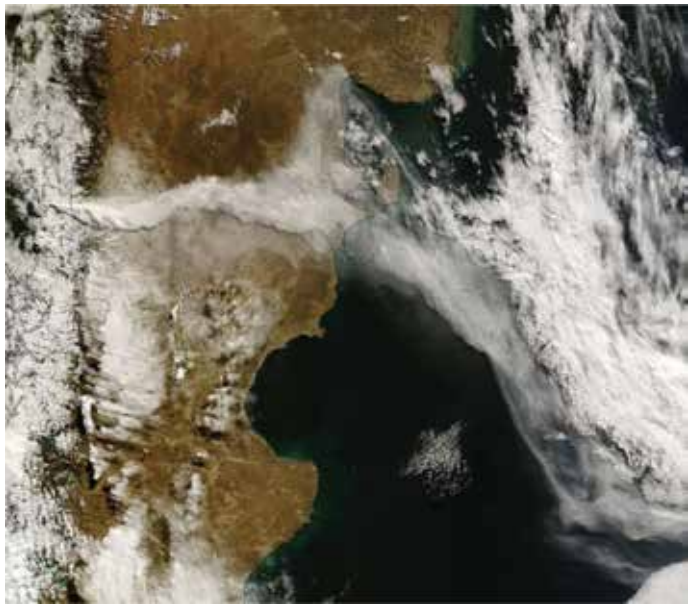

Figure 4. Rainfall May 2008 in South Africa, but a significant increasing rainfall during 21–31 May was attributed to the migration of the eruption cloud from the Chaitén volcano in Chile following the eruption on 2 May 2008 (Courtesy of South Africa Weather Service).

Figure 5. Rainfall in June 2008 in South Africa, but a heavy rainfall was attributed to the migration of the eruption cloud from the Chaitén volcano in Chile following the eruption on 2 May 2008 (Courtesy of South Africa Weather Service).

http://dx.doi.org/10.5772/00000

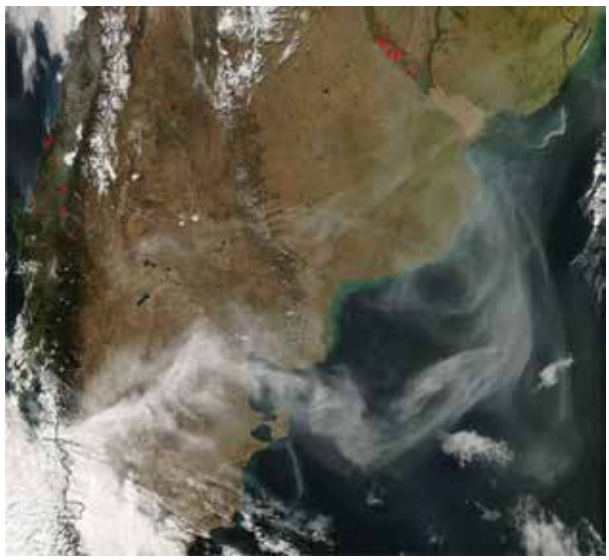

Figure 6. The annual rainfall of Hong Kong from 1947 to 2009 (Courtesy of the Hong Kong Observatory).

3. Satellite tracking of eruption cloud

Images of the eruption cloud recorded by NASA-MODIS using the Terra and Aqua MODIS sensors are shown as examples as in **Figures 7–12**.

Figure 7. May 2, 13:50 UT: Chile (MODIS).

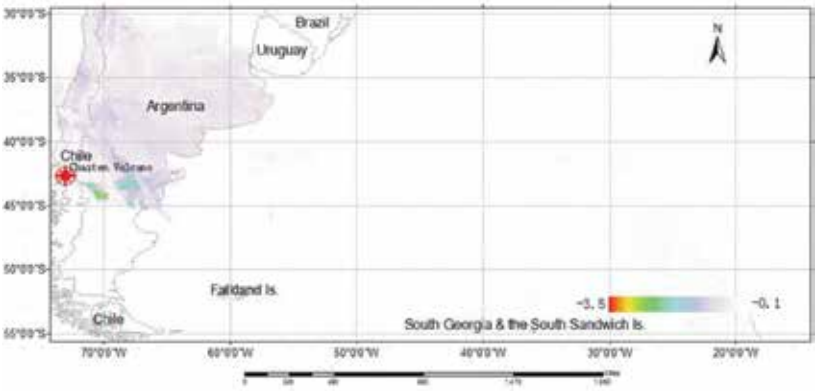

Figure 8. May 3, 14:35 UT: Chile (MODIS).

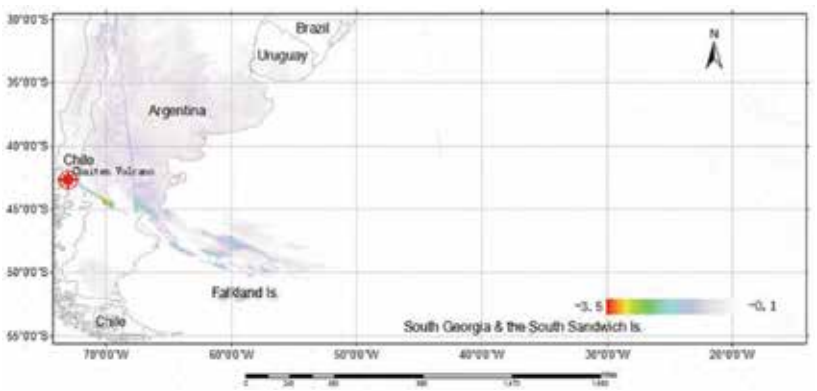

Figure 9. May 5, 14:25 UT: Chile (MODIS).

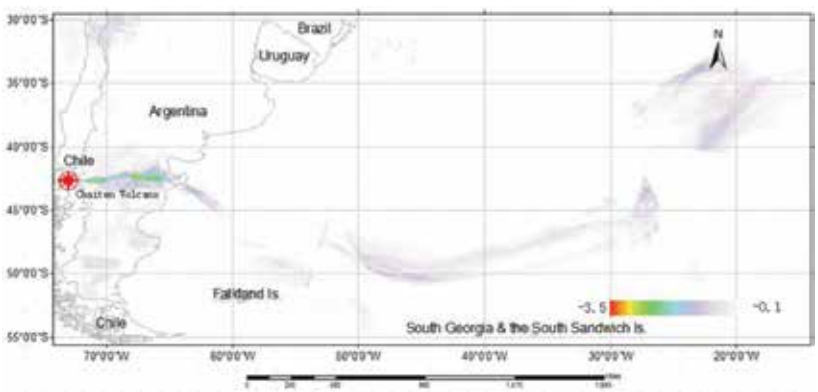

Figure 10. May 6, 15:05 UT: Chile (MODIS).

http://dx.doi.org/10.5772/00000

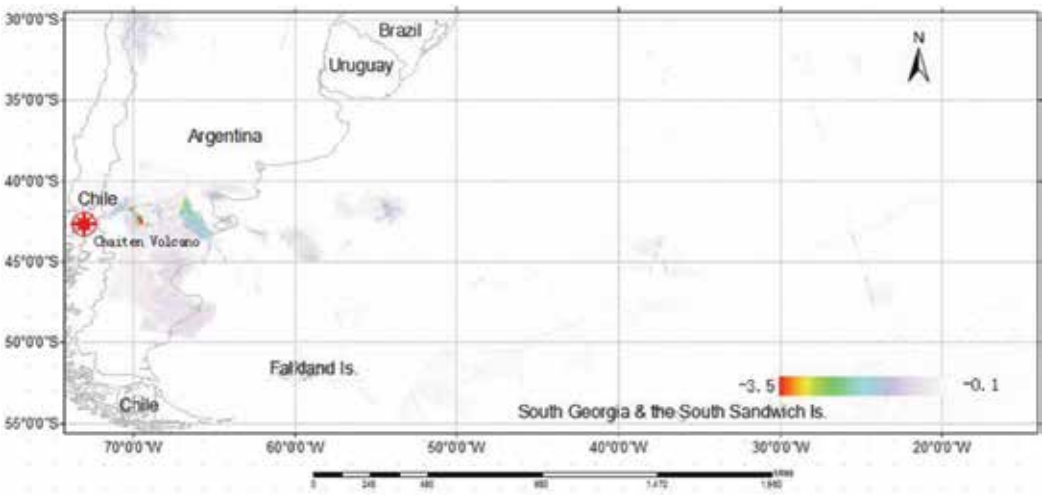

Figure 11. May 9, 18:10 UT: Chile (MODIS).

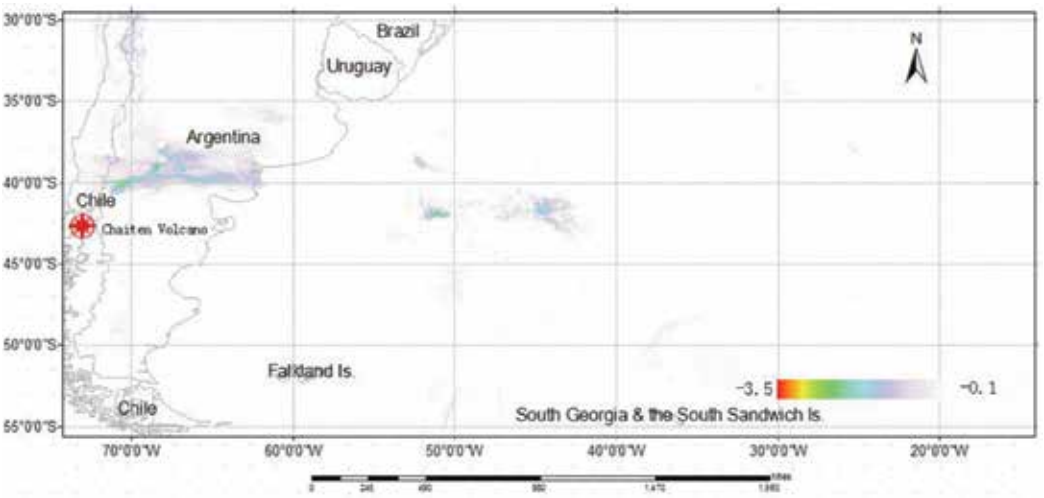

Figure 12. May 10, 14:40 UT: Chile (MODIS).

4. Results and discussion

4.1. Eruption cloud tracking

Applying Eqs (3) and (4), the eruption cloud tracking BTD images can be calculated from MODIS images data shown as in **Figures 13–20**.

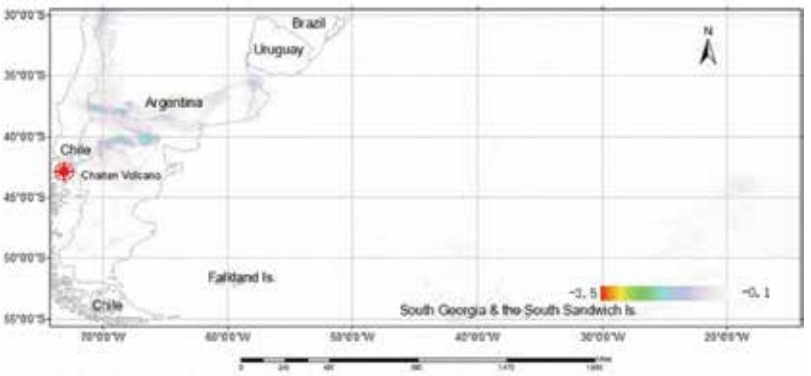

Figure 13. Chaitén eruption cloud on 3 May 2008.

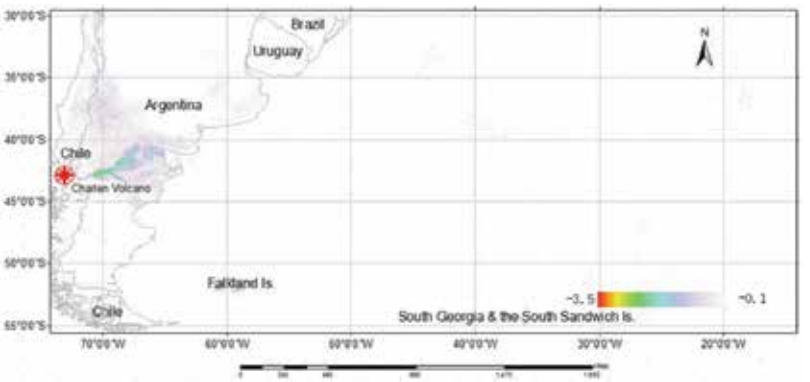

Figure 14. Chaitén eruption cloud on 4 May 2008.

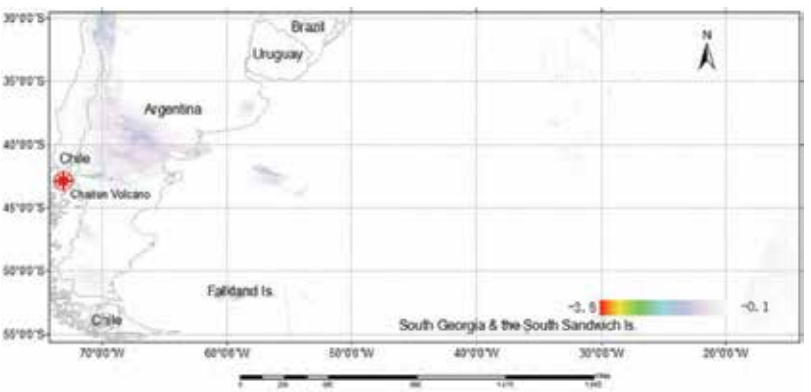

Figure 15. Chaitén eruption cloud on 5 May 2008.

http://dx.doi.org/10.5772/00000

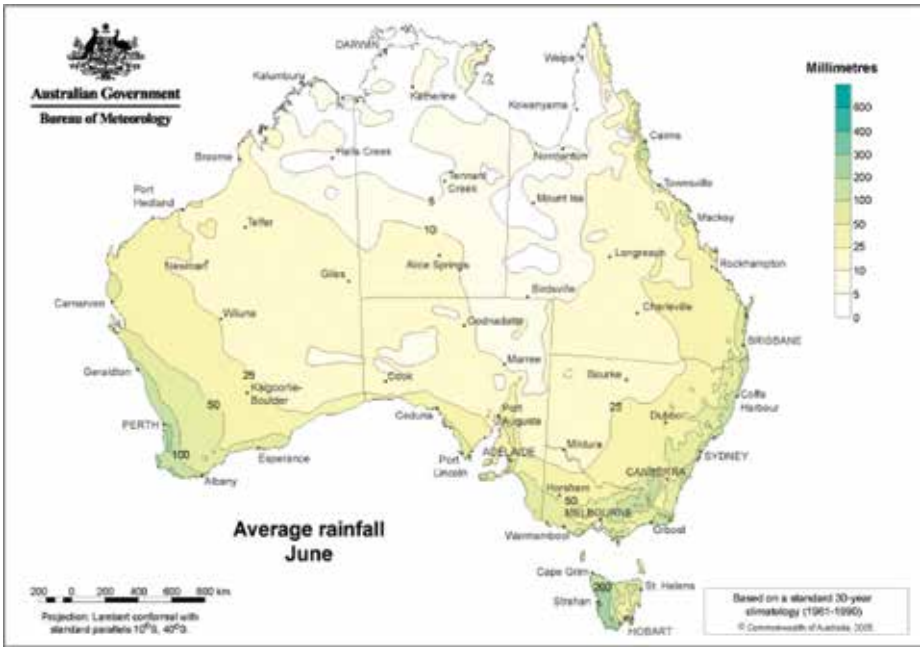

Figure 16. Chaitén eruption cloud on 6 May 2008.

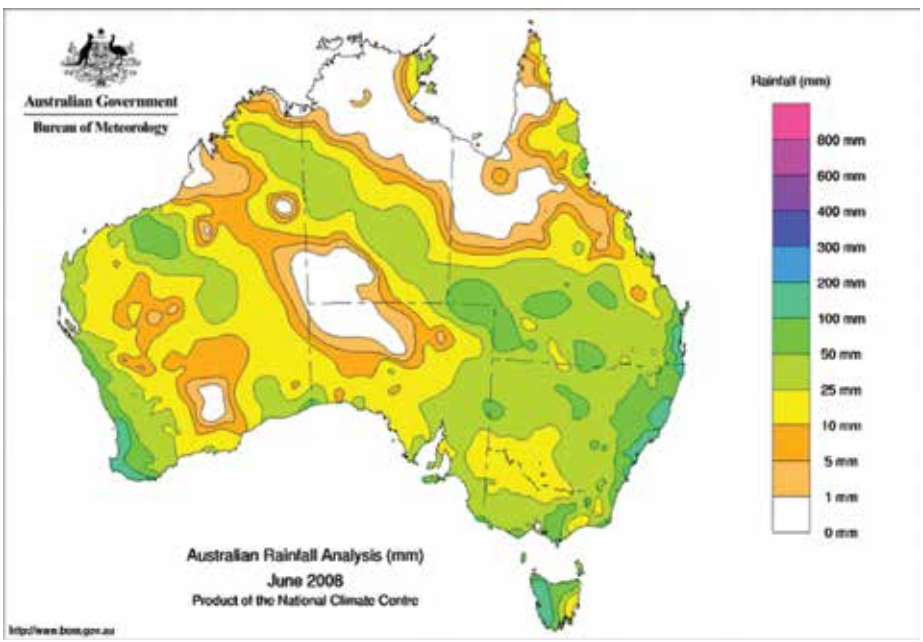

Figure 17. Chaitén eruption cloud on 7 May 2008.

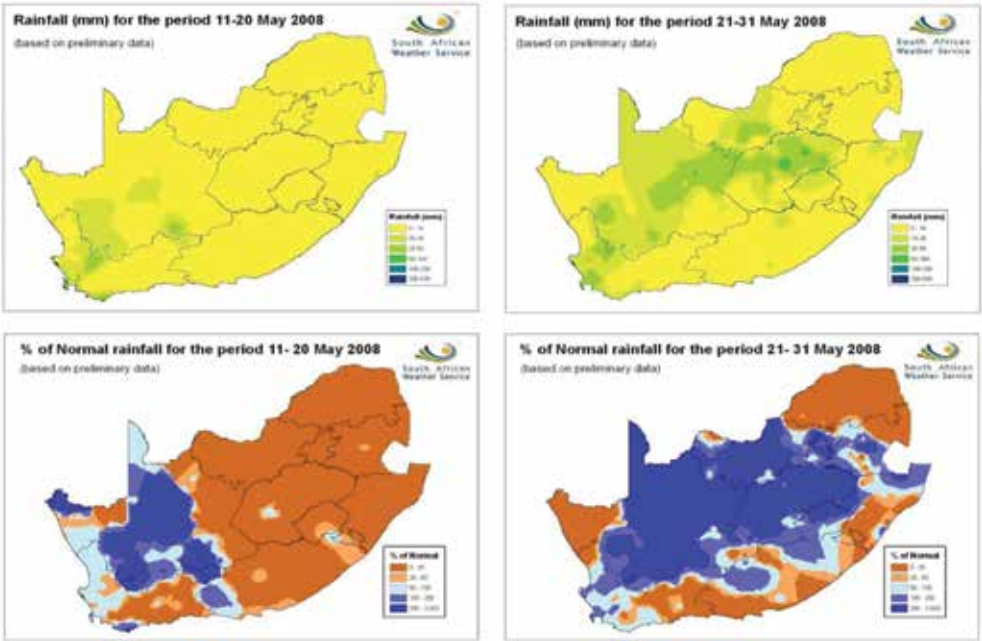

Figure 18. Chaitén eruption on 8 May 2008.

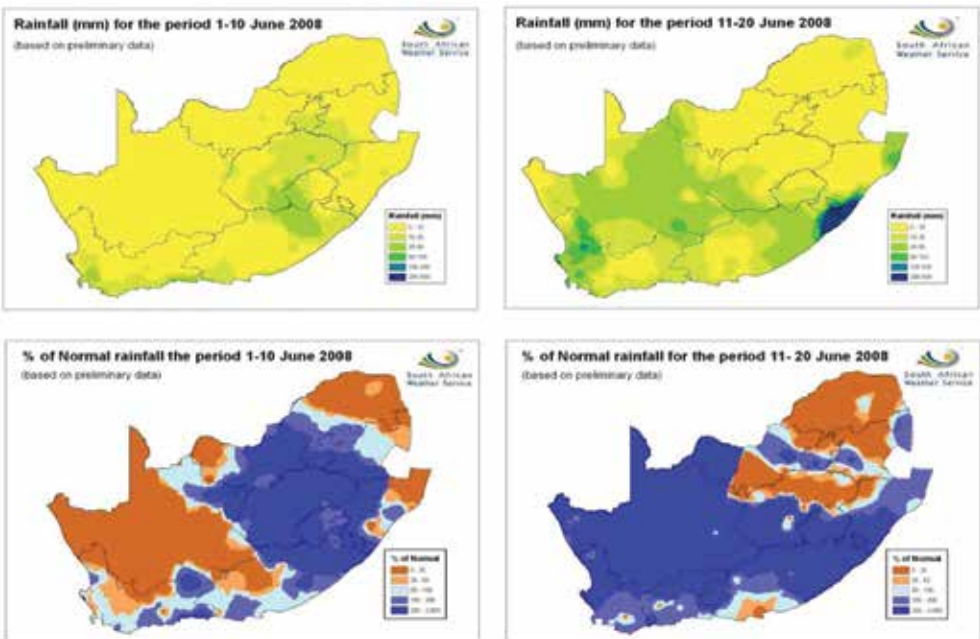

Figure 19. Chaitén eruption cloud on 9 May 2008.

http://dx.doi.org/10.5772/00000

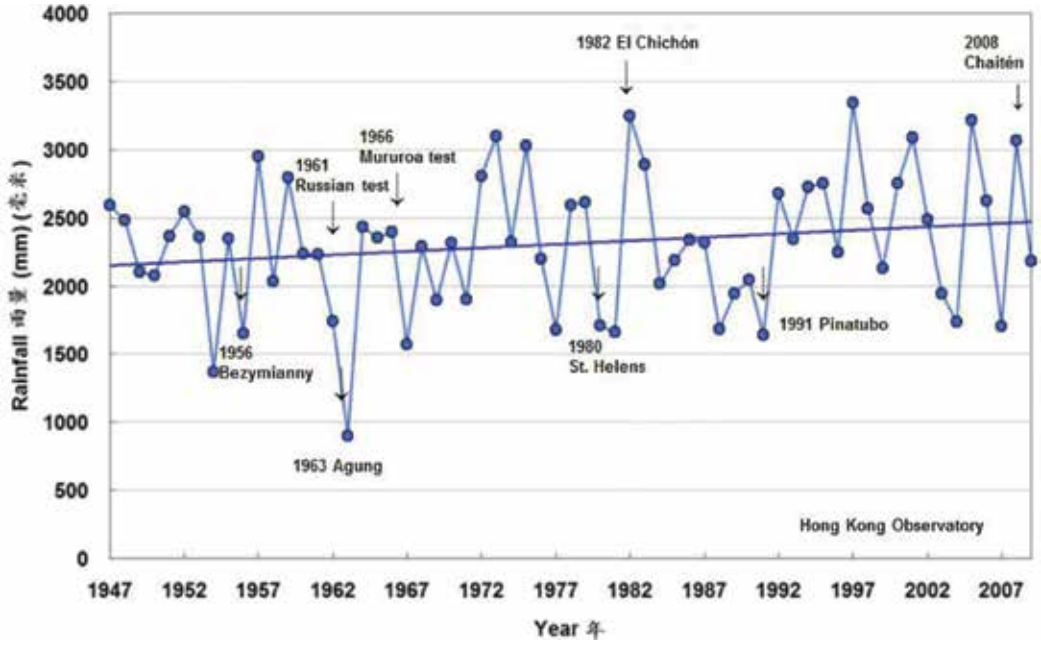

Figure 20. Chaitén eruption cloud on 10 May 2008.

Based on the results of monitoring the volcanic ashes using MODIS in this study and the referred reports, the following inferences can be drawn as below:

(1) On 3 May (**Figure 13**)—The eruption cloud formed a continuous, linear, and sharp-edged plume. The cloud-drifted southeastward reaching the Atlantic coast of Argentina

(2) On 4 May (**Figure 14**)—The volcanic ash fallout direction is toward the southeast which is similar to 3 May. The Chilean town of Futaleufu, located at about 75 km from the volcano, received copious fallout where ash deposition of10–30 cm in thickness is reported in [23] (3) On 5 May (**Figure 15**)—A continuous linear plume with an easterly orientation passed over the Atlantic Ocean. Large quantities of fine ash were reported at Trelew, Rawson and Madryn in [23] in Argentina and several Argentinian regional airports were shut down due to the lack of visibility.

(4) On 6 May (**Figure 16**)—It is reported that the eruption entered a more intense but short-lived phase with column height up to 30 km estimated. This eruption produced a cloud that drifted northeastwards across the Andes into Argentina.

(5) On 7 May (**Figure 17**)—The eruption cloud continued to drift in a northeast direction. Light fallout was reported at Bahia Blanca and Mar del Plata in Argentina in [23], located at more than 1000 km away from the volcano.

(6) On 8 May (**Figure 18**)—The eruption cloud moved in a northeasterly and northerly direction.

(7) On 9 May (**Figure 19**)—There was an increase in eruption activity on 9 May compared to 8 May. The volcanic ash drifted northeastwards reaching the Atlantic coast of Argentina.

(8) On 10 May (**Figure 20**)—A light eruption occurred on 10 May and the volcanic ash drifted eastwards.

4.2. Precipitation impact further downstream

Two examples of downstream precipitation impact over the continent of Australia are shown in **Figures 2** and **3**. It can be clear that the rainfall in June 2008 was much more over that of the Australian continent in the average of 1961–1990 normal. The link with the spread of the Chaitén eruption cloud is supported by the detection of stratospheric aerosol drifting over southeastern Australia by Cloud-Aerosol Lidar with Orthogonal Polarization (CALIOP) in [2]. Similarly torrential June rainfall occurred in South Africa (**Figure 5**) and over Hong Kong (**Figure 6**) in southern China in [24]. From **Figures 4** and **5**, it is obviously that late May, early and middle June 2008 in South Africa, the rainfall had a significant increase compared with that early May. It is reported that heavy rainfall on June 19 across parts of South Africa prompted severe flooding and mudslides. According to reports, Scottburgh, KwaZulu-Natal received a total of 128 mm of rain within 24-h (NOAA). June 2008 in Hong Kong with 1364.1 mm rainfall was the wettest month since record began in 1884. This included a rainstorm with a return period of 1100 years which led to over 2400 landslides on Lantau Island in [25]. The spread of stratospheric aerosols across the Intertropical Convergence Zone was likely to have been assisted by the timing of the early May eruption date which was during the southern hemisphere autumn when solar radiation intensity was decreasing in the southern hemisphere and increasing in the northern hemisphere.

5. Conclusions and future work

We have tracked the transport and deposition of volcanic ash during the first 8 days of May 2008 Chaiten volcano activity in Chile from 3 May to 10 May using MODIS images. The purpose was to learn the dispersion pattern of the eruption cloud and to analyze the possible impacts on rainfall. The volcanic ash detection procedure used in this study is based on the BTD algorithm using the thermal infrared channels centered on 11 and 12 μm of a multispectral satellite sensor. The results of BTD volcanic ash retrieval algorithm have been found to show good agreement with RGB images recorded by NASA-MODIS Terra and Aqua sensors. The eruption cloud was found to drift northeastwards, southeastwards and eastwards following the eruptions, reaching the Atlantic coast of Argentina and beyond over a 8-day period. The timing of heavy rainfall during May/June in South Africa, during June 2008 in central Australia and during June in Hong Kong (the wettest since record began in 1884) was thought to have been connected to the dispersion of particulates further downstream. However, the effective radius of volcanic ash particles and optical depths of clouds detection were not included in this research, but will be considered in our future work.

http://dx.doi.org/10.5772/00000

Acknowledgements

This research is supported by an Open Research Program at State Key Laboratory of Geological Processes and Mineral Resources (GPMR), China University of Geosciences in 2015. MODIS images data from NASA, rainfall images of Australian and South Africa from Australian Bureau of Meteorology and from the website of South Africa Weather Service, and the Hong Kong's annual rainfall data from Hong Kong Observatory (HKO) were acknowledged. The reviewer and editor's critical comments are helpful for improving the manuscript.

Author details

Yuanzhi Zhang[1,2*], Jin Yeu Tsou[2], Zhaojun Huang[2], Jinrong Hu[2] and Wyss W.-S. Yim[3]

*Address all correspondence to: yuanzhizhang@hotmail.com

1 Key Lab of Lunar and Deep-Space Exploration, Chinese Academy of Sciences, Beijing, China

2 Center for Housing Innovations, the Chinese University of Hong Kong, Shatin, Hong Kong

3 Department of Earth Sciences, the University of Hong Kong, Pok Fu Lam, Hong Kong

References

[1] Ellrod, G. P. and Connell, B. H., 2003. Improved detection of airborne volcanic ash using multispectral infrared satellite data, J. Geophys. Res., Vol. 108(D12), 4356.

[2] Carn, S. A., Pallister, J. S., Lara, L., Ewert, J. W., Watt, S., Prata, A. J., Thomas, R. J. and Villarosa, G. 2009. The unexpected awakening of Chaitén volcano, Chile, EOS Trans., Vol. 90(24), 205–206.

[3] Watt, F. L. and Pyle, D. M., 2009. Fallout and distribution of volcanic ash over Argentina following the May 2008 explosive eruption of Chaitén, Chile, J. Geophys. Res., Vol. 114, B04207, doi:10.1029/2008JB006219.

[4] Lara, L. E., 2009. The 2008 eruption of the Chaitén volcano, Chile: a preliminary report, Andean Geol., Vol. 36(1), 125–129.

[5] Scasso, R., Corbell, H., and Tiberi, T., 1994. Sedimentological analysis of the tephra from the 12–15 August 1991 eruption of Hudson volcano, Bull. Volcanol., Vol. 56, 121–133.

[6] Naranjo, J. and Stern, C., 2004. Holocene tephrochronology of the southern most Part (42°30′-45°S) of the Andean Southern Volcanic Zone, Revista Geolgica de Chile, Vol. 31, 225–240.

[7] Guffanti, M., Benitez, C., Andrioli, M., Romero, R. and Casadevall, T. J., 2008. Widespread effects on aviation of the 2008 eruption of Chaitén volcano, Chile, EOS Trans. AGU, Vol. 89(53), Fall Meet. Suppl., Abstract, V42C-03.

[8] NOAA: http://www.ncdc.noaa.gov/sotc/hazards/2008/6

[9] Prata, A. J., 1989a. Observations of volcanic ash clouds in 10–12 μm window using AVHRR/2 data, Int. J. Remote Sens., Vol. 10, 751–761.

[10] Prata, A. J., 1989b. Infrared radiative transfer calculations for volcanic ash clouds, Geophys. Res. Lett., Vol. 16(11), 1293–1296.

[11] Wen, S. and Rose, W. I., 1994. Retrieval of sizes and total masses of particles in volcanic clouds using AVHRR bands 4 and 5, J. Geophys. Res., Vol. 99(D3), 5421–5431.

[12] Hillger, D. W. and Clark, J. D., 2002. Principal component image analysis of MODIS for volcanic ash. Part I: most important bands and implications for future GOES imagers, J. Appl. Meteorol., 41, 985–1001.

[13] Watson, I. M., Realmuto, V. J., Rose, W. I., Prata, A. J., Bluth,G. J. S., Gu, Y., Bader, C. E., and Yu, T., 2004. Thermal infrared remote sensing of volcanic emissions using the moderate resolution imaging spectroradiometer, J. Volcanol. Geoth. Res., 135, 75–89.

[14] Tupper, A., Carn, S., Davey, J., Kamada, Y., Potts, R., and Prata, F., 2004. An evaluation of volcanic cloud detection techniques during recent significant eruption in the western Ring of Fire, Remote Sens. Environ., 91, 27–46.

[15] Corradini, S., Spinetti, C., Carboni, E., Tirelli, C., Buongiorno, M. F., Pugnaghi, S., and Gangale, G., 2008a. Mt. Etna tropospheric ash retrievaland sensitivity analysis using Moderate Resolution Imaging Spectroradiometer measurements, J. Atmos. Remote. Sens., 2, 023550, doi:10.1117/1.3046674.

[16] Corradini, S., Merucci, L., Prata, A. J., and Piscini, A., 2010. Volcanic ash and SO_2 in the 2008 Kasatochi eruption: retrievals comparison from different IR satellite sensors, J. Geophys. Res., 115, D00L21, doi:10.1029/2009JD013634.

[17] Corradini, S., Merucci, L., and Arnau, F., 2011. Volcanic ash cloud properties: comparison between MODIS satellite retrievals and FALL3D transport model, IEEE Geosci. Remote Sens. Lett., 8, 248–252.

[18] Yu T, Rose W. I., Prata A. J. 2002. Atmospheric correction for satellite-based volcanic ash mapping and retrievals using split window IR data from GEOS and AVHRR, J. Geophys. Res. 107 (D16):4311.doi:10.1029/2001JD000706.

http://dx.doi.org/10.5772/00000

[19] Prata, A. J. and Kerkmann, J 2007. Simultaneous retrieval of volcanic ash and SO_2 using MSG-SEVIRI measurements. Geophys. Res. Lett., 34:L05813.doi: 10.1029/2006GL028691.

[20] Pujol, G. C., Rabolli, M., Kalemkarian, M., 2008. Volcanic ash detection, monitoring and environment impact, Servicio Metorologico. Macional. (SMN), 7–17.

[21] Spinetti, C. and Corradini, S., 2007. Volcanic ash retrieval at Mt. Etna using AVHRR and MODIS data, Proc. of SPIE, Vol. 6749, 1–3.

[22] Jiang, L. P. and Qin, Z. H., 2006. Program splits window algorithm to retrieve land surface temperature for MODIS data using IDL, Geomat. Spat.l Inf. Technol., Vol. 29, No.3 Jun., 115–116.

[23] Folch, A., Jirba, O. and Viramonte, J., 2008. Volcanic ash forecast-application to the May 2008 Chaiten eruption, Nat. Hazards Earth Syst. Sci., 8, 927–940.

[24] Yim, W. 2010. Chilean volcano produces trail of destruction. Imperial Engineer, 12(Spring), 10–11.

[25] Kwan, J. S. H., Hui, T. H. H. and Ho, K. K. S., 2011. Modelling the motion of mobile debris flows in Hong Kong. Proc. of Second World Landslide Forum, 3–7 October 2011, Rome, 6 p.

Chapter 4

Increasing the Adaptive Capacity of Indigenous People to Environmental Change: The Potential Use of an Innovative, Web-Based, Collaborative-Geomatics Informatics Tool to Reduce the Degree of Exposure of First Nations Cree to Hazardous Travel Routes

Christine D. Barbeau, Donald Cowan and
Leonard J.S. Tsuji

Additional information is available at the end of the chapter

http://dx.doi.org/10.5772/103394

Abstract

The arctic and subarctic regions of Canada are experiencing amplified climate change impacts, which are disproportionately impacting Canadian indigenous populations' ability to safely travel on land to acquire resources. Less predictable and more dangerous travel conditions are impacting not only the health and safety of individuals but also the traditional lifestyles that are vital to the cultural well-being of these indigenous communities. The University of Waterloo's Computer Systems Group has developed a novel decision-support tool termed "Collaborative-Geomatics." This web-based informatics tool can allow for the community to monitor, in real-time, the safety of travel routes. Using handheld GPS tracking systems, the utility of the geomatics system to present real-time travel conditions was carried out in a Canadian First Nations community, located along the Western James Bay coast. The results of this study showed that the collaborative-geomatics tool offers the potential to monitor and store information on the safety of travel routes, helping to promote adaptive capacity and aid in knowledge transfer within arctic and subarctic indigenous communities.

Keywords: arctic, indigenous, climate change, collaborative-geomatics, safe-travel

1. Introduction

1.1. Global and arctic climate change

With the release of the Fifth Assessment Report by the Intergovernmental Panel on Climate Change (IPCC), it is now unequivocally certain that global warming is due to anthropogenic emissions, resulting in widespread social and ecological impacts [1, 2]. Globally, the atmosphere and oceans have warmed, and there have been more frequent heavy precipitation events and Heat waves [3]. It is becoming apparent that social systems, like ecological ones, are vulnerable to climate change, especially to extreme environmental events [3]. The spatial convergence of climate change impacts will likely compound risks to already vulnerable populations, globally [4]. Regions such as the Arctic are predicted to experience disproportionally greater ecological and social impacts from global warming [5]. Indeed, the duration of the sea-ice-free season has decreased in the arctic–subarctic region of Canada [6], and sea levels have changed and will continue to change [7, 8].

The Canadian arctic and subarctic regions have already experienced a general warming of up to 5°C, the most rapid rates of increasing average surface temperatures in the world [9–11]. Thinning Arctic Sea ice has been documented since 1979 [12]. Satellite imagery of Arctic Sea ice has shown a disturbing pattern in the rate of decline in ice extent. Winter months show a rate of decline in ice occurring at 3.5–4.1% per decade, while summer shows a rate of decline of 9.4–13.6% per decade [12]. Current models are predicting a continued and unprecedented decline in sea ice in the Arctic. Sea ice retreat in the Arctic will significantly impact arctic precipitation; the resulting increase in surface evaporation will lead to an amplified arctic hydrological cycle [13].

Climate models and precipitation trends indicate that there will be a significant increase in rainfall in arctic regions [6, 14–17]. By the end of the twenty-first century, it is predicted that precipitation rates in arctic regions will increase by 50% and will peak during the autumn and winter months, resulting in a likely increase in river discharge [13]. It is very likely that continued warming will result in changes to spring snow and river melt timing, pushing the spring peak flows earlier [18].

Increased atmospheric warming has also impacted permafrost in the Arctic. Since the early 1980s, permafrost temperatures have warmed by approximately 3°C, resulting in an overall thinning and loss in the extent of permafrost. The southern boundary of continuous permafrost in the arctic–subarctic region has already advanced northward by approximately 50 km [12]. Warming global temperatures are producing climate extremes. Arctic regions have already recorded increased wind speeds in all seasons [18]. Changes to sea-level pressure around mid-latitudes have resulted in longer and more frequent winter storms over the lower Canadian arctic [18]. Continued global warming is predicted to not only have devastating and irreversible ecological impacts on the arctic–subarctic environment, but it is now becoming apparent that there will also be equally significant social impacts on the individuals and communities who call this region home.

http://dx.doi.org/10.5772/103394

1.2. Risk and challenges associated with climate-related impacts

Globally, indigenous groups represent some of the most vulnerable populations, but are rarely considered in climate change discourse [19]. It is expected that the world's indigenous populations, living in arctic and subarctic regions, are some of the most vulnerable and will experience the greatest impacts of climate change [20, 21]. Within Canada, indigenous communities are defined as including First Nations, Inuit, and Métis people. The 2011 Canadian National Household Survey determined that just over 4% of Canada's population, approximately 1.4 million people, is indigenous [22]. Canadian indigenous people experience many inequalities compared to Canadian nonindigenous people, such as shorter life expectancy, higher rates of diabetes and infectious disease (e.g., tuberculosis), and higher rates of suicide and substance abuse [23, 24]. Approximately half of Canada's indigenous population—referred to as Aboriginal Peoples in the Canadian Constitution—live in northern Canada, on reserves, or in rural and remote communities [25]. Remote indigenous populations usually share close relationships with the land and practice traditional land-based lifestyles [26, 27]. Thus, indigenous groups living in Canada's arctic and subarctic regions are particularly vulnerable to climate change due to their interconnectedness with the land [25, 28].

Traditional ways of living include hunting and harvesting practices that are guided by seasonal cycles. Using environmental indicators such as seasonal cycles, indigenous groups have been able to predict seasonable changes and weather patterns [29]. This indigenous knowledge about the land, termed "traditional ecological knowledge (TEK)" can be defined as being "a body of knowledge and beliefs transmitted through oral tradition and first-hand observation. It includes … a set of empirical observations about the local environment … With its roots firmly in the past, TEK is both cumulative and dynamic, building upon the experience of earlier generations and adapting to the new technological and socioeconomic changes of the present" [30]. Therefore, this knowledge played an important role in the adaptation to environmental conditions on a seasonal and yearly basis [31]. However, social inequalities such as the introduction of residential schools in Canada in the 1930s have resulted in a loss of language, culture and knowledge, and the disruption of transmission of TEK between generations [24, 32]. This loss of TEK, coupled with preexisting marginalization, and the increase in unpredictable environmental changes (e.g., increase in the number and severity of storms, increased flooding, sea ice, and river changes) as a result of climate change reveal the vulnerability of northern Canadian indigenous communities. Climate-induced changes are expected to create challenges for indigenous people living in Canada's north, some of which are already being seen. These challenges, both observed and predicted, can be related to access to resources, and health and safety [33].

The ability to travel on land, ice, snow, and by water to acquire resources is an integral part of many indigenous peoples' lifestyles. Traditional ways of life for many indigenous communities involve the consumption of seasonal foods, such as waterfowl, game mammals, and fish [29]. Changes to the timing of ice breakup and river depths can affect access to family hunting camps. Often traveling by boat or snowmobile, changes to ice depths, snow type, river depths, and ice-free areas can significantly hinder the ability to get to these camps along with the length of time that can be spent there [33]. A recent study showed that one of the most significant

impacts of changing winter conditions is the inability to travel onto the land and participate in traditional harvesting activities, resulting in emotional feelings of being trapped and imprisoned [34]. Furthermore, participants reported changes to their eating habits, consuming more costly and less nutritious store-bought foods.

Related to this ability to access traditional resources and the importance behind such resources, the safety of indigenous people while out on the land is an important challenge when facing the impacts of climate change. Younger generations, especially, are viewing the land with more fear and uncertainty and believe that it is less accessible [35, 36]. Many safety issues are arising in relation to sea ice and early spring thaws. In many indigenous communities, sea ice is important for winter hunting activities such as hunting sea mammals [33]. However, ice conditions are less reliable, and sudden changes in ice conditions are becoming more common, resulting in safety issues for those who are out on the land and water. Changes in ice thickness, ice condition, ice movement, and the extent of open water can become a safety issue While out on the ice hunting. Also, early thawing of ice and ground along bush trails is resulting in stranded snowmobiles and increased risk of drowning and hypothermia [37]. Sudden changes to wind conditions often occur rapidly, resulting in dangerous and potentially life-threatening conditions for those already out on the land and water, making navigation difficult. Research has shown that the incident rate of accidents in northern coastal indigenous communities has increased as a result of changes in weather [37]. Furthermore, an increase in extreme weather events, such as an increase in unpredictable and intense summer storms, presents a risk to boaters out on the water [37, 38].

Cultural impacts as a result of these climate-induced changes are affecting the psychological status of many indigenous people [39]. Since traditional harvesting activities allow for the development of social relationships and the processing and consumption of traditional foods [39], any disruption to these activities negatively impacts indigenous culture.

Safety while out on the land relates to the predictability of environmental conditions (e.g., weather) [33]. Historically, indigenous people have been able to predict environmental conditions through their intimate knowledge of the land; however, it has become more difficult to use traditional knowledge to predict environmental events (e.g., ice breakup and weather patterns), as these things are occurring "at the wrong time" [33]. There is concern that as adaptive and flexible as TEK is, the rate and magnitude of climate-induced change might be too unpredictable for TEK to adapt [33, 40]. Therefore, there is a need for decision-support tools that are culturally appropriate and community-informed that can display real-time information on the safety of travel routes in arctic and subarctic indigenous communities [41–43].

1.3. Using geomatics to make travel safer

Since the 1990s, indigenous communities throughout Canada have been using Geographic Information Systems (GIS) for mapping [44], defined as "an organized collection of specific computer hardware, software, geographic data and personnel designed to efficiently capture, store, update, manipulate, analyze and display all forms of geographically referenced information (e.g., raster/vector) that can be drawn from different sources" [45, 46]. Within indige-

http://dx.doi.org/10.5772/103394

nous communities, GIS have been used to map information, such as traditional land use (e.g. hunting, fishing, and harvesting) [44, 47]. The ability to map traditional land-use activities and assets has played an important role in the collection and storage of TEK. Unlike traditional paper maps, GIS maps have the ability to be easily developed and modified to represent and archive current environmental conditions and/or traditions [44]. However, there has been concern, within the academic arena, that GIS can be a marginalizing technology [48]. Concern over how people, space, and the environment were represented by GIS systems has resulted in the shift from GIS technology to public participation GIS (PPGIS).

PPGIS draws upon conventional GIS techniques and builds upon them, allowing for what has been described as "a wider, more distributed use and development of geographic data, information, and knowledge" [49]. Although hard to define, PPGIS has been described as "the use of geographic information systems (GIS) to broaden public involvement in policy making as well as to the value of GIS to promote the goals of nongovernmental organizations, grassroots groups and community-based organizations" [49, 50]. PPGIS supports a range of interactive approaches and web-based applications that focus on ease of use and accessibility to support youth, elders, women, First Nations, and other vulnerable segments of society that have often been marginalized and excluded from decision-making processes [48]. Within arctic and subarctic indigenous communities, PPGIS offers the opportunity for communities to work together and build a database of value-based information [50]. This collection of information can lead to increased adaptation with respect to the impacts of climate change, through empowerment and knowledge sharing, between community and family members. Travel route (e.g., bush trails, ice roads) mapping on a real-time basis can help community members to be proactive and make informed decisions, on the safety of trail and ice-road conditions prior to heading out onto the land. It is with this knowledge, and First Nations community involvement, that the Computer Systems Group at the University of Waterloo developed a PPGIS termed "Collaborative-Geomatics."

Geomatics is a method used to link geospatial data (e.g., cities, regions, and countries) and attribute data (e.g., social, economic, ecological, and cultural data) [51]. Collaborative-geomatics is a PPGIS mapping tool based on geo-web technology where participants can collaborate, discuss, and communicate about community-based cultural asset maps and databases [49, 52]. The use of the collaborative-geomatics informatics tool by First Nation groups has been shown to build capacity in the communities through the complementary archiving of Western science and TEK [53], while having the potential to use the collaborative real-time function to plan and deal with the complex and dynamic nature of environmental change within subarctic environments. In this context, we worked with a subarctic First Nation community to develop and implement a collaborative-geomatics informatics tool that can use real-time geospatially referenced environmental change information to reduce the degree of exposure to unsafe travel routes and support the growth of community-wide adaptive capacity. In this chapter, we will present results from the initial step in our iterative process, related to the development of a decision-support tool (i.e., the collaborative-geomatics informatics tool) to reduce the degree of exposure of First Nations Cree people to hazardous bush travel routes.

2. Methods

2.1. Study location

The western James Bay region of Ontario, Canada, is populated by ~10,000 First Nation Cree who inhabit four coastal First Nations communities and one town (i.e., Moosonee; **Figure 1**) [54]. Within Canada, First Nation Cree make up the largest and most widely distributed populations of Aboriginal groups. Our focal community, Fort Albany, is located on the Albany River (52°15′N, 81°35′W), being a remote fly-in community with a population of approximately 900 people. Year-round access to the village is by aircraft only, with ice-road access in the winter. The James Bay winter road is 312 km long and connects the First Nations community of Attawapiskat in the north to Moose Cree First Nation (i.e., the community of Moose Factory) in the south, running by the First Nations communities of Kashechewan and Fort Albany (**Figure 1**). The winter road is a vital connection for First Nations communities along the western James Bay coast. These roads provide access to hunting camps, fishing sites, firewood collection areas, and other important subsistence activity sites. The winter road is also a lifeline that connects families that are spread out between the communities along the coast. With access to Moose Factory and Moosonee in the winter (Moosonee is the northern terminus of the rail line),more northern communities have the ability to purchase less-expensive food and household supplies. Fiber-optics and/or satellite Internet connections are

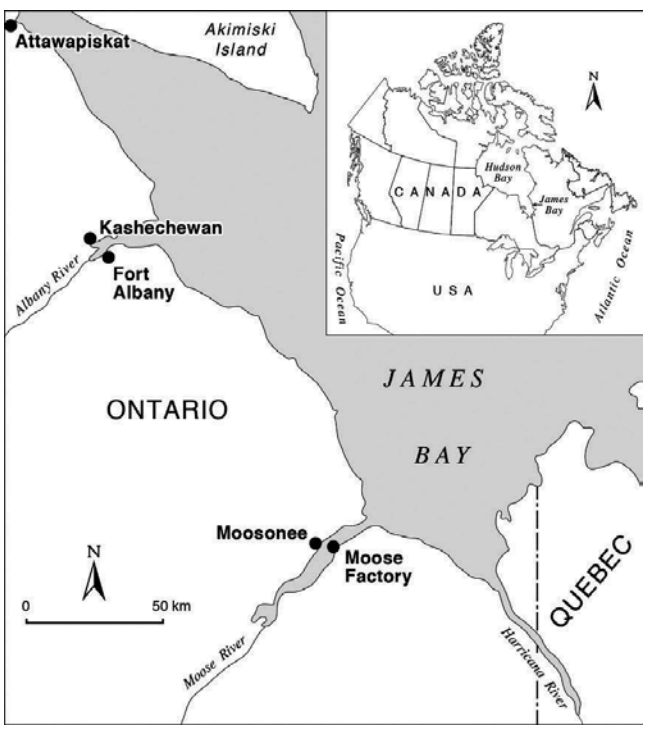

Figure 1. Map of the Mushkegowuk Cree First Nations territory, Western James Bay, Ontario, Canada.

http://dx.doi.org/10.5772/103394

available in all the western James Bay communities, with cell phone service only available in Moose Factory and Moosonee.

Fort Albany lies within the Mushkegowuk Territory (i.e., the western James Bay region), which is composed of ecologically important muskeg and wetlands. This region provides resources that many First Nations rely upon for subsistence, such as traditional game species (e.g., large ungulates, small mammals, game birds, fish), which are also socially and culturally important [55, 56]. Seasonal harvest of traditional foods is still an important part of life for First Nation Cree along the James Bay coast [29, 54]. The spring harvest, which begins in the middle of March, with the setting up of spring camps, is an important time of the year for the harvesting of traditional food that will be stored for consumption throughout the year. This time spent out on the land is also an important time where families come together to reaffirm their culture [57]. The spring hunt continues until river breakup, late April or early May [29, 58].

With respect to climate change, this region has already experienced significantly earlier sea-ice breakup events (0.8 days/year) and significantly longer sea-ice-free seasons (0.32–0.55 days/year) [6, 56, 59]. The Albany River and Attawapiskat River have also seen earlier breakup dates impacting the communities along their banks [56, 58]. Sudden warming events in the late spring combined with increased rainfall events have been attributed to extreme flooding events in the First Nations communities along the Albany River [60]. It is predicted that by the year 2100, in the western James Bay region, summer temperatures will increase by 4.1°C and winter temperatures by 7.5°C, along with an increase in extreme weather events [11].

2.2. The collaborative-geomatics informatics tool

The term collaborative geomatics is defined as "a participatory approach to both the development and use of online, distributed-authority, geomatics applications" [46]. Similar to neogeography, collaborative-geomatics builds upon the concept of PPGIS and collaborative GIS, where public participation is paramount [46]. Collaborative-geomatics is a system that is "centered on the designs, processes, and methods that integrate people, spatial data, exploratory tools, and structured discussions for planning, problem solving, and decision-making" [61].

What makes our geomatics decision-support tool unique is that it is based on the declarative application engine termed Web Informatics Development Environment (WIDE). The WIDE software toolkit [52] was developed over the last 17 years by the University of Waterloo Computer Systems Group (http://csg.uwaterloo.ca/) to construct, design, deploy, and maintain relatively inexpensive, secure, complex, web-based, and mobile systems [62]. The WIDE toolkit allows for a forms/wizards-based approach to system construction that supports the rapid development and modification of the tool. The WIDE toolkit is based on HTML, JavaScript, and PHP, and is provided as a software service over the Internet while supporting standard web browsers [46]. The security model is role-based.

The collaborative-geomatics informatics tool first deployed in 1992 supports a common high-resolution imagery reference map, similar to how Google Earth® presents data [49] (**Figure 2**). Some of the basic features of the tool include the entry of real-time geospatial information

(oral, written, and visual [photographic, video]) that is securely housed within the system through accessibility safeguards (user names and passwords). The ability to develop groups within the system and send both public and private messages, similar to Facebook® Messenger®, supports the development of social networks (**Figure 3**). Furthermore, a forums section within the system allows for members to discuss a variety of topics with other users in their community network (**Figure 4**).

Figure 2. Satellite imagery on the collaborative-geomatics informatics tool of Fort Albany First Nations.

Figure 3. Group development application on the collaborative-geomatics informatics tool.

http://dx.doi.org/10.5772/103394

Figure 4. Forum development application on the collaborative-geomatics informatics tool.

The WIDE toolkit and collaborative-geomatics system is a proven technology that has been successfully used in over 80 governmental, community, resource management, and cultural heritage applications [46, 49]. One question that had been raised in the initial development of the geomatics tool with chiefs and councils of Fort Albany First Nations, and community members, was that of the security/confidentiality of TEK such as locations of hunting camps and community bush trails that will be collected and stored in the informatics tool. As TEK is an intellectual property, the security of TEK is of utmost importance. It was explained that all data (including TEK) would be stored only on secure servers within the communities (and/or secured data vaults off-site). Added to the physical security aspect of the tool, TEK would also be operationally secure with access to TEK on the tool being password-protected through profiles vetted by the chosen representatives of the individual communities. In some cases, differential access would be controlled by the chiefs and councils, while in other cases by family gatekeepers [49]. Granting of differential access was dependent on the type of TEK and the proposed use of TEK [46, 49]. It should be emphasized that other iterations of the informatics tool have provided storage for sensitive data for government ministries using exactly the same safeguards as described above [46]. Even the researchers do not have access to TEK on the tool unless granted by a gatekeeper. Our approach is guided by the indigenous principles of OCAP [63]: community Ownership, Control, Access, and Possession of their data. With the data housed within the communities and with the applications accessible through any Internet connection, the short-term accessibility is not in question. Over the medium- to long-term, there were concerns about the sustainability of a system that requires upgrades and development from a third-party organization. Given this issue, a stand-alone version of WIDE toolkit is currently being developed to allow communities to create their own unique applications for their informatics tool [49]. With some basic training, community members could develop and evolve their system to meet the future geospatial knowledge needs; this is one of the unique features of the WIDE toolkit's wizards-based approach.

2.3. Field testing of the informatics tool

In 2016, using handheld Global Positioning Systems (GPS) (Garmin® Oregon® 550) alongside a mobile Apple iPhone® GPS tracking app (Track Kit®), the western James Bay winter road was tracked by vehicle and the associated .GPX files were uploaded onto the collaborative-geomatics informatics tool. The Garmin GPS units have been shown by previous research in the same subarctic community to be easy to transport and were easy to use when tracking and georeferencing important locations [64]. The Apple iPhone® GPS tracking app (Track Kit®) was chosen to act as a backup, and to support the tracking of travel routes, due to the low cost associated with this program and the fact that many community members in Fort Albany own and use Apple products, such as the iPhone®, iPad®, and iPod®, all of which are supported by the Track Kit® app. Prior to using the app, the associated background map of the western James Bay coast was loaded from an Internet connection.

While mapping the winter road, important river crossings and areas known to flood were marked as waypoints and photographed. These waypoints and photographs were then uploaded onto the informatics tool. Community bush trails as identified by community members were also tracked using the same GPS devices. With the help of a community elder, these trails were driven by snow machine, and the use and cultural importance of these travel routes were discussed. These tracks were saved as .GPX files and uploaded onto the informatics tool as a bush-trail layer. Important landmarks were also marked using waypoints and photographed using both the GPS cameras and Apple iPhone® camera. The collaborative-geomatics informatics tool supports photographs uploaded in either .JPG, .PNG, or .GIF file format. The initial evaluation of the potential use of the collaborative-geomatics informatics tool was qualitative, using a combination of field notes and participant observations [64–66].

3. Results and discussion

3.1. Ease of use (hands-on testing)

With the use of handheld GPS tracking systems, the community bush trails and the winter ice road were successfully tracked and uploaded as .GPX files onto the collaborative-geomatics informatics tool. Pictures and important locations were also noted and marked as waypoints and uploaded (as .JPG files) onto the informatics tool (**Figure 5**). The ability to add geospatial information in the form of photographs/videos in real-time has the ability to provide even more detailed information on travel conditions.

Travel conditions were color-coded according to road and trail conditions (white = clear conditions; yellow = use caution, some areas may become dangerous; red = avoid use, dangerous conditions). Five of the most frequently used community bush trails were mapped along with the 312 km James Bay winter road, both north (**Figure 6**) and south of Fort Albany. Overall, the ability to track and map community travel routes and upload them as a layer onto the informatics tool was simple and accurate; we could visualize the winter road on our base layer, satellite imagery, to check the accuracy of the waypoints uploaded. While the Garmin®

http://dx.doi.org/10.5772/103394

GPS units were easy to use, the ease of use and ability to take detailed pictures and notes on the mobile App made the Track Kit® app the most useful GPS unit in mapping travel routes. Furthermore, the preloaded high-resolution imagery on the App allowed for navigation while traveling along the bush trails and winter road.

Figure 5. Geospatially referenced photograph of a river-crossing located on the James Bay winter road.

Figure 6. James Bay winter road, north of Fort Albany First Nations to Attawapiskat First Nation, tracked via handheld GPS units and uploaded as a layer onto the collaborative-geomatics informatics tool.

3.2. Potential use of the collaborative-geomatics informatics tool to build adaptive capacity

The meanings of names and relationships with the land are often propagated in narratives from elders to children. This oral history helps First Nation children to develop a sense of place within their environment from a very young age. This sense of place with the land and the

memories and connections to a place are responsible for guiding future societal activities, land uses, oral history, and cultural transmissions of traditional knowledge. It is widely recognized that First Nations have developed an extensive understanding of the environment [67]. In the past, this knowledge of the environment was transmitted within and between generations, solely through oral traditions. This knowledge allowed First Nations to sustain their subsistence lifestyles and adapt to environmental change. Historically, northern indigenous communities addressed changes in the environment through TEK and skillsets acquired over generations on the land [33, 38]. Due to rapid changes in the environment as a result of a warming climate, knowledge once used to respond and adapt is becoming increasingly difficult to apply, thus decreasing First Nations' adaptive capacity [33, 38]. As environmental change continues in the arctic and subarctic regions, the resulting direct and indirect impacts have affected and will affect traditional lifestyles [11, 56]. At present, there is a great disconnect between what is currently being done on a global climate scale in terms of adaptation measures to climate change and what is needed locally [33, 68]. Increasing a community's adaptive capacity is one way in which vulnerability can be reduced [69, 70]. The collaborative-geomatics informatics tool is a decision-support tool that has the potential to increase the adaptive capacity of northern Canadian indigenous people to climate change impacts.

The following factors have resulted in less predictable and more dangerous travel routes: changes in the extent and extant of ice on lakes and rivers; later ice formation; earlier and more rapid spring melting; changes in the quality and amount of snow; increased precipitation, especially in the form of freezing rain; increased wind events; unpredictable wind directions; and an increased number of storms [42, 71–73]. The biophysical impacts of climate change on the safety of travel routes in the Canadian arctic and subarctic are having negative physical, social, cultural, and economic impacts on the indigenous communities in the region [27, 36, 41, 72, 74]. The collaborative-geomatics informatics tool has the potential to act as a decision-support tool to make bush travel safer, by promoting informed decisions prior to bush travel. The real-time capabilities of the tool can help determine the safest and most appropriate travel time and route prior to heading onto the land. This knowledge can not only directly protect the health and safety of individuals but also help relieve the anxiety associated with the unpredictability of travel routes, thus allowing for greater ability to practice traditional land use.

The collaborative-geomatics informatics tool would allow for the support of social networks where real-time travel information in the form of mapped trails/commentary/picture/videos can be posted online, allowing for further networking and discussion. The sharing of information via social networks can further help to rapidly mobilize community response in times of crisis [38]. Indeed, Pennesi et al. noted that one of the main barriers toward climate change adaptation in the arctic was the lack of social networks to support the informed decision on the safety of land-based activities [74]. Historically, community and family units played an important role in supporting adaptive capacity in northern indigenous communities [38]. However, with changes to the social and cultural structures, many indigenous communities have seen radical changes in lifestyles, resulting in the erosion of the social networks that have historically supported adaptation to environmental challenges [38]. The building and support

http://dx.doi.org/10.5772/103394

of social networks in arctic indigenous communities to build relationships of support and trust have been identified as key components in contributing to adaptability [38]. The collaborative-geomatics informatics tool has the potential to support the use of multiple social networks, where users can invite others to join a group and share specific information with those members.

Thus, the collaborative-geomatics informatics tool has the potential to increase the adaptive capacity of arctic–subarctic indigenous communities by supporting the transfer of TEK (**Table 1**). The transfer of information can be horizontal across age groups and/or vertical between age groups [57, 64]. Adaptive capacity has been described as "a set of resources that represent an asset base from which adaptations can be made" [41]. TEK plays a pivotal role in the manifestation of adaptive capacity and is considered to be a vital component in the effectiveness of adaptive strategies [5, 41, 57, 74].

Features of the informatics tool	Importance
Geospatial information (oral, written, visual [picture/video])	• Ability to store geospatial information on culturally important locations, such as bush trails [64, 43]
	• Linking youth and elders through technology and traditional knowledge in the form of oral history [43]
Social networking (groups and forum development)	• Allows for social networking to help decrease the risks associated with heading out onto the land
	• Formation of groups and forums within the geomatics tool to share information and discuss experiences [43]
	• Communication can foster the collaboration and exchange of information between individuals and communities along the coast that share resources and travel routes [38]
Real-time capabilities	• Real-time travel information will allow families and community members to determine the safest time to travel and empower youth to travel onto the land
	• Greater safety can allow for more travel between communities and the resulting transfer of knowledge
	• Real-time capabilities can help with the selection of the safest travel route going out on the land

Table 1. Key features of the collaborative-geomatics informatics tool important for the monitoring of unsafe travel routes.

Access to TEK is important in the formation of appropriate adaptive responses that together support the building of adaptive capacity. The effectiveness and strength of an adaptive

measure is directly related to the quality of information available [42]. Individuals and communities that readily have access to TEK will possess the depth of knowledge required to develop strong adaptive responses toward hazardous and unpredictable travel routes. Three areas of adaptive responses, *flexibility, hazard avoidance*, and *emergency preparedness*, have been identified as being important in building adaptive capacity in the arctic [4, 42]. The collaborative-geomatics informatics tool has the ability to support each of these adaptive responses.

The diversity and flexibility in travel routes and resources are vital in the adaptability toward unpredictable climate events and dangerous travel conditions [38]. The collaborative-geomatics informatics tool imbues flexibility, by allowing for modification and adjustments to travel routes prior to heading out onto the land. Based on real-time trail and road conditions, decisions can be made with respect to changes in the modes of transportation, harvesting equipment, and location of harvesting activities [41, 75]. Flexibility and diversity in behavior lead to the development of new skills and knowledge, which can further support the ability to make flexible and diverse decisions, resulting in increased adaptive capacity. There are some constraints to behavioral flexibility that can be addressed through features of the collaborative-geomatics informatics tool. Income constraints have been shown to restrict the flexibility and diversity of behaviors [75]. Changes in the mode of transportation and type of harvesting equipment are resource-dependent and can act as barriers to adaptation. Social networking, such as discussion forums and group settings, supported by the informatics tool, can link community members together to share resources, exchange ideas, and develop groups that could pool their resources and travel together.

Hazard avoidance of dangerous and unsafe travel routes is another adaptive response important to the development of increased adaptive capacity. Technology has been shown to play an important role in the avoidance of hazards [41]. Geospatial information provided in the informatics tool acts as a knowledge base from which individuals and groups can accurately identify real-time hazardous locations and determine the safest way to travel or whether to travel at all. Photographs and videos uploaded onto the tool can also provide valuable in-depth detail and real-time travel information of hazards to be consulted prior to heading out onto the land. The real-time capabilities of the informatics tool can also support more efficient maintenance and repair of hazardous locations on travel routes. Geospatial information uploaded onto the tool can inform ice-road maintenance crews of the exact locations of hazardous conditions, allowing for quicker and more efficient resource use.

When facing unpredictable environmental conditions, emergency preparedness is an important adaptive response. Anticipating adverse travel conditions prior to traveling can help avoid dangerous and potentially deadly situations. The collaborative-geomatics informatics tool can serve as a decision-support tool that allows individuals and groups to make informed decisions on travel conditions before heading out. Some of these decisions are regarding the equipment and supplies required to travel safely. The modification of equipment used while on the land, such as more powerful boat engines and snowmobiles, can reduce the degree of exposure to dangerous situations [38]. The packing of extra and/or emergency supplies (e.g., extra gas, food, water, and warm clothing) is a proactive adaptive response to hazardous (or potentially hazardous) situations while traveling on the land. The informatics tool can help in emergency

http://dx.doi.org/10.5772/103394

preparedness through proactive route planning. Individuals or groups heading out onto the land can geospatially mark locations on the tool, prior to heading out, to identify where they could be located if any issues were to arise. Furthermore, the social networking abilities of the tool can help to bring individuals together to form traveling groups, reducing the likelihood of emergencies and sharing of supplies to reduce the costs associated with bush travel. In this way, communities can build their adaptive capacity to deal with an unpredictable environment.

A dimension of adaptive capacity is the ability for a community to be innovative [46, 76]. Innovation can be defined as an "initiative, product, process, or program that profoundly changes the basic routines, resources, and authority flows or beliefs of any social system" [46, 76]. The collaborative-geomatics informatics tool can not only help reduce the degree of exposure to unsafe travel routes, but it can also allow communities to monitor, store, and analyze various forms of information to help monitor cumulative impacts of environmental change in the area. The ability of the informatics tool to nurture diversity and flexibility of different forms of knowledge is a key attribute to the development of innovation [46]. Increased innovation would allow for subarctic First Nations communities to not only adapt to climate-related impacts, but also actively engage in community-based land-use planning, increasing the community's ability to respond to change associated with the ever-increasing developmental pressures in the region [46].

3.3. Future development of the informatics tool

The next step in the development and implementation of this real-time informatics tool will be to work toward developing it as a mobile App supported by Apple iPhone®, iPad®, iPod®, and Andriod® phones. This would allow for the tracking and mapping of not only community travel routes, but also personal and family trails. With the development of a collaborative-geomatics informatics tool mobile App, the tracking of travel routes and the storage of TEK could be accomplished without the expense of having to purchase GPS tracking devices. Furthermore, due to privacy concerns around third party Apps, a mobile geomatics App would allow individuals to have control over their own information. Having a handheld informatics tool that could seamlessly track travel routes and automatically upload trails without the use of cables and computers would allow for greater accessibility by community members who might not have access to computers and the skills to use traditional GPS devices. Another added benefit of developing a handheld mobile version of the informatics tool would be using the tool for navigation. High-resolution base maps used in the current geomatics system, when loaded onto the tool prior to heading out onto the land, could act as a navigation tool to help guide individuals or groups around hazardous areas or during emergencies.

Although the monitoring and mapping of real-time safe-travel routes is a specific application, this collaborative-geomatics informatics tool could also be used for other purposes [64]. Once the collaborative-geomatics informatics tool has been fully community-tested and modified to meet the community's needs, the informatics tool will be given to the community, as a stand-alone secure system, at no cost to the community. It should be emphasized that this type of innovative approach and technology has the potential to help other indigenous communities

in the Canadian arctic and subarctic, as well as indigenous communities located outside of Canada.

4. Conclusion

It is clear from numerous scientific studies that global air temperatures are rising at a rate never experienced before. This elevation in temperatures impacts Earth's ecosystems, resulting in changes in snowfall, rainfall, sea levels, and species distributions. Such environmental changes have been well documented, but there has been relatively little research into the impacts of climate change on social systems. As the global population continues to rise and the divide between the rich and poor widens, it is expected that climate change effects will disproportionately impact already marginalized populations. Furthermore, experts predict that northern latitudes will experience the greatest impacts of environmental change due to global warming. First Nations communities in Canada have a history of marginalization and social inequalities, especially in communities located in the northern regions of the country. Despite these differences, there has been relatively little done to mitigate the impacts of environmental change on indigenous people. The ability to travel on land, ice, snow, and by water to acquire resources is an integral part of many indigenous people's lifestyles. However, changes to the extent and extant of ice on lakes and rivers, changes in the quality and quantity of snow, increased precipitation especially in the form of freezing rain, and unpredictable storms have resulted in less predictable and more dangerous travel conditions, impacting not only the health and safety of individuals but also the traditional lifestyle that is vital to the cultural well-being of these indigenous communities.

This study set out to examine the potential of a novel decision-support tool to reduce the degree of exposure to unsafe travel routes for James Bay Cree. It is clear from this research that the collaborative-geomatics informatics tool developed by the University of Waterloo's Computer Systems Groups has the potential to allow for the community to monitor, in real-time, the safety of travel routes. The ability to monitor and store information, on the safety of travel routes, has the potential to promote adaptive capacity and aid in knowledge transfer within arctic and subarctic First Nations Cree communities. The use of TEK and Western science as complementary knowledge system should be encouraged [77]. Increased adaptive capacity can lead to social and ecological resilience, allowing indigenous communities to better withstand the shocks and stresses that further environmental change and future resource development will bring [70, 78, 79].

Acknowledgements

We thank all participants, the community of Fort Albany First Nations and acknowledge support from the Social Sciences and Humanities Research Council of Canada, the National Science and Engineering Research Council of Canada, and the Canadian Institutes of Health Research (IPH #143068).

Author details

Christine D. Barbeau[1*], Donald Cowan[2] and Leonard J.S. Tsuji[3]

*Address all correspondence to: cbarbeau@uwaterloo.ca

1 School of Environment, Resources and Sustainability, University of Waterloo, Waterloo, ON, Canada

2 David R. Cheriton School of Computer Science, University of Waterloo, Waterloo, ON, Canada

3 Health Studies, Department of Physical and Environmental Sciences, University of Toronto Scarborough, Toronto, ON, Canada

References

[1] IPCC. Climate Change 2014 Synthesis Report Summary for Policy Makers. 2014. Available from: http://www.ipcc.ch/pdf/assessment-report/ar5/syr/AR5_SYR_FINAL_SPM.pdf [accessed: 2016-01-01].

[2] IPCC. Climate Change 2014: Synthesis Report. Contribution of Working Groups I, II and III to the Fifth Assessment Report of the Intergovernmental Panel on Climate Change [Core Writing Team, Pachauri RK, Meyer LA (eds.)]. Geneva, Switzerland, IPCC. 2014. p. 151.

[3] Wilbanks TJ, Romero Lankao P, Bao M, Berkhout F, Cairncross S, Ceron JP, et al. Industry, settlement and society. In: Climate Change 2007: Impacts, Adaptation and Vulnerability. Contribution of Working Group II to the Fourth Assessment Report of the Intergovernmental Panel on Climate Change [Parry ML, Canziani OF, Palutikof JP, van der Linden PJ, Hanson CE (eds.)]. Cambridge, Cambridge University Press. 2007. p. 357–390.

[4] Noble IR, Huq S, Anokhin YA, Carmin J, Goudou D, Lansigan FB, Osman-Elasha B, Villamizar A. Adaptation Needs and Options. In: Climate Change 2014: Impacts, Adaptation, and Vulnerability. Part A: Global and Sectoral Aspects. Contribution of Working Group II to the Fifth Assessment Report of the Intergovernmental Panel on Climate Change [Field CB, Barros VR, Dokken DJ, Mach KJ, Mastrandrea MD, Bilir TE, et al. (eds.)]. Cambridge, United Kingdom and New York, NY, USA, Cambridge University Press. 2014. p. 833–868.

[5] IPCC. Climate Change 2014: Impacts, Adaptation, and Vulnerability. Part A: Global and Sectoral Aspects. In: Contribution of Working Group II to the Fifth Assessment Report of the Intergovernmental Panel on Climate Change [Field CB, Barros VR,

Dokken DJ, Mach KJ, Mastrandrea MD, Bilir TE, et al. (eds.)]. Cambridge, United Kingdom and New York, NY, USA, Cambridge University Press. 2014. p. 1132.

[6] Gough WA, Cornwell A, Tsuji LJS. Trends in seasonal sea ice duration in southwestern Hudson Bay. Arctic. 2004;57:299–305. DOI: 10.14430/arctic507

[7] Tsuji LJS, Gomez N, Mitrovica JX, Kendall R. Post-glacial isostatic adjustment and global warming in sub-arctic Canada: Implications for islands of the James Bay region. Arctic. 2009;62:458–467. DOI: 10.14430/arctic176

[8] Tsuji LJS, Daradich A, Gomez N, Hay C, Mitrovica JX. Sea-level change in the western James Bay region of sub-arctic Ontario: Emergent land and implications for treaty No. 9. Arctic. 2016;69:99–107. Available from: http://arctic.journalhosting.ucalgary.ca/arctic/index.php/arctic/article/view/4542/4690 [accessed 2016-03-03].

[9] Anisimov O, Vaughan D, Callaghan T, Furgal C, Marchant H, Prowse T, et al. Polar regions (Arctic and Antarctic). Climate Change 2007: Impacts, Adaptation and Vulnerability. In: Contribution of Working Group II to the Fourth Assessment Report of the Intergovernmental Panel on Climate Change [Parry M, Canziani O, Palutikof J, van der Linden P, Hanson C. (eds.)]. Cambridge, Cambridge University Press. 2007. p. 653–685.

[10] Gagnon AS, Gough WA. Hydro-climatic trends in the Hudson Bay region, Canada. Can Water Resour J. 2002;27(3):245–262. Available from: http://www.tandfonline.com/doi/pdf/10.4296/cwrj2703245 [accessed: 2015-10-11].

[11] Hori Y, Tam B, Gough WA, Ho-Foong E, Karagatzides JD, Liberda EN, Tsuji LJS. The use of traditional environmental knowledge to assess the impact of climate change on subsistence fishing in the James Bay Region of Northern Ontario, Canada. Rural Remote Health. 2012;12:1878.

[12] IPCC. Climate Change 2013: The Physical Science Basis. Contribution of Working Group I to the Fifth Assessment Report of the Intergovernmental Panel on Climate Change [Stocker TF, Qin D, Plattner GK, Tignor M, Allen SK, Boschung J, et al. (eds.)]. Cambridge, United Kingdom and New York, NY, USA, Cambridge University Press. 2013. p. 1535

[13] Bintanja R, Selten FM. Future increases in Arctic precipitation linked to local evaporation and sea-ice retreat. Nature. 2014;509:479–482. DOI: 10.1038/nature13259

[14] IPCC. Climate Change 2007: Synthesis Report. In: Contribution of Working Groups I, II and III to the Fourth Assessment Report of the Intergovernmental Panel on Climate Change [Pachauri RK, Reisinger A (eds.)]. Geneva, Switzerland, IPCC. 2007. p. 104.

[15] Gough WA, Gagnon AS, Lau HP. Interannual variability of Hudson bay ice thickness. Polar Geo. 2004;28(3):222–238. DOI: 10.1080/789610188

[16] Stirling I, Parkinson C. Possible effects of climate warming on selected populations of polar bears (*Ursus maritimus*) in the Canadian Arctic. Arctic. 2006;59:261–275. DOI: 10.1093/icb/44.2.163

[17] Christensen JH, Hewitson B, Busuioc A, Chen A, Gao X, Held I, et al. Climate Change 2007: The Physical Science Basis. In: Contribution of Working Group I to the Fourth Assessment Report of the Intergovernmental Panel on Climate Change [Solomon S, Qin D, Manning M, Chen Z, Marquis M, Averyt KB, et al. (eds.)]. Cambridge, UK; New York, NY, USA, Cambridge University Press. 2007.

[18] IPCC. Managing the Risks of Extreme Events and Disasters to Advance Climate Change Adaptation. In: A Special Report of Working Groups I and II of the Intergovernmental Panel on Climate Change [Field CB, Barros V, Stocker TF, Qin D, Dokken DJ, Ebi KL., et al. (eds.)]. Cambridge, UK, and New York, NY, USA, Cambridge University Press. 2012. p. 582.

[19] Salick J, Byg A. Indigenous Peoples and Climate Change. A Tyndall Centre Publication Tyndall Centre for Climate Change Research, Oxford. 2007.

[20] Parry ML, Canziani OF, Palutikof JP, van der Linden PJ, Hansen CE. Contribution of Working Group II to the Fourth Assessment Report of the Intergovernmental Panel of Climate Change. Cambridge, Cambridge University Press. 2007.

[21] Buhrich A. Literature Review: Climate Change and Indigenous Communities. Australia, James Cook University. 2010. p. 1–20.

[22] Statistics Canada. Aboriginal Peoples in Canada: First Nations People, Métis and Inuit. National Household Survey. 2011. Catalogue No. 99-011-X2011001. ISBN: 978-1-100-22203-5. Available from: http://www12.statcan.gc.ca/nhs-enm/2011/as-sa/99-011-x/99-011-x2011001-eng.pdf [accessed: 2016-10-01].

[23] Macdonald ME, Rigillo N, Brassard P. Urban aboriginal understandings and experiences of tuberculosis in Montreal, Quebec, Canada. Qual Health Res. 2010;20(4):506–523. DOI: 10.1177/1049732309360538

[24] MacMillan H, MacMillan A, Offord D, Dingle J. Aboriginal health. Can Med Assoc J. 1996;155(11):1569–1578.

[25] Ford JD, Pearce T, Duerden F, Furgal C, Smit B. Climate change policy responses for Canada's Inuit population: The importance of and opportunities for adaptation. Glob Environ Change. 2010;20:177–191. DOI: 10.1016/j.gloenvcha.2009.10.008

[26] Richmond CM, Ross NA. The determinants of First Nation and Inuit health: A critical population health approach. Health Place. 2009;15:403–411. DOI: 10.1016/j.healthplace.2008.07.004

[27] Durkalec A, Furgal C, Skinner MW, Sheldon T. Climate change influences on environment as a determinant of Indigenous health: Relationships to place, sea ice, and health

in an Inuit community. Soc Sci Med. 2015;17:136–137. DOI: 10.1016/j.socscimed.2015.04.026

[28] Herrmann TM, Royer MJS, Cuciurean R. Understanding subarctic wildlife in Eastern James Bay under changing climatic and socio-environmental conditions: Bringing together Cree hunters' ecological knowledge and scientific observations. Polar Geogr. 2012;35(3–4):245–270. DOI: 10.1080/1088937x.2011.654356

[29] McDonald M, Arragutainaq L, Novalinga Z. Voices from the Bay: Traditional Ecological Knowledge of Inuit and Cree in the Hudson Bay Bioregion. Ottawa, Ontario: Canadian Arctic Resources Committee and the Environmental Committee of Municipality of Sanikiluaq. 1997. Available from: http://arctic.journalhosting.ucalgary.ca/arctic/index.php/arctic/article/viewFile/1156/1182 [accessed: 2016-01-01].

[30] Stevenson MG. Indigenous knowledge in environmental assessment. Arctic. 1996;49(3):278–291.

[31] Laidler GJ, Ford JD, Gough WA, Ikummaq T, Gagnon AS, Kowal S, et al. Travelling and hunting in a changing Arctic: Assessing Inuit vulnerability to sea ice change in Igloolik, Nunavut. Clim Change. 2009;94:363–397. DOI: 10.1007/s10584-008-9512-z

[32] Ball J. As if Indigenous Knowledge and Communities Mattered: Transformative Education in First Nations Communities in Canada. Summer, University of Nebraska Press. 2004. p. 454–479.

[33] Berkes F, Jolly D. Adapting to climate change: Social-ecological resilience in a Canadian western arctic community. Conserv Ecol. 2001;5(2):1–18. Available from: http://www.ecologyandsociety.org/vol5/iss2/art18/ [accessed: 2016-06-16].

[34] Wolf J, Allice I, Bell T. Values, climate change, and implications for adaptation: Evidence from two communities in Labrador, Canada. Global Environ Chang. 2012;23(2):548–562. DOI: 10.1016/j.gloenvcha.2012.11.007

[35] Wesche SD, Chan HM. Adapting to the impacts of climate change on food security among Inuit in the western Canadian Arctic. EcoHealth. 2010;7:361–373. DOI: 10.1007/s10393-010-0344-8

[36] Ford JD, McDowell G, Pearce, T. The adaptation challenge in the Arctic. Nat Clim Change. 2015;5:1046–1053. DOI: 10.1038/nclimate2723

[37] Furgal C, Prowse TD. Northern Canada. In: From Impacts to Adaptation: Canada in a Changing Climate 2007 [Lemmen DD, Warren FJ, Larcoix J, Bush E (eds.)]. Ottawa, Ontario, Government of Canada. 2008. p. 57–118.

[38] Ford JD, Smit B, Wandel J. Vulnerability to climate change in the Arctic: A case study from Arctic Bay, Canada. Global Environ Chang. 2006;16(2):145–160. DOI: 10.1016/j.gloenvcha.2005.11.007

[39] Ford JD, Keskitalo ECH, Smith T, Pearce T, Berrang-Ford L, Duerden F, et al. Case study and analogue methodologies in climate change vulnerability research. Clim Change. 2010;1(3):374–392. DOI: 10.1002/wcc.48

[40] Sydneysmith R, Andrachuk M, Smit B, Hovelsrud, GK. Vulnerability and Adaptive Capacity in Arctic Communities. In: Adaptive Capacity and Environmental Governance, Springer Series on Environmental Management [Armitage D, Plummer R (eds.)]. Berlin, Springer-Verlag. 2010.

[41] Pearce T, Ford J, Willox AC, Smit B. Inuit traditional ecological knowledge (TEK), subsistence hunting and adaptation to climate change in the canadian Arctic. Arctic. 2015;68(2):233–245. DOI: 10.14430/arctic4475

[42] Pearce T, Ford JD, Caron A, Kudlak PB. Climate change adaptation planning in remote, resource-dependent communities: An Arctic example. Reg Environ Change. 2012;12:825–837. DOI: 10.1007/s10113-012-0297-2

[43] Barbeau CD, Charania NA, Isogai AD, McCarthy DD, Cowan D, Tsuji LJS. Fostering adaptive capacity and resilience to environmental change in sub-arctic first nations: The use of collaborative geomatics, an interactive, web-based informatics tool. Int J Technol Knowl Soc. 2011;7(1):117–134.

[44] Eades G, Sieber R. Geospatial Technologies and the Representation of Cree Knowledge. In: Dialoguing Knowledges: Finding Our Way to Respect and Relationship [Scott C, Brown P, Labrecque L (eds.)]. Vancouver, British Columbia, UBC Press. 2011.

[45] European Commission. Glossary. 2000. Available from: http://ec.europa.eu/agriculture/publi/landscape/gloss.htm [accessed: 2015-02-03].

[46] McCarthy DDP, Whitelaw GS, Anderson S, Cowan D, McGarry F, Robins A, et al. Collaborative geomatics and the Mushkegowuk Cree first nations: Fostering adaptive capacity for community based sub-arctic natural resource management. Geoforum. 2012;43:305–314. DOI: 10.1016/j.geoforum.2011.07.015

[47] Tsuji LJS, Manson H, Wainman BC, Vanspronsen EP, Shecapio-Blacksmith J, Rabbitskin T. Identifying potential receptors and routes of contaminant exposure in the traditional territory of the Ouje-Bougoumou Cree: Land use and a geographical information system. Environ Monit Assess. 2007;127:293–306. DOI: 10.1007/s10661-006-9280-z

[48] Stewart EJ, Jacobson D, Draper D. Public participation geographic information systems (PPGIS): Challenges of implementation in Churchill, Manitoba. Can Geogr. 2008;52(3):351–366. DOI: 10.1111/j.1541-0064.2008.00217.x

[49] McCarthy DD, Whitelaw G, King C, King C, Viswanathan L, et al. Collaborative geomatics and the Mississaugas of the new credit first nation: Triaging requests for planning development consultation. Int J Technol Knowl Soc. 2013;9:1–15. Available

from: http://www.queensu.ca/pwip/sites/webpublish.queensu.ca.pwipwww/files/files/publications/collaborative-geomatics.pdf [accessed: 2016-02-28].

[50] Sieber R. Public participation geographic information systems: A literature review and framework. Ann Assoc Am Geogr. 2006;96(3):491–507. Available from: http://www.arch.mcgill.ca/prof/luka/urbandesignhousing/klwb/holding/fordham/Sieber2006_0702.pdf [accessed: 2016-01-15].

[51] Cusimano M, Chipman M, Glazier R, Rinner C, Marshall S. Geomatics in injury prevention: The science, the potential and the limitations. Inj Prev. 2007;13(1):51–56. DOI: 10.1136/ip.2006.012468

[52] Cowan D, Fenton S, Mulholland D. The Web-based Informatics Development Environment (WIDE). 2006. Available from: http://csg.uwaterloo.ca/wide.htm [accessed: 2011-06-10].

[53] Gardner-Youden HL, Barbeau C, McCarthy DD, Edwards V, Cowan D, Tsuji LJS. Indigenous mapping technologies: The past, present and future of the collaborative geomatics web-based tool. KM4D J. 2011;7(3):340–353. DOI: 10.1080/19474199.2012.684500

[54] Tsuji L, Nieboer E. A question of sustainability in Cree harvesting practices: The seasons, technological and cultural changes in the western James Bay region of northern Ontario, Canada. Can J Native Stud. 1999;19:169–192. Available from: https://www.researchgate.net/publication/237309842_A_QUESTION_OF_SUSTAINABlll-TY_IN_CREE_HARVESTING_PRACTICES_THE_SEASONS_TECHNOLOGICAL_AND_CULTURAL_CHANGES_IN_THE_WESTERN_JAMES_BAY_REGION_OF_NORTHERN_ONTARIO_CANADA [accessed: 2016-02-01].

[55] Tsuji L, Kataquapit J, Katapatuk B, Iannucci G. Remediation of Site 050 of the Mid-Canada Radar Line: Identifying potential sites of concern utilizing traditional environmental knowledge. Can J Native Studies. 2001;21(1):149–160. Available from: http://www3.brandonu.ca/library/cjns/21.1/cjnsv21no1_pg149-160.pdf [accessed: 2016-02-02].

[56] Tam B, Gough WA, Tsuji LJS. The impact of warming on the appearance of furunculosis in fish of the James Bay region, Quebec, Canada. Reg Environ Change. 2011;11:123–132. DOI: 10.1007/s10113-010-0122-8

[57] Barbeau C, Yukari H, Gough WA, Karagatzides JD, McCarthy DD, Cowan D, et al. The potential use of an interactive web-based informatics tool to decrease the incidence of human-polar bear encounters along the western James Bay Coast of Ontario, Canada. Int J Technol Knowl Soc. 2012;8:113–127.

[58] Ho E, Tsuji LJS, Gough WA. Trends in river-ice break-up data for the western James Bay region of Canada. Polar Geogr. 2005;29(1):291–299. DOI: 10.1080/789610144

[59] Gagnon A, Gough W. Climate change scenarios for the Hudson Bay region: An intermodel comparison. Clim Change. 2005;69:269–297. DOI: 10.1007/s10584-005-1815-8

[60] Adbelnour R. Albany River 2008 Ice Breakup: Forecasting the Flood Event, Observations of the River during the Spring Breakup and the Potential for Mitigating the Flooding Risk of the Kashechewan and Fort Albany First Nation. In: CGU HS Committee on River Ice Processes and the Environment 17th Workshop on River Ice. Edmonton, Alberta, Canada. 2013. Available from: http://cripe.civil.ualberta.ca/Downloads/17th_Workshop/Abdelnour-2013.pdf [accessed: 2016-03-01].

[61] Balram S, Dragicevic S. Collaborative Geographic Information Systems: Origins, Boundaries, and Structures. In: Collaborative Geographic Information Systems [Balram S, Dragicevic S (eds.)]. Hershey, PA, Idea Group. 2006. p. 1–22.

[62] Charania NA, Cowan D, Tsuji LJS. Health care delivery in remote and isolated first nations communities in Canada: The need for a collaborative health informatics system. Int J Technol Knowl Soc. 2013;8:71–84.

[63] First Nations Centre. OCAP: Ownership, Control, Access and Possession. Sanctioned by the First Nations Information Governance Committee, Assembly of First Nations. Ottawa, National Aboriginal Health Organization. 2007. Available from: http://cahr.uvic.ca/nearbc/documents/2009/FNC-OCAP.pdf [accessed: 2015-09-12].

[64] Isogai AD, Alexiuk E, Gardner HL, McCarthy DD, Edwards V, Spiegelaar N, et al. Sustaining a local-food security initiative in a remote subarctic community: Engaging Canadian First Nation youth in agroforestry-community gardens. Int J Soc Sust Econ Soc Cult Context. 2015;10(3–4):1–17.

[65] Churchill D, Kennedy D, Flint D, Cotton N. Using handhelds to support students' outdoor education activities. ICICTE. 2010;20(10):54–71. DOI: 10.1504/IJCEELL.2010.031648

[66] Bryman A. Social Research Methods. New York, Oxford University Press. 2001.

[67] CEAA. Considering Aboriginal Traditional Knowledge in Environmental Assessments Conducted under the Canadian Environmental Assessment Act, Interim Principles. 2010. Available from: http://www.ceaa.gc.ca/default.asp?lang=En&n=4A795E76-1 [accessed 2011-03-04].

[68] Wilbanks TJ, Kates RW. Global change in local places: How scale matters. Clim Change. 1999;43:601–628. DOI: 10.1023/A:1005418924748

[69] Smit B, Wandel J. Adaptation, adaptive capacity and vulnerability. Glob Environ Change. 2006;16:282–292. DOI: 10.1016/j.gloenvcha.2006.03.008

[70] Walker B, Salt D. Resilience Thinking: Sustaining Ecosystems and People in a Changing World. Washington, DC, Island Press. 2006.

[71] Ford JD. Indigenous health and climate change. Am J Public Health. 2012;102(7):1260–1266. DOI: 10.2105/AJPH.2012.300752

[72] Prno J, Bradshaw B, Wandel J, Pearce T, Smit B, Tozer, L. Community vulnerability to climate change in the context of other exposure-sensitivities in Kugluktuk, Nunavut. Polar Res. 2011;30:7363. DOI: 10.3402/polar.v30i0.7363

[73] Berkes F, Jolly D. Adapting to climate change: Social-ecological resilience in a Canadian Western Arctic community. Conserv Ecol. 2002;5(2):18. Available from: https://dlc.dlib.indiana.edu/dlc/bitstream/handle/10535/2746/Berkes.pdf?sequence=1&isAllowed=y [accessed 2015-09-01].

[74] Pennesi K, Arokium J, McBean G. Integrating local and scientific weather knowledge as a strategy for adaptation to climate change in the Arctic. Mitig Adapt Strateg Glob Change. 2012;17:897–922. DOI: 10.1007/s11027-011-9351-5

[75] Pearce T, Smit B, Duerden F, Ford JD, Goose A, Kataoyak F. Inuit vulnerability and adaptive capacity to climate change in Ulukhaktok, Northwest Territories, Canada. Polar Rec. 2010;46:157–177. Available from: http://www.uoguelph.ca/gecg/images/userimages/Pearce%20et%20al.%20(2009)_%20Ulukhaktok.pdf [accessed 2015-10-01].

[76] Westley F. Social Innovation. Available from: http://www.sig.uwaterloo.ca/social_innovation.html [accessed 2009-07-01].

[77] Tsuji LJS, Ho E. Traditional environmental knowledge and western science: In search of common ground. Can J Native Stud. 2002;22:327–360. Available from: http://iportal.usask.ca/docs/ind_art_cjns_v22/cjnsv.22no.2_pg327-360.pdf [accessed 2016-03-03].

[78] Armitage D. Adaptive capacity and community-based natural resource management. Environ Manage. 2005;35(6):703–715. DOI: 10.1007/s00267-004-0076-z

[79] Gunderson L, Holling C. Panarchy: Understanding Transformations in Human and Natural Systems. Washington, DC, Island Press. 2002.

Chapter 5

Estimation and Uncertainty Assessment of Surface Microclimate Indicators at Local Scale Using Airborne Infrared Thermography and Multispectral Imagery

Serge Olivier Kotchi, Nathalie Barrette, Alain A. Viau, Jae-Dong Jang, Valéry Gond and Mir Abolfazl Mostafavi

Additional information is available at the end of the chapter

http://dx.doi.org/10.5772/64527

Abstract

A precise estimation and the characterization of the spatial variability of microclimate conditions (MCCs) are essential for risk assessment and site-specific management of vector-borne diseases and crop pests. The objective of this study was to estimate at local scale, and assess the uncertainties of Surface Microclimate Indicators (SMIs) derived from airborne infrared thermography and multispectral imaging. SMIs including Surface Temperature (ST) were estimated in southern Quebec, Canada. The formulation of their uncertainties was based on in-situ observations and the law of propagation of uncertainty. SMIs showed strong local variability and intra-plot variability of MCCs in the study area. The ST values ranged from 290 K to 331 K. They varied more than 17 K on vegetable crop fields. The correlation between ST and in-situ observations was very high ($r = 0.99$, $p = 0.010$). The uncertainty and the bias of ST compared to in-situ observations were 0.73 K and ±1.42 K respectively. This study demonstrated that very high spatial resolution multispectral imaging and infrared thermography present a good potential for the characterization of the MCCs that govern the abundance and the behavior of disease vectors and crop pests in a given area.

Keywords: airborne remote sensing, infrared thermography, microclimate indicators, uncertainty, local scale, crop, pests and diseases

1. Introduction

Microclimates which are defined by agrometeorological conditions are key factors governing crop development and growth. They influence the abundance, development, and behavior of diseases and pests which can significantly reduce crop yield [1–6]. A regular use of pesticides for pest control can result, along with the risk to environmental and human health that pesticides pose. Microclimate variability induced by agrometeorological conditions represents around 80% of the variability of agricultural production [7]. These conditions are defined through variables such as the amount of vegetation, surface temperature, surface moisture, air temperature (AT), relative humidity (RH), solar radiation, evapotranspiration, wind speed and direction, rainfall, etc. Indicators such as percent vegetation cover (PVC) and leaf area index (LAI) [8, 9], duration of leaf wetness [2, 10], thermal units [11], degree days, vapor pressure deficit [7, 11, 12], potential evapotranspiration [13], water stress indices [12, 14, 15], drought indices [16], precipitation indices [17], etc., are related to these variables, and they are used to quantify and monitor agrometeorological and microclimate conditions on a given territory. They are also used to identify appropriate times in the management of various agricultural practices like sowing, irrigation, disease and pest screening, applying manure and pesticides, and harvesting. These variables and their related indicators are defined in this work as microclimate indicators (MCIs). MCIs, which are related to vegetation, temperature, and humidity levels, are considered critical indicators [18–24] and are used for the prediction and management of agricultural practices. They are the main input variables of models used to estimate other MCIs [2, 7, 25], models of growth and yield forecasting [25–28], models of disease and pest predictions [10, 23, 29], and models of climate prediction and adaptation to climate change [30, 31].

Several MCIs are commonly observed using weather stations [18, 32, 33] or in situ sensors [28, 34]. However, data from weather stations are point data that represent the specific conditions of the observing site. Their spatial representation on a larger area is not always valid [2, 7] because of the spatial heterogeneity of landscape and microclimate conditions [35]. The low number of weather stations and their generally sparse geographical distribution does not often allow for the characterization of the spatial variability of a microclimate within a given area [18, 32, 33, 36]. The cost and the maintenance of a more densified weather station networks to ensure better characterization of the spatial variability of microclimates is very high and could not be supported by the users [32]. In addition, meteorological data are often missing or erroneous in many parts of the world [7, 34, 36], which limits the application of simulation models [37, 38] and the management of agricultural practices. Some MCIs are considered secondary variables and are not commonly observed by weather stations [7], and punctual observations are not appropriate because of their large spatial variability [29, 39, 40]. Compared to MCIs related to atmospheric conditions (air temperature, relative humidity), those related to surface conditions (surface microclimate indicators, SMIs) like vegetation amount, surface temperature (ST), surface moisture and leaf wetness duration are often not observed by weather stations [10, 25, 41]. These SMIs are more directly related to microclimate conditions which affect water status and crop growth as well as the abundance, behavior and development of crop pests and diseases. And, weather stations where these SMIs are actually observed

http://dx.doi.org/10.5772/64527

frequently report missing or erroneous data due to equipment failure [25]. Punctual in situ observations over crop fields to address the lack of data on those SMIs are time and resource consuming, and they do not always result in a good characterization of their spatial variability [42]. Finally, for some of these SMIs, like leaf wetness, there is no commonly accepted standard for their measurement [2]. Due to all these limitations, weather station networks are not always able to meet the requirements for characterization of microclimate conditions in agriculture, or more specifically in precision agriculture and site-specific pest management [40]. This also concerns several other applications which require the characterization of the microclimate conditions.

While SMIs related to surface conditions are less frequently observed by weather stations, they are the primary variables derived from satellite images. Thus, the estimation of SMIs using satellite images overcomes the problem of sparse meteorological station networks and the nonavailability of meteorological data [18]. Some agricultural management programs are based on MCIs estimated by satellite images, where meteorological ground station data are not available [39]. These images offer a unique advantage for the estimation and the monitoring of microclimate conditions in the soil-vegetation-atmosphere interface over vast territories and at different spatial and temporal resolutions [43–46]. The spatial density of data derived from satellite images exceeds that of observations from weather stations. These data allow a better characterization of the spatial variability of microclimate conditions. Compared to point data acquired in fields, they are less costly in time and money [34]. Vegetation indices (VIs) derived from satellite images are used to estimate indicators of the amount of vegetation like percent vegetation cover (PVC) [8, 9, 47, 48] and leaf area index (LAI) [28, 49–51]. The normalized difference vegetation index (NDVI) is the best known and most widely used VI [11, 28, 34, 45, 46, 51, 52]. It is used in many other applications including estimating biophysical variables such as photosynthetically active radiation (PAR) and evapotranspiration [53, 54], monitoring crop growth and development [39, 46, 52], yield forecasting [55–57], and drought monitoring [16, 34, 58]. Surface temperature (ST) is a key variable to understanding and to characterizing heat and water exchanges between the surface and the atmosphere [20, 59, 60]. It can be estimated using several Earth observation systems like GOES, MSG/SEVIRI, NOAA/AVHRR, Terra, Aqua/MODIS, ASTER, and Landsat-8/TIRS. ST is used for the estimation of other MCIs such as air temperature [18] and evapotranspiration [37], for the detection of water deficits and the monitoring of drought conditions [16, 61], and for risk assessment of the occurrence of diseases and pests [32]. For example, the temperature condition index (TCI), based on the ST derived from satellite images, is one of the most used to track drought conditions and their impact on regional and global scales [16]. Variations of surface moisture in the short and long term and its impact on vegetation can be monitored using stress indices based on ST and IVs derived from satellite images [56]. The TVDI is one of the most used indices to estimate surface moisture [21, 24, 62, 63]. Chen et al. [64] used the TVDI estimated using MODIS images to characterize the spatial variability of surface moisture and to link it with rice farming systems in the Mekong Delta, Vietnam. Holzman et al. [56] also used the TVDI derived from MODIS images to estimate soil water availability and to assess crop yield at the regional scale.

SMIs which are derived from satellite images have a good potential to be used in regional agro-meteorological systems [35]. Several products related to surface temperature and to vegetation indices, such as those of MODIS, are also available in the form of time series. These products are frequently used to study climate and other dynamic phenomena in space and time [65]. However, applications of SMIs are limited either by the low spatial resolution or by the low temporal resolution of Earth observation systems which are used [60]. ST is derived from systems such as GOES and MSG/SEVIRI with a very high temporal resolution (15 min). However, these systems are characterized by a very low spatial resolution (3–5 km). Sensors like MODIS and AVHRR, which are mostly used to estimate surface temperature in many applications, are characterized by a high temporal resolution (1 day), but are associated with a low spatial resolution (1 km). Earth observation systems including Landsat-5/TM, Landsat-7/ETM+, and Landsat-8/TIRS are those with the best spatial resolution in thermal bands (120, 60, and 100 m, respectively). However, they are limited by a very low temporal resolution (16 days). The low spatial resolution satellite images used to estimate SMIs often lead to mixed pixels that combine different elements like bare soil, vegetation, water, impervious surfaces, and clouds, especially in environments with a strong spatial heterogeneity [32, 48, 59, 66]. These mixed pixels could lead to significant errors in the estimation of SMIs [32, 66]. This low spatial resolution also makes it difficult to link data from satellite images and data collected in the field [45, 48]. Moreover, the presence of clouds limits time series continuity [62]. That is even more problematic with low temporal resolution Earth observation systems.

Indicators such as ST are characterized by high spatial and temporal variability so they require observations both at a very high spatial and at a very high temporal resolution [59]. The low spatial resolution of satellite image products which are associated with ST limits several agricultural applications that require the characterization of the microclimate and the intra-plot variability. Site-specific management of crop pests, as well as management of agricultural inputs and irrigation, requires accurate estimates of crop status and agro-meteorological conditions and characterizations of their intra-plot variability [42]. Several authors are unanimous on the fact that management of diseases and pests, characterized by a high spatial and temporal dynamics, requires specific agro-meteorological information at the field and microclimate scales [67–69]. Matese et al. [70], for example, have shown that the microclimate of vineyards is characterized by high spatial variability (intravignoble and intervignoble) meaning that measurements from meteorological stations located outside of these vineyards do not effectively reflect the microclimate conditions occurring there. Agricultural practices rely increasingly on data acquired at fine scales in order to characterize the spatial and temporal variability of growth factors within the fields in order to improve management of crop diseases and pests and agricultural inputs, and to reduce the costs for producers and the toll on the environment and human health. Airborne remote sensing offers several advantages that can meet this need. Technological advances in recent years in the field of thermal infrared remote sensing led to the development of very high spatial resolution airborne sensors which allow the observation of ST at very fine scales [20]. According to Wood et al. [71], airborne remote sensing is an effective approach to producing accurate information in near real-time to improve the management of agricultural practices (prevention and control of crop diseases and pests, fertilizer application, irrigation, etc.) in a precision farming context. It provides accurate

http://dx.doi.org/10.5772/64527

mapping solutions with flexibility of choice regarding spatial and temporal scales that meet specific needs [42, 72] such as integrated pest management. It was thus demonstrated that images at very high spatial resolution are more appropriate to map riparian vegetation which is characterized by great complexity, great diversity, and spatial variability that manifests itself in very short scales [73]. Wood et al. [71] used airborne images to map the intra-plot variability in wheat fields. Zhang et al. [74] used airborne images to assess the effectiveness of different herbicides in cotton fields. The airborne thermal imagery acquired using infrared thermography cameras was among those used for the detection of water stress [42]. The characterization of the spatial variability of microclimate conditions at fine scales also requires accurate data [42, 68, 69, 75, 76]. This requires the assessment of the uncertainties related to tools and methods used to estimate SMIs.

The aim of our study was to estimate, evaluate uncertainties, and characterize the spatial variability of surface microclimate indicators (amount of vegetation, surface temperature, and surface moisture) derived from airborne infrared thermography and airborne multispectral imaging in the context of prevention and control of vegetable crop diseases and pests.

2. Method

2.1. Study area

The study area is located in the valley of the St. Lawrence River, in the Montérégie West region, in the south of the metropolitan area, and in the southern part of the province of Quebec, Canada (**Figure 1**). The terrain is relatively flat in this study area. Elevations vary between 50

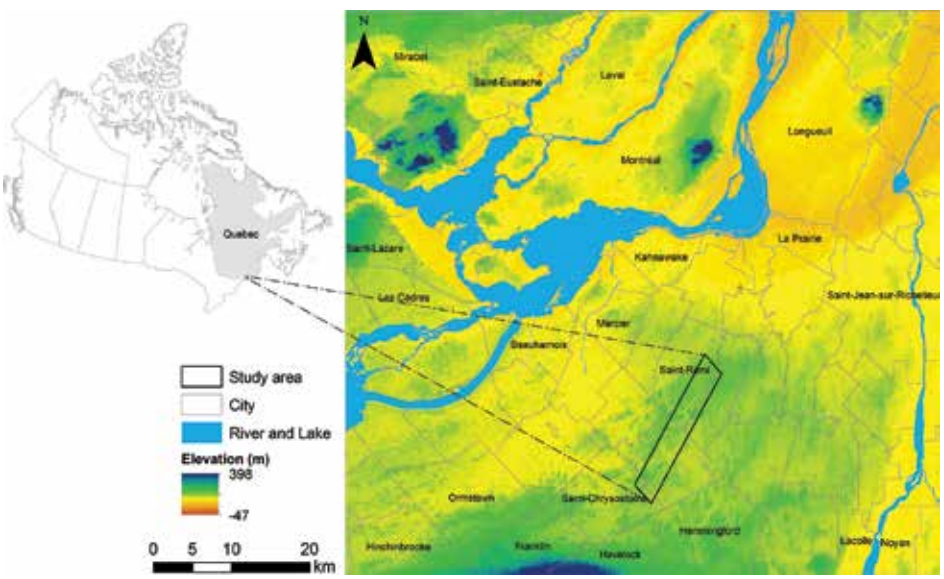

Figure 1. Study area.

and 73 m (average elevation of 60 m), with slopes varying between 0 and 6.14% (average slope of 0.77%) (Canadian Digital Elevation Data [77]). Elevations are higher in the northern half of the study area. Black soil (organic soil) dominates the southern half part, while the northern half is mainly occupied by mineral soil. Forest and wooded areas are mainly located in the south. Agricultural lands are mainly used for vegetable crops (potato, lettuce, onion, carrot, celery, cabbage, etc.) and field crops (soybean and maize). These crops are respectively distributed in the northern part and in the southern part of the study area. Airborne imagery acquisition and in situ measurements were performed on July 14, 2006. Ground recognition was conducted from July 13 to 14, 2006.

2.2. Data acquisition

Figure 2 presents the overall schema of data acquisition and processing.

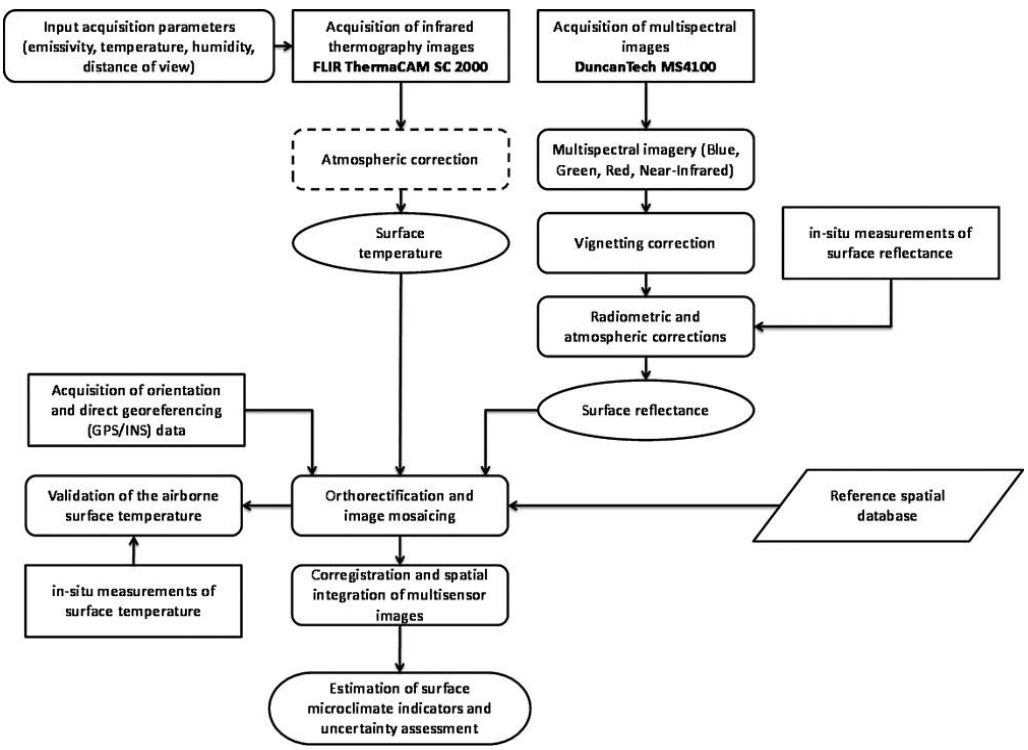

Figure 2. Overall schema of airborne remote sensing data acquisition and processing.

2.2.1. Airborne multispectral imagery and infrared thermography

The MS4100 camera (Duncan Tech, Auburn, CA) was used for the acquisition of airborne multispectral images. It was configured to operate with the spectral bands blue (437–483 nm), green (520–560 nm), red (640–680 nm), and near infrared (767–833). This camera is character-

http://dx.doi.org/10.5772/64527

ized by an image plane of 14.2 × 8 mm^2, a pixel size of 7.4 microns, an image resolution of 1920 × 1080 pixels, a focal length of 17 mm, and a field of view of 49° × 28.6° (Duncan Tech 2005).

The acquisition of infrared thermography images was performed with the ThermaCAM SC2000 camera (FLIR Systems Inc., Boston, MA, www.flir.ca). This camera operates in the spectral band of 7.5–13 μm. Its imaging system is a focal plane array (FPA), with an uncooled microbolometer detector of 240 × 320 pixels. It has a spatial resolution (instantaneous field of view, IFOV) of 1.3 mrad and a field of view (FOV) of 24° × 18°, with a minimum view distance of 0.3 m. This latter parameter allows a maximum spatial resolution of 0.4 × 0.4 mm (absolute size of each pixel at a distance of 0.3 m). Its thermal resolution or thermal sensitivity is 0.07°C at an ambient temperature of 30°C, with an absolute precision (systematic bias) of +/−2°C or +/−2%.

Images were acquired at a flying height of 1200 m, with 13 flying lines oriented south-west/north-east in the direction of the length. The flying height was determined from an expected spatial resolution of 1.5 m on the infrared thermographic images and an equivalent expected spatial resolution of 0.25 m on the multispectral images. A minimum of 30% lateral (side) overlap was used between images of adjacent flying lines, and a minimum of 60% longitudinal overlap was used between adjacent images of the same flying line. The calculation of these overlaps was based on the technical specifications of the infrared thermography camera. In addition to the remote sensing sensors, the acquisition system also included an integrated Global Positioning System/Inertial Navigation System (GPS/INS), which is a Position and Orientation Solutions for Direct Georeferencing (POS/DG) designed by the Applanix Corporation (Richmond Hill, Ontario, Canada, www.applanix.com). The acquisition system was mounted on an airborne platform carried by a Cessna 310L airplane. Image acquisition took place between 9:15 and 11:06 a.m. Eastern Standard Time, from the western boundary to the eastern boundary of the study area (**Figure 1**).

2.2.2. Field investigation and in-situ measurements

A field reconnaissance was conducted before, during, and after the acquisition of airborne images. It allowed the identification of crop varieties and their phenological stages, the identification of infield problems related to drainage, water and nutrient stress, abiotic damage, stress and damage caused by crop pests and diseases, and yield variation. In situ measurements were carried out for air temperature, relative humidity, surface reflectance, and surface temperature on various sites in the study area during the acquisition of airborne images. These measures were used to correct remote sensing images and to assess the accuracy of estimating agro-meteorological indicators.

2.2.2.1. Air temperature and relative humidity

Air temperature (AT) and relative humidity (RH) were observed from 13 sample points distributed over the study site. These observations were synchronized to the acquisition of airborne images. They were carried out at a height of 1.5 m from the surface using hygrothermometers (model 6301032 NexxTech, ORBYX electronics, Concord, ON). These instruments

have an absolute accuracy of ±1.8°C between 0 and 40°C. A series of nine repeated measurements at 5 s intervals was carried out by sampling point in order to obtain an average measure with a resultant uncertainty of ±0.6°C. A device was used to protect the hygrothermometers from wind and direct sunlight. Continuous measurements at 10-min intervals were undertaken during the acquisition of airborne images, using two hygrothermometers installed at two weather station sites. The comparison of these measures with those acquired by meteorological stations at the same time was used to adjust hygrothermometer measurements to those of the meteorological stations.

2.2.2.2. Surface reflectance

Surface reflectance measurements were performed using a spectroradiometer FieldSpec Pro (ASD Inc., Boulder, CO, www.asdi.com) at two calibration sites (calibration site 1, CS1, and calibration site 2, CS2). On site CS1, reflectance measurements were performed on a white tarpaulin and on green grass. On site CS2, these measures were performed on a water surface (irrigation pond), bare soil (black soil), and on an onion crop surface. Each reflectance measurement was preceded by a calibration of the spectroradiometer using a Spectralon (white reference). Reflectance measurements were carried out simultaneously with the acquisition of airborne images.

2.2.2.3. Surface temperature

Surface temperature was measured on the same calibration surfaces used for surface reflectance, during and after the acquisition of airborne images. Infrared thermometer OS643E-LS (Omega, Stamford, CT) was used for these measurements. This instrument measures the temperature using the radiation emitted in the 6–14-μm-wide spectral band (thermal infrared). It has a reading accuracy of ±2%, a display resolution of 1°C, and a field of view of 65 mm diameter at 1 m. Surface temperature measurements were performed vertically at a target distance of about 1 m, except for water surface which required an oblique view and a greater distance for reasons of accessibility. Nine measuring points were sampled across each calibration surface. Two types of measurements were performed with the infrared thermometer. The first, called "calibration measurements of the infrared thermometer," was used to establish the relationship between the measurements of the thermometer and the infrared thermography camera and in order to use the thermometer readings as reference data for the assessment of the uncertainty of the surface temperature derived from the airborne infrared thermography. The calibration measurements of the infrared thermometer were performed at four sites, on a white tarpaulin that served as a reference surface. The geometry of the measurement was configured such that the two sensors covered the same field of view on the tarpaulin. The second type of measurement was used as a validation measure of the estimation of the surface temperature by airborne infrared thermography. These measures were synchronized with the acquired airborne images.

http://dx.doi.org/10.5772/64527

2.3. Data processing

2.3.1. Radiometric and atmospheric corrections

2.3.1.1. Multispectral imagery data

A gradual darkening effect from the center to the edges was found when reading the multispectral images. This phenomenon is known as vignetting [78–80]. It was corrected using the equations proposed by Hasler and Süsstrunk [81].

The empirical line method [82] was used to perform the atmospheric correction of the multispectral images. This method assumes that there is in the image at least one low reflectance target (value close to 0) and one high reflectance target (value close to 1) in each spectral band of the sensor [82–84]. A linear equation that models the relationship between the luminance (or the digital count) and the surface reflectance is set to convert the digital counts in surface reflectance values. Although this approach corrects both radiometric and atmospheric effects and overcomes having to use atmospheric measurements and a radiative transfer model, it does require reflectance measurements on target surfaces with simultaneous image acquisition; this was performed in the present study. The average values of surface reflectance and digital count of the calibration panels were used to establish regression models and derive the equation of the empirical line in each spectral band of the sensor. Three target surfaces were used to determine the empirical line in each spectral band.

2.3.1.2. Infrared thermography data

The infrared camera ThermaCAM SC 2000 is designed for industrial applications and for research and development applications conducted primarily in laboratory. The format of the camera output data does not meet the needs of a geospatial application. The ThermaCAM Researcher software 2001 (FLIR Systems AB, Rinkebyvägen, Danderyd) was used to export the thermography to a MatLab file (.mat). The structure of this file contains information like date and time of data acquisition, object signal, emissivity, temperature, characteristics of the black body and the trigger signal number. From this data structure, the surface temperature matrix was converted into a 32-bit georeferenced Tagged Image File Format (GeoTIFF) image file.

The radiometric calibration and atmospheric correction are internal to the thermal camera. The calibration is performed by measuring digital counts over a blackbody with a known emitted luminance, surface temperature, surface emissivity, and target distance. The data derived from this calibration are used to produce a curve associating digital numbers to luminance values and to establish the relationship between the input luminance of the sensor and the surface temperature of the target. The latter conversion is made using a series of lookup tables (LUTs) stored in the camera. These LUTs establish the relationship between luminance values and blackbody temperatures. When a measurement is made, the system identifies the LUT which is associated with the digital number signal generated and calculates the temperature value related to the measurement. The surface temperature calculated by the camera is based on the law of total radiation [85, 86] by using the infrared radiation emitted by the surface, the

reflected infrared radiation emitted by the surrounding heat sources, and the thermal radiation of the atmosphere Eq. (1).

$$T_{\text{cam}}{}^4 = \varepsilon\tau \text{ST}^4 + \left(1-\varepsilon\right)\tau T_{\text{amb}}{}^4 + \left(1-\tau\right)T_{\text{atm}}{}^4 \quad (1)$$

where $T_{\text{cam,}}$ input temperature of the camera (K); ε, surface emissivity; τ, transmissivity of the atmosphere; ST, surface temperature (K); $T_{\text{amb,}}$ reflected ambient temperature (K); $T_{\text{atm,}}$ temperature of the atmosphere (K).

The input parameters used by the thermal camera to solve Eq. (1) were surface emissivity, ambient temperature (temperature of the ambient air from the environment of the object), temperature of the atmosphere (temperature of the air between the object and the camera), the target distance, and the relative humidity of the air. These parameters were provided to the camera before the measurements and were used in post processing to correct the infrared thermography images. The ThermaCAM Researcher software (FLIR Systems, Boston, MA) was used for the acquisition and correction of infrared thermography images. The surface emissivity value was set to 1 in order to calculate an apparent atmospherically corrected blackbody temperature because the acquisition and processing software accepts only one emissivity value by image. However, the surface emissivity varies over the image with the spatial heterogeneity of the observed territory. The surface temperature was subsequently calculated using the apparent blackbody temperature and a surface emissivity map (Section 2.5.2).

2.3.2. Orthorectification and spatial integration

Airborne remote sensing data acquisition was completed with an average of 350 images per flight line for a total of 4500 images per sensor. A conventional aerial triangulation was carried out on subsets of images of different flight lines in order to perform the internal calibration of the sensors and solve the linear and angular eccentricities of the GPS/INS/camera system. A total of 30 images and a minimum of 5 control/tie points per image were used for this calibration. The images used for the calibration are those whose centers coincide with a point that can be defined as a control point (intersection of roads, trails, rivers, or center of irrigation pond, etc.). An algorithm was developed to mark the center of the images to identify those suitable for the calibration. The resolution of eccentricities consisted of comparing the exterior orientation parameters calculated by the conventional aerial triangulation method and those from the GPS/INS system data. Image orthorectification and mosaicking were subsequently performed automatically for each flight line. Then, a mosaic of different image lines was completed. The internal orientation parameters and the values of eccentricity from the calibration, the external orientation parameters from the GPS/INS system data, and a digital elevation model were used as input data in the OrthoEngine module of Geomatica software (PCI Geomatics, Richmond Hill, ON) to perform the orthorectification. Data from the *Base de Données Topographiques du Québec* (BDTQ, topographic database of the province of Quebec,

http://dx.doi.org/10.5772/64527

1/20000) was used as spatial reference to collect control points to assess the overall accuracy of the orthorectified multispectral image and infrared thermography image.

Estimating SMIs by using multisensor data requires a good spatial integration of these data to ensure the linking of homologous pixels from multispectral and thermal images. To achieve this, an average filter of 5 × 5 pixels and a resampling to the resolution of 5 m were successively applied to the 1.5-m resolution images.

2.4. Image classification

A maximum likelihood supervised classification (MLSC) [87, 88] was performed using airborne multispectral and infrared thermography images to map land use and land cover (LULC). The MLSC was conducted according to different thematic classes including: full cover vegetable crop (FCVC), partial cover vegetable crop (PCVC) (vegetation and visible bare soil), large-scale farming (LSF), hay and grazing land (HGL), organic bare soil (OBS), mineral bare soil (MBS), herbaceous, forest, impervious surface (IS), and water. Field reconnaissance data and the Insured Crop Database (ICDB) of the *Financière agricole du Québec* (www.fadq.qc.ca) were used to collect both training and validation sites. Error statistics like overall accuracy, kappa coefficient, producer accuracy, and user accuracy [89, 90] were used to assess the quality of the classification. The polygons associated with the thematic classes of the classified image were used to evaluate the spatial variability of SMIs according to these classes.

2.5. Estimation of surface microclimate indicators and uncertainty assessment

2.5.1. Vegetation quantity

The normalized difference vegetation index (NDVI) [91] and percent vegetation cover (PVC) were used to express the amount of vegetation and the spatial variability of phenological stages observed in the field. Formulas of NDVI and PVC are, respectively, presented in Eqs. (2) and (3). Vegetation indices (VIs) can be considered as indicators of the amount of vegetation and vegetation biomass [92]. The NDVI is one of the best known and most used of VIs [28, 45, 51, 93], particularly for estimating the amount of vegetation and monitoring crop phenology [34, 46]. The NDVI was estimated using airborne multispectral images, as formulated in Eq. (2). PVC was estimated using the NDVI [94] according to Eq. (3). In a comparative study based on airborne images, Nagler et al. [48] showed that the NDVI gave a better result for estimating PVC, compared to soil-adjusted vegetation index (SAVI) and enhanced vegetation index (EVI). The uncertainty of the NDVI was evaluated by validation using in situ measurements (Eq. (4)). The formulation of the uncertainty of the PVC (Eq. (5)) was based on the law of propagation of uncertainty (LPU) and the combined standard uncertainty assessment approach proposed by the guide to the expression of uncertainty in measurement (GUM) [95].

$$\mathrm{NDVI} = \frac{\rho_{\mathrm{NIR}} - \rho_{\mathrm{R}}}{\rho_{\mathrm{NIR}} + \rho_{\mathrm{R}}} \tag{2}$$

where NDVI, normalized difference vegetation index; $\varrho_{R,}$ reflectance of the red band; $\varrho_{NIR,}$ reflectance of the near infrared band.

$$PVC = \left[\frac{NDVI - NDVI_{min}}{NDVI_{max} - NDVI_{min}} \right]^2 \quad (3)$$

where PVC, percent vegetation cover; $NDVI_{min,}$ NDVI minimum; $NDVI_{max,}$ NDVI maximum.

The parameters $NDVI_{min}$ and $NDVI_{max}$, respectively, correspond to the NDVI of bare soil and the NDVI of full vegetation cover. They were estimated using the classified image according to the average NDVI values, respectively, associated with FCVC and PCVC classes.

$$u\left(NDVI_{airborne}\right) = \sqrt{\frac{1}{N-2}\sum_{i=1}^{N}\left(NDVI_{airborne\,i} - \left(b + aNDVI_{in\ situ\,i}\right)\right)^2} \quad (4)$$

where $u(NDVI_{airborne})$, uncertainty of the NDVI derived from airborne multispectral imagery; $NDVI_{airborne,}$ NDVI derived from airborne multispectral imagery; $NDVI_{in\ situ,}$ NDVI derived from in situ spectroradiometric measurements; N, number of observations of the pair ($NDVI_{in\ situ}$, $NDVI_{airborne}$); a, slope of the linear regression $NDVI_{in\ situ}/NDVI_{airborne;}$ b, intercept of the linear regression $NDVI_{in\ situ}/NDVI_{airborne.}$

$$u\left(PCV\right)^2 = 8PCV^2 u\left(NDVI\right)^2 \left[\left(\frac{1}{NDVI - NDVI_{min}} \right)^2 - \left(\frac{1}{NDVI_{max} - NDVI_{min}} \right)^2 \right] \quad (5)$$

where u(PCV), PVC estimation uncertainty; u(NDVI), NDVI estimation uncertainty; $NDVI_{min,}$ NDVI minimum threshold corresponding to bare soil; $NDVI_{max,}$ NDVI maximum threshold corresponding to full vegetation cover.

2.5.2. Surface temperature

Surface temperature (ST) was estimated using (Eq. (6)) [96, 97], based on the apparent blackbody temperature derived from the airborne infrared thermography and the surface emissivity model (SEM) estimated according to Sobrino and Raissouni [98]. The largest source of uncertainties in the estimation of the ST derived from airborne infrared thermography are related to the input parameters of the temperature model (Eq. (1)). They include surface emissivity model, ambient temperature, temperature of the atmosphere, relative humidity of the air, viewing distance, error induced by the ambient infrared radiation reflected by the surface, estimation error of the transmissivity of the atmosphere, and atmospheric radiation [99]. The surface emissivity model is the most important source of uncertainty [99, 100]. Orthorectification and image coregistration and mosaicking are other non-negligible sources

http://dx.doi.org/10.5772/64527

of uncertainty. Considering all these uncertainty components, the formal assessment of the resultant uncertainty of the ST derived from airborne infrared thermography ($ST_{airborne}$) using analytical methods such as LPU is not easy to achieve. The uncertainty of the $ST_{airborne}$ was estimated by validation, as an experimental uncertainty combining all the above uncertainty components. The assessment of the experimental uncertainty was performed using in situ measurements carried out by infrared thermometry ($ST_{in\ situ}$) (Eq. (7)).

$$ST = \frac{T_b}{\varepsilon_s^{\frac{1}{4}}} \tag{6}$$

where ST, surface temperature (K); $T_{b,}$ apparent blackbody temperature (K); $\varepsilon_{s,}$ surface emissivity (0, 1).

$$u\left(ST_{airborne}\right) = \sqrt{\frac{1}{N-2}\sum_{i=1}^{N}\left(ST_{airborne\,i} - \left(b + aST_{in\ situ\,i}\right)\right)^2} \tag{7}$$

where $u(ST_{airborne})$, uncertainty of the surface temperature derived from airborne infrared thermography (K); $ST_{airborne,}$ surface temperature derived from airborne infrared thermography (K); $ST_{in\ situ,}$ surface temperature derived from in situ infrared thermometry (K); N, number of observations of the pair ($ST_{in\ situ}$, $ST_{airborne}$); a, slope of the linear regression $ST_{in\ situ}/ST_{airborne;}$ b, intercept of the linear regression $ST_{in\ situ}/ST_{airborne.}$

2.5.3. Surface humidity

Surface humidity (SH) was estimated using the temperature/vegetation dryness index (TVDI) proposed by Sandholt et al. [101]. This index is based on the principle that the direct relationship between soil moisture and ST is not easy to assess. However, soil moisture is an important factor in the spatial and temporal variability of ST. It influences ST via evapotranspiration and the thermal properties of the surface [101]. Also, the status of the vegetation cover is a function of soil water content. Thus, the curve relating ST and NDVI, commonly known as the ST/NDVI space, allows the assessment of the moisture conditions of the surface and the estimation of soil water status [24, 34, 56, 101–105]. For a given site, the point cloud of the relationship TS/NDVI defines a trapezoidal space. This space is a set of isolines representing different states of surface moisture [105]. Its left vertical edge represents bare soil, from a dry state corresponding to an absence of evapotranspiration (E_{null}), to a wet state corresponding to a maximum of evapotranspiration (E_{max}). The horizontal line of the lower limit of the trapezoid defines the wet edge with minimum values of ST (ST_{min}). It reflects the increase of the green vegetation amount along the x axis (increasing NDVI). The slope of the line representing the upper limit of the trapezoid is defined as the dry edge with maximum values of ST (ST_{max}). Eq. (8) shows the formulation of the TVDI, which varies between 0 and 1. A value of 1 corresponds

to dry conditions and is associated with limited water availability. The value 0 corresponds to maximum evapotranspiration and unlimited water availability.

$$\mathrm{TVDI} = \frac{\mathrm{ST} - \mathrm{ST}_{\min}}{\mathrm{ST}_{\max} - \mathrm{ST}_{\min}} \tag{8}$$

where ST, surface temperature (K); $\mathrm{ST}_{\min,}$ line of the wet edge defining the minimum value of ST (K); $\mathrm{ST}_{\max,}$ line of the dry edge defining the maximum value of ST (K).

The line of the dry edge is defined as follows:

$$\mathrm{ST}_{\max} = a + b \times \mathrm{NDVI} \tag{9}$$

The parameters *a* and *b* are the coefficients of the linear regression ST/NDVI determined using the points defining the upper limit of the ST/NDVI space.

The calculation of TVDI is based on the presence of pixels of full vegetation cover, pixels of bare soil, and mixed pixels of vegetation and bare soil in the ST/NDVI space. The classified image was used to identify those pixels in order to compute the point cloud of the ST/NDVI space and to estimate the edge lines needed for the calculation of the TVDI.

The uncertainty of the TVDI was formulated in Eq. (10) on the basis of the LPU [95].

$$u\left(\mathrm{TVDI}\right)^2 = \mathrm{TVDI}^2 \left[\begin{array}{l} \left(\dfrac{u\left(\mathrm{ST}\right)}{\mathrm{ST} - \mathrm{ST}_{\min}} \right)^2 + \left(\dfrac{u\left(\mathrm{ST}_{\max}\right)}{\mathrm{ST}_{\max} - \mathrm{ST}_{\min}} \right)^2 + \\ \left(\dfrac{1}{\mathrm{ST}_{\max} - \mathrm{ST}_{\min}} + \dfrac{1}{\mathrm{ST} - \mathrm{ST}_{\min}} \right)^2 u\left(\mathrm{ST}_{\min}\right)^2 \end{array} \right] \tag{10}$$

where u(TVDI), uncertainty of the temperature/vegetation dryness index; u(ST), uncertainty of the surface temperature (K); $u(\mathrm{ST}_{\max})$, uncertainty of the surface temperature related to the dry edge of the ST/NDVI space (K); $u(\mathrm{ST}_{\min})$, uncertainty of the surface temperature related to the wet edge of the ST/NDVI space (K).

The uncertainty u(ST) is equal to $u(\mathrm{ST}_{\mathrm{airborne}})$ (Eq. (7)). Uncertainties $u(\mathrm{ST}_{\max})$ and $u(\mathrm{ST}_{\min})$ were estimated using the variance of the residuals of the regression lines, respectively, associated with the upper edge (Eq. (11)) and the lower edge (Eq. (12)) of the ST/NDVI space.

$$u\left(\mathrm{ST}_{\max}\right) = \sqrt{\frac{1}{N_{\mathrm{pls}} - 2} \sum_{i=1}^{N_{\mathrm{pls}}} \left(\mathrm{ST}_{\max i} - \left(a + b \times \mathrm{NDVI}_i\right)\right)^2} \tag{11}$$

where $u(ST_{max})$, uncertainty of the surface temperature related to the dry edge of the ST/NDVI space (K); $ST_{max,}$ surface temperature of the dry edge of the ST/NDVI space (K); NDVI, normalized difference vegetation index (−1, 1); a and b, intercept and slope of the line of the dry edge of the ST/NDVI space; $N_{pls,}$ number of pixels used to define the line of the dry edge of the ST/NDVI space.

$$u\left(ST_{\min}\right) = \sqrt{\frac{1}{N_{\text{pli}} - 1}\sum_{i=1}^{N_{\text{pli}}}\left(ST_{\min i} - \overline{ST}_{\min}\right)^2} \tag{12}$$

where $u(ST_{min})$, uncertainty of the surface temperature related to the wet edge of the ST/NDVI space (K); ST_{min}, surface temperature related to the wet edge of the ST/NDVI space (K); $\overline{ST}_{min,}$ average surface temperature of the wet edge of the ST/NDVI space (K); N_{pli}, = number of pixels used to define the line of the wet edge of the ST/NDVI space.

The TVDI estimated from airborne images was validated using in situ measurements of AT and HR, as surface moisture was not measured during the field campaign. This validation is based on the assumption that conditions of high surface moisture are locally associated with lower values of AT and higher values of HR. Conversely, dry surface conditions are locally associated with higher AT values and lower HR values.

3. Results

3.1. Land use and land cover

Airborne multispectral imaging and infrared thermography helped achieve good classification results in the study area. Overall accuracy and kappa coefficient of the supervised classification were, respectively, 84.87% and 0.85. The classified image showed that agricultural surfaces represent the main LULC of the study area (53.25%). The proportion of this area occupied by the other LULC themes is 28.82% for forests, 11.66% for hay and grazing land, 2.63% for impervious surfaces, and 0.28% for water (**Figure 3**). Vegetable crops and large-scale farming are the main components of agricultural surfaces. They occupy 23.50 and 17.58%, respectively, of the study area. The proximity of vegetable crops with organic bare soil (OBS) shows that they are mainly grown on this type of soil. The presence of OBS on vegetable crop fields denotes the high variability that could characterize the microclimate of these environments.

3.2. Vegetation quantity

The NDVI derived from airborne multispectral imaging ($NDVI_{aero}$) varies in the study area between −0.73 and 0.84 (**Figure 4**), with an average value of 0.34 and a standard deviation of ±0.31. It is strongly correlated with the NDVI derived from in situ observations (r = 0.994; p = 0.006) (**Figure 5**). Uncertainty and bias of the $NDVI_{aero}$, based on in situ observations, are, respectively, ±0.045 and −0.118. On average, the $NDVI_{aero}$ underestimates the NDVI values by

about 0.118. The NDVI map shows three major classes of LULC in the study area (**Figure 4**). In the first group, IS, dry crop residues, and MBS have NDVI values less than 0. In the second group, water, OBS, and PCVC have NDVI values between 0 and 0.33. In this category, OBS is characterized by NDVI values between 0 and 0.29, with an average value of 0.10 and a standard deviation of ±0.045. The third group includes forest and FCVC surfaces, which are characterized by the highest values of NDVI (NDVI mean = 0.60).

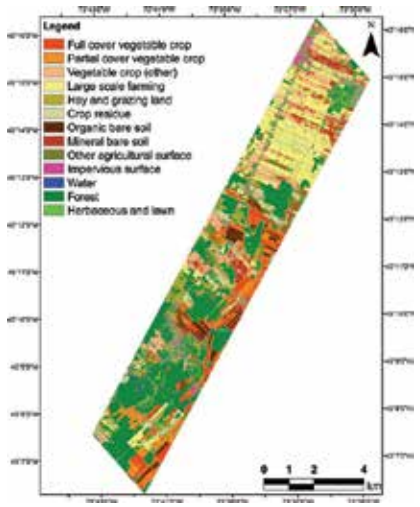

Figure 3. Classification of the land use and land cover using airborne multispectral imagery and infrared thermography.

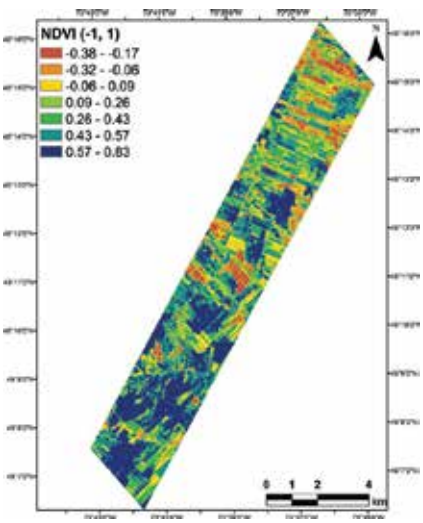

Figure 4. Variation of the normalized difference vegetation index (NDVI) over the study area.

http://dx.doi.org/10.5772/64527

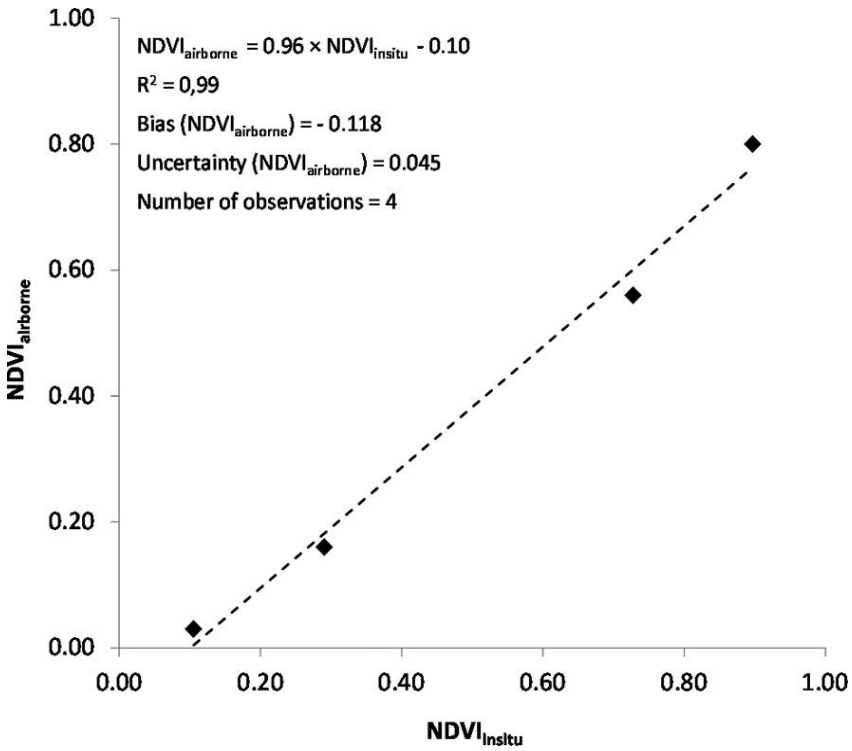

Figure 5. Validation and uncertainty assessment of the NDVI derived from airborne multispectral imagery with in-situ observations.

Average values of NDVI associated with OBS (0.10) and full vegetation cover (0.60) were, respectively, used as minimum and maximum values of NDVI for the estimation of PVC (Eq. (3)). **Figure 6** shows the map of the variation of PVC over the study area. It varies between 0 and 1, with an average value of 0.48 and a standard deviation of ±0.42. Its resultant uncertainty varies between 0 and ±0.365 over the study area (**Figure 7**). The variation of PVC and its resultant uncertainty according to NDVI is illustrated by **Figure 8**. PVC uncertainty increases with NDVI values. Thus, highest PVC uncertainties are observed on areas with greater vegetation cover and lowest PVC uncertainties are observed on areas with smaller vegetation cover (**Figure 8**). The average value of PVC on FCVC surfaces is 0.70, with an average uncertainty of ±0.279, while PCVC surfaces have an average value of 0.48 PVC, with an average uncertainty of ±0.215. Comparatively, forest cover is characterized by an average value equal to 0.90 PVC, with an average uncertainty of ±0.338. PVC is characterized by a lower spatial variability compared to NDVI, because all NDVI values less than or equal to 0.10 have a PVC value equal to 0 and, all NDVI values greater than or equal to 0.60 have a PVC value of 1. However, the spatial dynamics of agricultural surfaces, ranging from bare soil (PCV = 0) to complete vegetation cover (PCV = 1), is best described by PVC rather than NDVI. To illustrate this, **Figure 9** show the variation of NDVI and PVC values on potato crop fields in different phenological stages.

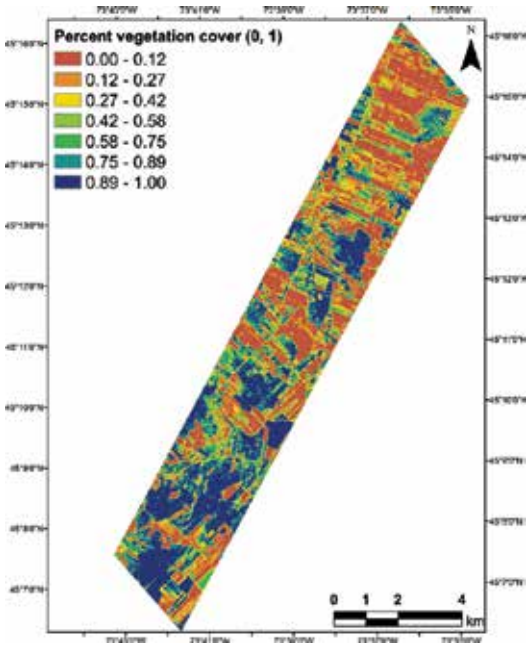

Figure 6. Variation of the percent vegetation cover (PVC) over the study area.

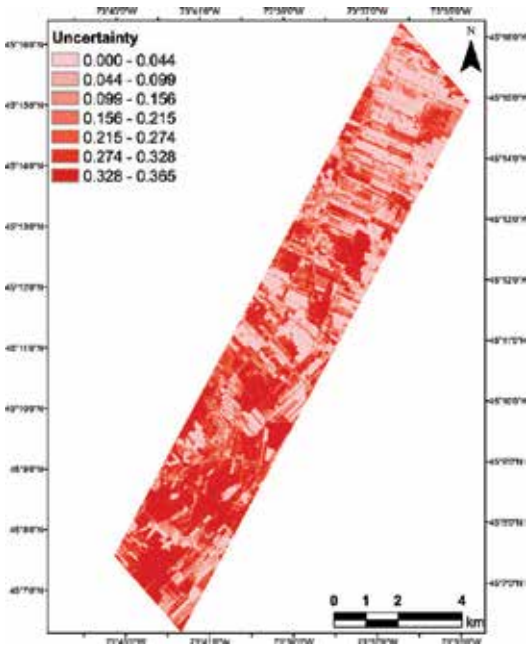

Figure 7. Variation of the uncertainty of the percent vegetation cover (PVC) over the study area.

http://dx.doi.org/10.5772/64527

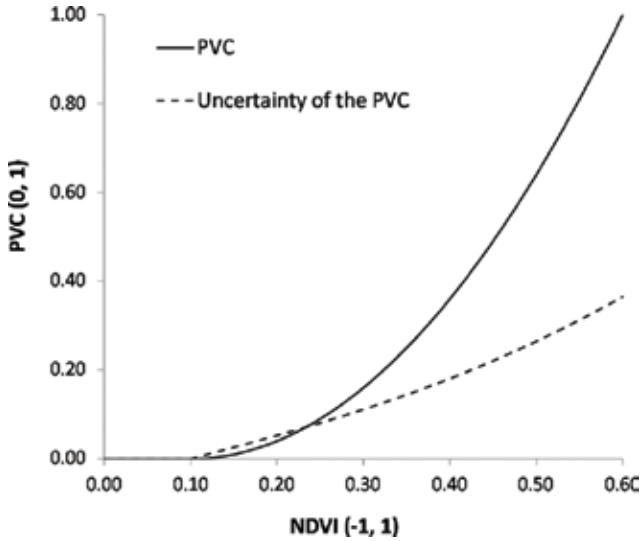

Figure 8. Variation of the percent vegetation cover (PVC) and its uncertainty according to the normalized difference vegetation index (NDVI).

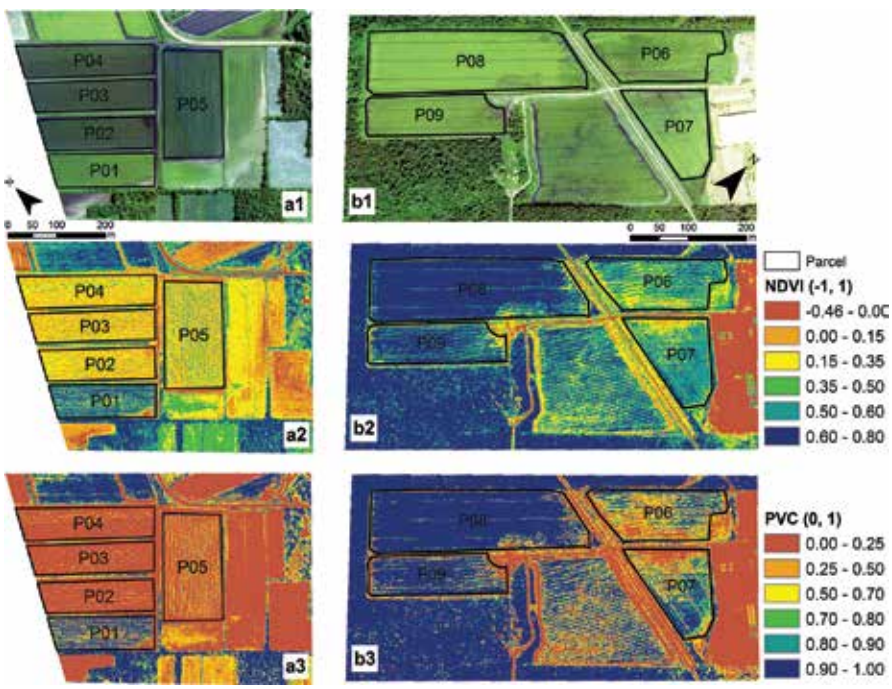

Figure 9. Variation of the normalized difference vegetation index (NDVI) and the percent vegetation cover (PVC) over potato crops at different phenological stages.

3.3. Surface temperature

Surface temperature estimated by airborne infrared thermography ($ST_{airborne}$) demonstrates a very high thermal spatial variability over the study area (**Figure 10**). This variability occurs both at the intra-plot and local scales. In the period of airborne data acquisition (09:10–11:00 am) and across the study area, the $ST_{airborne}$ varies from 290 to 331 K, with an average value of 300.60 K (SD = ±3.42 K). This represents a spatiotemporal variation of more than 40 K over an area of 56 km^2 and a period of about 2 h. The correlation between $ST_{airborne}$ and $ST_{in\ situ}$ is very high (r = 0.99; p = 0.010) (**Figure 11**). The experimental uncertainty and the bias of the $ST_{airborne}$ compared to in situ observations are, respectively, 0.73 and ±1.42 K.

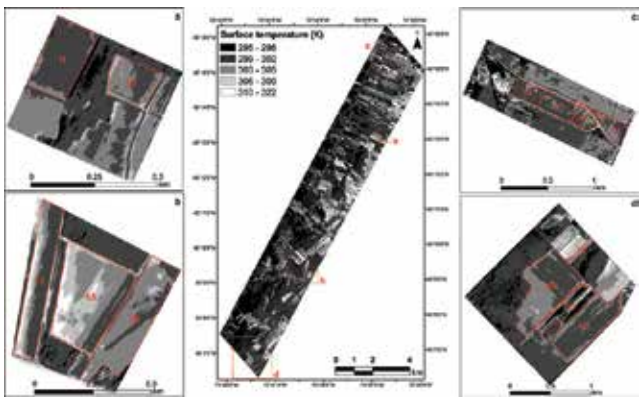

Figure 10. Variation of the surface temperature (ST) over the study area: (a) ST variation according to soil type, (b) ST variation according to soil quality, (c) ST variation on crop surfaces according to soil drainage, and (d) ST variation according to crop varieties and phenological stages.

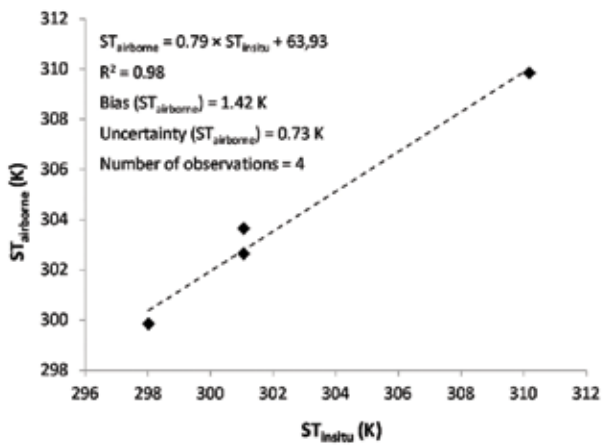

Figure 11. Validation and uncertainty assessment of the surface temperature (ST) derived from airborne infrared thermography with in situ observations.

http://dx.doi.org/10.5772/64527

Table 1 shows the variations of $ST_{airborne}$ on various classes of LULC. Highest temperature values and highest temperature variations are observed on impervious surfaces (ST_{mean} = 309.99 K, SD = ±5.12 K, ST_{max}–ST_{min} = 39.5 K). Lowest temperature values and lowest temperature variations are observed on surface waters (ST_{mean} = 296.67 K, SD = ±0.74 K). The standard deviation of the temperature associated with this class is very close to the uncertainty of $ST_{airborne}$. Among vegetation areas, forests present the lowest temperature values and the lowest temperature variations (ST_{mean} = 297.87 K, SD = ±0.97 K). Surface temperature values and variations of full cover vegetable crops (ST_{mean} = 298.91 K, SD = ± 1.43 K) are close to those of large scale farming (ST_{mean} = 298.01 K; SD = ± 1.57 K), while ST values and variations of partial cover vegetable crops (ST_{mean} = 302.22 K; SD = ± 2.60 K) are closer to those of hay and grazing surfaces (ST_{mean} = 302.01 K; SD = ± 2.55 K). Temperature variation reached 8 K on full cover vegetable crop surfaces, while ST varied over 17 K on partial cover vegetable crops. These large variations are mainly due to soil temperature. ST values are on average higher and vary much more on organic bare soil (ST_{mean} = 307.36 K; SD = ± 3.87 K) than on mineral bare soil (ST_{mean} = 304.65 K; SD = ± 2.52 K). The variations of ST on organic bare soil reached 20.33 K and the difference between the ST of vegetable crops and the ST of organic bare soil reached 21.44 K. This very high variation of ST on organic bare soil may be due to water status and the high spatial and temporal dynamics of the temperature of this type of surface.

	Surface temperature (K)			
	Minimum	**Maximum**	**Mean**	**Standard deviation**
Impervious surface	291.66	331.16	309.88	5.12
Water	293.73	298.91	296.67	0.74
Forest	294.84	303.36	297.87	0.97
Hay and grazing land	295.75	311.32	302.01	2.55
Full cover vegetable crop	296.25	304.33	298.91	1.43
Partial cover vegetable crop	297.13	314.16	302.22	2.6
Large scale farming	294.92	305.7	298.01	1.57
Mineral bare soil	297.45	314.31	304.65	2.52
Organic bare soil	297.36	317.69	307.36	3.87

Table 1. Variation of the surface temperature derived from airborne infrared thermography in the study area according to land use and land cover.

Field survey and in situ observations show that intra-field variability of $ST_{airborne}$ observed in vegetable crops are associated with spatial patterns which are related to

- Topographic variation
- Variation of soil type (organic versus mineral soil)
- Different states of organic matter in black soil crops (decomposed soil, not decomposed soil, loam)

- Soil drainage problems in certain areas of the field
- Bare soil versus vegetation areas
- Presence of different crop varieties on the same plot
- Variation of crop phenology on the same field due to different planting dates of crop units
- Water and mineral stress
- Abiotic damage due to phenomena like strong wind, heavy rain, heat stress, farm machinery, and pesticides
- Stress and biotic damage caused by disease and pests
- Proximity to windbreaks (windproof effect)
- Yield variation

The study area is mainly composed of organic and mineral soil. Organic soils are mostly located in the south part which was formerly covered by lakes. Hence, a strong relationship between land elevation and soil type in the area. The values of ST are higher on organic soil compared to mineral soil. Loam soils are sometime present on organic soil fields. **Figure 10a** shows a strong variability of ST between a loam zone (higher values of ST) and an organic soil zone (lower ST values) on field 53. On some fields, the organic soil is not well decomposed. Its nutritional quality is reduced. This causes growth problems and gives rise to a high intra-field variability of ST, which is the case with field 15 on which is grown Chinese cabbage (**Figure 10b**). Poor drainage and flooding caused by underground tanks, for example, can hamper crop growth and lead to a strong spatial variability of ST due to lower vegetation cover in the problematic areas of the field. **Figure 10c** shows a maize crop field affected by poor soil drainage. The temperatures are higher on the problematic areas of the field due to lower vegetation cover.

Intra-field variation from bare soil to full vegetation cover is associated with the highest temperature variabilities observed on the fields (**Figure 10d**, field G3). ST values are much higher on bare soil than on full cover vegetable crops. **Figure 10d** shows temperature variations above 14 K on field G3, which is a mix of bare soil and vegetation. Different crop varieties are characterized by varying phenology, canopy structure, and planting dates. This causes a spatial variability of ST. **Figure 10d** shows temperature variations between lettuce, celery, and potato crops. Subdivision of fields according to different planting dates results in a variation of phenological stages within the same crop variety, hence a variation of percent vegetation cover and ST within the field. Spatial variability of ST on field M3 (celery crop) (**Figure 10d**) is primarily a function of growth stages associated with different planting dates. The lowest temperatures are those of the vegetation cover of the most mature plants. While higher temperatures are associated with younger plants, which are characterized by a lower percent vegetation cover. Spatial variability of ST on crop surfaces are related not only to the variability of soil and crop varieties but also to several other agrometeorological factors such as soil moisture, nutrient and water stress, abiotic damage by weather conditions or cultural practices, and damage caused by pests. Thus, a high spatial variability of ST over a field or crop unit

http://dx.doi.org/10.5772/64527

may indicate a crop growth problem and therefore reflect variability in yield. Temperature variability of the field presented at **Figure 10c** is strongly correlated with yield maps (not presented here—yield maps were shown by the farmer).

3.4. Surface humidity

3.4.1. Lines of dry and wet edges of the TS/NDVI space and their uncertainties

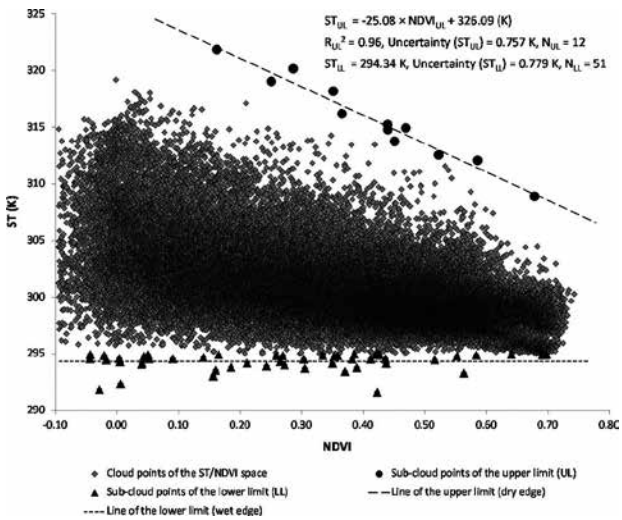

Figure 12. Cloud points of the ST/NDVI space and estimation of dry edge and wet edge lines.

Cloud points of the ST/NDVI space established with airborne infrared thermography and airborne multispectral images describe a trapezoidal area where the upper edge is associated with the highest dry conditions and the lower edge is associated with the highest moisture conditions (**Figure 12**). The cloud points of the upper edge were used to establish the equation of the dry limit (ST = −25.08 × NDVI + 326.09 (K)) with an uncertainty of ±0.757 K, and the cloud points of the lower edge was used to establish the equation of the wet limit (ST = 291.61 K) with an uncertainty of ±0.779 K. Both uncertainty values are close to the one of $ST_{airborne}$. The points of the wet limit are mainly located on the western edge of the study area, while a large majority of the points of the dry limits are located on the eastern boundary. The western boundary is the location of the first flight lines' images, acquired in the morning during the period of the lowest ST values. The points of the wet limit are located on vegetation surfaces and on bare soil with low ST values. The eastern boundary is the location of the last flight lines' images, acquired late in the morning when ST values are higher.

3.4.2. Surface moisture variability and uncertainty components of the TVDI

The map of the TVDI confirms that the wetter surfaces are located on the western side of the study area and the driest surfaces are located on the eastern part (**Figure 13**). There are

however, some drought islands (TVDI > 0.50) in the wetter zone and some moisture islands (TVDI < 0.30) in the driest zones. Among the drought islands, there are hay, organic bare soil, and low cover vegetable crops on organic soil (PCV < 0.25). Organic bare soil, full cover vegetable crops, and partial cover vegetable crops are among the moisture islands observed in the driest areas. Over the study area and the period of observation, the TVDI ranges between 0 and 1, with a mean value of 0.35 (SD = ±0.097). Its uncertainty varies between ±0.021 and ±0.126 (**Figure 14**), with an average value of ±0.055 (SD = ±0.016). The histogram of the uncertainty of the TVDI shows three peaks around the values ±0.033, ±0.040, and ±0.068 (**Figure 15**). The map of the uncertainty confirms these three peaks which are associated with three types of surfaces (**Figure 14**). The first type corresponds to surfaces of low values of NDVI such as mineral bare soil, hay, and grazing lands. The second type also corresponds to surfaces of low NDVI values such as organic bare soil and low cover vegetable crops on organic soil. Areas with a high percent vegetation cover, dominated by forests and full cover crops, compose the third type of surface on which higher values of uncertainty are observed (**Figure 14**). This shows that the uncertainty of the TVDI increases with the NDVI (**Figure 16**). **Figures 17** and **18** show that this uncertainty also increases when the ST or the temperature of the dry limit (ST_{max}) are near the temperature of the wet limit (TS_{min}). However, this situation generally corresponds to a high vegetation cover with low ST values, therefore a tendency to observe low values of TVDI and higher surface moisture values. These conditions converge toward the wet limit (**Figure 19**).

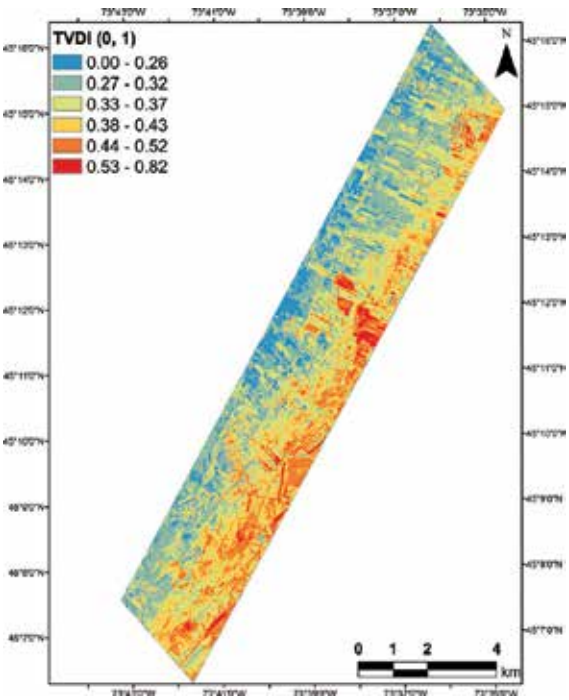

Figure 13. Variation of the temperature/vegetation dryness index (TVDI) over the study area.

http://dx.doi.org/10.5772/64527

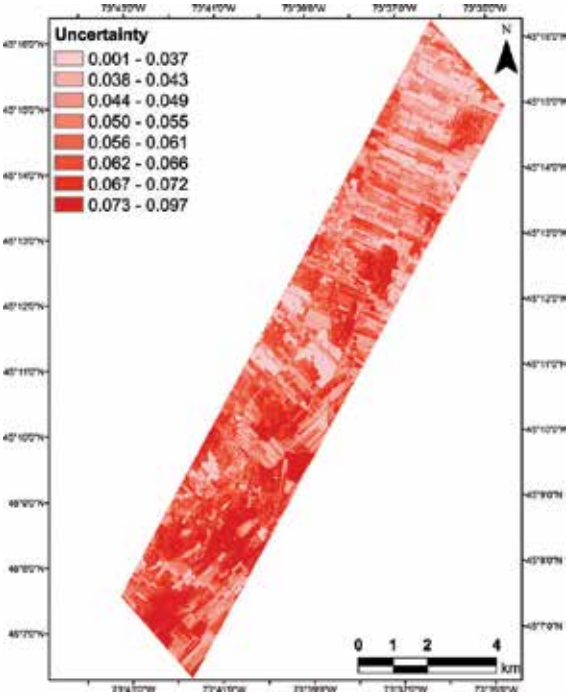

Figure 14. Variation of the uncertainty of the temperature/vegetation dryness index (TVDI) over the study area.

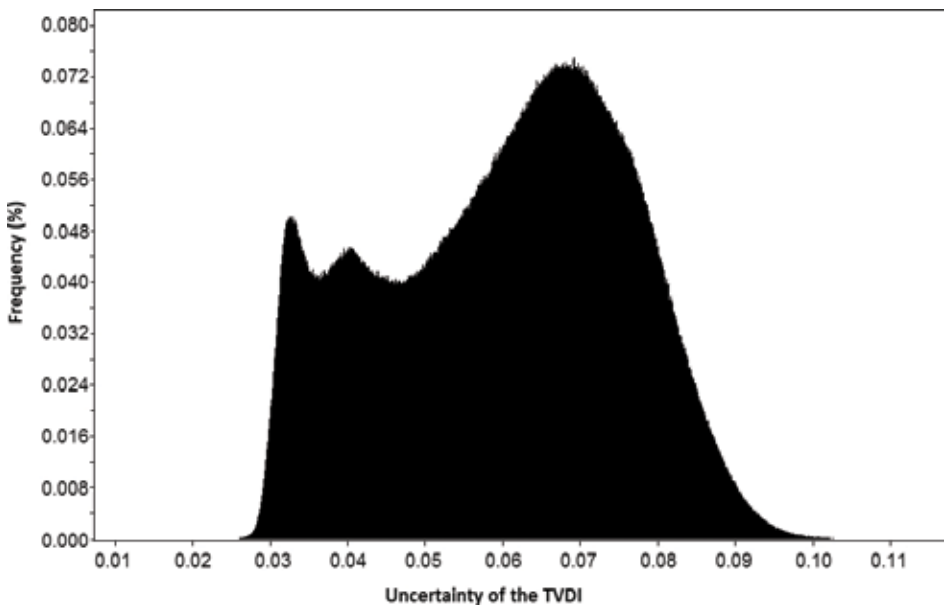

Figure 15. Histogram of the uncertainty of the temperature/vegetation dryness index (TVDI) over the study area.

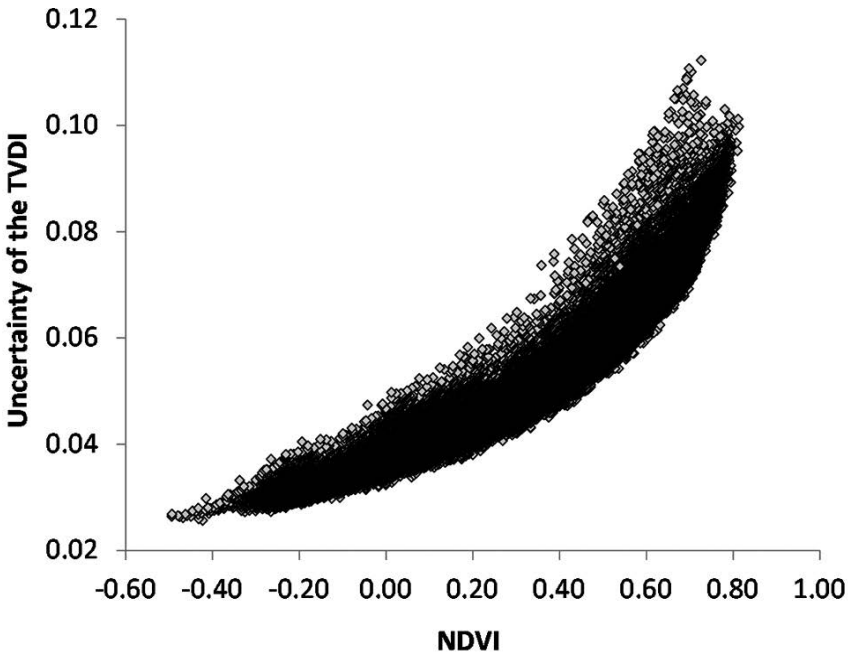

Figure 16. Variation of the uncertainty of the temperature/vegetation dryness index (TVDI) according to the normalized difference vegetation index (NDVI).

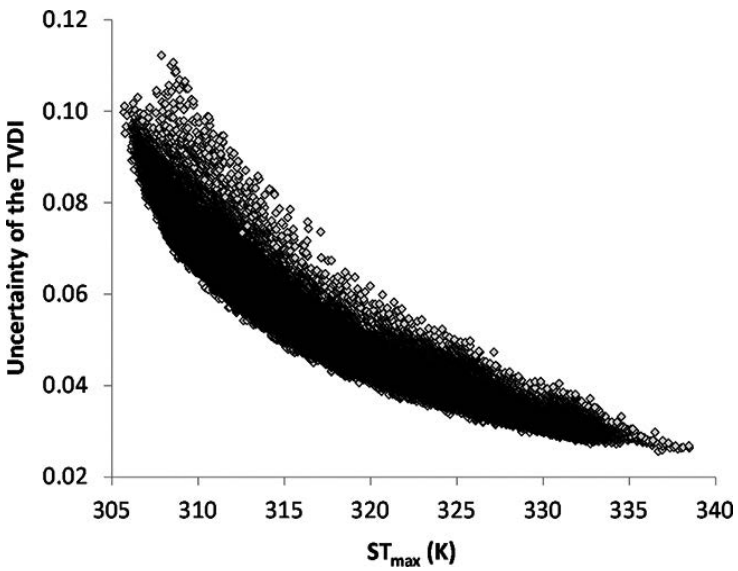

Figure 17. Variation of the uncertainty of the temperature/vegetation dryness index (TVDI) according to the surface temperature of the dry edge (STmax).

http://dx.doi.org/10.5772/64527

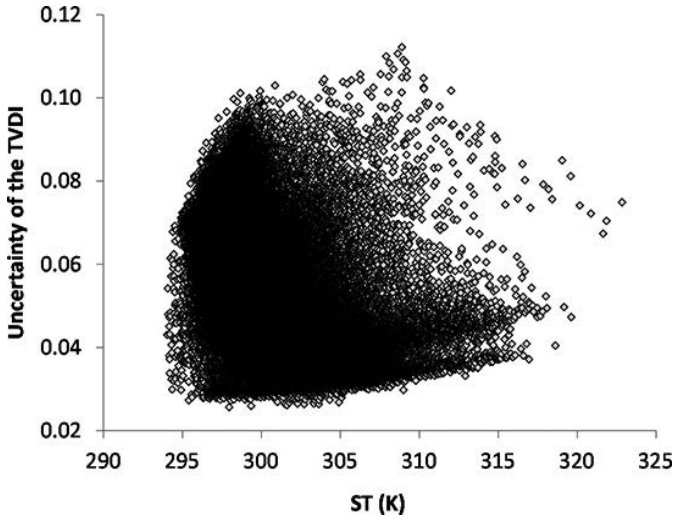

Figure 18. Variation of the uncertainty of the temperature/vegetation dryness index (TVDI) according to the surface temperature (ST).

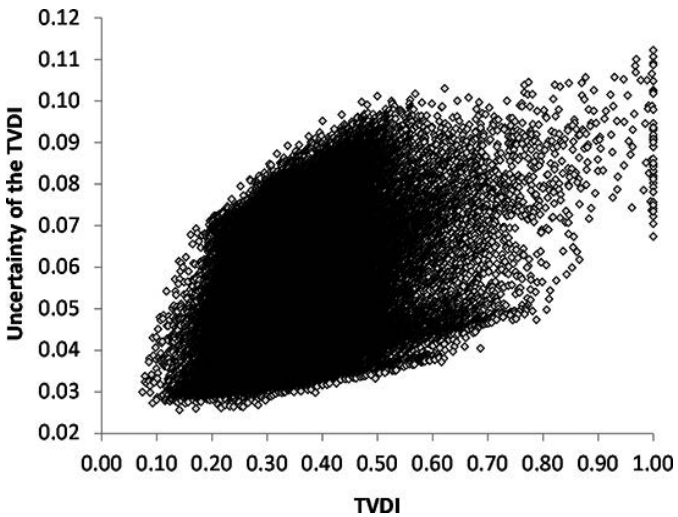

Figure 19. Variation of the uncertainty of the temperature/vegetation dryness index (TVDI) according to the TVDI.

3.4.3. Spatial variability of the TVDI on agricultural surfaces

The TVDI varies between 0.20 and 0.70 across full cover vegetable crop surfaces, with an average value of 0.39 (SD = ±0.076) and an average uncertainty of ±0.067 (SD = ±0.006). This shows that the surface moisture is much lower in some agricultural parcels compared to others. However, full cover vegetable crops are on average wet surfaces rather than dry. This trend

is also observed on partial cover vegetable crop surfaces where the TVDI varies between 0.15 and 0.93, with an average value of 0.44 (SD = ±0.093) and an average uncertainty value of ±0.058 (SD = ±0.011). Much drier surfaces are observed on partial cover vegetable crops compared to full cover vegetable crops. On average, surface moisture was higher on large-scale crops compared to vegetable crops. The TVDI values of the first ones vary from 0.14 to 0.83, with an average value of 0.31 (SD = ±0.065) and an average uncertainty value of ±0.064 (SD = ±0.009). Surface moisture of organic bare soils is highly variable (TVDI: AV = 0.48, SD = ±0.116), with very wet surfaces (TVDI < 0.25) and very dry surfaces (TVDI > 0.75), while mineral bare soil surfaces are wetter on average (TVDI: AV = 0.33, SD = ±0.063).

3.4.4. Relationship between the TVDI and in situ observations of air temperature and relative humidity

The relationship between the TVDI and in situ observations shows that it is highly correlated with air temperature ($r = 0.88$, $p = 0.004$, **Figure 20**). However, it does not present a correlation with relative humidity ($r = 0.09$; $p = 0.826$). The correlation between the TVDI and air temperature verifies the hypothesis that conditions of higher surface moisture (the TVDI value tends toward 0) are locally associated with lower values of air temperature, while the conditions of lower surface moisture (the TVDI value tends toward 1) are associated with higher values of air temperature (**Figure 20**). **Figure 20** shows that the locations at which in situ observations were made are predominantly wet surfaces (TVDI < 0.50). That did not permit the assessment of the relationship between the TVDI and in situ observations of air temperature and relative humidity in drier conditions.

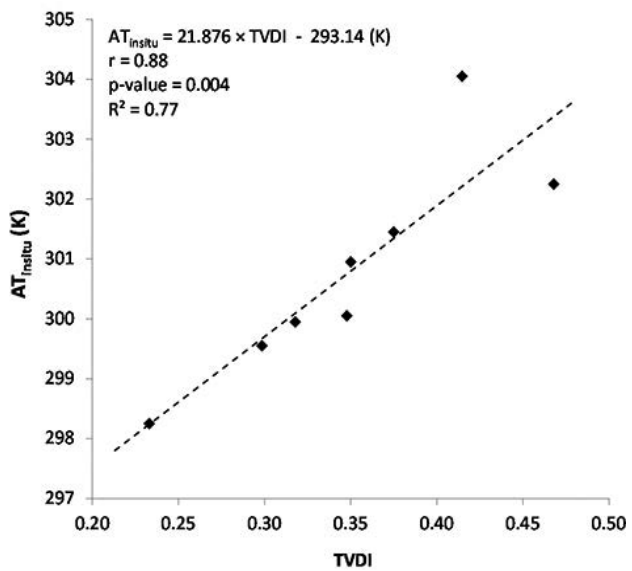

Figure 20. Correlation between the temperature/vegetation dryness index (TVDI) derived from airborne imagery and in situ observations of air temperature (AT).

http://dx.doi.org/10.5772/64527

4. Discussion

4.1. Vegetation index and percent vegetation cover

The NDVI estimated using airborne multispectral imaging ($NDVI_{airborne}$) is an important indicator of the spatial heterogeneity of agricultural surfaces and their intra-plot variability. It allows the easy distinguishing of different states of agricultural lands like full vegetation cover, partial vegetation cover, and bare soil. NDVI values which are associated with these thematic classes were, respectively, estimated at 0.58 (SD = 0.087), 0.37 (SD = 0.172), and 0.10 (SD = 0.071) for vegetable crops on organic soil. These values are close to those observed in different studies using in situ observations if we consider the bias of 0.118 between $NDVI_{airborne}$ and $NDVI_{in\ situ}$. For example, Van De Griend and Owe [92] report a value of 0.157 for the NDVI of bare soil (sandy loam). Considering all potential sources of error mentioned above and the uncertainty of NDVI values reported by different studies [106], the uncertainty of ±0.045 of $NDVI_{airborne}$ is satisfactory. Nagol [106] reports NDVI uncertainty values varying between ±0.023 and ±0.085 according to different types of vegetation and weather conditions. Compared to NDVI, PVC refers more to a vegetation cover rate and a quantity of biomass. Full cover vegetation has a maximum PVC value and an absence of vegetation have a zero value. Thus, PVC allows a better characterization of the amount of vegetation, from bare soil to full vegetation cover. This characterization would allow a better assessment of phenological stages.

4.2. Airborne infrared thermography, surface temperature of agricultural lands and crop management

The estimation of ST using airborne infrared thermography ($ST_{airborne}$) allowed the characterization of the intra-plot variability of agricultural lands over the study area. This variability is mainly associated with a variation in the percent vegetation cover, the type of vegetation, surface moisture conditions, and different types of soil. $ST_{airborne}$ thus helps to reveal the changing microclimate conditions across crop fields. It is a useful variable for the modeling and estimation of MCIs at local scales. And it offers a high potential for crop management given its ability to detect problematic areas in the field. The $ST_{airborne}$ was estimated with an uncertainty of ±0.73 K and a bias of 1.42 K with respect to in situ observations. The uncertainty of $ST_{airborne}$ is greater than the sensitivity of the infrared thermography camera (±0.007 K), but its estimated bias is lower than the accuracy of the camera (2.00 K). The uncertainty of $ST_{airborne}$ is due to the measurement accuracy of the camera, the uncertainty of the surface emissivity estimated by using in-situ observations and airborne multispectral imagery, the uncertainty of the atmospheric correction, and the uncertainties of the orthorectification and image mosaicking. The uncertainty of $ST_{airborne}$ is relatively good considering all these sources of uncertainties. Some conditions and components of the method helped to achieve this good result in the present study: (1) the clear sky during the acquisition of the airborne images, (2) the low altitude used for this acquisition which resulted in a low optical thickness, and (3) the mapping of surface emissivity which helped to reduce the influence of the main source of uncertainty in the estimation of the $ST_{airborne}$. The estimation of $ST_{airborne}$ in clear sky conditions with a relatively low uncertainty, aligns with the observations of Moran et al. [107] who report

that in these conditions where visibility is high and water vapor content is low, the atmospheric correction of thermal images is not necessary because the absorption by atmospheric particles is balanced by the thermal emission of these components. The uncertainty and the bias of the $ST_{airborne}$ is close to those of the ST estimated using other airborne sensors [108–110] or earth observation satellites [108, 111–116]. Considering the high intra-plot variability of ST, even if on full cover vegetation surfaces, the uncertainty of $ST_{airborne}$ is satisfactory to characterize the microclimate conditions of agricultural lands. Using airborne infrared thermography is a promising approach to characterizing agricultural surfaces and a promising diagnostic and decision-making tool for crop management. This allows the characterization of growing conditions along with the occurrence and behavior of diseases and pests through the estimation of several other MCIs like surface humidity and near surface air temperature.

4.3. The TVDI indicator of surface moisture

The trapezoidal space ST/NDVI and the TVDI estimated using airborne multispectral imaging and infrared thermography allowed a good characterization of the spatial variability of surface moisture and its temporal variability induced by successive acquisition flight lines. The variation of humidity conditions over the study area, from the wet limit to the dry one, is thus both time and space dependent. This study shows that the ST/NDVI space and the limit lines defining the TVDI could be established on an intra-seasonal and inter-seasonal basis to assess surface moisture and could take into account not only prevailing moisture conditions at the time of image acquisition but also taking into account the dynamics of these conditions throughout the season and between seasons. The concept of sub-cloud points of wet and dry limits of the ST/NDVI space and their clear identification were used to improve the estimation of those limit lines and to assess their uncertainty. The use of sub-cloud points reduces the subjectivity of the estimation of the limit lines by calculating their uncertainty. Wang et al. [63] report about this subjectivity and the imprecision that it generates in the estimation of the TVDI. The concept of the sub-cloud points of the limit lines allows the assessment of this imprecision and allows this to be taken into account when estimating the uncertainty of the TVDI. The TVDI was estimated over the study area with a low uncertainty. The analysis of the components of this uncertainty showed that it is strongly related to the NDVI and the temperature of the dry limit. The uncertainty of the TVDI increases with the NDVI, and it decreases with the temperature of the dry limit. Each of these two variables allows a full expression of the minimum and maximum uncertainty of the TVDI for a given percent vegetation cover. These results confirm those of Li et al. [21] who also report that the uncertainty of the TVDI increases with the NDVI and the approximation of the isolines. The TVDI showed that the intra-plot variability of surface moisture may be quite high on vegetable crop surfaces. Of two neighboring fields, the spatial extent of one can be mainly characterized by surface moisture conditions close to those of the wet limit while that of the other one can be mainly characterized by surface moisture conditions close to those of the dry limit. This reflects the high spatial variability of the agro-meteorological conditions that could influence the abundance of crop diseases and pests in the fields.

http://dx.doi.org/10.5772/64527

4.4. Added value of the integration of optical and microwave data for the characterization of microclimatic conditions and crop identification

The integration of microwave remote sensing data (passive or active) with optical (multispectral) and thermal data offers several advantages both for the characterization of microclimatic conditions and for the characterization of land use and land cover (LULC). This integration makes it possible to characterize both the microclimatic conditions of the surface (surface temperature and moisture) and the air near the surface (near surface air temperature) by using optical and thermal remote sensing data and the microclimatic conditions of the soil layers near the surface (soil temperature and moisture) by using microwave remote sensing data.

Soil temperature and soil moisture are two important agro-meteorological variables. The first has an influence on both the development of crops and several pests and pathogenic microorganisms in the soil. The second is more directly related to the water content of the soil, and thus to the amount of water available for the development and growth of crops. But in the conditions of the presence of vegetation and cloud cover, it is more difficult to estimate these two variables using optical and thermal remote sensing data. Indeed, in the presence of vegetation, surface temperature and moisture estimated by optical and thermal data are more related to the canopy or to a mixed surface composed of canopy and fraction of bare soil, while microwave remote sensing data offer a better potential for estimating soil temperature and soil humidity even in the presence of vegetation (low vegetation percent cover) and clouds [117–120]. For example, Manns et al. [118] used data from the airborne sensor Passive Active L-band System (PALS) to estimate soil moisture in agricultural and forest areas. However, some disadvantages are associated with the use of microwave remote sensing for estimating soil temperature or soil moisture depends on the type of system used. The major one is the low spatial resolution of passive microwave sensors [117, 119]. The use of radar sensors (active microwave) has the advantage of a better spatial resolution compared to passive microwave sensors. However, the estimation of soil moisture using radar images is more difficult because these data are more sensitive to the surface roughness and to the structure of the canopy [117].

Different crop varieties may have different canopy structures (size and geometry of the canopy, canopy density, leaf orientation, row direction) at certain phenological stages [121]. As the radar remote sensing data are highly sensitive to this structural variation [117], their integration with optical data acquired at specific periods of the season optimizes the accuracy of the algorithms used to perform classification of crops [121].

4.5. About the use of airborne-based technologies versus spaceborne-based technologies

Airborne data offer many advantages for the characterization of microclimatic conditions, identification of different crop varieties, and monitoring of crop condition and phenology. One of the most important advantages is the flexibility of the choice of spatial resolution, spectral resolution, and temporal resolution at which the images will be acquired.

Compared to satellite images for which the spatial, temporal, and spectral resolutions are already set, those of airborne images can be defined according to the needs and constraints of the user. For example, very high spatial resolution images can be acquired at particular periods

of the season and at specific times of the day to meet precise needs in agriculture. However, the spatial, temporal, and spectral resolutions of satellite images would not allow to do so.

The growing interest in the use of drones for remote sensing applications and their rapid development open the way for a greater access to airborne imagery with reducing acquisition costs (aircraft rent and pilot fees, flight authorization, etc.), increasing autonomy (the purchase of a drone and the expertise to operate it are more accessible compared to an aircraft), and reducing constraints related to airborne mission (minimum permitted flight height, the spatial resolution increases with the decrease of the flight height).

5. Conclusion

Infrared thermography and airborne multispectral imaging were used in this study to estimate surface microclimate indicators (SMIs) at local scale and to assess their uncertainties. Normalized difference vegetation index (NDVI), percent cegetation cover (PVC), surface temperature (ST) and the temperature/vegetation dryness index (TVDI) were used to characterize local and intra-plot variability of the amount of vegetation, the surface temperature, and surface moisture. The ST estimated by airborne infrared thermography offers a high potential for the management of vegetable crops, as it allows the detection and investigation of problematic zones in the fields. The spatial variability of surface temperature has been associated with several growth factors and management practices of agricultural lands such as soil type (mineral soil, black earth, loam), drainage and soil quality, soil moisture, crop varieties and their growth stage, and stress (water and nutrient deficit, abiotic damage). This thermal variability is the result of several agro-meteorological phenomena that govern crop yields, as well as the occurrence and behavior of crop pests and diseases. The TVDI demonstrated that intra-plot variability of surface moisture may be quite high on crop surfaces. This reflects the high variability of microclimate conditions that can affect diseases and pests that are present on these surfaces. The main limitation of the applications of SMIs derived from airborne remote sensing is the cost of images acquisition and processing. Planning airborne missions and using unmanned aerial vehicles (UAV) via a shared service that includes different stakeholders working in the same territory (agricultural producers, agroenvironmental consulting clubs, phytosanitary warning networks, etc.) would be able to meet the specific needs of crop management and integrated pest management (spatial and temporal resolution, periods and critical management areas), while significantly reducing the costs associated with the use of such data. Moreover, the rapid development of technologies related to Earth observation satellites and sensors has led to better spatial and temporal resolutions. The growing availability of Earth observation images due to a greater number of satellites in orbit, the advent of satellite constellations, and various integrated Earth observation programs will allow for greater frequency of image acquisition over vast territories and at finer scales. This will help reduce data gaps and enable better monitoring of microclimate and agrometeorological conditions at local scales.

http://dx.doi.org/10.5772/64527

Acknowledgements

This work is a part of the thesis study of the first author. It was carried out with the financial support of the Natural Sciences and Engineering Research Council of Canada (NSERC) and the Compagnie de Recherche Phytodata Inc., PRISME Consortium, Sherrington, Québec, Canada through the Industrial Postgraduate Scholarships (IPS) program. Thanks to Stéphanie Bourgon, Jocelyn Bluteau, Gilles Lavoie, Richard Picard, Guido Castellanos, Bakary Koné, and Aliou Diouf, all from Université Laval, for their help in acquisition and processing of GPS data, measurement of in situ meteorological and spectroradiometric data, and planning and acquisition of airborne remote sensing images. We also thank the staff of the PRISME Consortium, especially Luc Brodeur, Gerardo Gollo Gill, Caesar Chlela, Abdenour Boukhalfa, Mohammed Boudache, and Franck Bosquain who facilitated our research residency within their organization and supported our collection of data in the field.

Author details

Serge Olivier Kotchi[1,2,3*], Nathalie Barrette[2,4], Alain A. Viau[2,3], Jae-Dong Jang[5], Valéry Gond[6] and Mir Abolfazl Mostafavi[2,3]

*Address all correspondence to: serge-olivier.kotchi@phac-aspc.gc.ca

1 National Microbiology Laboratory (NML), Public Health Agency of Canada (PHAC), Saint-Hyacinthe, Quebec, Canada

2 Faculty of Forestry, Geography and Geomatics, Laval University, Quebec City, Quebec, Canada

3 Center for Research in Geomatics (CRG), Laval University, Quebec City, Quebec, Canada

4 Hydro-Quebec Institute in Environment, Development and Society (EDS Institute), Laval University, Quebec City, Quebec, Canada

5 National Meteorological Satellite Center (NMSC), Korean Meteorological Administration (KMA), Jincheon, South Korea

6 French Agricultural Research Centre for International Development (CIRAD), Montpellier, France

References

[1] Carisse O, Tremblay D-M, McDonald MR, Brodeur L, McRoberts N. Management of botrytis leaf blight of onion: the Québec experience of 20 years of continual improvement. Plant Disease. 2011;95(5):504–14.

[2] Dalla Marta A, Magarey RD, Orlandini S. Modelling leaf wetness duration and downy mildew simulation on grapevine in Italy. Agricultural and Forest Meteorology. 2005;132(1–2):84–95.

[3] Gordon TR, Koike ST. Management of Fusarium wilt of lettuce. Crop Protection. 2015;73:45–9.

[4] Park Y-L, Krell RK, Carroll M. Theory, technology, and practice of site-specific insect pest management. Journal of Asia-Pacific Entomology. 2007;10(2):89–101.

[5] Whitfield GH, Carruthers RI, Haynes DL. Phenology and control of the onion maggot (Diptera: Anthomyiidae) in Michigan onion production. Agriculture, Ecosystems & Environment. 1985;12(3):189–200.

[6] Wu BM, Subbarao KV, van Bruggen AHC. Analyses of the relationships between lettuce downy mildew and weather variables using geographic information system techniques. Plant Disease. 2005;89(1):90–6.

[7] Hoogenboom G. Contribution of agrometeorology to the simulation of crop production and its applications. Agricultural and Forest Meteorology. 2000;103(1–2):137–57.

[8] Delamater PL, Messina JP, Qi J, Cochrane MA. A hybrid visual estimation method for the collection of ground truth fractional coverage data in a humid tropical environment. International Journal of Applied Earth Observation and Geoinformation. 2012;18:504–14.

[9] Ju C, Cai T, Yang X. Topography-based modeling to estimate percent vegetation cover in semi-arid Mu Us sandy land, China. Computers and Electronics in Agriculture. 2008;64(2):133–9.

[10] Sentelhas PC, Dalla Marta A, Orlandini S, Santos EA, Gillespie TJ, Gleason ML. Suitability of relative humidity as an estimator of leaf wetness duration. Agricultural and Forest Meteorology. 2008;148(3):392–400.

[11] Dalezios NR, Loukas A, Bampzelis D. The role of agrometeorological and agrohydrological indices in the phenology of wheat in central Greece. Physics and Chemistry of the Earth, Parts A/B/C. 2002;27(23–24):1019–23.

[12] Pou A, Diago MP, Medrano H, Baluja J, Tardaguila J. Validation of thermal indices for water status identification in grapevine. Agricultural Water Management. 2014;134:60–72.

http://dx.doi.org/10.5772/64527

[13] Sentelhas PC, Gillespie TJ, Santos EA. Evaluation of FAO Penman–Monteith and alternative methods for estimating reference evapotranspiration with missing data in Southern Ontario, Canada. Agricultural Water Management. 2010;97(5):635–44.

[14] Erdem Y, Arin L, Erdem T, Polat S, Deveci M, Okursoy H, et al. Crop water stress index for assessing irrigation scheduling of drip irrigated broccoli (*Brassica oleracea* L. var. italica). Agricultural Water Management. 2010;98(1):148–56.

[15] Gontia NK, Tiwari KN. Development of crop water stress index of wheat crop for scheduling irrigation using infrared thermometry. Agricultural Water Management. 2008;95(10):1144–52.

[16] Du L, Tian Q, Yu T, Meng Q, Jancso T, Udvardy P, et al. A comprehensive drought monitoring method integrating MODIS and TRMM data. International Journal of Applied Earth Observation and Geoinformation. 2013;23:245–53.

[17] Kuśmierek-Tomaszewska R, Żarski J, Dudek S. Meteorological automated weather station data application for plant water requirements estimation. Computers and Electronics in Agriculture. 2012;88:44–51.

[18] Benali A, Carvalho AC, Nunes JP, Carvalhais N, Santos A. Estimating air surface temperature in Portugal using MODIS LST data. Remote Sensing of Environment. 2012;124:108–21.

[19] Chen T, Niu RQ, Wang Y, Zhang LP, Du B. Percentage of vegetation cover change monitoring in Wuhan region based on remote sensing. Procedia Environmental Sciences. 2011;10, Part B:1466–72.

[20] Deng C, Wu C. Estimating very high resolution urban surface temperature using a spectral unmixing and thermal mixing approach. International Journal of Applied Earth Observation and Geoinformation. 2013;23:155–64.

[21] Li Z, Wang Y, Zhou Q, Wu J, Peng J, Chang H. Spatiotemporal variability of land surface moisture based on vegetation and temperature characteristics in Northern Shaanxi Loess Plateau, China. Journal of Arid Environments. 2008;72(6):974–85.

[22] Mondal P, Jain M, DeFries RS, Galford GL, Small C. Sensitivity of crop cover to climate variability: Insights from two Indian agro-ecoregions. Journal of Environmental Management. 2015;148:21–30.

[23] Orlandini S, Massetti L, Marta AD. An agrometeorological approach for the simulation of *Plasmopara viticola*. Computers and Electronics in Agriculture. 2008;64(2):149–61.

[24] Zhang F, Zhang L-W, Shi J-J, Huang J-F. Soil moisture monitoring based on land surface temperature-vegetation index space derived from MODIS data. Pedosphere. 2014;24(4):450–60.

[25] Abraha MG, Savage MJ. Comparison of estimates of daily solar radiation from air temperature range for application in crop simulations. Agricultural and Forest Meteorology. 2008;148(3):401–16.

[26] Ehret DL, Hill BD, Helmer T, Edwards DR. Neural network modeling of greenhouse tomato yield, growth and water use from automated crop monitoring data. Computers and Electronics in Agriculture. 2011;79(1):82–9.

[27] Garcia y Garcia A, Guerra LC, Hoogenboom G. Impact of generated solar radiation on simulated crop growth and yield. Ecological Modelling. 2008;210(3):312–26.

[28] Kross A, McNairn H, Lapen D, Sunohara M, Champagne C. Assessment of RapidEye vegetation indices for estimation of leaf area index and biomass in corn and soybean crops. International Journal of Applied Earth Observation and Geoinformation. 2015;34:235–48.

[29] Cicogna A, Dietrich S, Gani M, Giovanardi R, Sandra M. Use of meteorological radar to estimate leaf wetness as data input for application of territorial epidemiological model (downy mildew—*Plasmopara viticola*). Physics and Chemistry of the Earth, Parts A/B/C. 2005;30(1–3):201–7.

[30] Moonen AC, Ercoli L, Mariotti M, Masoni A. Climate change in Italy indicated by agrometeorological indices over 122 years. Agricultural and Forest Meteorology. 2002;111(1):13–27.

[31] Paterson RRM, Sariah M, Lima N. How will climate change affect oil palm fungal diseases? Crop Protection. 2013;46:113–20.

[32] Marques da Silva JR, Damásio CV, Sousa AMO, Bugalho L, Pessanha L, Quaresma P. Agriculture pest and disease risk maps considering MSG satellite data and land surface temperature. International Journal of Applied Earth Observation and Geoinformation. 2015;38:40–50.

[33] Vancutsem C, Ceccato P, Dinku T, Connor SJ. Evaluation of MODIS land surface temperature data to estimate air temperature in different ecosystems over Africa. Remote Sensing of Environment. 2010;114(2):449–65.

[34] Rahimzadeh-Bajgiran P, Omasa K, Shimizu Y. Comparative evaluation of the vegetation dryness index (VDI), the temperature vegetation dryness index (TVDI) and the improved TVDI (iTVDI) for water stress detection in semi-arid regions of Iran. ISPRS Journal of Photogrammetry and Remote Sensing. 2012;68:1–12.

[35] de Wit AJW, Boogaard HL, van Diepen CA. Using NOAA-AVHRR estimates of land surface temperature for regional agrometeorogical modelling. International Journal of Applied Earth Observation and Geoinformation. 2004;5(3):187–204.

[36] Seiler RA, Kogan F, Wei G, Vinocur M. Seasonal and interannual responses of the vegetation and production of crops in Cordoba–Argentina assessed by AVHRR derived vegetation indices. Advances in Space Research. 2007;39(1):88–94.

[37] Corbari C, Bissolati M, Mancini M. Multi-scales and multi-satellites estimates of evapotranspiration with a residual energy balance model in the Muzza agricultural district in Northern Italy. Journal of Hydrology. 2015;524:243–54.

[38] Wu W, Liu H-B, Hoogenboom G, White JW. Evaluating the accuracy of VEMAP daily weather data for application in crop simulations on a regional scale. European Journal of Agronomy. 2010;32(3):187–94.

[39] Doraiswamy PC, Pasteris PA, Jones KC, Motha RP, Nejedlik P. Techniques for methods of collection, database management and distribution of agrometeorological data. Agricultural and Forest Meteorology. 2000;103(1–2):83–97.

[40] Laurence H, Fabry F, Dutilleul P, Bourgeois G, Zawadzki I. Estimation of the spatial pattern of surface relative humidity using ground based radar measurements and its application to disease risk assessment. Agricultural and Forest Meteorology. 2002;111(3):223–31.

[41] Sentelhas PC, Gillespie TJ, Gleason ML, Monteiro JEBM, Pezzopane JRM, Pedro Jr MJ. Evaluation of a Penman–Monteith approach to provide "reference" and crop canopy leaf wetness duration estimates. Agricultural and Forest Meteorology. 2006;141(2–4): 105–17.

[42] Gonzalez-Dugo V, Zarco-Tejada PJ, Fereres E. Applicability and limitations of using the crop water stress index as an indicator of water deficits in citrus orchards. Agricultural and Forest Meteorology. 2014;198–199:94–104.

[43] Cruz-Blanco M, Lorite IJ, Santos C. An innovative remote sensing based reference evapotranspiration method to support irrigation water management under semi-arid conditions. Agricultural Water Management. 2014;131:135–45.

[44] De Pauw E, Göbel W, Adam H. Agrometeorological aspects of agriculture and forestry in the arid zones. Agricultural and Forest Meteorology. 2000;103(1–2):43–58.

[45] He Y. The effect of precipitation on vegetation cover over three landscape units in a protected semi-arid grassland: Temporal dynamics and suitable climatic index. Journal of Arid Environments. 2014;109:74–82.

[46] Jin H, Eklundh L. A physically based vegetation index for improved monitoring of plant phenology. Remote Sensing of Environment. 2014;152:512–25.

[47] Eckert S, Engesser M. Assessing vegetation cover and biomass in restored erosion areas in Iceland using SPOT satellite data. Applied Geography. 2013;40:179–90.

[48] Nagler PL, Glenn EP, Huete AR. Assessment of spectral vegetation indices for riparian vegetation in the Colorado River delta, Mexico. Journal of Arid Environments. 2001;49(1):91–110.

[49] Du Q, Chang N-B, Yang C, Srilakshmi KR. Combination of multispectral remote sensing, variable rate technology and environmental modeling for citrus pest management. Journal of Environmental Management. 2008;86(1):14–26.

[50] Duchemin B, Hadria R, Erraki S, Boulet G, Maisongrande P, Chehbouni A, et al. Monitoring wheat phenology and irrigation in Central Morocco: On the use of relationships between evapotranspiration, crops coefficients, leaf area index and remotely-sensed vegetation indices. Agricultural Water Management. 2006;79(1):1–27.

[51] Liu J, Pattey E, Jégo G. Assessment of vegetation indices for regional crop green LAI estimation from Landsat images over multiple growing seasons. Remote Sensing of Environment. 2012;123:347–58.

[52] Pan Z, Huang J, Zhou Q, Wang L, Cheng Y, Zhang H, et al. Mapping crop phenology using NDVI time-series derived from HJ-1 A/B data. International Journal of Applied Earth Observation and Geoinformation. 2015;34:188–97.

[53] Dong J, Xiao X, Wagle P, Zhang G, Zhou Y, Jin C, et al. Comparison of four EVI-based models for estimating gross primary production of maize and soybean croplands and tallgrass prairie under severe drought. Remote Sensing of Environment. 2015;162:154–68.

[54] Er-Raki S, Rodriguez JC, Garatuza-Payan J, Watts CJ, Chehbouni A. Determination of crop evapotranspiration of table grapes in a semi-arid region of Northwest Mexico using multi-spectral vegetation index. Agricultural Water Management. 2013;122:12–9.

[55] Bolton DK, Friedl MA. Forecasting crop yield using remotely sensed vegetation indices and crop phenology metrics. Agricultural and Forest Meteorology. 2013;173:74–84.

[56] Holzman ME, Rivas R, Piccolo MC. Estimating soil moisture and the relationship with crop yield using surface temperature and vegetation index. International Journal of Applied Earth Observation and Geoinformation. 2014;28:181–92.

[57] Wang Y, Zia S, Owusu-Adu S, Gerhards R, Müller J. Early detection of fungal diseases in winter wheat by multi-optical sensors. APCBEE Procedia. 2014;8:199–203.

[58] Romano G, Zia S, Spreer W, Sanchez C, Cairns J, Araus JL, et al. Use of thermography for high throughput phenotyping of tropical maize adaptation in water stress. Computers and Electronics in Agriculture. 2011;79(1):67–74.

[59] Ghosh A, Joshi PK. Hyperspectral imagery for disaggregation of land surface temperature with selected regression algorithms over different land use land cover scenes. ISPRS Journal of Photogrammetry and Remote Sensing. 2014;96:76–93.

[60] Wu P, Shen H, Zhang L, Göttsche F-M. Integrated fusion of multi-scale polar-orbiting and geostationary satellite observations for the mapping of high spatial and temporal resolution land surface temperature. Remote Sensing of Environment. 2015;156:169–81.

[61] Sruthi S, Aslam MAM. Agricultural drought analysis using the NDVI and land surface temperature data; a case study of Raichur District. Aquatic Procedia. 2015;4:1258–64.

[62] Garcia M, Fernández N, Villagarcía L, Domingo F, Puigdefábregas J, Sandholt I. Accuracy of the temperature–vegetation dryness index using MODIS under water-limited vs. energy-limited evapotranspiration conditions. Remote Sensing of Environment. 2014;149:100–17.

[63] Wang H, Li X, Long H, Xu X, Bao Y. Monitoring the effects of land use and cover type changes on soil moisture using remote-sensing data: A case study in China's Yongding River basin. Catena. 2010;82(3):135–45.

[64] Chen C-F, Son N-T, Chang L-Y, Chen C-C. Monitoring of soil moisture variability in relation to rice cropping systems in the Vietnamese Mekong Delta using MODIS data. Applied Geography. 2011;31(2):463–75.

[65] Schwarz N, Lautenbach S, Seppelt R. Exploring indicators for quantifying surface urban heat islands of European cities with MODIS land surface temperatures. Remote Sensing of Environment. 2011;115(12):3175–86.

[66] Pan Y, Li L, Zhang J, Liang S, Zhu X, Sulla-Menashe D. Winter wheat area estimation from MODIS-EVI time series data using the Crop Proportion Phenology Index. Remote Sensing of Environment. 2012;119:232–42.

[67] Crowder DW, Harwood JD. Promoting biological control in a rapidly changing world. Biological Control. 2014;75:1–7.

[68] Qin Z, Zhang M. Detection of rice sheath blight for in-season disease management using multispectral remote sensing. International Journal of Applied Earth Observation and Geoinformation. 2005;7(2):115–28.

[69] Tripathy AK, Adinarayana J, Vijayalakshmi K, Merchant SN, Desai UB, Ninomiya S, et al. Knowledge discovery and leaf spot dynamics of groundnut crop through wireless sensor network and data mining techniques. Computers and Electronics in Agriculture. 2014;107:104–14.

[70] Matese A, Crisci A, Di Gennaro SF, Primicerio J, Tomasi D, Marcuzzo P, et al. Spatial variability of meteorological conditions at different scales in viticulture. Agricultural and Forest Meteorology. 2014;189–190:159–67.

[71] Wood GA, Taylor JC, Godwin RJ. Calibration methodology for mapping within-field crop variability using remote sensing. Biosystems Engineering. 2003;84(4):409–23.

[72] Lamb DW, Brown RB. PA--precision agriculture: Remote-sensing and mapping of weeds in crops. Journal of Agricultural Engineering Research. 2001;78(2):117–25.

[73] Akasheh OZ, Neale CMU, Jayanthi H. Detailed mapping of riparian vegetation in the middle Rio Grande River using high resolution multi-spectral airborne remote sensing. Journal of Arid Environments. 2008;72(9):1734–44.

[74] Zhang H, Lan Y, Suh CPC, Westbrook J, Clint Hoffmann W, Yang C, et al. Fusion of remotely sensed data from airborne and ground-based sensors to enhance detection of cotton plants. Computers and Electronics in Agriculture. 2013;93:55–9.

[75] Agam N, Cohen Y, Berni JAJ, Alchanatis V, Kool D, Dag A, et al. An insight to the performance of crop water stress index for olive trees. Agricultural Water Management. 2013;118:79–86.

[76] Ramos JG, Cratchley CR, Kay JA, Casterad MA, Martínez-Cob A, Domínguez R. Evaluation of satellite evapotranspiration estimates using ground-meteorological data available for the Flumen District into the Ebro Valley of N.E. Spain. Agricultural Water Management. 2009;96(4):638–52.

[77] Government of Canada. Canadian Digital Elevation Data (CDED). In: Natural Resources Canada, Earth Sciences Sector, Centre for Topographic Information, editors. Sherbrooke, Quebec, Canada: Centre for Topographic Information; 2000.

[78] Gitin AV. Radiometry of optical systems with quasi-homogeneous sources: A linear systems approach. Optik – International Journal for Light and Electron Optics. 2011;122(19):1713–8.

[79] Pasher J, King DJ. Multivariate forest structure modelling and mapping using high resolution airborne imagery and topographic information. Remote Sensing of Environment. 2010;114(8):1718–32.

[80] Doutre C, Nasiopoulos P, editors. Fast vignetting correction and color matching for panoramic image stitching. 16th IEEE International Conference on Image Processing (ICIP); November 7–10, 2009; Cairo, Egypt.

[81] Hasler D, Süsstrunk S. Mapping colour in image stitching applications. Journal of Visual Communication and Image Representation. 2004;15(1):65–90.

[82] Smith GM, Milton EJ. The use of the empirical line method to calibrate remotely sensed data to reflectance. International Journal of Remote Sensing. 1999;20:2653–62.

[83] Moran MS, Bryant R, Thome K, Ni W, Nouvellon Y, Gonzalez-Dugo MP, et al. A refined empirical line approach for reflectance factor retrieval from Landsat-5 TM and Landsat-7 ETM+. Remote Sensing of Environment. 2001;78(1–2):71–82.

[84] Xu JF, Huang JF. Refined empirical line method to calibrate IKONOS imagery. Journal of Zhejiang University – Science A. 2006;7(4):641–6.

[85] Matlock TS, Hargus WA, Larson CW. Thermographic Characterization and Comparison of 200 W and 600 W Hall Thrusters. Ft. Belvoir: Defense Technical Information Center; 2007; Available from: http://handle.dtic.mil/100.2/ADA471080.

[86] Holst GC. Common Sense Approach to Thermal Imaging. Winter Park, FL, Bellingham, WA: JCD Pub.; co-published by SPIE Optical Engineering Press; 2000. xiii, 377 pp.

[87] Jensen JR. Introductory Digital Image Processing: A Remote Sensing Perspective. 3rd ed. Upper Saddle River, NJ: Prentice Hall; 2005. xv, 526 pp.

[88] Sun J, Yang J, Zhang C, Yun W, Qu J. Automatic remotely sensed image classification in a grid environment based on the maximum likelihood method. Mathematical and Computer Modelling. 2013;58(3–4):573–81.

[89] Smits PC, Dellepiane SG, Schowengerdt RA. Quality assessment of image classification algorithms for land-cover mapping: A review and a proposal for a cost-based approach. International Journal of Remote Sensing. 1999;20(8):1461–86.

[90] Skirvin SM, Kepner WG, Marsh SE, Drake SE, Maingi JK, Edmonds CM, et al. Assessing the accuracy of satellite-derived land-cover classification using historical aerial photography, digital orthophoto quadrangles, and airborne video data. In: Lunetta R, Lyon JG, editors. Remote Sensing and GIS Accuracy Assessment. Boca Raton, FL: CRC Press; 2004. p. 115–31.

[91] Rouse JW, Haas RH, Schell JA, Deering DW, Harlan JC. Monitoring the vernal advancements and retrogradation (greenwave effect) of nature vegetation. Texas A&M Univ.; Remote Sensing Center.; College Station, TX, United States: National Aeronautics and Space Administration (NASA), 1974 Contract No.: NAS5–21857.

[92] Van De Griend AA, Owe M. On the relationship between thermal emissivity and the normalized difference vegetation index for natural surfaces. International Journal of Remote Sensing. 1993;14(6):1119–31.

[93] Dalezios NR, Loukas A, Bampzelis D. Assessment of NDVI and agrometeorological indices for major crops in central Greece. Physics and Chemistry of the Earth, Parts A/B/C. 2002;27(23–24):1025–9.

[94] Carlson TN, Ripley DA. On the relation between NDVI, fractional vegetation cover, and leaf area index. Remote Sensing of Environment. 1997;62(3):241–52.

[95] ISO. Uncertainty of measurement – Part 3: Guide to the expression of uncertainty in measurement (GUM:1995). Geneva, Switzerland: International Organization for Standardization (ISO), ISO/IEC Guide 98–3:2008, 2008.

[96] Bonn F, Rochon G. Précis de télédétection. Volume 1, Principes et méthodes. Sainte-Foy: Presses de l'Université du Québec; 1992.

[97] Bonn F, Escadafal R. La télédétection appliquée aux sols. In: Presses de lșuniversité du Québec, editor. Précis de télédétection, Volume 2, applications thématiques. Sainte-Foy/Montréal: Bonn, F.; 1996. p. 633 pages.

[98] Sobrino JA, Raissouni N. Toward remote sensing methods for land cover dynamic monitoring: Application to Morocco. International Journal of Remote Sensing. 2000;21(2):353–66.

[99] Minkina W, Dudzik S. Infrared Thermography: Errors and Uncertainties. Chippenham, Wiltshire, Great Britain: John Wiley & Sons; 2009. Available from: http://onlinelibrary.wiley.com/book/10.1002/9780470682234.

[100] Hamrelius T. Accurate Temperature-Measurement in Thermography – an Overview of Relevant Features, Parameters and Definitions. Proceedings of the Society of Photo-Optical Instrumentation Engineers (SPIE). 1991;1467:448-57.

[101] Sandholt I, Rasmussen K, Andersen J. A simple interpretation of the surface temperature/vegetation index space for assessment of surface moisture status. Remote Sensing of Environment. 2002;79(2–3):213–24.

[102] Gao Z, Gao W, Chang N-B. Integrating temperature vegetation dryness index (TVDI) and regional water stress index (RWSI) for drought assessment with the aid of LANDSAT TM/ETM+ images. International Journal of Applied Earth Observation and Geoinformation. 2011;13(3):495–503.

[103] Liu Z, Shi X, Warner E, Ge Y, Yu D, Ni S, et al. Relationship between oriental migratory locust plague and soil moisture extracted from MODIS data. International Journal of Applied Earth Observation and Geoinformation. 2008;10(1):84–91.

[104] Naira C, Robert L, Ramata M, Marouane T. Surface soil moisture status over the Mackenzie River Basin using a temperature/vegetation index. Geoscience and Remote Sensing Symposium, 2007 IGARSS 2007 IEEE International [Internet]. 2007, pp. 1846-8 pp. Available from: http://ieeexplore.ieee.org/stamp/stamp.jsp?tp=&arnumber=4423182&isnumber=4422708.

[105] Xin J, Tian G, Liu Q, Chen L. Combining vegetation index and remotely sensed temperature for estimation of soil moisture in China. International Journal of Remote Sensing. 2006;27:2071–5.

[106] Nagol JR. Quantification of error in AVHRR NDVI data [thesis]. College Park, Maryland: University of Maryland; 2011.

[107] Moran MS, Inoue Y, Barnes EM. Opportunities and limitations for image-based remote sensing in precision crop management. Remote Sensing of Environment. 1997;61(3): 319–46.

[108] Coll C, Caselles V, Rubio E, Sospedra F, Valor E. Temperature and emissivity separation from calibrated data of the digital airborne imaging spectrometer. Remote Sensing of Environment. 2001;76(2):250–9.

[109] Rahkonen J, Jokela H. Infrared radiometry for measuring plant leaf temperature during thermal weed control treatment. Biosystems Engineering. 2003;86(3):257–66.

[110] Wanjura DF, Upchurch DR. Infrared thermometer calibration and viewing method effects on canopy temperature-measurement. Agricultural and Forest Meteorology. 1991;55(3-4):309–21.

[111] Kerr YH, Lagouarde JP, Imbernon J. Accurate land surface-temperature retrieval from AVHRR data with use of an improved split window algorithm. Remote Sensing of Environment. 1992;41(2-3):197–209.

[112] Li ZL, Tang BH, Wu H, Ren HZ, Yan GJ, Wan ZM, et al. Satellite-derived land surface temperature: Current status and perspectives. Remote Sensing of Environment. 2013;131:14–37.

[113] Mallick J, Singh CK, Shashtri S, Rahman A, Mukherjee S. Land surface emissivity retrieval based on moisture index from LANDSAT TM satellite data over heterogeneous surfaces of Delhi city. International Journal of Applied Earth Observation and Geoinformation. 2012;19:348–58.

[114] Niclòs R, Galve JM, Valiente JA, Estrela MJ, Coll C. Accuracy assessment of land surface temperature retrievals from MSG2-SEVIRI data. Remote Sensing of Environment. 2011;115(8):2126–40.

[115] Norman JM, Divakarla M, Goel NS. Algorithms for extracting information from remote thermal-IR observations of the earth's surface. Remote Sensing of Environment. 1995;51(1):157–68.

[116] Srivastava PK, Majumdar TJ, Bhattacharya AK. Surface temperature estimation in Singhbhum Shear Zone of India using Landsat-7 ETM+ thermal infrared data. Advances in Space Research. 2009;43(10):1563–74.

[117] Lee WS, Alchanatis V, Yang C, Hirafuji M, Moshou D, Li C. Sensing technologies for precision specialty crop production. Computers and Electronics in Agriculture. 2010;74(1):2–33.

[118] Manns HR, Berg AA, Colliander A. Soil organic carbon as a factor in passive microwave retrievals of soil water content over agricultural croplands. Journal of Hydrology. 2015;528:643–51.

[119] Merlin O, Chehbouni A, Kerr YH, Goodrich DC. A downscaling method for distributing surface soil moisture within a microwave pixel: Application to the Monsoon '90 data. Remote Sensing of Environment. 2006;101(3):379–89.

[120] Moran MS, Vidal A, Troufleau D, Qi J, Clarke TR, Pinter Jr PJ, et al. Combining multifrequency microwave and optical data for crop management. Remote Sensing of Environment. 1997;61(1):96–109.

[121] McNairn H, Champagne C, Shang J, Holmstrom D, Reichert G. Integration of optical and synthetic aperture radar (SAR) imagery for delivering operational annual crop inventories. ISPRS Journal of Photogrammetry and Remote Sensing. 2009;64(5):434–49.

Chapter 6

Participatory Mapping to Disrupt Unjust Urban Trajectories in Lima

Rita Lambert and Adriana Allen

Additional information is available at the end of the chapter

http://dx.doi.org/10.5772/64303

Abstract

This chapter shares the experience of two action research projects ReMap Lima and cLIMA sin Riego, where mapping has been used with three main objectives: to make visible what is otherwise 'invisible'; to open up dialogue between different stakeholders in the city and to arrive at concrete actions, collectively negotiated between citizens and policy makers. Two case study sites were chosen in Lima, Peru: Barrios Altos (BA) in the historic centre and José Carlos Mariátegui (JCM) at the edge of the city. The approach adopted applies a participatory action methodology based on grounded applications and advanced technologies for community-led mapping and visualisation. The chapter reflects upon three interrelated sites of the mapping process: the reading, writing and audiencing of maps and explores how these can provide opportunities to break away from the polar positions often established between Claimant/ marginalised group and the state, thus aiming to contribute to a process of spatial co-learning across typically confronted actors. The two case studies show different possibilities for interrogating the city to provide a spatially and socially grounded way of co-producing knowledge for action that can contribute to the planning of just urban futures.

Keywords: Participatory mapping, Counter-mapping, Drones, Spatial justice, Critical cartography, Urban Global South, Lima

1. Introduction

Acknowledging that maps plays a key role in urban planning and the design and implementation of policies, a critical engagement with the 'work' they do, how they operate and how they come to be made, is important. In many cities across the Global South, the use of maps in decision-

making is increasing. Although maps are often seen as technical means, a shift to positioning them as political devices brings to view the political economy and the unequal development landscape that characterises these cities.

In Lima, the state is investing considerable resources in the production of cartographic information. However, this production is predominantly linked to particular projects or mega-infrastructural developments, making evident the fragmented cartographic landscape of the city where certain areas are over-mapped while others remain under-mapped.

For several decades, Lima has developed through land invasions rather than formal planning [1, 2]. Since the 1940s, the city has undergone an explosive demographic growth to reach an estimated 9 million population in 2015. This process has been underpinned by the inability of city authorities to keep up with the required provision of housing and basic services and also accurately record the extent of Lima. Although a detailed updated overall map of the city does not exist, certain areas have been recurrently mapped supporting dominant visions of how the city is and should develop.

We understand maps as 'neither neutral nor unproblematic with respect to representation, positionality, and partiality of knowledge' (p. 101 in Ref. [3]). Because maps are statements that support the actualisation of ideas [4–6], there is a close relationship between the way in which space is framed and the actions that are given potential with this framing. In this sense, hegemonic representations of how the city should develop can play a role in fostering exclusionary socio-environmental processes. We hereby seek to contribute to the growing critical cartographic and development planning literature to understand how and under what conditions mapping can support socially and environmentally just processes and outcomes.

Much has been written about how maps are part and parcel of dispossession and control, but also resistance. Of particular weight, due to the number of academic contributions, is the link made between map-making and hegemony of the state that dominates map production [7, 8]. An insightful addition to this body of the literature is the notion of 'unmapping' as a form of control. Roy [9], in her article on informality, argues that systems of deregulation and unmapping are interlinked and that regimes of urban governance often operate through them. She explores how state purposefully leaves the peri-urban areas of Calcutta unmapped because doing so allows considerable 'territorialized flexibility to alter land use, deploy eminent domain, and to acquire land' (p. 81 in Ref. [9]). Thus, 'unmapping' can be interpreted as a means of control as well as accumulation.

In recent years, there has been a growing literature in development planning focussing on the role of mapping as a tool for resistance in response to the marginalising authoritative maps produced by state agencies. Here, mapping is adopted as a tactic to enhance the negotiation capacity of excluded groups when fighting towards just processes of recognition and equitable distribution of resources [3]. Several scholars have explored how the mapping of indigenous territories has been used to bolster the legitimacy of customary claims over resources in legal battles [10, 11]. In the urban context, grassroots actors are adopting mapping as a means to contest evictions and relocations [12] and to claim their entitlement to services and urban infrastructure [13, 14].

http://dx.doi.org/10.5772/64303

These accounts can be understood as various forms of 'counter-mapping': a term pioneered by Peluso and defined by Harris and Hazen as 'any effort that fundamentally questions the assumptions or biases of cartographic conventions, that challenges power effects of mapping, or that engages in mapping in ways that upset power relations' (p. 115 in Ref. [3]). One of the dominant aspects in counter-mapping is the fundamental polar positions established between the 'us' (the claimant and marginalised group) against the 'them' (the state). This contributes to very long battles where the power and action space is constantly struggled over. Moreover, counter-mapping does not preclude participation and indeed it can solely be expert-led [15].

This chapter explores the possibility of opening up participation in counter-mapping to include a wide range of actors in two research projects led by the authors: ReMap Lima[1] and cLIMA sin Riesgo[2]. Adopting a Participatory Action Research methodology that promotes the 'plurality of knowledges', the mapping process is explored as an opportunity for spatial co-learning through an incremental process of network building among ordinary citizens, planners, policy makers, researchers, and advocates. Adapting Rose's visual methodologies approach [18], the chapter explores how new possibilities for transformative change might be created through three interrelated sites in the mapping process: *reading*, *writing* and *audiencing of maps* [19].

Two case study sites are chosen: Barrios Altos (BA) in the historic centre of Lima and José Carlos Mariátegui (JCM) at the edge of the city. These two neighbourhoods are contrasting not only because of their geographic location but also because the centre has been over-mapped, while the periphery has been rarely recorded through official mapping efforts. Thus, these two areas capture distinct processes of cartographic marginalisation: those of misrepresentation and omission.

2. An overview of the case studies

2.1. Barrios Altos in the historic centre

Barrios Altos (BA) is a deprived and overcrowded area which experienced a steady decline in the living conditions since the 1970s due to a general lack of public and private investment. Local dwellers, mostly impoverished tenants, face the risk of health problems related to inadequate basic services, the structural collapse of buildings and frequent fires caused by precarious electricity connections. Despite being declared a UNESCO world heritage site in 1991, the area is undergoing rapid changes propelled by an illegal land market (**Figure 1**). Due

[1] ReMap Lima is an 18 month project led by the authors that began in November 2013 to interrogate the nature of cartographic representations of marginalised neighbourhoods in Lima In addition, the project explored the possibilities of opening up the writing of maps to ordinary citizens through the adoption of grounded applications and advanced technologies for community-led mapping and visualisation. For more information, see Ref. [16].

[2] Building on ReMap Lima, cLIMA sin Riesgo was launched in February 2015 with support from Climate and Development Knowledge Network (CDKN). This action-research project focusses on everyday risks that often go unnoticed, examining how they are produced, where they accumulate and who they affect. It evaluates the public and private investments that are made to cope with and mitigate risk and seeks to produce knowledge and co-funding mechanisms to disrupt urban risk cycles (for more information, see Ref. [17]).

to its strategic location at the geographic centre of the city, and in close proximity to several planned infrastructure projects as well as the central market of Metropolitan Lima, the land is in high demand. Land traffickers use various techniques from coercion to violence to take possession of residential properties and illegally changing them to more profitable uses such as storage facilities for the central market (**Figure 2**). In this way, many of the historic buildings are quietly converted while keeping the facades intact, where new structures are erected replacing the antique interiors. This process affects negatively the built environment eroding the cultural heritage and leading to the eviction of many vulnerable inhabitants who have lived there for generations. These processes are somewhat 'invisible' as they are often physically hidden from the street and tolerated by the Municipal authorities.

Figure 1. A building in Barrios Altos marked as 'Property under litigation', a sign that illustrates the disputes and conflict with land traffickers posing as owners. Source: Photo by Rita Lambert.

Over time, the city centre has been repeatedly mapped from different perspectives. Existing thematic maps produced by government agencies depict Barrios Altos as a poor zone, overcrowded, with high criminality and at risk of physical collapse. These thematic maps are compiled by PROLIMA, a special municipal body in charge of the strategic vision for the renovation of the historic centre and the Masterplan 2025 [20]. They substantiate the argument for the demolition of 40% of the area [21] and its renovation through private investment which would capitalise on the cultural heritage but in effect lead to gentrification [22, 23].

An interview with the former architect of the plan for the historic centre reveals the assumptions underpinning the mapping of the area to substantiate current redevelopment plans:

'*This area is like a black hole, it is difficult to extract information, as it is difficult to access … Moreover, many properties are not registered. Not everything can be mapped. We have limited capacity so we concentrated our efforts on certain parts and we second guess what happens in other parts*' (interview with the head architects of PROLIMA, May 2014).

http://dx.doi.org/10.5772/64303

Figure 2. The storage facilities that violate the building height restrictions for the historic centre and come to replace the old structures within an area deemed of monumental value. Source: Photo by Rita Lambert.

Most of the illegal land use changes into storage facilities are not recorded by official maps. Moreover, when representing risk, institutional maps mainly take into account the construction materials of the buildings and the probability of their collapse in the event of an earthquake, thereby disregarding other man-made risks (**Figure 3**).

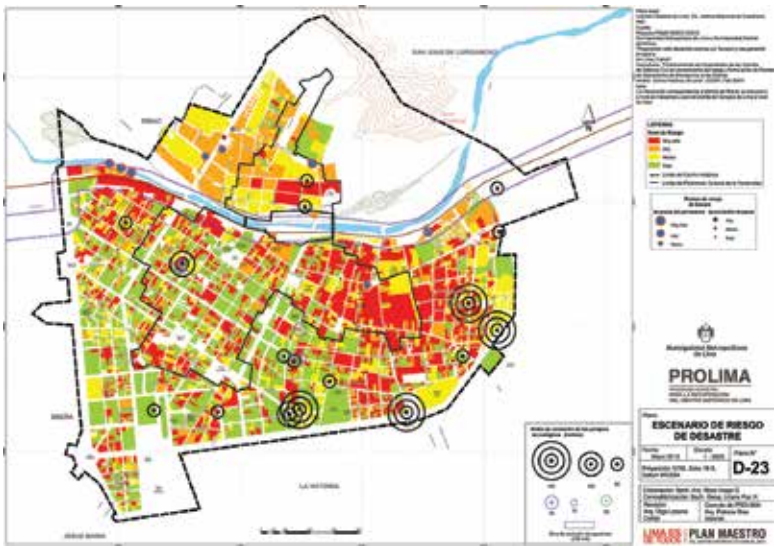

Figure 3. Map showing the scenario of risk of disaster in the event of an earthquake. The map depicts most of Barrios Altos in red at the highest risk of physical collapse. Source: PROLIMA 2013.

Official maps of the area do not consider the daily risks that threaten the most vulnerable segments of the local population, such as fires due to sparks created from exposed cables compounded by the flammable materials held in the storage facilities, or the spread of epidemics due to lack of adequate water and sanitation. For example, a diagnostic map from the public water utility company SEDAPAL portrays this area as well serviced with potable water (**Figure 4**). However, the last infrastructure investments made in this area date back to 1970 (interview with SEDAPAL, May 2015), and the infrastructure is old and prone to leakages. This leads to the contamination of potable water as well as the weakening of the traditional adobe building structures due to the humidity generated. Furthermore, not all households are serviced with potable water. One house, that used to accommodate a single family, is now typically subdivided to accommodate several families of tenants, who, in many cases, rely on a single water point in the courtyard of the *quinta* or multi-family housing unit. In some instances, water is rationed by the inhabitants themselves, as they often rely on one metre and share the bill.

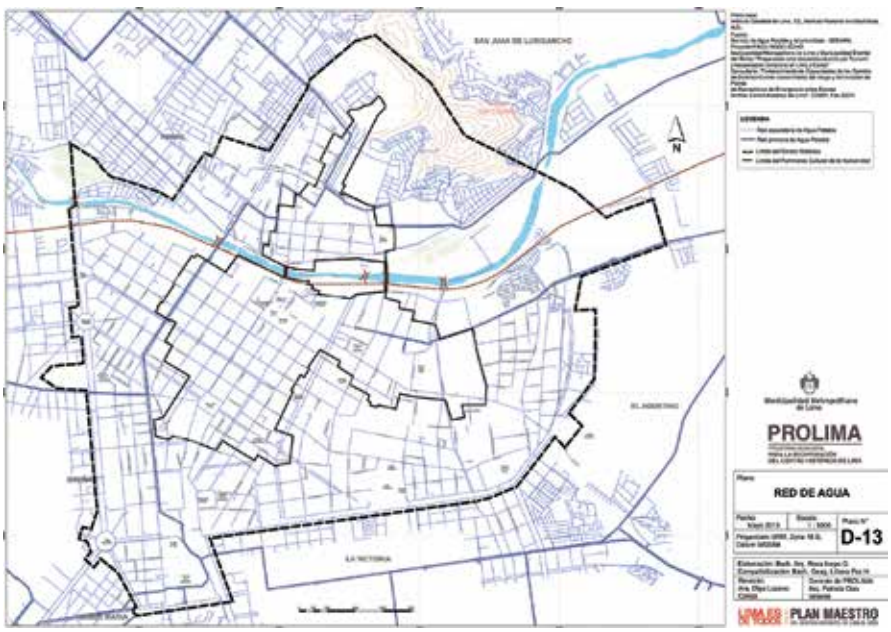

Figure 4. SEDAPAL map showing an extensive water network in the whole historic centre, portraying the area as well served with potable water but in effect hiding the reality of many residents who do not enjoy individual water connections. Source: PROLIMA 2013.

This type of map conceals the severity of the problem, funnelling public investments elsewhere whilst thousands of residents struggle to access water in an area considered the foundation of the city of Lima. Although the historic centre has been over-mapped through time and is, at the moment, at the centre of government projects, everyday risks are rendered invisible. Moreover, because the renovation of the area remains a top-down endeavour with the diagnostic and proposal stages removed from the reality experienced by tenants on the ground

http://dx.doi.org/10.5772/64303

and with no active intervention to stop the negative processes, the loss of the cultural heritage, which includes its people, is rapidly occurring. The vacuum in effective management, the lack of a robust diagnosis of the lived reality in the area and the exclusion of inhabitants from participating in decision-making processes to redevelop the area, limit the scope of urban renovation projects and programmes.

2.2. José Carlos Mariátegui at the periphery of the city

In the absence of a national housing policy and affordable land in the central areas of Lima, the urban poor are forced to occupy informal settlements on the steep slopes at the city's edge. Many of these areas coincide with the local ravine ecosystem or '*Lomas Costeras*': an essential ecological infrastructure for recharging the aquifers that guarantee water for Lima and regulate the effects of climate variability. Located in San Juan de Lurigancho, the most populated and poorest district of Lima, José Carlos Mariátegui (JCM) is one of these areas and was established in the 1990s through a first wave of invasions. Constituted by various settlements, each working within its own boundary, JCM suffers from uncoordinated actions and fragmented planning, which contribute to the production and reproduction of conditions of risk for the local dwellers (**Figures 5** and **6**).

Figure 5. The continuous occupation of the steep slopes in JCM leads to the production and reproduction of risks and the increased vulnerability of the inhabitants. Source: Photo by Rita Lambert.

Figure 6. As people flatten the plots to then build their house, they contribute to the instability of the slope and increase the risk for others. Source: Photo by Rita Lambert.

Overall, the area is rapidly urbanising with the continuous influx of people. Moreover, large-scale land traffickers operate here to capitalise on the barren areas of land upslope by opening up new roads, dividing the land into plots and selling them off. The never-ending occupation of the steep slope is exacerbating the vulnerability of the population, as access to basic services becomes ever more difficult for those located in the upper part and the increased instability of the slope worsens the risk of rockfalls and structural collapse of retaining walls.

In contrast with BA, JCM is under-mapped with few and often outdated maps produced by municipal authorities and Civil Defence. These maps only partially capture the risks that threaten the area and exclude the newly established settlements, as these have emerged after the stipulated cutoff date of 31 December 2004 for formal land titling by the National Government. As the residents consolidate these settlements under precarious physical and legal conditions, they are often excluded from public plans and investments to improve housing, basic services and social facilities.

In order to gain official recognition from the district government, local community organisations—also known as *Agrupación Familiar* (AF)[3] —hire professional topographers to produce schematic plans of their own settlements, which are then submitted to the local municipality (**Figure 7**). Only once these plans have been certified by the latter, can the inhabitants begin the process of requesting basic services such as water and electricity.

[3] An AF is a community organisation that governs by the facto all collective affairs in the neighbourhood and operates as the interface with governmental institutions and programmes, as well as with neighbouring settlements and informal land traffickers.

http://dx.doi.org/10.5772/64303

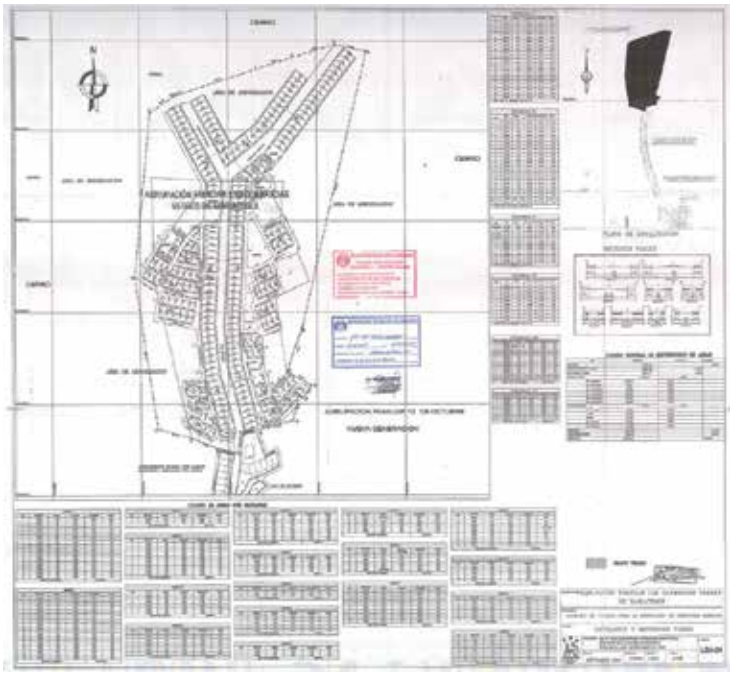

Figure 7. An example of a certified map. Source: Quebrada Verde, JCM.

Figure 8. The vertical staircases of JCM are planned and built in such a way that they increasing the risk of accidental falls. Source: Photo by Rita Lambert.

These plans or maps are diagrammatic and lack any details of the context, such as adjacent settlements or contour lines. They represent the terrain as flat, thereby failing to record the risks associated with the occupation of the steep slopes. The lines on the map are directly transposed onto the ground, demarcating the plots that will soon be occupied. In most cases, the layout works against the contour lines making it difficult to access the plots through the resultant steep stairs and paths and increasing the risk of accidental falls (**Figure 8**).

These plans are also used by community organisations to subdivide plots further up slope. In the absence of public recognition and investments, the selling of new plots carved out of the slopes is often regarded as the only viable financial source to improve the liveability of the most consolidated parts of the settlement. In short, these abstract plans do not reflect the challenges associated with the exponentially increasing risks produced by the urbanisation of the area.

Landing in these conflict-ridden contexts, the research projects ReMap Lima and cLIMA sin Riesgo built upon an existing network of partner organisations and local community groups with whom the authors established a productive working relationship in 2012, in support of existing processes for transformative change. These projects have a strong mapping component where the reading, writing and audiencing stages are used to improve the spatial knowledge of these areas and to identify how risk is distributed and with what consequences for the most vulnerable. Besides the ambition of producing robust evidence and counter-map how these areas are represented, the mapping process is designed to bring together various stakeholders from state authorities, local communities, academics, NGOs, and to open up critical reflection and foster the design of integrated responses and co-financing mechanisms to reduce and prevent risk.

3. Sites of participatory mapping

3.1. The site of reading

The reading of maps refers to the critical questioning of 'who' maps and what is included/excluded. Focussing on official maps that dominate the framing of particular areas helps to bring into view who and what is left 'off the map' and why. This interrogation contributes to the examination of the socio-environmental power struggles at play and the actions that are justified through cartographic devices. The process of reading maps as texts that bring forth particular arguments [24, 25] facilitates the identification of those cartographic devices to be rewritten to contest hegemonic representations. Recent literature has provided valuable insights into how maps work, arguing that maps are not fixed representations but are rather in constant flux, as each encounter with a map produces new meanings and engagements with the world [26]. Although reading is subjective, we contend that a collective reflective position can be attained when the reading of maps is a debated process.

The projects seek to create such spaces for critical reflection to interrogate why certain representations and ways of mapping are stabilised, what consequences these might have and

http://dx.doi.org/10.5772/64303

how new possibilities can be imagined for more inclusive representations that can effectively contribute to breaking risk accumulation cycles. For example, cLIMA sin Riesgo facilitated several forums bringing together public entities who work on disaster risk management, preservation of cultural heritage, urban regeneration, infrastructural service provision, urban development planning and land use zoning. One of the objectives was to contrast and evaluate the different methodologies adopted by these organisations to map risk.

The discussion confirmed that everyday risks and episodic disasters are often disregarded. Most institutions define risk management strategies, relying on sectoral statistics and often outdated and non-georeferenced data. Agreeing that this approach limits a comprehensive understanding of the spatial distribution of risk and its accumulation over time and also hinders the design of effective structural solutions, participants agreed on the importance of reconsidering how risks are cartographically captured. Moreover, public institutions confirmed that they rely mostly on scientific studies and the prediction of large-scale disasters as principal tools to identify and visualise risk on official maps. Last, but not least, they acknowledged the need to take into account everyday risks to enable a prospective approach to risk management and prevention.

However, the established official way of mapping risk overlooks the potential of knowledge co-production through participatory mapping processes in the identification of small-scale hazards. Integrating interdisciplinary and inter-institutional platforms into the mapping process has proven to be effective in bridging the 'them' and 'us' divide and questioning the entrenched institutional modes of framing risk as well as marginalised areas and how they are cartographically represented.

Figure 9. The aerial photographs produced by the drones were used in various workshops and focus groups, with local dwellers actively engaging in their critical reading. Source: Photo by Rita Lambert.

Moreover, the production of robust data that make visible many of the otherwise 'invisible' changes occurring in the study areas creates more traction to address such changes.

In February 2014, the ReMap Lima project started with the production of high resolution 2D and 3D images captured through drones. The unregulated environment in Lima regarding the use of drones made it possible to produce these images. As one of the co-investigators notes, this would not have been possible to do in London and such a high resolution image cannot be attained (interview with Andy Hudson-Smith, June 2015). Although there is controversy regarding the application of drones, as they are typically associated with military use and surveillance, if used sensitively, they can help advance the visualisation of recurrently disregarded realities. We could not rely on satellite images because they were outdated and did not provide the level of detail required to analyse and capture dynamic ongoing changes. The images produced were highly revealing and easier to read than any other drawn map, particularly for the inhabitants that had never seen their neighbourhood from this perspective (**Figure 9**). A new reading of the areas could be attained through two important factors: the level of detail captured, and the scale jump which the bird's-eye view provided.

In BA, the view from above made visible the otherwise 'unseen' processes occurring behind both conserved and deteriorating facades. This included the storage facilities and the buildings, which had experienced eviction (**Figure 10**). Moreover, from the 3D digital model, one could discern the violation of building height restrictions stipulated for the historic centre, which occur behind facades that mask such processes (**Figure 11**).

Figure 10. Close-up detail on the 2D image of BA showing the eviction of one muti-family housing unit, Isaias Clivio. Source: ReMap Lima.

http://dx.doi.org/10.5772/64303

Figure 11. 3D point cloud produced with the drone to show building heights in BA. Source: ReMap Lima.

In JCM, the high-quality images exposed the different practices adopted by land traffickers, such as the tracing of plots to be urbanised and the opening up of new roads. Unlike the maps produced by the AFs, the 3D image revealed the topography and the risk produced by the continuous urbanisation of the steep slopes. Furthermore, this image captured the whole ravine, showing the shifting borders and the loss of ecological infrastructure as the *lomas* are encroached (**Figure 12**). It also made evident the disjunctures between the various settlements, raising awareness of the ravine as a system which needs consolidated planning efforts at a larger scale. As a JCM inhabitant and mapper notes:

'*People often don't know what is happening at the back of their own settlement … Working with this technology has meant that a lot of information was gathered about the risk areas. With the drone images, the leaders realised that new roads were being opened and they started to pay attention to the matter, raising awareness of their community and promoting the planning and safeguarding of open spaces*' (interview with JCM inhabitant, May 2015).

Figure 12. 3D point cloud of JCM. Source: ReMap Lima.

The production of cartographic images that can be easily read is crucial to engage local dwellers and gives them a sense of empowerment. As one of the local partners and co-investigator notes

in the case of BA: '*for the neighbours, having this aerial photo, is like having the urban block in their hands… it has given a lot of information… the mapping process has helped to strengthen social organisation*' (interview with Silvia de los Rios, July 2015).

01-3D scanning using drones SenseFly eBee drones were used to capture aerial images, as well as point clouds with the height of building and terrain. 	**02-Generation of Mesh** Using a 3D computer program (Rhino), the point cloud was triangulated and converted into a mesh. 
03-Digital Modeling Based on the 3D mesh, the buildings were modeled in detail. The heights were provided by the mesh whilst the details of the buildings were taken from the 2D aerial images. 	**04-3D printing** The digital file produced was 3D printed in ABS plastic with a 3D Maker-Bot. As this is an automated process, it permits the completion of models in a short period of time. 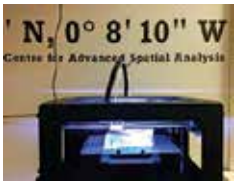
05-Final details on the physical model To make it easier to identify buildings, photographs of the facades were adjoined to the models and the aerial images were used as a base. 	**06-Projection on physical models**. Various variables collected were projected onto the models to facilitate their reading. 

Table 1. The process from the drone image capture to the printing of 3D models for planning for real workshops.

Table 1 explains the process adopted to use the drone data to make physical models that can be used in planning for real workshops with community groups. Being able to produce various outputs—from a model of the whole ravine in JCM which can be handheld to a large aerial image where people can immerse themselves—helped to grasp the spatiality of problems at various scales and to guide discussions about the scale of action required, as well as informing the site of writing of new maps.

http://dx.doi.org/10.5772/64303

3.2. The site of writing

The site of writing focuses on the collective decision of what to map, how to map and towards what end. It also encompasses the actual process of data gathering in the field and its representation on maps. The writing process began with a discussion of 'why to map' together with community mappers comprised of women and men inhabitants and community leaders from the two areas. Mapping was identified by the participants as a means to document and denounce otherwise invisible practices. It was also seen as a strategic activity to understand trends and ongoing processes of change by institutions and real estate developers. Moreover, the process was also seen as a useful means to identify the social and material resources of a neighbourhood and to promote strategic interventions.

Subsequently, transect walks were designed together with local dwellers (**Figure 13**), and the variables to be recorded were also agreed. A manual, as well as a digital process, was used to gather the data (**Figure 14**).

Figure 13. The mappers of BA collecting information during the transect walk. Source: Photo by Rita Lambert.

The manual process involved the use of the drone images as base maps and the annotation of relevant information identified through the transect walks. The map was completed with the stories, experiences and knowledge of local dwellers through photographs and short-filmed

interviews, which were keyed into online maps. In parallel, the digital process used a number of open source mobile phone applications such as Epicollect+, MyTracks and Twitter[4], which helped the systematic data collection, and the speedy integration of the georeferenced surveys in Quantum GIS. We organised training workshops in order for participants to learn how to use these programmes and to visualise the information gathered. Although there was differential engagement among community mappers due to the agility required to work with such technologies, the main aim of these workshops was to allow everyone involved to become familiar with the way the technology works and its possibilities. The capacities required within each of the mapping teams were flexible enough to allow different roles to be comfortably filled by participants.

Figure 14. Preparing for the transect walk together with community mappers. Source: Photo by Flora Roumpani.

For cLIMA sin Riesgo, a total of 700 georeferenced surveys were undertaken at different scales, including information at the household level in both areas, at the block and multi-family housing unit level in BA, and at the settlement level in JCM. The survey questionnaires contain social and economic aspects such as the local dwellers' individual and collective capacity to save and investments made to mitigate risk. The questionnaires also recorded physical aspects such as living conditions, construction materials and the type and state of available infrastructure and services, as well as the specific hazard that affect each area. This knowledge complements scientific and sectoral studies, determining with more precision the location of physical threats and revealing other sources of risk and vulnerabilities. Moreover, it allows an under-

[4] Epicollect+ provided the recording of a number of variables in a survey format at point location; MyTracks was useful for line tracing, and Twitter was experimented with as a real-time collector ideal for purposes of emergency reporting.

http://dx.doi.org/10.5772/64303

standing of the inhabitants' perception of risk and the identification of the capacities required to respond to these risks effectively and preventively.

The information-gathering process in the field promoted the interaction of community mappers with a large number of women and men dwelling in both areas. In the case of JCM, mapping across settlements was important to establish new social relations, reflect collectively upon common problems and discuss ways to consolidate efforts, halt urban expansion and plan this area. The mapping process was articulated to a series of capacity-building workshops run by CENCA (Instituto de Desarollo Urbano), a progressive NGO and partner in cLIMA sin Riesgo with a long-established presence in the area. The entire process helped raise awareness and strengthen local capacities and encouraged the participation of community leaders and local inhabitants. This process was particularly targeted towards young people, who were trained as community mappers, enabling them to gain a better understanding of the reality affecting their own neighbourhoods. In BA, the leaders took the opportunity to reach out to their neighbours, explaining the importance of self-enumeration and mapping, not only to make visible the conditions in which they live but also as a means to strengthen social organisation and collective action. As stated by two of the mappers in BA:

'*They* [those involved in ReMap Lima] *began mapping from the air and then we walked from door to door. As community leaders, we became aware of many problems: lack of water services, lack of electricity, collapsed sewerage pipes. Despite being in the modern era, we still live precariously*' (interview with local leader and BA mapper, May 2015).

'*The mapping process was useful to me and the other mappers and helped us to understand the reality of the neighbourhood. For us tenants, the project helped us to see that we have to organise ourselves to fight for better housing conditions*' (interview with BA mapper, May 2015).

3.3. The site of audiencing

The site of audiencing involves making collective decisions on who should see the maps, where they should be displayed and how to frame new interpretations emanating from the contrasting of existing and newly written maps. A cyclical process is thereby established as one moves back to the site of reading, evaluating the meanings that emerge from new written maps.

An important consideration concerns the exposure of sensitive information, particularly when working with vulnerable and highly contested territories such as BA and JCM. In both areas, if misappropriated, the data collected could be used against its intended aims and further promote land trafficking. Because the mapping process includes government institutions and various actors, which might have multiple and overlapping identities (for example, a local leader might have vested interests to engage in the pirate subdivision of plots), issues of co-option and questions of who owns the process and the Information need careful consideration [27].

Foreseeing how the cartographic information produced could be misappropriated and by whom is an important aspect of counter-mapping. As demonstrated by various scholars, serious questions are raised regarding the unintended negative consequences of counter-mapping [10, 11, 28, 29]. In the two projects discussed, the researchers from UCL and the

partner NGO hold the bulk of the sensitive information. However, as sharing what emerged throughout the research process is strategically important to expand the network of allies and advocates and provide a learning platform, various forums were devised. On the one hand, workshops, exhibitions and international conferences[5] provided the space to attract a wide audience, including community-based organisations, government institutions, academics, activists and even remote mappers.[6] On the other hand, we provided an online platform to share non-confidential qualitative and quantitative information produced throughout the research. This takes the form of a publicly accessible 'Online Story Maps' hosted by (ESRI) digital platform (**Figure 15**). These maps offer a nuanced reading of the actual conditions shaping urban risk and allow those involved in the research, as well as other audiences, to understand how risk accumulation cycles operate, thus enabling a reframed diagnosis of the process of urbanisation in risk, but without disclosing information that could potentially exacerbate such process.

Figure 15. Online story map publicly available can be easily navigated to apprehend: (1) the different causes of everyday risk and episodic disasters; (2) where and why potential impacts manifest; (3) who is affected, why and where; (4) the relationship between different types of risk; and (5) the actions and investments made to mitigate or reduce risk.

Displaying the information with a clear narrative, which includes photographs and video testimonies from local dwellers, and structuring the information under different themes for

[5] The projects were exhibited at the COP21 in Lima, public exhibitions in London (The Building Centre, July 2015) and at various sites in Lima since November 2015, reaching over 3000 visitors. Moreover, they were presented at various conferences including: GISRUK Leeds 15–17 April 2015 and Foro Centro Vivo, Lima 28 April 2016.

[6] The projects drew in the unforeseen involvement of remote mappers. Within three days that the 2D drone image was donated to OpenStreetMap, mappers from afar staked their piece of the earth. JCM was traced discerning the dirt roads, staircases and building structured. Examining Lima on OpenStreetMap, one sees that this is the only area in the periphery that has been mapped with such detail.

http://dx.doi.org/10.5772/64303

each area, guide viewers in the reading of these maps, reframing the problematic and the actions that need to be taken. All the while providing credible quantitative evidence accompanied by the actual voices of those living in that reality, the online story maps move away from using strict cartographic conventions. They thus suspend the need to 'appropriate the state's techniques and manner of representation to bolster the legitimacy [of claims]' (p. 384 in Ref. [10]), which reveal but inherently abstract, efface and omit [11, 10, 30]. Many negative unintended consequences of counter-mapping (especially of indigenous territories) have been attributed to the 'forced' adoption of the cartographic conventions in order for the information not to be dismissed in dialogue with authorities.

4. Concluding remarks

The two action-research projects examined in this chapter have provided an invaluable experimentation space to push new possibilities for the spatial analysis of marginalised areas that are altogether omitted or misrepresented in official maps. It has also shown how the articulation of different types of knowledge throughout the mapping process can offer a more precise and comprehensive spatial and social diagnosis.

The three sites of mapping, reading writing and audiencing, show different opportunities for how one can interrogate the city and provide a spatially and socially grounded way of producing knowledge for action. Besides enabling the creation of legitimate and robust evidence for the understanding of risk, these sites play different roles in facilitating co-learning and the co-production of knowledge through an incremental process of network building among local dwellers, researchers, planners and advocates. These three sites are not only interrelated but also iterative.

Reaching beyond the local site of map production by those putting forward their claims, the chapter shows that it is possible and effective for counter-mapping initiatives to consider at points the inclusion of the very institutions that play a role in propagating the dominant framings of the areas. Also, one cannot strictly pertain to the hegemony of the state and see institutions that constitute it, as a solid impenetrable unit. The research reveals that officials have the capacity and the will to reflect on what needs to be changed and aspire to work towards more socially and spatially just outcomes. More needs to be done on this front to open up spaces for collective reflection and to move beyond the everyday constraints that might limit such opportunities, as one official notes: '*we are so busy earning a living, we have no time or energy to think about how and why things could be different … we do what has been done because it is less trouble … but if we have a chance to stop and think, anything is possible*' (interview with official from Civil Defence, October 2015). Overall the challenge is always to sustain and scale up multiple engagements and carve new avenues for those excluded in the city to have a voice in urban policy and planning issues and conceptions. Notwithstanding that knowledge production is a site of power struggles, using the mapping process to foster a political space for dialogue, can open-up new opportunities to coordinate the transformative actions required to interrupt unjust urban trajectories.

With respect to scaling up, there have been some advancements made in cLIMA sin riesgo, propelled to a large extent by the mapping process, that relate to the setting up of local observatories[7]. These are platforms devised with local communities and institutions that will continue monitoring through mapping how risk operates and how it can be addressed.

On another note, ensuring that the mapping from the air using drones and mapping from the ground with community mappers goes hand in hand was a crucial aspect for the demystification of technology. The articulations of various mapping methods served the very practical purpose of enabling local dwellers to have accessible means to engage with the problematic and analyse it at different scales, raising awareness and critical reflection and promoting alternative framings and imaginations of the future. As the potential impact of such technologies in these kinds of contexts is still unknown, it is crucial to critically evaluate the potentials and limitations of such tools in advancing grassroots practices and claims for resistance.

In our experience, one has to acknowledge the role that the technology itself and innovative visualisations can play in fostering progressive and constructive iterations in the reading, writing and audiencing of maps; whether this is linked to the possibility of grounding such methods to enable local dwellers to become active players in the use and construction of cartographic devices, or by attracting the attention of institutions to seek more efficient ways to capture how cities change and why. The participation of citizens in state mapping initiatives can be problematic if it is only a means for the efficient and cheap collection of data. Although questions of co-optation are still present, the writing of inclusive representations of the city is an avenue towards the planning of more socially and environmentally just cities. Towards this end, counter-mapping, together with other processes, can play a key role in fostering genuine commitment towards participation in knowledge production and spatial co-learning.

Acknowledgements

We would like to express our gratitude to the people of Barrios Altos and José Carlos Mariátegui for their active participation in the design and development of the mapping process that inspired this chapter, as well as to the government institutions, academics and various organisations that took part in both projects. We would also like to thank the funders: The Bartlett Materialisation Grant for ReMapLima and the Climate and Development Knowledge Network (CDKN) for the grant awarded to cLIMA sin Riesgo. Finally, we would like to thank our local NGO partners in CENCA, CIDAP and Foro Ciudades para la Vida for their sustained support and participation on this initiative since 2012 and our partners at UCL, the Centre for Advanced Spatial Analysis (CASA), as well as Drone Adventures, the makers of the senseFly eBee drones, who collaborated by donating their time as well as the drone images produced for the project.

[7] In BA the observatory brings together the Ministry of Culture, Ministry of Housing, UNESCO, Municipality of Lima, amongst others to work on (1) a deeper diagnosis of the situation, (2) a way of responding to emergencies and (3) the design and implementation of regeneration projects [31, 32].

http://dx.doi.org/10.5772/64303

Author details

Rita Lambert* and Adriana Allen

*Address all correspondence to: rita.lambert@ucl.ac.uk

The Bartlett Development Planning Unit, UCL Faculty of the Built Environment, London, United Kingdom

References

[1] Collier, D. (1976). *Barriadas y Elites: de Odria a Velasco*. Baltimore and London: The Johns Hopkins University Press.

[2] Riofrio, G. (1991). *Producir la ciudad (popular) de los '90*. Lima: DESCO.

[3] Harris, L. M., & Hazen, H. D. (2006). Power of Maps: (Counter) Mapping for Conservation. *Acme an Interantional Ejournal for Critical Geographies, 4*(1), 99–130.

[4] Abrams, J., & Hall, P. (2006). *Else/Where: Mapping New Cartographies of Networks and Territories*. Minneapolis: University of Minnesota Press.

[5] Corner, J. (1999). The Agency of Mapping: Speculation, Critique and Invention. In D. Cosgrove (Ed.), *Mappings* London; (Vol. 2, pp. 213–252). Reaktion Books. Retrieved from http://peterahall.com/mapping/corner-agency_of_mapping.pdf

[6] Dodge, M., Kitchin, R., & Perkins, C. (2009). *Rethinking Maps: New Frontiers in Cartographic Theory*. New York: Routledge.

[7] Black, J. (2002). Maps, Power, and Truth. *The Lancet, 359*, 449.

[8] Edney, M. H. (2011). Cartography without "Progress": Reinterpreting the Nature and Historical Development of Map Making. In M. Dodge (Ed.), *Classics in Cartography: Reflections on Influential Articles from Cartographica* (pp. 305–329). John Wiley & Sons Hoboken, New Jersey.

[9] Roy, A. (2009). Why India cannot plan its cities: Informality, insurgence and the idiom of urbanization. *Planning Theory, 8*(1), 76–87.

[10] Peluso, N. (1995). Whose woods are these? Counter-mapping forest territories in Kalimantan, Indonesia. *Antipode*, 27(4), 383–406. doi:10.1111/j.1467-8330.1995.tb00286.x

[11] Fox, J., Krisnawati, S., & Hershock, P. (2005). *Mapping Communities: Ethics, Values, Practice*. Honolulu: East-West Centre.

[12] Patel, S., & Baptist, C. (2012). Editorial: Documenting by the Undocumented. *Environment and Urbanization* 24 (1), 3–12. doi:10.1177/0956247812438364

[13] Glockner, H. (2004). Local empowerment through community mapping for water and sanitation in Dar es Salaam. *Environment and Urbanization* 16 (1), 185–198. doi: 10.1177/095624780401600115

[14] Hasan, A. (2006). Orangi pilot project: The expansion of work beyond Orangi and the mapping of informal settlements and infrastructure. *Environment and Urbanization* 18 (2), 451–480. doi:10.1177/0956247806069626

[15] Smith, D. (2003). Participatory mapping of community lands and hunting yields among the bugle of Western Panama. *Human Organization, 62*(4), 332–343.

[16] ReMap Lima (2013). ReMap Lima: A participatory approach to mapping. Available from: http://remaplima.blogspot.co.uk/ [Accessed: 2016-05-08].

[17] cLIMA sin Riesgo (2015). Disrupting urban 'risk traps': Bridging finance and knowledge for climate resilient infrastructural planning in Lima. Available from: http://www.climasinriesgo.net/ [Accessed: 2016-05-08].

[18] Rose, G. (1996). Teaching visualised geographies: Towards a methodology for the interpretation of visual materials. *Journal of Geography in Higher Education, 20*(3), 281–294. doi:10.1080/03098269608709373

[19] Allen, A., & Lambert, R. (2015). Learning through mapping. In B. Campkin & R. Ross (Eds.), *Urban Pamphleteer* (pp. 40–42). Municipalidad Metropolitana de Lima. London: UCL Urban Laboratory.

[20] PROLIMA. (2014). *Plan Maestro del Centro Historico de Lima al 2025.* Lima.

[21] Lizarzaburu, J. (2015). *Lima Milenaria: Gestión Castañeda prepara la demolición de cerca del 40% del Centro Histórico de Lima*. Available from http://www.limamilenaria.blogspot.com [Accessed: 2016-05-08].

[22] Akyuz, S., Nebelung, N., Reyes Aldasoro, C., Chang, C., Kuroda, I., Llanos, M. B., … Yang, J. H. (2013). Barrios Altos. In A. Allen & R. Lambert (Eds.), *Urban Renovation with Life and Memory* (pp. 69–111). London: Development Planning Unit, UCL.

[23] Braga, L., Fourrier, A., Kameja, K., Kosolsak, M., Monteiro, E., Qin, W., … Zhakanova, M. (2014). Barrios Altos – co-producing the right to the centre. In A. Allen & R. Lambert (Eds.), *Transformative Planning for Environmental Justice in Metropolitan Lima: Water, Risk and Urban Development: Present Outlooks, Possible Futures* (pp. 43–73). London: Development Planning Unit, UCL.

[24] Harley, J. (1989). Deconstructing the map. *Cartographica the International Journal for Geographic Information and Geovisualization*, 26(2), 1–20. doi:10.3138/E635-7827-1757-9T53

[25] Pickles, J. (1991). Texts, hermeneutics and propaganda maps. In T. J. Barnes & J. S. Duncan (Eds.), *Writing Worlds Discourse Text and Metaphor in the Representation of Landscape* (pp. 193–230). London: Routledge.

[26] Dodge, M., Kitchin, R., & Perkins, C. (Eds.). (2011). *The Map Reader*. West Sussex: Wiley-Blackwell.

[27] Allen, A., Lambert, R., Apsan Frediani, A., & Ome, T. (2015). Can participatory mapping activate spatial and political practices? Mapping popular resistance and dwelling practices in Bogotá Eastern Hills. *Area* 47 (3), 261–271. doi:10.1111/area.12187

[28] Wainwright, J., & Bryan, J. (2009). Cartography, territory, property: Postcolonial reflections on indigenous counter-mapping in Nicaragua and Belize. *Cultural Geographies*, 16, 153.

[29] Willow, A. (2013). Doing sovereignty in native North America: Anishinaabe counter-mapping and the struggle for land-based self-determination. *Human Ecology, 41*, 871–884.

[30] Roth, R. (2009). The challenges of mapping complex indigenous spatiality: From abstract space to dwelling space. *Cultural Geographies, 16*(2), 207–227. doi: 10.1177/1474474008101517

[31] UNESCO (2015). UNESCO Perú participó en el Lanzamiento del Observatorio del Centro Histórico de Lima. Available from: http://www.unesco.org/new/es/culture/themes/dynamic-content-single-view/news/unesco_peru_participo_en_el_lanzamiento_del_observatorio_del_centro_historico_de_lima/#.VmCD6nbhAuU [Accessed: 2016-05-08].

[32] Ministerio de Cultura del Peru (2015). Observatorio del Centro Histórico de Lima. Available from: http://www.cultura.gob.pe/es/tags/observatorio-del-centro-historico-de-lima [Accessed: 2016-05-08].

Chapter 7

Satellite SAR Interferometry for Earth's Crust Deformation Monitoring and Geological Phenomena Analysis

Giuseppe Solaro, Pasquale Imperatore and Antonio Pepe

Additional information is available at the end of the chapter

http://dx.doi.org/ 10.5772/64250

Abstract

Synthetic aperture radar interferometry (InSAR) and the related processing techniques provide a unique tool for the quantitative measurement of the Earth's surface deformation associated with certain geophysical processes (such as volcanic eruptions, landslides and earthquakes), thus making possible long-term monitoring of surface deformation and analysis of relevant geodynamic phenomena. This chapter provides an application-oriented perspective on the spaceborne InSAR technology with emphasis on subsequent geophysical investigations. First, the fundamentals of radar interferometry and differential interferometry, as well as error sources, are briefly introduced. Emphasis is then placed on the realistic simulation of the underlying geophysics processes, thus offering an unfolded perspective on both analytical and numerical approaches for modeling deformation sources. Finally, various experimental investigations conducted by acquiring SAR multitemporal observations on areas subject to deformation processes of particular geological interest are presented and discussed.

Keywords: deformation modeling, geodesy, SAR interferometry

1. Introduction

Synthetic aperture radar interferometry (InSAR) is a consolidated technique that can be used to measure crustal deformation (associated with volcanic and seismic activity) by exploiting the phase of coherent electromagnetic signal. Specifically, theoretical foundation of the space-

borne (across-track) SAR interferometry and multitemporal advanced processing (e.g., persistent-scatters and small-baseline based) methods are introduced. First, we methodologically address the InSAR methods allowing the detection, mapping and monitoring of the Earth's crust dynamic processes (surface displacements) over large temporal and spatial scales with centimeter to millimeter accuracy. Then, emphasis is placed on the geological processes taking place within the Earth's crust, such as the movement of a seismogenic fault, the accumulation of magma, variation of pressure in the magmatic reservoirs, subsidence. All these phenomena can cause deformations of the Earth's surface and can then be investigated by suitably exploiting satellite observations. For such a purpose, different approaches are possible; most of them are based on the inversion of a suitable model describing the underlying geophysical phenomenon. Specifically, in order to model the deformation sources both analytical and numerical approaches have been adopted. Within the analytical framework, we first address the most commonly adopted models, which can reproduce the observed deformations in a sufficiently realistic way by using simple functions characterized by a limited number of parameters. Although these analytical models neglect several aspects (e.g., the properties of magma inside the source, including its compressibility, the asperities along the fault plane, the crustal heterogeneity), they still constitute a valuable tool for a preliminary evaluation on the localization and geometric characteristics of the sources. Numerical modeling, which is a powerful tool allowing a realistic simulation of geophysical processes, using heterogeneous information and efficient computational methods, is also discussed. Specifically, various numerical modeling techniques exist; one of the most used in the Earth Sciences community is the finite element method (FEM) technique. In fact, both the increase in knowledge about geophysical systems and technological development of numerical techniques have enabled the implementation of complex modeling approaches, which are able to represent the spatiotemporal variability of the geophysical parameters of interest. In this context, the use of FEM multiphysics tools represent a new frontier for the understanding of the spatial and temporal evolution of different geodynamic settings, such as volcanic and seismic areas and those with a hydrogeological instability. Therefore, a comprehensive and updated perspective is offered in this chapter, encompassing advanced remote sensing and geophysical methodologies addressed to the analysis of several natural phenomena resulting in the deformation of the Earth's crust. Furthermore, a wide range of case studies is shown, which have systematically been investigated by considering data acquired by different SAR sensors (e.g., ENVISAT, RADARSAT-2) on diverse hazardous geologically zones of interest (e.g., areas interested by seismic and volcanic activity).

2. SAR interferometry principles

Synthetic aperture radar (SAR) [1–3] is a coherent active microwave remote sensing system widely used for the Earth remote sensing. SAR instruments can be mounted on-board aircraft or satellite platforms; they work by transmitting microwave pulses toward the Earth surface and by measuring the microwave echoes scattered back to the sensor platform. SAR is an imaging system with all-weather, day and night sensing capability that nowadays plays a key

http://dx.doi.org/ 10.5772/64250

role for the remote sensing of the environment, and in particular it is extensively used for the monitoring and analysis of several geophysical phenomena. A SAR image can be represented as a two-dimensional (2D) complex signal in the (range, azimuth) plane, whose amplitude gives information about the backscattering coefficient of the ground and the phase includes information about the distance traveled by the emitted electromagnetic pulses from the transmitting to the receiving antennas (i.e., twice the sensor-to-target distance). *Range* (or cross-track) direction is associated with the "line-of-sight" distance from the radar to the target, whereas *azimuth* (along-track) direction is parallel to the flight track.

One of the major applications of the SAR technology is represented by the SAR interferometry (InSAR) technique [4–8], which is based on the measurements of the phase pattern difference between two complex-valued SAR images acquired from two different orbital positions, and allows the measurements of geomorphological characteristics of the ground, such as the topography height and its modifications over time (e.g., the surface deformation) due to earthquakes, volcano eruptions, or other geophysical phenomena. Historically, the main application of InSAR was the retrieval of the terrain topography [4–6]. Depending on the time when SAR acquisitions are collected and the orbital position of the SAR platform, different InSAR configurations can be distinguished. *Cross-track* interferometry is a basic SAR interferometric configuration in which two antennas are arranged across the track of the platform, as sketched in **Figure 1**.

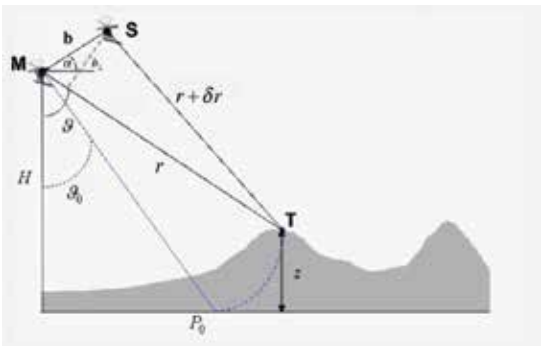

Figure 1. SAR interferometric configuration. The black lines show radar signal paths for an interferogram pair formed by the antennas M and S.

Within this context, two different acquisition modes can be distinguished: *single-pass* mode is characterized by two distinct antennas on the same platform (in the standard form, the former (master) operating in a receive/transmit mode and the latter (slave) in the receive mode only), the *repeat-pass* mode concerns two separate passes of a single SAR mission over the same area [8]. In addition to the standard cross-track interferometric configuration, we also mention the *along-track* interferometry (ATI), which is a single-pass configuration with two antennas displaced with a baseline parallel to the direction of motion: airborne ATI has been mainly used for measurement of ocean currents.

Let us consider again the imaging geometry depicted in **Figure 1**, where the first SAR image (i.e., the master image) is taken from the orbital position labeled to as M, and the second one (i.e., the slave image) is captured from the orbital position labeled to as S, at a distance b (typically referred to as *baseline*) from M. Taking into account simple geometrical considerations relevant to the considered geometry, it is possible to uniquely locate each imaged targets on the ground and get an estimate of their heights (namely, z) above the reference plane. As evident by inspection of **Figure 1**, if a same target (namely, T) is observed from two orbital positions (master and slave), the difference between the path lengths to the target can be correctly measured and the target height z above the assumed zero-altitude plane can be unambiguously determined. This is obtained by taking into account the following two equations (see **Figure 1**):

$$(r + \delta r)^2 = r^2 + b^2 - 2\, r\, b \sin(\vartheta - \alpha) \tag{1}$$

$$z = H - r\cos\vartheta \tag{2}$$

where δr and $\delta + \delta r$ represent the radar ranges from the corresponding antennas to the target point being observed, ϑ is the radar look angle, α represents the angle of the baseline relative to the horizontal, z denotes the scatterer height above the flat-earth reference, H is the height of the sensor above the reference surface, and b is the physical separation of the antennas that is referred to as the *baseline* of the interferometer. Notice that (1) derives from the application of the cosine rule to the MST triangle and (2) is a simple geometric relationship linking the target topography (z), the sensor height (H), and the radar side-looking angle (ϑ). The ability in successfully reconstructing the unknown topography (z) is strictly dependent on the capability to precisely measure the slant-range difference δr, which represents one of the known terms of the system of Eqs. (1) and (2).

Historically, a first methodology to get an estimate of δr was represented by the radar stereometry [8]. In such a method, the master/slave sensor-to-target slant-range difference δr is measured by searching for the position of the same target in the two coregistered SAR images (being the coregistration the operation needed to spatially aligned one SAR image to another) [9, 10]. As a matter of fact, the attainable accuracy in estimating δr is on the order of the system slant-range resolution. However, it can be proved that the errors in the estimation of δr is magnified by a factor on the order of the ratio $\left(\frac{r}{b}\right)$ when they are transferred to height measurements [3], thus leading to an inaccurate measurement of the target height (z). For instance, we consider ENVISAT platform parameters $\left(\frac{r}{b} = \frac{800\text{km}}{100\text{m}}\right)$ and suppose being able to discriminate reasonable range displacements of 1/16th of the pixel spacing through use of correlation digital processing (i.e., the accuracy in measurement of δr is equal to 0.5 m). Accordingly, the achievable height accuracy turns out to be on the order of kilometers, and it is evidently unacceptable. This is the main reason of InSAR success with respect to radar-stereometry. Indeed, the intrinsic limitation of radar stereometry due to the low attainable accuracy of

http://dx.doi.org/ 10.5772/64250

topography is fully overcome by SAR interferometry, which allows estimates of the master/slave slant-range difference δr with centimeter accuracy over region of hundreds of kilometers in size at a resolution of a few meters.

In the following, we primarily refer to the repeat-pass cross-track SAR interferometry configuration. Let us consider again the imaging geometry depicted in **Figure 1** and assume the radar system has infinite bandwidth and hence with point-wise image pixels [4]; under this condition the master and slave complex-valued SAR images (pixel-by-pixel) can be mathematically represented as follows:

$$\hat{\gamma}_1 = \gamma_1 exp\left[-j\frac{4\pi}{\lambda}r\right] \tag{3}$$

$$\hat{\gamma}_2 = \gamma_2 exp\left[-j\frac{4\pi}{\lambda}(r+\delta r)\right] \tag{4}$$

where γ_1 and γ_2 are the complex reflectivity functions of the master and slave scene, respectively, and λ denotes the operative radar wavelength. It is worth mentioning that the phase of each single-channel radar signal is composed of two parts: the first represents the propagation phase that depends on the radar-scene distance, the second depends on the inherent electromagnetic scattering process. The interferometric phase map (so called *interferogram*) is formed on a pixel-by-pixel basis starting from two coregistered (complex) SAR images as follows. For each pixel, the phase difference between the two SAR images is extracted by simply multiplying the first image (master) by the complex conjugate of the second image (slave) and then by extracting its phase term.

From (3), we get the radar observable (interferometric phase):

$$\tilde{\psi} = arg[\hat{\gamma}_1\hat{\gamma}_2^*] = arg\left[\gamma_1\gamma_2^* exp(j\frac{4\pi}{\lambda}\delta r)\right] \tag{5}$$

where the asterisk denotes the complex conjugate operation, and the symbol arg[·] refers to the phase extraction operation (i.e., the operator that extracts the phase of a complex number restricted to the $]-\pi, \pi]$ interval). Assuming that the scattering mechanism on the ground has not significantly changed ($arg[\gamma_1] = arg[\gamma_2]$) between the two passages of the sensor over the illuminated area (mutually coherent observations), the measured interferometric phase $\tilde{\psi}$ depends upon purely geometric information on the path difference δr only:

$$\tilde{\psi} = arg\left[exp(j\frac{4\pi}{\lambda}\delta r)\right] \tag{6}$$

The observed interferometic phase $\tilde{\psi}$ is 2π-ambiguous, and the obtained image is called an *interferogram*; the pattern formed by the iso-phase contours is commonly referred to as fringe pattern. Since the ambiguity of the phase measured modulo 2π, the information on range difference δr is then retrieved from the interferogram by applying the *phase unwrapping* operation [11, 12], thus estimating the inherent *absolute* interferometric phase ψ, which is given by:

$$\psi = \frac{4\pi}{\lambda}\delta r \tag{7}$$

Note also that: $\tilde{\psi} = W(\psi)$, where W is the so called *wrapping operator* [13].

The difference in range from the scatterer to the two aperture phase centers is well approximated (since $b \ll r$, the commonly referred to as *parallel-ray* assumption is reasonable) as $\delta r = -b\sin(\vartheta - \alpha)$, where $b_{||} = -b\sin(\vartheta - \alpha)$ is just the projection of the baseline along the line of sight (LOS) (**Figure 1**). Thus, the interferometric phase is given by:

$$\psi = -\frac{4\pi}{\lambda} b\sin(\vartheta - \alpha) \tag{8}$$

It is worth highlighting the height sensitivity of ψ, through the dependence of the actual look angle ϑ, on the altitude $z = H - r\cos\vartheta$, where H is the height of the sensor above the reference surface. By considering the standard interferometric configuration depicted in **Figure 1**, it is possible to relate the computed interferometric phase to the (unknown) height topography [4]. At first order, we obtain:

$$\psi \approx \psi_0 + \frac{\partial\psi}{\partial z} z = -\frac{4\pi}{\lambda} b sin(\vartheta_0 - \alpha) - \frac{4\pi}{\lambda}\frac{b_\perp}{r\sin\vartheta_0} z \tag{9}$$

where z is the topography height above the flat earth reference, ϑ_0 is the look angle to the point target assuming zero local height, $b_\perp = b\cos(\vartheta_0 - \alpha)$ represents the projection of the baseline normal to the line of sight from the radar to the target and it is an important parameter referred to as *orthogonal baseline*. The first term in (9), $\psi_0 = \frac{4\pi}{\lambda} b\sin(\vartheta_0 - \alpha)$, accounts for phase contribution generated by an ideally *flat-earth* ($z = 0$); this term is present even in the absence of any height elevation above the reference surface. Indeed, across the image swath there will be an equivalent flat-earth variation in phase resulting from the corresponding change of incidence angle from near to far swath edge. In order to avoid that the result be biased with position across the swath, the flat earth variation needs to be removed from the recorded phase, thus removing (*interferogram flattening*) the high-frequency modulation induced by the "flat earth" phase variations to facilitate further processing. The second term in (9), $\Delta\psi = \frac{\partial\psi}{\partial z} z$, is the resulting "flattened" phase difference, with the *height sensitivity* of the interferometer given by

http://dx.doi.org/ 10.5772/64250

$\frac{\partial \psi}{\partial z} = -\frac{4\pi}{\lambda}\frac{b_\perp}{r\sin\vartheta_0}$. From (9), it is clear that the sensitivity of the interferometer could be improved by increasing the baseline. The perpendicular baseline, however, cannot exceed the limiting case (*critical baseline*) for which the variation in the interferometric phase difference across a single ground range resolution element is 2π. Indeed, the arising decorrelation phenomena lead to significant noise disturbances in the computed interferogram [14], hence fraction of the critical baseline are typically used in practice. As a result, a compromise is needed for the selection of the optimal baseline: on the one hand, large interferometric baselines would guarantee more accurate estimates of height topography, on the other hand, large baseline interferograms are more affected by decorrelation noise.

2.1. Detecting surface deformation

In this section, we shortly review the basic principles of differential SAR interferometry. Indeed, satellite SAR interferometry nowadays is mostly used for the detection/monitoring of surface changes occurring between the two passages of the radar sensor over the same scene. In such a case, as a slightly change across the two SAR acquisition times occurs in the imaged scene (due to, for instance, subsidence, landslide, or earthquake phenomena), an additive term associated with the radar line of sight (LOS) component of the surface displacement arises in the interferometric phase, in addition to the phase dependence on topography. By the inspection of the imaging geometry depicted in **Figure 2**, at the first-order we get:

$$\Delta\psi = \frac{\partial\psi}{\partial z}\Delta z + \frac{\partial\psi}{\partial d_{LOS}}\Delta d_{LOS} = -\frac{4\pi}{\lambda}\frac{b_\perp}{r\sin\vartheta}\Delta z + \frac{4\pi}{\lambda}\Delta d_{LOS} \tag{10}$$

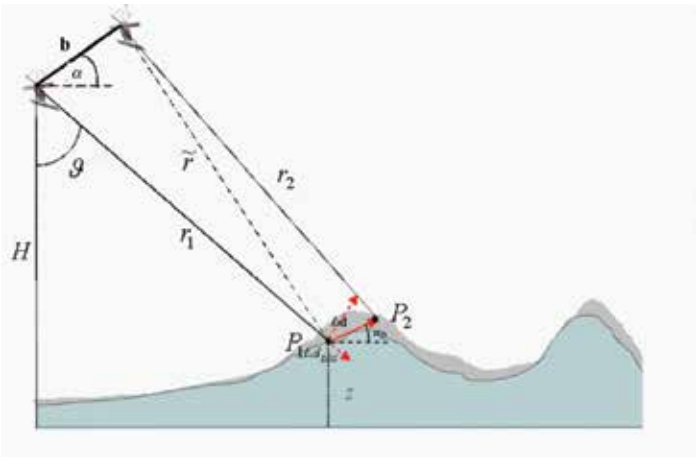

Figure 2. Differential SAR interferometry geometry. Note that $r_2 - r_1 = (r_2 - \tilde{r}) + (\tilde{r} - r_1) \cong \Delta d_{\mathrm{LOS}} + \delta r$, where $\delta r = \tilde{r} - r_1$ is the path difference in the absence of any ground displacement, and the LOS displacement, Δd_{LOS}, is given by $\Delta d_{\mathrm{LOS}} = \Delta d \sin(\vartheta - \alpha_{\mathrm{D}})$, with Δd representing the amplitude of the displacement from P_1 to P_2.

where Δd_{LOS} represents the projection of the surface-displacement vector onto LOS (range) direction, ϑ is the look angle to the point target with respect to the nominal local height, and Δz denotes the residual topographic variation. Note that it is reasonable to assume that the radar echoes remain correlated since the surface displacements are assumed small with respect to a resolution cell. It is also important to note that a much more sensitive dependence of phase (10) results from surface displacement Δd_{LOS} than from residual topographic variation Δz, insofar as the distance r typically is very much greater than the orthogonal baseline distance $b_{\perp}$. Notice that, in order to isolate (measure) the interferometric phase term associated with the displacement, it is necessary to remove the interferometric phase contribution pertinent to the underlying topography in Eq. (10). Specifically, the so-called differential SAR interferometry (DInSAR) basically consists in the synthesis of a simulated topographic phase screen from an available *digital elevation model* (DEM) of the area (using the so so-called back-geocoding process) and to subtract on pixel basis these synthetic fringes leaving only the terms associated with the displacement (see Eq. (10)) [4].

In this ideal configuration, the DInSAR technique gets an unambiguously measurement of the LOS displacement of the order of fractions of wavelength: note that a differential phase change of 2π is converted to a LOS displacement of $\lambda/2$. As an example, since the error on the estimate is of a fraction of π and the wavelength is of the order of centimeters (e.g., for the ERS-1/2 case λ = 5.6 cm), we could measure LOS displacement down to millimeter accuracy, provided that coherence of the differential interferograms is sufficiently high. Computed differential SAR interferograms however contain, in addition to the deformation component, some (unwanted) phase terms arising from unavoidably inaccuracies in the knowledge of the actual topographic pattern and/or of the orbital parameters. In particular, the variation of the interferometric phase can be expressed more in general in the form:

$$\Delta\psi = \Delta\psi_{disp} + \Delta\psi_{topo} + \Delta\psi_{orb} + \Delta\psi_{prop} + \Delta\psi_{noise} \tag{11}$$

where:

- $\Delta\psi_{disp} = \frac{4\pi}{\lambda}\Delta d_{LOs}$ accounts for a possible displacement of the scatterer between observations, where Δd_{LOS} denotes the projection of the relevant displacement vector on the line of sight;
- $\Delta\psi_{topo} = \frac{4\pi}{\lambda}\frac{b_{\perp}}{r\sin\vartheta}\Delta z$ represents the residual-topography induced phase due to a nonperfect knowledge of the actual height profile (i.e., the DEM errors Δz);
- $\Delta\psi_{orb}$ accounts for residual fringes due the use of inaccurate orbital information in the synthesis of the topographic phase;
- $\Delta\psi_{prop}$ denotes the phase components due to the variation of propagation conditions (pertinent to the change in the atmospheric and ionospheric dielectric constant) between the two master/slave acquisitions;

http://dx.doi.org/ 10.5772/64250

- $\Delta\psi_{noise}$ accounts for decorrelation phenomena: spatial baseline decorrelation, Doppler centroid decorrelation, thermal decorrelation, and temporal decorrelation (including any change in scattering behavior) [14].

As a final remark, we observe that another source of misinterpretation upon the measured deformation is intrinsic to the InSAR technique itself, and it is due to phase unwrapping errors. Evidently, phase unwrapping errors are integer multiples of 2π but they can propagate within the inversion process, thus significantly affecting the deformation measurements [3].

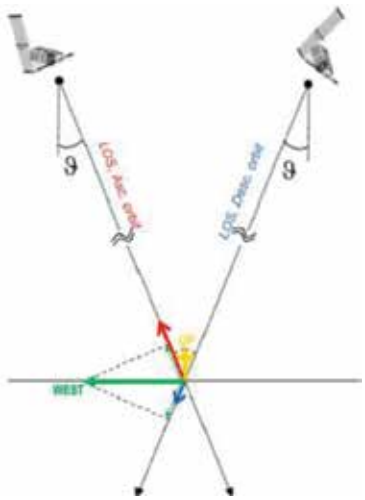

Figure 3. Geometric scheme for the deformation components.

Availability of InSAR results computed from SAR data obtained from ascending and descending orbits allows the retrieval of the east-west (E-W) and the up-down (U-D) components of the detected deformation [15, 16]. Let us assume the target "observed" from both the *ascending* and the *descending* satellite passes, and assume the displacement components along the ascending and descending radar LOS directions have been estimated. For the sake of simplicity, the following assumptions are made: (i) ascending and descending radar LOS directions ($d_{\mathrm{LOS}}^{(\mathrm{asc})}$ and $d_{\mathrm{LOS}}^{(\mathrm{desc})}$, respectively) lay on the plane identified by east and –z directions, and (ii) the sensor look angle ϑ is approximately the same for both the ascending and descending observations. In particular, for all the pixels that are common to both radar geometries, the sum and the difference of LOS-projected deformations computed (over approximately the same time period) for the ascending and the descending orbits can be calculated. Based on simple geometric considerations, the E-W and up-down components of the measured surface deformation can be estimated as follows:

$$d_{LOS}^{(East)} = \frac{d_{LOS}^{(desc)} - d_{LOS}^{(asc)}}{2\sin\vartheta} \tag{12}$$

$$d_{LOS}^{(Up)} = \frac{d_{LOS}^{(desc)} + d_{LOS}^{(asc)}}{2\cos\vartheta} \tag{13}$$

Notice that, because of the namely polar sensor orbit direction, the north-south (N-S) component of the deformation cannot be reliably singled out. Geometric scheme to interpret the deformation component is portrayed in **Figure 3**.

Finally, we emphasize that a fundamental advantage of InSAR technology, with respect to global positioning system (GPS) networks, resides in its dense spatial sampling of the displacement field.

3. Multichannel SAR interferometry

Differential SAR interferometry methodology has first been applied to investigate single deformation events. At the present days, however, it is chiefly applied for the computation of displacement time-series through the so-called multitemporal (or multichannel) interferometric SAR approaches [17–25]. These advanced methods are based on the processing of sequences of multitemporal interferograms relevant to an area of interest and are aimed at recovering the expected LOS-projected time-series of deformation. A short overview of the main algorithms proposed up to now is here reported. Generally speaking, multichannel interferometric techniques can be categorized into two broad families, those focused on analyzing *persistent scatterers*, that is to say point-like targets that are not significantly affected by decorrelation effects [17–19], and the *small baseline* (SB) [20–26] methodologies, relying on the investigation of deformation signals related to distributed scatterers (DS) on the ground, which can be however severely corrupted by decorrelation effects. In this latter case, an *a priori* selection of the exploited SAR data pairs with small baseline values is required to reduce the noise level in the generated interferograms. Despite of their intrinsic differences, both the PS and SB algorithms have successfully been used to detect and monitor deformation phenomena, due to several natural and anthropic hazards, such as volcanic events, earthquakes, landslides, damages to man-made infrastructures in urbanized areas caused by underground, and tunneling excavations and/or gas and water exploitation [27–37]. Very recently, a plethora of different PS- and SB-oriented approaches have been implemented and public InSAR toolboxes [17–26] are available to users. Recently, some innovative approaches based on the joint exploitation of spatial and temporal relationships among sequences of interferograms and of the statistical characteristics of SAR images involved in their formation have been proposed for the analysis of deformations affecting DS targets [38–42]. In particular, the method proposed in [40], which is known in literature to as *SqueeSAR*, is aimed at retrieving the displacement time-series of DS that are identified by preliminarily studying the statistical homogeneity of adjacent pixels in long sequences of amplitude SAR images, and then by averaging the interferometric phase only on the set of statistically homogeneous (SH) pixels [40, 41]. In addition, the average interferometric phases (associated with couples of images) are jointly employed (for each pixel of the SAR scene) to obtain estimates of the phase relevant

http://dx.doi.org/ 10.5772/64250

to SAR acquisitions [40], thus finally retrieving (for each SH target) a time-series of deformation. This method allows increasing the number of detectable DS targets, but at the expenses of ad-hoc processing for the generation of average (multilook) InSAR interferograms. At variance with the SqueeSAR and other recently proposed multitemporal filtering techniques (e.g., [41, 42]), the method proposed in [41] (and also detailed in [42]) used conventional multilook interferograms, which can be generated by using any of existing InSAR toolboxes and without any preselection of SH targets. This leads to the nonapplicability of statistical framework adopted in [40], which is based on the distributed scattering hypothesis under which the probability density function (pdf) of the complex-valued SAR image may be regarded as being a zero-mean multivariate circular normal distribution. This issue is not considered a very limiting factor in [43], where "conventional" multilook interferograms (also potentially prefiltered using other space-based noise filtering techniques [44]) are filtered in time with the aim to isolate and discard the noise components that are not conservative in time from generated time-series of deformation. The mathematical framework of this new improved SBAS-oriented processing chain is illustrated in [43, 45] where the method is fully detailed. In the following, we focus on the *small baseline subset* (SBAS) algorithm, originally proposed in [20], by analyzing the underlying basic principles. Let us consider a set of Q *single-look-complex* (SLC) SAR data acquired over a certain area of interest. One of them is assumed as the reference (master) image, with respect to which the images are properly coregistered. This set is characterized by the corresponding acquisition times $\{t_1,\ldots, t_Q\}$ and perpendicular baselines $\{b_{\perp 1},\ldots, b_{\perp Q}\}$ evaluated with respect to the reference image. Application of the standard SBAS technique starts with the generation of a number, namely M, of small baseline multilook (differential) interferograms. The *multichannel phase unwrapping* (MCh-PhU) problem consists in the jointly retrieval of the original (unwrapped) phase signals from the modulo-2π measured (wrapped) phases relevant to the considered stack of interferograms. The MCh-PhU operation can be straightforwardly implemented through various 2D [46–48] and 3D approaches [44, 49–51] (and/or hybrid ones [13, 52]). The variation of the interferometric phase pertinent to the kth SAR data pair can be expressed as (see also (10)):

$$\Delta\psi^k = \frac{4\pi}{\lambda}\Delta d^k_{\mathrm{LOS}} - \frac{4\pi}{\lambda}\frac{b^k_{\perp}}{r\sin\vartheta^k}\Delta z + \Delta\psi^k_{\mathrm{orb}} + \Delta\psi^k_{\mathrm{prop}} + \Delta\psi^k_{\mathrm{noise}} \tag{14}$$

where $k \in \{1,\ldots, M\}$ specifies the considered interferometric pair (master/slave) of the multiple baseline configuration used for the generation of the relevant interferogram. Readers are referred to [20] for further details. Once the phase associated to each SAR acquisition, as well as the residual topography, are estimated, the phases are converted to deformation and the atmospheric phase screen (APS) is computed and filtered out from the obtained deformation time-series. APS removal is achieved by exploiting the assumption that APS is spatially correlated and uncorrelated in time, thus processing atmospheric corrupted time-series is performed with a spatial low-pass (LP) filter and a time high-pass (HP) filter [17, 20]. The quality of retrieved LOS time-series is finally evaluated pixel-by-pixel by calculating the values of the *temporal coherence* factor, defined in [52]. Residual orbital fringes are also estimated and

filtered out in the conventional SBAS processing chain by searching for (in each interferogram) any possible phase ramp, which can be directly related to errors in the knowledge of sensor position along its orbit. Such residual phase ramps (see also [38, 39]) are jointly analyzed to correct orbits state vectors. Finally, for pixels with high temporal coherence the map of LOS mean deformation rate over the analyzed time-periods is computed. Note that, whenever ascending/descending SAR data-tracks are available, SBAS processing can be applied for the two complementary orbits. Thus, the ascending/descending rates of deformation can be composed, as described in the previous section, to retrieve the east-west and up-down displacement rates over the time-period span by the available SAR scenes. Finally, we highlight that a parallel computational model for SBAS algorithm is discussed in [13, 26].

4. Geological models and applications

In this section, we describe the technical aspects related on how to retrieve the characteristics of a deformation source from satellite InSAR data, focusing the attention on the seismic, volcanic, and landslide activities. We present the state-of-the-art of the techniques concerning this problem, describing the most commonly used analytical and numerical models, and also providing appropriate geological examples for each kind of modeling approach.

4.1. Analytic modeling

The increasingly widespread use of space geodesy has resulted in numerous, high-quality surface deformation data sets. For example, a dense array of more than 1000 continuous GPS (global positioning system) stations are distributed throughout Japan [53] and more than 700 GPS stations are operating in the California area [http://earthquake.usgs.gov/monitoring/deformation/]. Many geologically active areas, such as Hawaii, Mt. Etna, Campi Flegrei, and Long Valley caldera, have regional GPS networks as well [55–58]. At the same time, DInSAR is a well-established technique for studying and analyzing tectonically active areas characterized by wide spatial extent of the inherent deformation [5]. These geodetic data can provide important constraints on fault geometry, its slip distribution and also type and position of a magmatic source. For this reason, over last years, many researchers have developed robust and semiautomatic methods for inverting suitable models to infer the source type and geometry from surface deformation [54]. Most of these methods use elasticity theory and a trial-and-error approach to find geologically plausible deformation models that fit the major features of the observed deformation field [55]. Other authors have systematically searched through a large set of feasible models, comparing the model predictions to the data, and choosing the model that minimizes the misfit [56].

The knowledge of source geometry from geodetic data primarily requires a forward model describing how the crust responds to various kinds of deformation sources. The most commonly used crustal model is the homogeneous, isotropic, linear and elastic half-space [57]. In spite of its limitations, the elastic half-space model is widely used to simulate surface defor-

http://dx.doi.org/ 10.5772/64250

mation, primarily due to its mathematical simplicity. Sources models commonly used in many papers are [58, 59]:

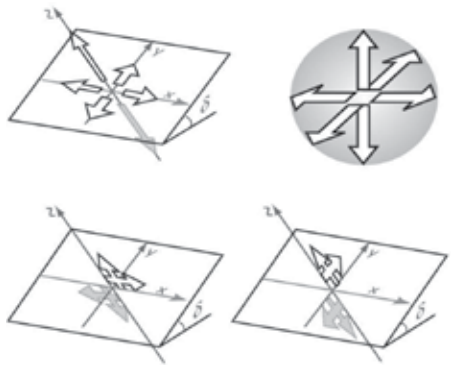

Figure 4. Four types of buried point dislocation sources: tensile, dilatational, strike slip, and dip slip (from [58]).

- The elastic dislocation of a finite rectangular source (Okada model): it is one of the most used model to simulate the surface displacement due to an earthquake, represented as a shear dislocation over a finite rectangular fault [60]. Moreover, the Okada model can also be used to describe magma intrusion like sills or dykes, interseismic and postseismic displacement. Pertinent source parameters are east and north position, depth, length, width, strike angle, dip angle, dislocation (or slip), dislocation angle (rake), opening (for magmatic intrusion) (**Figure 4**).
- The point pressure source (Mogi model): it is one of the simplest and effective sources used in volcanology, as its description requires only four parameters: depth, east and north position, volume/pressure variation [61] (**Figure 5**).
- The finite spherical pressure source relies on the assumption that the radius of the source cannot be separated from the pressure change. This means that we can only obtain estimates of the depth, location, and power of the source [58]. In [62], the mathematical expressions to approximate the deformation due to a pressurized finite spherical cavity were derived by applying higher order corrections for stresses reflected back on the source by its image.
- The closed pipe: a model for a plugged conduit or a cigar-shaped magma chamber. It includes a conduit to transport magma from the chamber to the surface. During quiescence period, the magma tends to cool and forms a plug, and the pressure in the magmatic system can increase [58]. The distribution of surface deformation from inflation of a closed pipe is quite different from that previously described for a sphere and this is mainly related to two main aspects: (1) most conduits are quite small relative to magma chambers, and (2) the near-field deformation from an elongate embedded source depends on the value of Poisson's ratio [63].
- The open pipe: a composite model for the filling of an open conduit. In [64], it is presented a dislocation model for surface deformation from magma rising in a conduit that is open at

the top. A constant cylindrical dislocation is used to model portions of the conduit subject to a uniform pressure change [58].

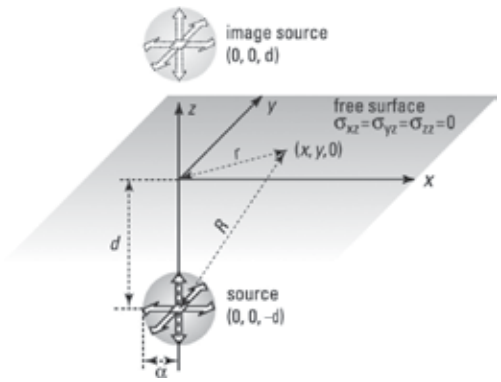

Figure 5. Surface deformation from an embedded point pressure source (Mogi model) (from [58]).

In spite of its limitations, the elastic half-space models are widely used to model surface deformation caused by uniform rectangular dislocations [60] and point sources [61]. Moreover, until recently, most geodetic data were not of sufficiently high quality to justify more complex crustal models.

For almost all the listed models, the geometric parameters (position, depth, dimension, orientation, etc.) are nonlinearly related to the surface displacement. On the contrary, other parameters, as the dislocation for the Okada model or the pressure change for a Mogi model, have a linear dependency with the surface displacement [59]. The estimation of nonlinear and linear parameters from geodetic data follows different inversion strategies, which are explained in the next section.

4.1.1. Inversion strategies for source parameters estimation

The relationship between the measured deformation field (which for instance can be inferred through InSAR technique, as discussed in Sections 2 and 3) and the source geometry can be expressed by the following equation:

$$\mathbf{d} = G(\mathbf{m}) + \varepsilon \tag{15}$$

where **d** is the deformation data vector, **m** is the source parameter vector (e.g., for a fault, length, width, depth, dip, strike, location, slip are the source parameters to be estimated), and *G* describes the specific functional form. The **ε** term is a vector of observation errors. For the source geometry estimation problem the data, in general, are nonlinearly related to the source parameters. For this reason, source estimation reduces to nonlinear optimization [54]. Therefore, we systematically search the finite dimensional parameter space for **m**, using G to predict the deformation field for a given **m**. The geodetic signal contains unmodeled deformation such

http://dx.doi.org/ 10.5772/64250

as those arising from elastic heterogeneity or anisotropy, which may contribute to the misfit, thus our best estimated source model is always conditional on the assumptions intrinsic to the forward model.

Derivative-based algorithms, Levenberg-Marquardt or the method of conjugate gradients, offer straightforward and efficient strategies for solving the mentioned optimization problem [54]. These algorithms depend on the gradient and higher-order derivatives to guide them through misfit space; however, due to the nonlinear nature of the *G* functional form, they can get trapped in the first local minimum that they encounter and never find or even approach the global minimum. Consequently, these algorithms work well only when the initial guess is near the global minimum. *A priori* information can often provide a good initial guess. Clearly, whether a derivative-based method reaches the global minimum depends on where it starts. Moreover, in [54], it was found that particularly in the case of low measured displacement, the misfit space often contains numerous local minima and lacks a deep, well-defined global minimum. Therefore, derivative-based methods offer a practical approach for retrieving the solution to the geodetic inversion problem only in cases characterized by high measured displacement and good geologic insights, such as the type and location of the deformation source [54].

In spite of their inefficiency, exhaustive and random searches do not have the limitation to remain trapped in a local minimum. In the past, mathematicians have sought algorithms that combined the efficiency of a derivative-based method with the robustness of a random search. The result was the Monte Carlo class of algorithms. The common feature that all algorithms of this class share is an element of randomness that permits an occasional uphill move, that is, the algorithms will not always move from a candidate model with higher misfit to a model with lower misfit [54]. The most common Monte Carlo algorithms are the simulated annealing [65] and the random cost algorithm [66]. Another class of Monte Carlo algorithm includes the genetic algorithms [67].

Simulated annealing. In such a kind of algorithm, the possibility to choose a higher misfit model compared to a lower one mainly depends on the state of the annealing process at the time of the choice [54]. The algorithm gives an estimate of this state dependence in terms of a global time-varying parameter called temperature. At high temperatures, all source models have roughly equal chances of getting picked, whereas at low temperatures the algorithm favors low misfit models. The specific annealing algorithm adopted here follows from the work by Yu and Rundle [65] and Berg [68]. It is called the "heat bath" algorithm and proceeds as follows. The initialization procedure consists of two steps: (1) set bounds on the values for all the model parameters (these bounds can come from geologic constraints or physical limitations) and (2) randomly pick an initial starting model. Cycle through the individual model parameters. The most significant complication to the simulated annealing algorithm is the cooling schedule, i.e., how the temperature changes as the annealing progresses. This plays a crucial role in the successor failure of the optimization. In [69], a critical temperature at which the bulk of the annealing should, for maximum efficiency, occur was defined. In brief, at the critical temperature the system remains cool enough to favor low misfits but still high enough to escape local minima.

Random cost. This algorithm is an alternative Monte Carlo approach for nonlinear optimization problems characterized by many local minima in a broad misfit space [66]. It considers a stochastic process to enforce a random walk in misfit space, which allows it to overcome the increase of misfit and to find the global minimum. In [54], the authors indicate that this algorithm is significantly less efficient than simulated annealing, but it is much easier to implement because it does not require a specific cooling schedule. The random cost approach begins by generating a set of trial models that span a region about an arbitrary *a priori* model [54].

4.1.2. Geological applications

In this section, we present two examples of deformation sources in volcanic (Lazufre, Chile) and seismic (2012, Emilia earthquake, Italy) environment, by applying the analytic modeling. In the first case, the simulated-annealing-based approach is adopted, while in the second case we apply the Levemberg-Marquardt algorithm (see Section 4.1.1).

4.1.3. Sill and finite spherical sources: the case of Lazufre (Chile) volcano

The Lazufre volcanic area is located on the Chilean-Argentinean border at ~300 km east of the subduction trench (**Figure 6**). The area contains several morphologically distinct volcanic centers [71, 72]. Only one of these, the Lastarria volcano (~5700 m asl), shows strong and persistent fumarolic activity localized on the recent crater borders and on the western flank (**Figure 6**).

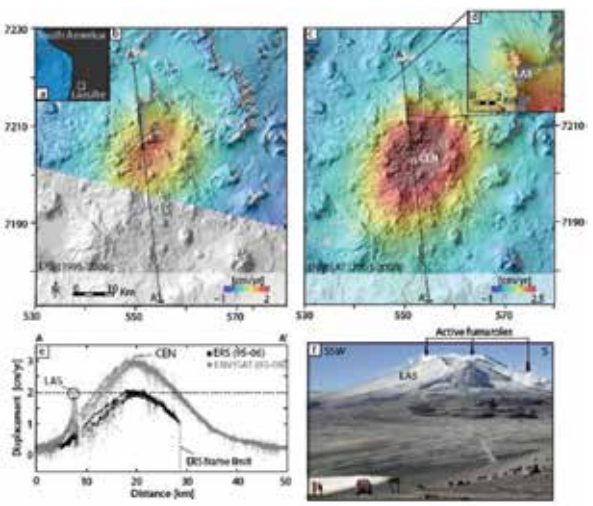

Figure 6. Deformation at the Lazufre volcanic area: (a) location of Lazufre; (b) InSAR observation for the period June 1995–December 2006 acquired by ERS; (c) InSAR observation for the period April 2003–January 2008 acquired by ENVISAT; (d) details of Lastarria volcano; (e) NNW-SSE profiles across the deformation areas for the ERS dataset (black) and for the ENVISAT dataset (gray); (f) photograph of the Lastarria volcano from the northwest, 10 km distant from the summit [70].

http://dx.doi.org/ 10.5772/64250

Through InSAR observations, a large-scale elliptical deformation pattern was detected during the period from 1995 to 2008, with a deformation rate ranging from 1.8 to 3.2 cm/year [70]. The observed displacement rate at LAS reaches up to 2 cm/year from 2003 to 2008, with a part of this signal being related to the large-scale deformation field. To retrieve the mean deformation velocity maps of the area the SBAS algorithm (see Section 3) was applied to two SAR datasets acquired by the European Satellite missions ERS-1/2 and the ASAR sensor onboard the ENVISAT satellite, operating both in descending orbits.

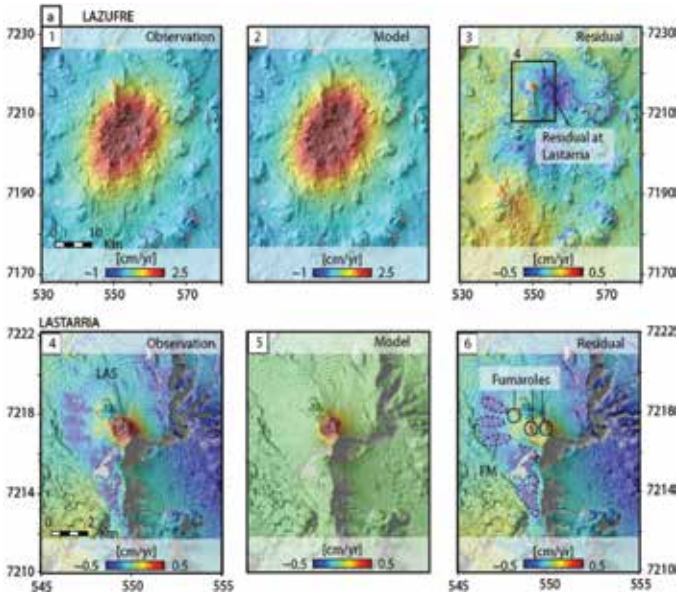

Figure 7. Inversion results of the Lazufre deformation data from 2003 to 2008: (1) observation data, (2) analytic models, and (3) residuals. Lastarria displacement result by simulating a finite spherical source showing (4) the observation data, (5) the analytic model, and (6) residuals highlighting three fumarolic areas (black circles). Dashed lines indicate flank movements (FM), on the western flank of the Lastarria volcano [70].

In order to quantify the sources that are responsible for the observed two-scale deformations [70], the considered analytical models were inverted by applying the simulated annealing method. To isolate the displacement pattern the authors followed two main steps: (1) a linear Pearson correlation coefficient [73] and a search of pixels falling within 95% of a similar trend to the maximum displacement observation point (see CEN in **Figure 6**) were applied; pixels that are not affected by the deformation were automatically excluded; (2) a subsampling of the cross-correlated dataset using a regularly spaced grid (1 km), thus reducing significantly the computational time without affecting the parameter estimation performance, was applied. Because the observed main deformation pattern is very extended in space and its source is likely laterally extended, in [70] an expanded dislocation plane acting as a sill source model [65] has been assumed, and then its parameters has been estimated. For the sake of simplicity, the models were performed in an elastic half-space medium with a Poisson's ratio $v = 0.25$ and a Young's modulus of $E = 50$ GPa. Residuals are generally less than 0.2 cm/year with the

exception of a near radial-symmetric deformation signal with uplift rates larger than 1 cm/year centered on the Lastarria volcano affecting an area of about 50 km^2 (**Figure 7**).

To further investigate this residual deformation a spherical source model approximation is applied [62]. The residuals are again generally less than 0.2 cm/year, with the exception of the area where the three main fumarolic fields are located, which still shows a discrepancy (i.e., the difference between the satellite observation and retrieved model) up to 0.5 cm/year (**Figure 7**). The best fitting model suggests a shallow spherical source located between 0.6 and 0.9 km below the Lastarria summit. The source radius is ~0.3 km (between 230 and 360 m) and subject to a volume change of ~13,000 m^3/year [70].

4.1.4. Okada fault model: the case of the Emilia (Italy) earthquake

On May 20, 2012, a local magnitude (Ml) of 5.9 earthquake occurred near the town of Finale Emilia, in the Central Po alluvial Plain, Italy. The seismic sequence evolved with some decreasing magnitude aftershock events (Ml ≤ 5.1), until May 29, when a Ml = 5.8 seismic event occurred around the Mirandola village, about 10 km SW of the May 20 main shock epicenter (**Figure 8**). The focal mechanisms for these two seismic events show both a WNW-ESE and E-W oriented nodal planes, respectively, and a ~N-S compressional kinematics [74]. The large amount of data available for the considered area, acquired through InSAR analyses, geophysical and deep borehole geological investigations, allows extensively studying the relationship

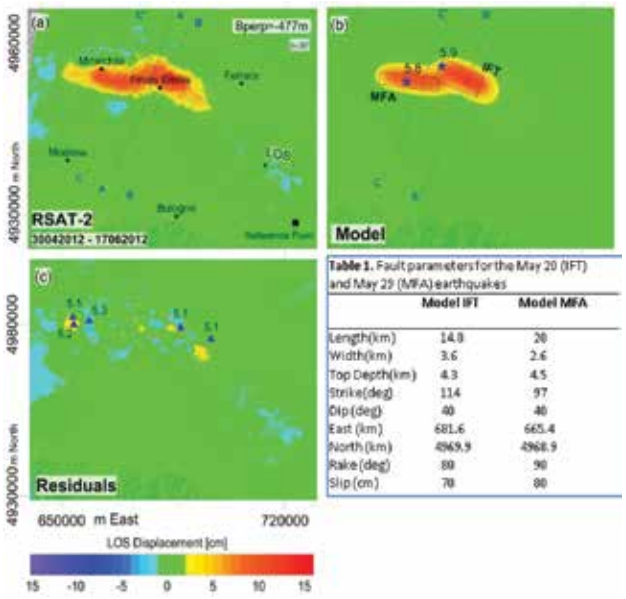

Figure 8. (a) April 30–June 17, 2012 RADARSAT-2 InSAR interferogram; $b_\perp$ =447m (perpendicular baseline), ϑ = 30° (look angle); the black square represents the InSAR reference point. Note that the red and blue colors correspond to a sensor-target range decrease and increase, respectively. (b) Analytic modeling of the RSAT-2 displacement map. The blue stars are the locations of the two main shock events and the black rectangles represent the surface projection of the best-fit Okada plane solutions. (c) Residuals map; the blue triangles indicate the locations of the Ml ≥ 5.0 aftershocks occurred after May 20. **Table 1** reports the retrieved fault parameters for IFT and MFA (modified from [74]).

between the ground deformation fields and the activated fault segments associated with the Ml 5.9 and Ml 5.8 main shocks.

To this aim, an analytic modeling was performed [74] by investigating a RADARSAT-2 (RSAT-2) interferogram (see Section 2) that, encompassing the two main earthquakes, allowed quickly identifying the upper crust regions affected by the faulting processes. In particular, in [74], the authors searched for the faults parameters, by using a nonlinear inversion based on the Levenberg-Marquardt Least-Squares approach [75]; the DInSAR data were subsampled through a QuadTree algorithm [76] over a mesh of about 4600 points. The best fit solution consists of two distinct reverse fault planes, corresponding to the south dipping Inner Ferrara Thrust (IFT) and Mirandola Ferrara Anticline (MFA) for the May 20 and the May 29 events, respectively (**Figure 8b** and **Table 1**) (more details are provided in [74]). The model shows a good fit with the measured InSAR data, as clearly highlighted by the residual map in **Figure 8c**, where values smaller than 2 cm are generally found. However, small areas with higher residuals are also noted; they appear at the locations corresponding to the few aftershocks with Ml ≥ 5.0 (not considered in the inversion procedure) occurred in the same time period covered by the RSAT-2 interferogram.

4.2. Numerical modeling: finite element method

Most of the analytical formulations are based on the assumption of a geologic source (seismic or magmatic) embedded in a homogeneous elastic half-space medium [77]. Analytical elastic models are attractive because of their straightforward formulation. However, active geological areas are usually characterized by severe heterogeneities, nonelastic rheologies and complex topography, which are responsible for significant shallow and surface effects. To meet this need, different numerical procedures can be applied in ground deformation studies to estimate how heterogeneity and topography can affect the deformation field solution.

To make numerical simulations practical, it is necessary to reduce the number of degrees of freedom of the object under study to a finite number. The reduction is called discretization. The product of the discretization process is the discrete model. The most popular numerical techniques in structural mechanics are *finite element method* and *boundary element method* (BEM). FEM is the most widely used. The basic concept in the physical FEM is the subdivision of the model into disjoint (nonoverlapping) components of simple geometry called finite elements. The response of each element is expressed in terms of a finite number of degrees of freedom characterized as the value of an unknown function, or functions, at a set of nodal points. The response of the model is then considered to be approximately that obtained by connecting or assembling the collection of all elements. A detailed discussion, which is however beyond the scope of this chapter, can be found in [78, 79].

4.2.1. Geological applications

Two examples of deformation sources in landslide (Ivanchich, Italy) and seismic (2012, Emilia earthquake, Italy) environment obtained by applying the numerical modeling are shown in the next sections.

4.2.2. A steady-state creep model: the case of the Ivancich (Italy) landslide

The Ivancich landslide is located in the southeast part of the historical town of Assisi municipality (Italy) and is affected by an active slow motion. Recurrent damages to buildings and infrastructures caused by the slow landslide evolution led local authorities to carry out geological and geotechnical investigations aimed at implementing effective remedial works and mitigation strategies. The kinematical evolution of the Ivancich unstable mass has been simulated by performing a two-dimensional time-dependent FEM of the active ground deformation [80]. We briefly report here the main results achieved in [80].

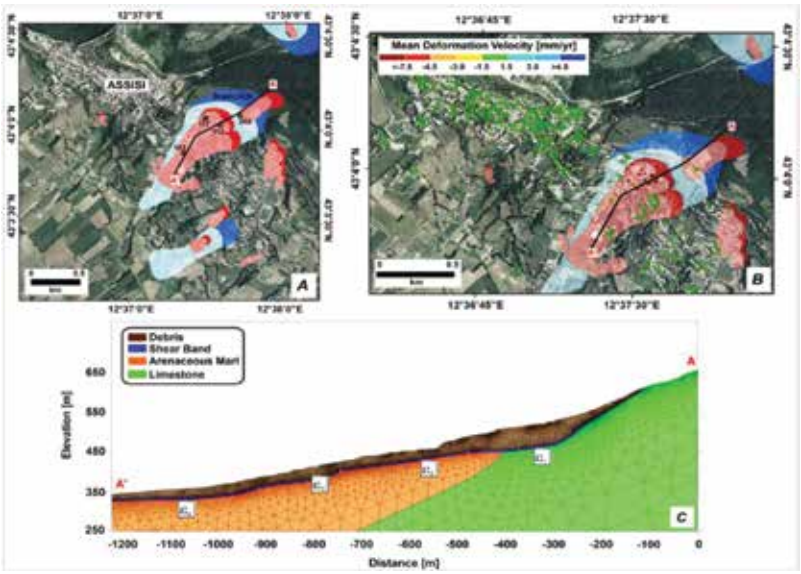

Figure 9. (A) The landslide inventory map of Assisi area; the location of four considered inclinometers is also reported. (B) ERS-ENVISAT mean deformation velocity map with location of the six considered SAR pixels. The thick black line shows the longitudinal cross section A-A' used for modeling, along which the sectors subdivision is reported. (C) A-A' 2D section reporting the model geometry of the landslide area with geological units, superimposed on the triangular FE mesh. For further details, see [80].

The longitudinal section along the A-A' line (**Figure 9**) has been reconstructed by using the available borehole information, the geomorphological evidences and the inclinometer readings.

In [80], the authors subdivided the slope modeling domain into four geomechanical units: (i) the landslide deposit (unsorted debris), (ii) the upper part of the slope is constituted by the limestone bedrock, (iii) the central part is the pelitic-sandstone bedrock, and (iv) the shear zone, with a thickness lower than 2 m, at a depth ranging between 20 and 60 m. In addition, the analysis of geomorphological evidences and InSAR displacement measurements allowed us to identify four areas showing similar kinematical behavior. InSAR data cover almost 20 years of ERS-1/2 and ENVISAT SAR images acquired between April 1992 and November 2010 and processed through the SBAS technique (see Section 3). Four different subsectors along the

http://dx.doi.org/ 10.5772/64250

landslide shear band, characterized by different creep rate parameters, have been assumed in the mesh domain. The authors chose a deviatoric creep model characterized by a creep rate, depending on the stress state deviatoric component to simulate the behavior of the soil in the shear band [81]. In particular, they proposed that the creep strain rate of the soil in the shear band is the unknown parameter, which can be obtained through an optimization procedure with field data. In **Figure 10**, a comparison between the time series of six selected SAR pixels and those calculated with the in LOS-projected model is shown. According to the authors, the modeling results highlights that a quasi-linear trend in LOS projection can reasonably describe the variation of the slope displacement over time. Higher displacement rates are calculated for the central portions of the landslide, whereas significantly lower rates are predicted in the upper and lower portions of the slope. Moreover, for the same creep model, they showed the comparison between the time series of the displacement at the top of four inclinometers located along the examined longitudinal section and the model results, and they found a good agreement between field data and model results for all considered inclinometers [80].

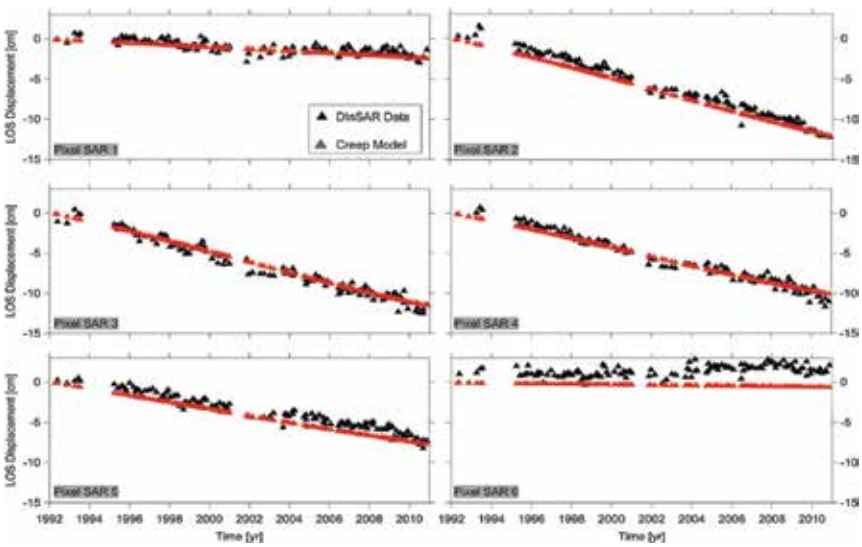

Figure 10. Comparison between the time series of six SAR pixels and the calculated secondary creep model in LOS [from 80].

4.2.3. Discretization of faults model: the case of Emilia (Italy) earthquake

A numerical modeling for the retrieved ground deformation of the two Emilia earthquakes, already described in Section 4.1.2, was performed in [74] by using FEM. This modeling approach permits us to take into account geological (rock types) and geophysical information available for the considered area. The two seismic events were analyzed in a structural mechanical context under the plane strain approximation mode, in order to solve for the retrieved displacements [82]. **Figure 11a** and **b** reports the geological and structural conditions on which the subdomain setting of the FEM model is based. In [74], a 2D structural geometric

domains of the region at depth along the AA′ line (**Figure 8a**) was derived. A 2D optimization was performed: the two BB′ and CC′ profiles, shown in **Figure 8a**, cross the areas of maximum deformation associated with the Ml 5.9 and Ml 5.8 seismic events, respectively. The model was made to evolve through two stages: during the first stage (preseismic), the model compacted under the weight of the rock successions (gravity loading) until it reached a stable equilibrium. At the second stage (coseismic), where the stresses were released through a nonuniform slip along the faults, an iterative optimization procedure based on a trial and error approach [82] was used, allowing us to follow the evolution of the faulting processes within the best fit solution retrieval. In [74], the authors applied the following boundary conditions (**Figure 11a** and **b**): the upper boundary representing the Earth's surface was not constrained; the bottom boundary was a fixed constraint; a symmetry condition was assumed for the SSW and NNE areas to make the edge effects as negligible. Moreover, they considered three different boundary settings to simulate the sedimentary and tectonic contacts between different rock

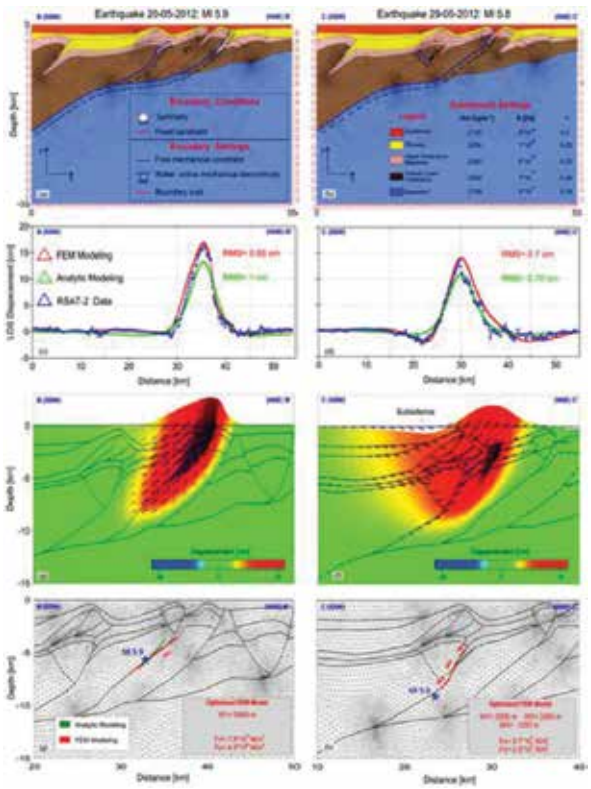

Figure 11. (a and b) 2D numerical model along the BB′ and CC′ profiles of (a) with the indication of the used boundaries and subdomain settings. The parameters rho, *E*, and *n* represent the density, Young's modulus, and Poisson's ratio, respectively (see [74] for more details). (c and d) Comparison of RSAT-2 (blue triangles), analytical model (green triangles), and FEM model (red triangles) data evaluated along the BB0 and CC0 profiles, respectively. (e and f) Sections of the displacement maps of the Ml 5.9 and Ml 5.8 seismic events, respectively. The arrows indicate the mean displacement directions. (g and h) Locations of the Okada (green lines) and FEM (red lines) fault solutions superimposed on the numerical model mesh. W1, W2, and W3 as well as Fx and Fy are the widths and active loads along the optimized faults, respectively (see [74] for more details).

http://dx.doi.org/ 10.5772/64250

successions (**Figure 11a** and **b**): (i) free mechanical constrains where the faults are kept locked; (ii) roller constraints, which allow the faults to freely slip under the applied stress field, thus the mechanical discontinuities are considered as active; (iii) boundary loads along which the forces are concentrated and transferred to the boundary subdomains. In **Figure 11c** and **d**, **a** comparison between the best fit solutions for the RSAT-2 data with the analytic and the heterogeneous FEM models along the BB′ and CC′ lines, respectively, is shown. From this analysis, a good fit between the FEM models developed along these profiles and the observed ground deformation pattern is evident, in terms of shape and amplitude of the signal, for both seismic events.

5. Conclusion

This chapter offers an updated and applications-oriented perspective on the satellite InSAR technology, with emphasis on subsequent geophysical investigations. Various phenomena occurring in hazardous geologically zones of interest (e.g., areas interested by earthquake, volcanic activity, or landslide), for which the inherent Earth's crust deformation pattern can be obtained by suitably processing data acquired by SAR sensors (e.g., ENVISAT, RADARSAT-2), have been investigated. Moreover, the adoption of appropriate geophysical models for the considered scenarios has also permitted to consistently explain the resulting deformation patterns. Finally, the obtained information can be suitably stored in geographic information system (GIS) for the geospatial data management, with important implications in terms of the assessment of geological risks (such as volcanic and seismic), damage assessment, and the proper prevention/planning of human activities.

Author details

Giuseppe Solaro*, Pasquale Imperatore and Antonio Pepe

*Address all correspondence to: solaro.g@irea.cnr.it

Institute for Electromagnetic Sensing of the Environment (IREA), National Research Council (CNR) of Italy, Napoli, Italy

References

[1] C. A. Wiley, "Synthetic aperture radars: a paradigm for technology evolution", IEEE Trans. Aerospace Electron. Syst., vol. AES-21, no. 3, pp. 440–443, May 1985.

[2] I. G. Cumming and F. H. Wong, Digital Processing of Synthetic Aperture Radar Data, Artech House, 2005.

[3] G. Franceschetti and R. Lanari, Synthetic Aperture Radar Processing. Boca Raton, FL, USA: CRC Press, 1999.

[4] R. M. Goldstein and H. A. Zebker, "Mappings mall elevation changes over large areas: differentia radar interferometry," J. Geophys. Res., vol. 94, no. B7, pp. 9183–9191, 1989.

[5] D. Massonnet and K. L. Feigl, "Radar interferometry and its application to changes in the Earth's surface," Rev. Geophys., vol. 36, pp. 441–500, 1998.

[6] Bürgmann, P. A. Rosen, and E. J. Fielding, "Synthetic aperture radar interferometry to measure Earth's surface topography and its deformation," Annu. Rev. Earth Planet. Sci., vol. 28, pp. 169–209, May 2000.

[7] P. A. Rosen, S. Hensley, I. R. Joughin, F. K. Li, S. R. Madsen, E. Rodriguez, and R. M. Goldstein, "Aperture radar interferometry," Proc. IEEE, vol. 88, no. 3, pp. 333–381, 2000.

[8] R. Bamler and P. Hartl, "Synthetic aperture radar interferometry," Inverse Problems, vol. 14, no. 4, R1, 1998.

[9] G. Fornaro and G. Franceschetti, "Image registration in interferometric SAR processing," IEE Proc.-Radar, Sonar Navig., 142, 1995.

[10] E. Sansosti, "A simple and exact solution for the interferometric and stereo SAR geolocation problem," IEEE Trans. Geosci. Rem. Sens., vol. 42, no. 8, pp. 1625–1634, August 2004.

[11] D. C. Ghiglia and M. D. Pritt, Two-Dimensional Phase Unwrapping: Theory, Algorithms and Software, New York: John Wiley, 1998.

[12] R. K. Ahuja, T. J. Magnanti, and J. B. Orlin, Network Flows: Theory, Algorithms, and Applications, New Jersey: Prentice Hall, 1993.

[13] P. Imperatore, A. Pepe, and R. Lanari, "Multichannel phase unwrapping: problem topology and dual-level parallel computational model," IEEE Trans. Geosci. Rem. Sens., vol. 53, no. 10, pp. 5774–5793, October 2015.

[14] H. A. Zebker and J. Villasenor, "Decorrelation in interferometric radar echoes," IEEE Trans. Geosci. Rem. Sens., vol. 30, pp. 950–959, September 1992.

[15] P. Lundgren, F. Casu, M. Manzo, A. Pepe, P. Berardino, E. Sansosti, and R. Lanari, "Gravity and magma induced spreading of Mount Etna volcano revealed by satellite radar interferometry," Geophys. Res. Lett., vol. 31, p. L04602, 2004.

[16] M. Manzo, G. P. Ricciardi, F. Casu, G. Ventura, G. Zeni, S. Borgstrom, P. Berardino, C. Del Gaudio, and R. Lanari, "Surface deformation analysis in the Ischia Island (Italy) based on spaceborne radar interferometry," J. Volcanol. Geotherm. Res. vol. 151, pp. 399–416, 2006.

[17] A. Ferretti, C. Prati, and F. Rocca, "Permanent scatterers in SAR interferometry," IEEE Trans. Geosci. Rem. Sens., vol. 39, no. 1, pp. 8–20, January 2001.

[18] B. M. Kampes, Radar Interferometry: Persistent Scatterer Technique, Springer, 2006.

[19] A. Hooper, H. Zebker, P. Segall, and B. M. Kampes, "A new method for measuring deformation on volcanoes and other natural terrains using InSAR persistent scatterers," Geophys. Res. Lett., vol. 31, no. 23, p. L23 611, December 2004, DOI: 10.1029/2004GL021737.

[20] P. Berardino, G. Fornaro, R. Lanari, and E. Sansosti, "A new algorithm for surface deformation monitoring based on small baseline differential SAR interferograms," IEEE Trans. Geosci. Remote Sens., vol. 40, no. 11, pp. 2375–2383, November 2002.

[21] M. Crosetto, B. Crippa, and E. Biescas, "Early detection and in-depth analysis of deformation phenomena by radar interferometry," Eng. Geol., vol. 79, no. 1/2, pp. 81–91, June 2005.

[22] O. Mora, J. J. Mallorquí, and A. Broquetas, "Linear and nonlinear terrain deformation maps from a reduced set of interferometric SAR images," IEEE Trans. Geosci. Remote Sens., vol. 41, no. 10, pp. 2243–2253, October 2003.

[23] S. Usai, "A least squares database approach for SAR interferometric data," IEEE Trans. Geosci. Rem. Sens., vol. 41, no 4, pp. 753–760, April 2003.

[24] M. P. Doin, S. Guillaso, R. Jolivet, C. Lasserre, F. Lodge, G. Ducret, et al., Presentation of the small baseline NSBAS processing chain on a case example: the Etna deformation monitoring from 2003 to 2010 using Envisat data, ESA FRINGE 2011 conference Frascati, Italy, 2011.

[25] E. A. Hetland, P. Muse, M. Simons, Y. N. Lin, P. S. Agram, and C. J. DiCaprio, "Multi-scale InSAR Time Series (MInTS) analysis of surface deformation," J. Geophys. Res.-Solid Earth, vol. 117, 2012.

[26] F. Casu, S. Elefante, P. Imperatore, I. Zinno, M. Manunta, C. De Luca, and R. Lanari, "SBAS-DInSAR parallel processing for deformation time series computation," IEEE J. Select. Top. Appl. Earth Observ. Rem. Sens., vol. 7, no. 8, pp. 3285–3296, August 2014.

[27] F. Bovenga, R. Nutricato, A. Refice, and J. Wasowski, "Application of multi-temporal differential interferometry to slope instability detection inurban/peri-urban areas," Eng. Geol., vol. 88, no. 3–4, pp. 218–239, December 15, 2006.

[28] L. Cascini, S. Ferlisi, G. Fornaro, R. Lanari, D. Peduto, and G. Zeni, "Subsidence monitoring in Sarno urban area via multi-temporal DInSAR technique," Int. J. Rem. Sens., vol. 27, no. 8, pp. 1709–1716, 2006.

[29] S. Stramondo et al., "Advanced DInSAR analysis on mining areas: La Union case study (Murcia, SE Spain)," Eng. Geol., vol. 90, no. 3–4, pp. 148–159, March 27, 2007.

[30] G. Peltzer and P. A. Rosen, "Surface displacement of the 17 May 1993 Eureka Valley earthquake observed by SAR interferometry," Science, vol. 268, no. 5215, pp. 1333–1336, June 1995.

[31] R. Lanari et al., "An overview of the small BAseline subset algorithm: a DInSAR technique for surface deformation analysis," Pure Appl. Geophys., vol. 164, no. 4, pp. 637–661, January 2007.

[32] P. Tizzani, M. Battaglia, G. Zeni, S. Atzori, P. Berardino, and R. Lanari, "Uplift and magma intrusion at Long Valley Caldera from InSAR and gravity measurements," Geology, vol. 37, no. 1, pp. 63–66, January 2009.

[33] M. Manzo, Y. Fialko, F. Casu, A. Pepe, and R. Lanari, "A quantitative assessment of DInSAR measurements of interseismic deformation: the Southern San Andreas fault case study," Pure Appl. Geophys., vol. 169, no. 8, pp. 1463–1482, August 2012.

[34] E. Trasatti et al., "The 2004–2006 uplift episode at Campi Flegrei caldera (Italy): constraints from SBAS-DInSAR ENVISAT data and Bayesian source inference," Geophys. Res. Lett., vol. 35, no. 7, p. L07308, April 2008.

[35] R. Lanari et al., "Surface displacements associated with the L'Aquila 2009 Mw 6.3 earthquake (Central Italy): new evidence from SBASDInSAR time series analysis," Geophys. Res. Lett., vol. 37, p. L20309, October 2010.

[36] M. Bonano, M. Manunta, A. Pepe, L. Paglia, and R. Lanari, "From previous C-band to new X-band SAR systems: assessment of the DInSAR mapping improvement for deformation time-series retrieval in urban areas," IEEE Trans. Geosci. Rem. Sens., vol. 51, no. 4, pp. 1973–1984, April 2013.

[37] E. Sansosti et al., "How second generation SAR systems are impacting the analysis of ground deformation," Int. J. Appl. Earth Observ., vol. 28, no. 1, pp. 1–11, 2014.

[38] A. Pepe, P. Berardino, M. Bonano, L. D. Euillades, R. Lanari, and E. Sansosti: " SBAS-based satellite orbit correction for the generation of DInSAR time-series: application to RADARSAT-1 data", IEEE Trans. Geosci. Rem. Sens., vol. 49, pp. 5150–5165, December 2011.

[39] M. Manzo, Y. Fialko, F. Casu, A. Pepe, and R. Lanari, "A quantitative assessment of DInSAR measurements of interseismic deformation: the Southern San Andreas Fault case study," Pure Appl. Geophys., vol. 169, no. 8, pp. 1463–1482, 2012.

[40] A. Ferretti, A. Fumagalli, F. Novali, C. Prati, F. Rocca, and A. Rucci, "A new algorithm for processing interferometric data-stacks: SqueeSAR," IEEE Trans. Geosci. Rem. Sens., vol. 49, pp. 3460–3470, September 2011.

[41] A. Parizzi and R. Brcic, "Adaptive InSAR stack multi-looking exploiting amplitude statistics: a comparison between different techniques and practical results," IEEE Geosci. Rem. Sens. Lett., vol. 8, no. 3, pp. 441–445, May 2011.

[42] B. Pinel-Puyssegur, R. Michel, and J. P. Avouac, "Multi-link InSAR time series: enhancement of a wrapped interferometric database," Sel. Top. Appl. Earth Observ. Rem. Sens., vol. 5, no. 3, pp. 784–794, June 2012.

[43] A. Pepe, Y. Yang, M. Manzo, R. Lanari, "Improved EMCF-SBAS processing chain based on advanced techniques for the noise-filtering and selection of small baseline multi-look DInSAR interferograms," IEEE Trans. Geosci. Rem. Sens., vol. 53, no. 8, pp. 4394–4417, August 2015.

[44] R. M. Goldstein and C. L. Werner, "Radar interferogram filtering for geophysical applications," Geophys. Res. Lett., vol. 25, no. 21, pp. 4035–4038, Nov. 1998.

[45] P. Imperatore and A. Pepe, "Topological characterization and advanced noise-filtering techniques for phase unwrapping of interferometric data stacks" in *Environmental Applications of Remote Sensing* (Ed. by M. Marghany), INTECH Publisher, 2016, ISBN 978-953-51-4628-5.

[46] M. Costantini and P. A. Rosen, "A generalized phase unwrapping approach for sparse data," Proc. IGARSS99, pp. 267–269, Hamburg (Germany), 1999.

[47] T. Flynn, "Two-dimensional phase unwrapping with minimum weighted discontinuity," J. Opt. Soc. Am. A, vol. 14, no. 10, pp. 2692–2701, 1997.

[48] M. D. Pritt and J. S. Shipman, "Least-squares two-dimensional phase unwrapping using FFTs," IEEE Trans. Geosci. Rem. Sens., vol. 32, no. 3, pp. 706–708, May 1994.

[49] A. Hooper and H. Zebker, "Phase unwrapping in three dimensions with applications to InSAR time series," J. Opt. Soc. Am. A, vol. 24, no. 9, pp. 2737–3747, August 2007.

[50] M. Costantini, S. Falco, F. Malvarosa, F. Minati, F. Trillo, and F. Vecchioli, "A general formulation for robust integration of finite differences and phase unwrapping on sparse multidimensional domains," in Proc. Fringe, Frascati, Italy, December 2009.

[51] A. P. Shanker and H. Zebker, "Edgelist phase unwrapping algorithm for time series InSAR analysis," J. Opt. Soc. Am. A, Opt. Image Sci. Vis., vol. 27, no. 3, pp. 605–612, March 2010.

[52] A. Pepe and R. Lanari, "On the extension of the minimum cost flow algorithm for phase unwrapping of multitemporal differential SAR interferograms," IEEE Trans. Geosci. Rem. Sens., vol. 44, no. 9, pp. 2374–2383, September 2006.

[53] T. Karo, G. S. El-Fiky, E. N. Oware, and S. Miyazaki, "Crustal strains in the Japanese Islans as deduced from dense GPS array", Geophys. Res. Lett., vol. 25, pp. 3445–3448, 1998.

[54] P. Cervelli, M. H. Murray, P. Segall, Y. Aoki, and T. Kato, "Estimating source parameters from deformation data, with an application to the March 1997 earthquake swarm off the Izu Peninsula, Japan," J. Geophys. Res., vol. 106, doi: 10.1029/2000JB900399, 2001.

[55] Y. Okada, and E. Yamamoto, "A model for the 1989 seismo-volcanic activity off Ito, Central Japan, derived from crustal movement data," J. Phys. Earth, vol. 39, pp. 177–195, 1991.

[56] G. A. Marshall, R. S. Stein, and W. Thatcher, "Faulting geometry and slip from co-seismic elevation changes: the 18 October 1989, Loma Prieta, California, Earthquake," Bull. Seismol. Soc. Am., vol. 81, no. 5, pp. 1660–1693, 1991.

[57] Y. Wang, Q. Zhang, C. Zhao, Z. Lu, and X. Ding, "Monitoring and inversion on land subsidence over mining area with InSAR technique," International Symposium on Lidar and Radar Mapping 2011 Technologies and Applications, 2011.

[58] M. Lisowski, "Analytical volcano deformation source models". In: Dzurisin (Ed.), Volcano Deformation, Springer, Berlin, Heidelberg, pp. 279–304, 2006.

[59] S. Atzori and S. Salvi "SAR data analysis in solid earth geophysics: from science to risk management, land applications of radar remote sensing," Dr. Damien Closson (Ed.), InTech, DOI: 10.5772/57479, 2014.

[60] Y. Okada, "Internal deformation due to shear and tensile faults in a half-space," Bull. Seismol. Soc. Am., vol. 82, pp. 1018–1040, 1992.

[61] K. Mogi, "Relations between the eruptions of various volcanoes and the deformations of the ground surface around them", Bull. Earth. Res. Inst., University of Tokyo, vol. 36, pp. 99–134, 1958.

[62] D. F. McTigue, "Elastic stress and deformation near a finite spherical magma body: resolution of the point source paradox", J. Geophys. Res., vol. 92, no. B12, pp. 12931–12940, doi:10.1029/JB092iB12p12931, 1987.

[63] G. Ranalli, Rheology of the Earth, London, Glasgow, Weinheim, New York, Tokyo, Melbourne, Madras: Chapman & Hall, 413 pp., 1995.

[64] A. Bonaccorso and P. M. Davis, "Models of ground deformation from vertical volcanic conduits with application to eruptions of Mount St. Helens and Mount Etna," J. Geophys. Res., vol. 104, pp. 10531–10542. 1999.

[65] T. T. Yu and J. B. Rundle, "Inverting for fault zone geometry using genetic algorithms (abstract), in: International Union of Geodesy and Geophysics XX I General Assembly, Week B 56, 1995.

[66] B. Berg, "Locating global minima in optimization problems by a random-cost approach", Nature, vol. 361, pp. 708–710, 1993.

[67] N. A. Metropolis, A. Rosenbluth, M. Rosenbluth, A. Teller, and E. Teller, "Equation of state calculations by fast computing machines," J. Chem. Phys., vol. 21, pp. 1087–1092, 1953.

[68] M. Cruetz, "Monte-Carlo study of quantized SU(2) gauge theory," Phys. Rev. D, vol. 21, pp. 2308–2315, 1984.

[69] D. H. Rothmann, "Nonlinear inversion, statistical mechanics, and residual statics estimation," Geophysics, vol. 5, no. 0, pp. 2784-2796, 1985.

[70] J. Ruch, A. Manconi, G. Zeni, G. Solaro, A. Pepe, M. Shirzaei, T. R. Walter, and R. Lanari, "Stress transfer in the Lazufre volcanic area, central Andes," Geophys. Res. Lett., vol. 36, p. L22303, doi:10.1029/2009GL041276, 2009.

[71] O. Oncken, D. Hindle, J. Kley, K. Elger, P. Victor, and K. Schemmann, "Deformation of the central Andean upper plate system—facts, fiction, and constraints for plateau models," in: O. Oncken et al. (Eds.), The Andes. Active Subduction Orogeny, Frontiers Earth Sci., vol. 1, pp. 3–27, Springer, Berlin, 2006.

[72] S. De Silva and P. W. Francis, Volcanoes of the Central Andes, 216 pp., Springer, Berlin, 1991.

[73] J. M. Stanton, "Galton, Pearson and the Peas: a brief history of linear regression for statistic instructors," J. Stat. Educ., vol. 9, no. 3, p. 1, 2001.

[74] P. Tizzani, R. Castaldo, G. Solaro, S. Pepe, M. Bonano, F. Casu, M. Manunta, M. Manzo, A. Pepe, S. Samsonov, R. Lanari, and E. Sansosti, "New insights into the 2012 Emilia (Italy) seismic sequence through advanced numerical modeling of ground deformation InSAR measurements," Geophys. Res. Lett., vol. 40, pp. 1971–1977, doi:10.1002/grl.50290, 2013.

[75] D. Marquardt, "An algorithm for least-squares estimation of nonlinear parameters," SIAM J. Appl. Math., vol. 11, pp. 431–441, doi:10.1137/0111030, 1963.

[76] S. Jonsson, H. Zebker, P. Segall, et al., "Fault slip distribution of the 1999 Mw7.1 Hector Mine, California, earthquake, estimated from satellite radar and GPS measurements," B. Seismol. Soc. Am., vol. 92, no. 4, pp. 1377–1389, 2002.

[77] Y. Sasai, "Tectonomagnetic modeling on the basic of the linear piezomagnetic effect," Bull. Earthq. Res. Inst., Univ. Tokyo, vol. 66, pp. 585-722, 1991.

[78] M. J. Fagan, Finite Elements Analysis: Theory and Practice, pp. 1–311, London, Prentice Hall, 1992.

[79] O. C. Zienkiewicz, R. L. Taylor, and J. Z. Zhu, The Finite Element Method: Its Basis And Fundamentals, 6th edition, Butterworth-Heinemann, Amsterdam, London: Elsevier, 2005.

[80] R. Castaldo, P. Tizzani, P. Lollino, F. Calò, F. Ardizzone, M. Manunta, F. Guzzetti, and R. Lanari, "The Ivancich active landslide process (Assisi, Central Italy) analysed via numerical modeling jointly optimized by DInSAR and inclinometric data," in G. Lollino et al. (Eds.), Engineering Geology for Society and Territory – Vol. 2, DOI: 10.1007/978-3-319-09057-3_268, Switzerland: Springer International Publishing, 2015.

[81] J. Betten, Creep Mechanics, Berlin: Springer, 2002.

[82] A. Tarantola, Inverse Problem Theory and Methods for Model Parameter Estimation, pp. 1–343, Philadelphia: SIAM Society for Industrial and Applied Mathematics, ISBN 0-89871-572-5, 2005.

Chapter 8

Collaborative Uses of Geospatial Technology to Support Climate Change Adaptation in Indigenous Communities of the Circumpolar North

Megan Sheremata, Leonard J.S. Tsuji and
William A. Gough

Additional information is available at the end of the chapter

http://dx.doi.org/10.5772/64214

Abstract

A literature review is conducted of geospatial technologies in community-based research on ice and mobility among Indigenous people of the circumpolar north. Numerous studies explore the use of traditional knowledge in the Arctic on sea ice, but limited evidence of community-based research in sub-Arctic communities and in freshwater ice systems is found. Geographical Information Systems (GIS) and remote sensing tools have been applied in a variety of ways in support of community adaptations. These include the production of living memory maps, ice classification systems, and geodatabases that reflect the relationship-building nature of collaborations between Indigenous traditional knowledge holders and scientists. Satellite imagery—particularly synthetic aperture radar (SAR)—is widely used to characterize traditional understandings of ice to help tailor geospatial tools, climate research, and early warning systems, so that they may be used more effectively to address community interests and needs. As numerous mapping platforms have been developed in the circumpolar north, there are important considerations with respect to data management, Indigenous rights, and data sharing. We see opportunities for further research in lake and river ice, and in further developing early warning systems to address the growing problem of unpredictable ice regimes in Arctic and sub-Arctic regions.

Keywords: circumpolar north, climate change, ice, traditional knowledge, geospatial technologies

1. Introduction

The climate system of the circumpolar north is undergoing transformative change. Average annual Arctic air temperatures have increased by 2.9°C since the start of the twentieth century [1]. As a result, significant sea ice declines through most of the Arctic have occurred over the past 30 years [2], while inland, freshwater ice systems have experienced shorter seasons of ice cover due to a significantly later freeze-up and earlier breakup [3]. The decline in sea ice leads to greater absorption of solar radiation in the Arctic Ocean in early autumn, which intensifies vertical fluxes of heat and moisture into the atmosphere, amplifying the effects of climate change in poles to approximately twice the global average [4].

Such changes have affected the mobility of Indigenous people of the north, who rely on the frozen landscape to move freely during winter months [5, 6]. Sea ice, frozen lakes, and rivers act as virtual highways in the north, while seasonal winter ice roads are constructed to provide access to the north for various industries, and are crucial for bringing year-round essentials, such as food, fuel, construction, and household items into remote communities [7, 8]. In recent years, travel to hunting grounds is less predictable, and ice persists for shorter periods of time, posing hazards to hunters [7]. Beyond direct impacts to traditional land use, these changes impact the northern community's well-being in terms of food security, health, culture, and spiritual life [9].

Regional characterizations of Arctic ice systems, which bring together information from satellite imagery, in situ observations, and climate models, are being used to help better simulate global climate projections [10–12], to forecast seasonal sea ice extent [13], to map potential new Arctic shipping routes [14], and to explore opportunities for natural resources development [15]. However, at the local level, a variety of geospatial tools have emerged in polar research to support Indigenous communities adapting to climate change. This chapter looks at what geospatial technologies have been used in Arctic and sub-Arctic regions to support adaptations to changing ice regimes. We will explore what outputs have emerged from geospatial research collaborations, and what lessons have been learned. We will then look at more recent concerns of data management, and how this has led to the establishment of numerous networks and mapping platforms in the circumpolar north (see Section 2 for the criteria used to delimit the region).

Community-based cartography in the Arctic is not new. Early Inuit maps were made with ephemeral pieces of the landscape, as charts were drawn into snow and sand, and detailed coastal relief maps were carved or assembled from sticks and stones [16–18]. It is said that maps of winter trails are etched in the minds of those who make and use them [5]. The communication of this collective traditional knowledge (traditional knowledge) is an oral tradition. Traditional knowledge has been defined in numerous ways across the literature, but is generally understood as accumulated bodies of knowledge rooted in the spiritual health, culture, and experiences of Indigenous peoples in the occupancy and use of a land base [19–22]. Traditional knowledge represents a cumulative, multigenerational knowledge of local and regional physiography, natural features, climate, wildlife, and an intimate understanding of the relationships between all aspects of the environment, including people [20]. Efforts to map

http://dx.doi.org/10.5772/64214

traditional knowledge among Indigenous peoples have been widespread since the 1970s in response to concerns about the erosion of traditional culture, the need to improve participatory natural resources management practices, and an interest in asserting legal claims of tenure over traditional lands and natural resources [23–27].

A specific interest in traditional ice use in the circumpolar north emerged in the 2000s, a period during which geospatial technologies experienced radical changes and greatly enabled mapping in the far north [28]. In 2000, the U.S. government began to allow the public to receive a nondegraded GPS signal globally, which facilitated its use in remote regions. The same year, ESRI released Arc IMS 3.0, a web-based Geographical Information Systems (GIS) platform that initiated a wave of innovation in online mapping. Moreover, space agencies and commercial companies began to make increasingly more available high-resolution satellite imagery every year [29].

At the same time, scientists have become interested in using Indigenous traditional knowledge in their research over the past few decades. This is particularly true in the circumpolar north, where the impacts of climate change on the cryosphere have created a sense of urgency to understanding the impacts of global warming to the region. Historical scientific climatological data in the circumpolar north are lacking, except for proxy measures (e.g., sediment cores), but over millennia Indigenous peoples have maintained traditional land-use practices and a detailed knowledge of natural processes. Thus, traditional knowledge can be used to fill key knowledge gaps at local scales [30, 31]. Indeed, many scientists work with traditional knowledge holders due to the paucity of weather- and ice-monitoring data in high-latitude regions of the world, and to increase their understanding of the impacts of climate change in a region. However, traditional knowledge plays a more foundational role than simply patching gaps in data records. It helps scientists to better frame their research in ways that can ultimately produce more usable knowledge to northern communities [32].

Northern Indigenous peoples have also been interested in collaborating with scientists, in the interest of documenting traditional knowledge for cultural preservation and to assert land-use claims over their traditional lands [26, 27, 33], and because rates of environmental change have surpassed anything experienced previously [34]. Indigenous peoples of the north are adaptive by nature [8, 35]; however, climate change has prompted communities to inquire how science and technology can be used alongside traditional knowledge of the land to support their efforts in adapting to climate change.

As a growing body of research has suggested, collaborative research with traditional knowledge holders is successful when it allows the time for a meaningful, co-productive process to develop [36, 37]. The tools and outputs of co-productive geospatial projects may act as boundary objects—collaborative tools or concepts that possess shared meaning within the collaboration—but whose significance differs markedly when collaborating individuals return to their own institutions or community contexts [38, 39]. In other words, traditional knowledge maps and databases can have very different roles in communities than they do in research. Thus, researchers, spatial analysts, and others involved in these collaborations who take the time to consider how the outputs of their research will be used by their collaborators tend to be more effective at creating viable tools that will be used by communities [36, 37].

2. Methodology

This review involved a search of peer-reviewed literature in Google, Scopus, and Web of Science databases in January, 2016. A search string was developed to identify articles that could help identify geospatial tools being used to support adaptations among Indigenous peoples to climate changes in the circumpolar north. Of specific interest were those adaptations pertaining to changes in the cryosphere and to impacts on mobility in the Arctic and sub-Arctic. Our demarcation of the circumpolar north follows that of Ford et al. [7] whose definition of the Arctic includes Alaska, Canada North of 60°N, together with northern Quebec and Labrador, all of Greenland, the Faroe Islands, Iceland, the northernmost regions of Norway, Sweden and Finland, and Russia—including the Murmansk Oblast, the Nenets, Yamalo-Nenets, Taimyr, and Chukotka autonomus okrugs, Vorkuta in the Komi Republic, Norilsk and Igsrka in Krasnoyarsky Kray, and those parts of the Sakha Republic whose boundaries lie closest to the Arctic Circle. However, we also include the Hudson Bay Lowlands (including James Bay) in Canada due to its physical geography and its sub-Arctic climatology. The resulting area has a population of approximately 4 million people, of whom approximately 400,000 and 1.3 million are Indigenous persons [7, 40, 41]. We wanted to know how geospatial technologies are being used in community-based, collaborative research with Indigenous communities. Thus, research that sought to integrate or use as complementary knowledge constructs—traditional knowledge and the natural sciences in geospatial contexts—with a focus on work that prioritizes community-based research and Indigenous ways of characterizing ice systems was the primary object of this literature review. The resultant search queries employed the following terms: "*climate change*," "*adaptation*"; "*Arctic*" or "*sub-arctic*"; "indigenous" or "Aboriginal"; "*GIS*" or "*Geospatial*" or "*remote sensing*" or "*mapping*"; "*ice*" or "*ice monitoring*"; and "community" or "*community-based*."

A limited review of the gray literature was conducted to evaluate and interpret trends in the literature, which included reviews of websites and correspondence with some Arctic scholars. Forward and reverse citations were conducted and produced the included publications on the theme of data management.

We limited our search to publication dates between January 2005 and January 2016 to exclude research using outdated technologies, and to focus on the period during which adaptation research in the circumpolar north has been concentrated (Ford et al. [7]). Excluded were those studies that did not emphasize the use of geospatial technologies, community-based collaboration, and the complementary use of traditional knowledge with the natural sciences, even where such studies may have applications in community-based research. We also excluded studies that focus exclusively on in situ monitoring and make no explicit mention of geospatial tools. We sought publications on sea, lake and river-ice systems, and on ice roads, as these all act as substrates for movement for the Indigenous peoples of the north. However, we expanded our criteria to include a study of icing of pastures, because we felt this work has some bearing on the other studies we looked at. Research that emphasizes bulk transportation through the Arctic was excluded, as were numerous papers in ecology and northern ecosystems. Also excluded were studies of permafrost and glacier systems.

http://dx.doi.org/10.5772/64214

The original search produced 470 peer-previewed articles. These were exported to Endnote for evaluation. Duplicates were removed, and a reading of the abstracts was conducted. After applying the exclusion criteria discussed above, we reviewed 30 articles. Qualitative analysis of the literature involved manual coding of emergent themes rather than coding according to theoretical constructs or previous empirical results [42]. Our reading included some interest in chronology to identify themes relevant to the present research context.

3. Results and discussion

The resulting community-based ice studies in our search are almost entirely centered in coastal Arctic Canada and Alaska, although not exclusively. All but one study focus on sea ice. The three primary themes that emerged were as follows: (1) the documentation of traditional knowledge in community-based research; (2) the complementary uses of traditional knowledge and science to understand local and regional contexts; and (3) the resulting need to manage geographical data appropriately and effectively (see **Table 1**). Here, we discuss these themes and their subthemes that emerged from our examination of the literature. First, we discuss how traditional knowledge documentation produces *living memory maps* that are of considerable value to both researchers and communities, and that act as discursive objects of ongoing research that have implications for how we design geodatabases. These maps are the basis of *ice classification systems*, and some studies further incorporate *remote sensing* with traditional knowledge for local ice monitoring to facilitate safe winter travel. A number of studies use these tools collectively with the aim of developing integrated *early warning systems (EWS).* In this light, the emergence of numerous collaborative geomatics platforms has led to numerous concerns regarding data management in recent years.

3.1. Production of living memory maps

The value of documenting collective memory is discussed throughout the literature as a discursive process. Aporta [5] and Gearheard et al. [43] collaborated with Inuit hunters to map winter trails and document traditional knowledge of wildlife and other features. The resulting maps, developed in consultation with elders and present-day hunters, are described as "living memory maps" [5, 43]. Along with Freeman's work of the 1970s [23–25], these collaborative maps have been among the first documents to show how extensive traditional land use of the circumpolar north is, reflecting a tenure of land that Aporta contrasts with the widely misplaced notion of an unused and largely barren Arctic landscape [5]. Winter trails across the ice, rather, provide important conduits that span the circumpolar north. They are reconstructed each year and are based on knowledge that has been shared orally over many generations. This knowledge includes detailed understandings of ice processes and travel safety, and represents the cumulative knowledge of present-day hunters and of the detailed, intergenerational knowledge held by the elders of a community [5, 44–47]. See **Figure 1** for examples of the kinds of knowledge that are used to create these maps.

Primary research themes	Geospatial application themes	Applications	Publication
Documenting traditional knowledge (TK)	Living memory maps of winter trails and ice use based on participatory TK research	Document of traditional land use and tenure systems	Aporta (2009), Fidel et al. (2014)
		Participatory mapping process enables researchers to actively engage with communities	Aporta (2009), Eisner et al. (2013), Eisner et al. (2009) Gearheard et al. (2010), Herrmann et al. (2012), Laidler et al. (2010)
		Maps of collective memory in a community can be used to facilitate the intergenerational transfer of TK from elders to youth	Isogai et al. (2013), Laidler et al. (2011)
Complementary uses of TK and science to understand local context	Ice classification systems	Classification and mapping of ice types	Druckenmiller et al. (2010), Laidler et al. (2010), Tremblay et al. (2006)
		Used to identify of climate change indicators	Laidler et al. (2010), Tremblay et al. (2006)
	Using TK with remote sensing	Used to identify vulnerabilities and adaptive capacities of communities to climate change	Druckenmiller et al. (2009), Ford et al. (2009), Laidler et al. (2009)
		Using TK validate remote sensing observations	Bell (2012), Gauthier et al. (2010), Kapsh et al. (2010), Laidler et al. (2011)
	Development of geospatially-based early warning systems	Establishment of networks of community-based monitoring teams that integrate TK using geospatial tools	Gauthier et al. (2010), Mahoney et al. (2009), Johnson et al. (2013)
		Integration of community-based ice observation networks, remote sensing tools, seasonal forecasts and decision-making to warn of unsafe conditions for hunting and/or travel	Bell et al. (2014), Druckenmiller et al. (2009) Mahoney et al. (201)
Data management	Development of Geomatics platforms	Designed primarily for engagement with community	Harrmann et al. (2012)

http://dx.doi.org/10.5772/64214

Primary research themes	Geospatial application themes	Applications	Publication
		Intended for ease of uptake and customization	Gardner-Youden (2012), Isogai et al. (2013), McCarthy et al. (2012)
		Employs complex relational databases for integrating multiple data types and sources for enrichment of TK	Eicken et al. (2014), Pulsifer et al. (2011)
		Highly interactive platform to facilitate education and public awareness of community-driven research while protecting intellectual property rights	HBC (2015)
		Large platform designed to enable information sharing and to establish early warning systems	Eicken (2014)
	Respecting indigenous rights	Designing accessible research to enable shared authorship with communities	Johnson et al. (2015), Pulsifer et al. (2015)

Table 1. Themes found in the use of geospatial technologies in community-based research in Arctic and sub-Arctic regions.

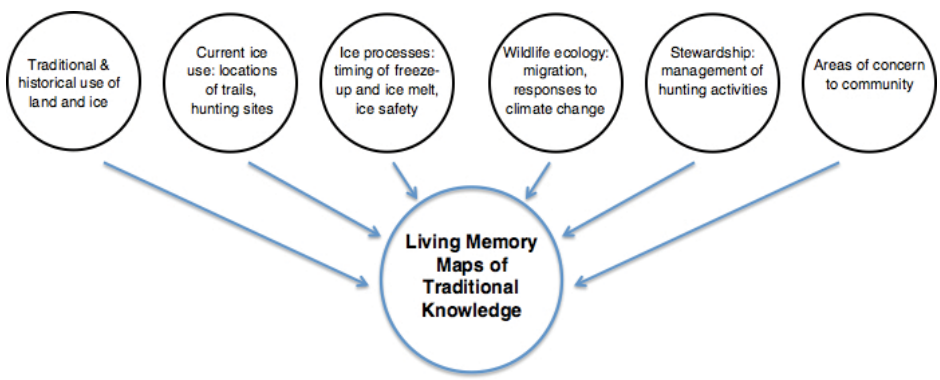

Figure 1. Examples of traditional knowledge used to create living memory maps.

These maps are of significant use to both researchers and community members, but often for different purposes, as illustrated in **Figure 2**. Scientists base much of their work on the details they provide of local ice processes and the potential they offer in helping to build meaningful relationships with communities [44, 45, 48]. On the other hand, communities have been interested in their potential to support local interests in land management, land-use claims,

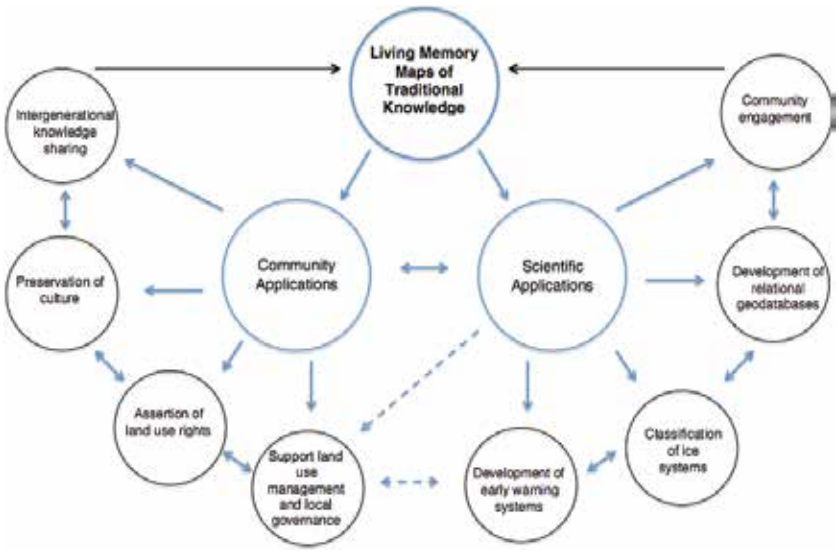

Figure 2. Examples of applications of living memory maps by communities and in research.

cultural preservation, and the sharing of traditional knowledge with younger generations [26, 27, 49]. In some instances, the value of these maps may be the reason why communities collaborate in the first place; so, care in their production and maintenance to reflect this value is important [32]. However, as has been observed elsewhere [50], their value to local governance and natural resources management is not adequately discussed in the literature (expressed by the dashed lines in **Figure 2**). This gap may have implications in terms of how useful the research ultimately is to communities.

In their study of Inuit sea ice use, Laidler et al. [47] use topographic maps in interviews with elder sea ice experts to document and map traditional knowledge of local sea ice. They cite the conversational value of large paper maps to dialog with sea ice experts, employing mylar overlays for documenting spatial information provided by elders, which are later digitized. The ability to converse respectfully and effectively with elders is an important aspect of the mapping process. However, accuracy is lost with digitization at rates inversely proportional to scale. Thus, this approach warrants consideration of the potential benefits of mapping directly into a GIS platform.

This view of traditional knowledge documentation as an ongoing dialog with community participants is a notable theme in community-based traditional knowledge mapping. For instance, there are practical challenges to mapping traditional knowledge due to the fact that traditional knowledge is usually intertwined with stories, place names, euphemisms, and other aspects of a community's culture that can render it incomplete in its documented form [51]. This has underscored the need for relational geodatabases (a topic we will address later in this chapter) to facilitate ongoing inputs of data as they are collected, so that waypoints associated with traditional knowledge documented in interviewed form may be enriched by stories, photography, and other data formats [32, 38]. To this end, one study employs participatory

http://dx.doi.org/10.5772/64214

photomapping as a method for documenting, contextualizing, and sharing Indigenous observations of environmental conditions [52].

Methods of traditional knowledge mapping require archival research as a precursor to any new traditional knowledge mapping studies. Of the many traditional knowledge mapping projects that have been already conducted to date, a significant number exist only in paper form, lie on old hard drives, or are essentially lost, having been inappropriately cataloged. Thus, methods for archiving any recovered work from previous traditional knowledge studies are essential [53].

3.2. Ice classification maps

A number of studies have created atlases of ice types based on characteristics drawn from traditional knowledge [6, 48, 54–57]. As Tremblay et al. [48] discuss, this allows a researcher to understand how ice dynamics are perceived from a community perspective, and to conduct ice research using scientific methods based on traditional knowledge of ice and ice safety. Often, based on living memory maps, these studies can include extensive interviews and field surveys with elders and local hunters to photograph and geolocate different kinds of ice, and describe how these ice types are used. Interviews and surveys may document names of ice types in the local language, identify features. and/or processes deemed important to hunters and fishers, and locate important fishing and/or hunting sites where different types of ice may be found. The maps that result establish classification systems of ice as baselines on which the impacts of environmental change and industrial development on ice systems can be evaluated [6, 54–56].

Some studies have identified indicators of environmental change and incorporated them into ice classification systems, either for analysis of potential impacts of climate extremes or climate change on safe travel over ice [48, 57, 58] or to help researchers understand the influences of local geography on ice systems [48]. As **Figure 3** illustrates, the resulting ice classification systems demonstrate how traditional knowledge, science, and geospatial tools can be used together to synthesize valuable tools for managing ice safety.

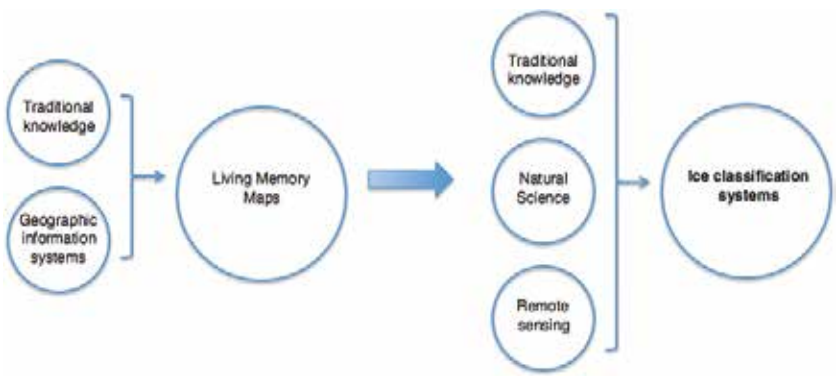

Figure 3. Ice classification systems are based on the complementary use of traditional knowledge, science, and geospatial technologies.

3.3. Synthetic aperture radar (SAR) imagery in ice monitoring for safe winter travel

A number of studies have explored the use of SAR imagery in ice safety monitoring. SAR uses an active microwave sensor that provides imagery, regardless of cloud cover or time of day (unlike optical imagery), and employs radar to interpret and map surface and near-surface characteristics of ice [59]. Its resolution is generally more appropriate for use at scales that are used by hunters [60]. Passive microwave imagery, which has a coarser resolution than SAR but broader spatial coverage, was used in one study of walrus hunting in Alaska to evaluate regional anomalies in sea ice concentrations, but the resultant anomalies were unable to be resolved with local sea ice use due to problems with scale and the resolution of the imagery [61].

Ice monitoring studies aim to provide communities with tailored remote sensing [54, 62] or map products [6, 55, 56] to help individuals in communities plan their travel across ice. Laidler et al. [62] evaluate an Inuit community's interests in tailored SAR products, and results indicate that Inuit hunters are interested in using satellite imagery (and were using it previous to the study), but would prefer to have the following: higher resolution and higher frequency SAR images; time series of images as well as supplemental optical imagery to help better elucidate details themselves from the images; image interpretation training; and opportunities for collaborations directly with the agency processing the SAR imagery, so that traditional knowledge could inform and improve on how images are interpreted on an ongoing basis.

Some studies have explored how traditional knowledge can do just that—that is, meaningfully inform the validation and processing of remote sensing imagery—for community use [6, 54]. For example, a study in Nunatsiavut (Labrador, Canada) aimed to develop a processing and validation methodology to incorporate sea ice thickness data and satellite imagery into a knowledge database of both Inuit- and WMO-based ice catalogs. Their goal is to streamline the generation of products that they process in accordance with user needs, and based on extensive community consultation.

In another study of river ice in Nunavik (Quebec), SAR imagery and the FRAZIL GIS-based hydrological modeling tool are used to create ice maps for safe winter travel planning [6]. This study is significant in that it demonstrates how advances in the RADARSAT-2 satellite technology (multipolarization, polarimetry, and higher spatial resolutions) have the ability to discriminate between freshwater types, and how improved image delivery times have enabled near real-time use of the technology [6]. However, the authors also indicate that validation of satellite imagery in their study was complicated by the difficulty in accessing key sites on the rugged, remote landscape of the study site. They opted to use ground-based cameras and aerial photogrammetry with limited success, and improvements to their radar mapping process were deemed necessary. Today, this could be made possible with unmanned aerial vehicle (UAV)-enabled photogrammetric validation, which has recently been studied for its potential in gaining access to remote Arctic and sub-Arctic sites as a remote sensing tool [63]. Other options for validation include the potential of community-based volunteer monitoring programs to work closely in collecting data, for which there is extensive guidance from previous research [64, 65].

http://dx.doi.org/10.5772/64214

As exemplified by Ford et al. [58], when climate indicators are obtained, sea ice observation data and classification systems can be used with sea ice charts (these are SAR-based maps of ice concentrations provided in Arctic coastal areas by the Canadian Ice Service) to better understand community vulnerabilities to climate change. Where SAR is available, sea ice concentrations can be studied directly as has been done in studies of walrus hunting in the Bering Strait of Russia and Alaska [66].

3.4. Use of other remote sensing imagery

While the majority of adaptation and ice monitoring research with Indigenous peoples has emerged out of North America [7, 37], in Eurasia the Sami reindeer-led initiative, the EALÁT Project, has used remote sensing and participatory Geographical Information Systems (GIS), with the end goal being the establishment of an early warning system with respect to seasonal climate impacts on herding grounds [67]. Remote sensing has been used in a collaborative classification system to identify where the seasonal icing of pastures occurs. Icing effectively "locks out" reindeer from their food source (lichen) and force nomadic herders out of traditional herding routes. EALÁT has developed vegetation indices collaboratively with herders using MODIS, SAR, and Lidar, and notably has developed an integrated approach that includes the seasonal forecasting of icing events to facilitate on-the-ground land-use decision-making during "lockout" seasons. This kind of early warning system, which brings traditional knowledge and seasonal forecasting together through extensive collaboration and knowledge coproduction, can allow for the early detection of unsafe conditions. This is what others have called for in other regions of the circumpolar north in the face of climate change [32].

3.5. Collaborative geospatial platforms and data management

With the growth of traditional knowledge mapping, rights to intellectual property and free and informed prior consent have featured prominently in the design of geospatial systems for research with Indigenous communities [33]. However, the numerous legal and ethics-based protocols that exist can be unclear for both the community and the researcher in terms of who has the authority to use or share data through community-based research [37]. Many technical solutions do exist—such as systems with multiple access roles, data encryption, and protection of sensitive sites—but these require highly technical skills that may be out of reach of some communities or research projects.

A number of geospatial platforms have emerged to provide geospatial services in traditional knowledge mapping, to work respectfully with communities, and to establish appropriate protocols for mapping and managing traditional knowledge data. These include the Exchange for Local Observations and Knowledge of the Arctic (ELOKA) program (National Snow and Ice Data Center), the Geomatics and Cartographic Research Centre's Inuit *SIKU* Sea Ice Atlas (Carleton University), the Interactive Knowledge Mapping Platform for Community-Driven Research (Arctic Eider Society), and an emerging collaborative geomatics tool being developed for use in sub-Arctic Canada (the Centre for Community Mapping and the Computer Systems Group, University of Waterloo). Each of these tools is rooted in research networks particular

to given regions, and brings together numerous local and regional projects into one platform [38, 68].

Some scientists have called for greater data sharing and partnerships to reduce ice-related hazards [56]. In light of this, data management has emerged as a prominent issue, particularly in the high Arctic, where most of the community-based traditional knowledge research on ice has occurred [37, 38, 69, 70]. Principles of "Indigenist data management" have been called for and are rooted in the context-specific nature of traditional knowledge, and the need for relationship-building and a respect for Indigenous values, culture, and language in research [38]. Enabling communities to share their own data at their own discretion at conferences or with other communities or researchers should be a priority for the design of geospatial platforms. Yet, this is complicated by the fact that data generated during research can be in diverse formats, such as recorded narratives, qualitative observations, transcripts, various types of multimedia, and geodatabases. Providing meaningful accessibility to archives of these assemblages of data remains a challenge [37, 70]. Additionally, a lack of access to technology and slow Internet speeds persist in the north, and must be reflected in the development of plans to store and share data [37].

3.6. Gaps in the literature

Studies involving sea ice are well characterized in the literature. However, comparable studies of ice use in brackish and inland freshwater systems were found to be notably underrepresented in community-based geospatial research. Neither lake-based nor ice road studies are represented at all, and only one community-based river ice study was found. This may be due to fewer remote sensing tools available in inland contexts; there are no ice charts, for example. Algorithms have yet to be developed with which to characterize river ice effectively in the processing of SAR imagery; however, anticipated enhancements to the RADARSAT constellation planned for 2018 may benefit freshwater research [59]. Additionally, in situ monitoring can be used effectively on freshwater lakes to validate imagery [10].

There was a concentration of research among communities that participated in the International Polar Year (IPY)-affiliated projects, which were centered in the high Arctic. This signifies both that the funding provided by the initiative was instrumental in advancing community-based geospatial research on ice systems, and that a lack of other sources of funding has hindered research where IPY research sites and priorities did not occur. Virtually, all of the work was in coastal communities, primarily in Canada, and to a lesser degree, Alaska. IPY Canada decidedly prioritized research that was community-based [69], indicating that the field of community-based research on ice has been advanced by the IPY initiative. By contrast, a paucity of community-based studies outside of Arctic North America was noted, and this was also seen with respect to the sub-Arctic regions of the world, including Canada. Studies conducted in freshwater regions and on ice roads have also been relatively rare, which is particularly noteworthy given their role in supporting northern livelihoods.

Finally, we agree that the potential for an early warning system approach to ice research should receive greater emphasis, as continued warming and amplification of polar temperatures in the polar regions will negatively impact ice-based travel in the Arctic and sub-Arctic regions

http://dx.doi.org/10.5772/64214

of the world. Such early warning systems may focus on establishing how geospatial technologies can be used to detect dangerous ice conditions earlier or in real time, and help communications within community and between communities located in high-latitude regions, increasing the adaptive capacity of these communities.

4. Conclusion

Geospatial technologies have helped scientists work with Indigenous peoples to document and map traditional knowledge, and develop tools for cataloging ice systems. This documentation process, more of a dialog than a series of data-collection procedures, has produced geodatabases and maps that are valuable to both researchers and communities for different reasons. Tools, both old and new, are used to create living memory maps and ice classification systems, which can be used to inform scientific inquiry on climate change, impacts to local ice systems, and ways of using the ice.

Remote sensing has been an important part of this process, and the current movement toward tailoring image products in collaboration with communities is exciting. However, the ultimate goal of creating community-based tools to improve ice safety requires expanding the scope of research to outside North America, to be inclusive of sub-Arctic regions of the world, as well as inland freshwater systems, since communities located in these regions and systems also are similarly impacted by climate change and resultant safe winter-travel concerns. Finally, the end goal of setting up an integrated early warning system will require greater partnership building between research teams and community members, and the establishment of meaningful data management systems that facilitate knowledge sharing while addressing community interests and concerns.

Acknowledgements

We acknowledge funding support from the Ontario Ministry of Environment and Climate Change, the National Science and Engineering Research Council of Canada, and the Canadian Institutes of Health Research (IPH #143068).

Author details

Megan Sheremata*, Leonard J.S. Tsuji and William A. Gough

*Address all correspondence to: megan.sheremata@utoronto.ca

University of Toronto Scarborough Campus, Toronto, Ontario, Canada

References

[1] Jeffries, M. O., Richter-Menge, J. and Overland, J. E., 2015. Arctic Report Card. NOAA, Pacific Marine Environmental Laboratory, Seattle, WA. 93 pp.

[2] Comiso, J. C. and Hall D. K., 2014. Climate trends in the Arctic as observed from space. *WIREs Climate Change* 5, pp. 389–409.

[3] Prowse, T., Alfredsen, K., Beltaos, S., Bonsal, B., Duguay, C., Korhola, A., McNamara, J., Vincent, W. F., Vuglinsky, V. and Weyhenmeyer, G. A., 2011. Arctic freshwater ice and its climatic role. *Ambio* 40(1), pp. 46–52.

[4] Screen, J. A., Simmonds, I., Deser, C. and Tomas, R., 2013. The atmospheric response to three decades of observed Arctic sea ice loss. *Journal of Climate*, 26(4), pp. 1230–1248.

[5] Aporta, C., 2009. The trail as home: Inuit and their pan-Arctic network of routes. *Human Ecology*, 37(2), pp. 131–146.

[6] Gauthier, Y., Tremblay, M., Bernier, M. and Furgal, C., 2010. Adaptation of a radar-based river ice mapping technology to the Nunavik context. *Canadian Journal of Remote Sensing*, 36(suppl 1), pp. S168–S185.

[7] Ford, J. D., McDowell, G. and Jones, J., 2014. The state of climate change adaptation in the Arctic. *Environmental Research Letters*, 9(10), p. 104005.

[8] Golden, D. M., Audet, C. and Smith, M. A., 2015. "Blue-ice": Framing climate change and reframing climate change adaptation from the indigenous peoples' perspective in the northern boreal forest of Ontario, Canada. *Climate and Development*, 7(5), pp. 401–413.

[9] Durkalec, A., Furgal, C., Skinner, M. W. and Sheldon, T., 2015. Climate change influences on environment as a determinant of Indigenous health: Relationships to place, sea ice, and health in an Inuit community. *Social Science & Medicine*, 136, pp. 17–26.

[10] Brown, L. C. and Duguay, C. R., 2010. The response and role of ice cover in lake-climate interactions. *Progress in Physical Geography*, 34(5), pp. 671–704.

[11] Holland, M. M., Serreze, M. C. and Stroeve, J., 2010. The sea ice mass budget of the Arctic and its future change as simulated by coupled climate models. *Climate Dynamics*, 34(2-3), pp. 185–200.

[12] Prowse, T., Alfredsen, K., Beltaos, S., Bonsal, B., Duguay, C., Korhola, A., McNamara, J., Vincent, W. F., Vuglinsky, V. and Weyhenmeyer, G. A., 2011. Arctic freshwater ice and its climatic role. *Ambio*, 40(1), pp. 46–52.

[13] Kauker, F., Kaminski, T., Ricker, R., Toudal-Pedersen, L., Dybkjaer, G., Melsheimer, C., Eastwood, S., Sumata, H., Karcher, M. and Gerdes, R., 2015. Seasonal sea ice predictions for the Arctic based on assimilation of remotely sensed observations. *The Cryosphere*, Discussions, 9, pp. 5521–5554.

http://dx.doi.org/10.5772/64214

[14] Stephenson, S. R. and Smith, L. C., 2015. Influence of climate model variability on projected Arctic shipping futures. *Earth's Future*, 3(11), pp. 331–343.

[15] Meier, W. N., Hovelsrud, G. K., Oort, B. E., Key, J. R., Kovacs, K. M., Michel, C., Haas, C., Granskog, M. A., Gerland, S., Perovich, D. K. and Makshtas, A., 2014. Arctic sea ice in transformation: A review of recent observed changes and impacts on biology and human activity. *Reviews of Geophysics*, 52(3), pp. 185–217.

[16] Fossett, R., 1996. Mapping Inuktut: Inuit views of the Real World. In Reading Beyond Words: Contexts for Native History, J. Brown and E. Vibert (Eds.). Broadview Press, Ontario. pp. 74–95.

[17] MacEachren, A. M., 1986. A linear view of the world: Strip maps as a unique form of cartographic representation. *The American Cartographer*, 13(1), pp. 7–26.

[18] Spink, J. and Donald M., 1972. Eskimo Maps from the Canadian Eastern Arctic. Cartographica, Monograph 5. Toronto: University of Toronto Press.

[19] Berkes, F., 1993. Traditional ecological knowledge in perspective. In: Traditional Ecological Knowledge: Concepts and Cases, J.T. Inglis, Ed., Canadian Museum of Nature/International Development Research Centre, International Program on Traditional Ecological Knowledge International Development Research Centre, Ottawa, Canada. p.1–9.

[20] Forest Stewardship Council Canada Working Group (FSCCWG), 2004. National boreal standard. Forest Stewardship Council Canada Working Group, Toronto, Ont. 181 pp.

[21] Stevenson, M. G., 1998. Traditional knowledge and environmental management: From commodity to process. Paper for NAFA Conference, Celebrating Partnerships. September 14–18, 1998. Prince Albert, SK.

[22] World Intellectual Property Organization (WIPO). 2005. The Protection of Traditional Knowledge and Folklore. Proceedings of the WIPO Intergovernmental Committee on Intellectual Property and Genetic Resources, Traditional Knowledge and Folklore, Eighth Session. Geneva, June 6–10, 2005.

[23] Anonymous, 1976. Fieldwork methodology: rationale and assessment. In: Milton Freeman (Ed.), Inuit Land Use and Occupancy Project. Volume Two: Supporting Studies. Minister of Supply and Services Canada. Ottawa, Canada. p. 47–59.

[24] Anonymous, 1976. Introduction. In: Milton Freeman (Ed.), Inuit Land Use and Occupancy Project. Volume Two: Supporting Studies. Minister of Supply and Services Canada, Ottawa, Canada. p. 103–104.

[25] Anonymous, 1976. Notes to Part II. Notes to Part III. In: Milton Freeman (Ed.), Inuit Land Use and Occupancy Project. Volume Three: Land Use Atlas. Minister of Supply and Services Canada, Ottawa, Canada. p. xxiii-unnumbered.

[26] Tobias, T. N., 2000. Chief Kerry's Moose: A Guidebook to Land Use and Occupancy Mapping, Research Design, and Data Collection. UBCIC/Ecotrust, Canada, 81 pp.

[27] Tobias, T., 2010. Living Proof: The Essential Data-collection Guide for Indigenous Use-and-Occupancy Map Surveys. UBCIC/Ecotrust, Canada, 486 pp.

[28] Gearheard, S., Pocernich, M., Stewart, R., Sanguya, J. and Huntington, H. P., 2009. Linking Inuit knowledge and meteorological station observations to understand changing wind patterns at clyde river, Nunavut. *Climatic Change*, 100(2), pp. 267–294.

[29] Kawasaki, A., Berman, M. L. and Guan, W., 2013. The growing role of web-based geospatial technology in disaster response and support. *Disasters*, 37(2), pp. 201–221.

[30] Huntington, H. P., 2011. Arctic science: The local perspective. *Nature*, 478(7368), pp. 182–183.

[31] Nichols, T., Berkes, F., Jolly, D. and Snow, N. B., 2004. Climate change and sea ice: Local observations from the Canadian Western Arctic. *Arctic*, pp. 68–79.

[32] Eicken, H., 2013. Ocean science: Arctic sea ice needs better forecasts. *Nature*, 497(7450), pp. 431–433.

[33] Scassa, T., Engler, N. J. and Taylor, D. F. (2015). Legal issues in mapping traditional knowledge: Digital cartography in the Canadian north. *The Cartographic Journal*, 52(1), pp. 41–50.

[34] Cochran, P., Huntington, O. H., Pungowiyi, C., Tom, S., Chapin III, F. S., Huntington, H. P., Maynard, N. G. and Trainor, S. F., 2013. Indigenous frameworks for observing and responding to climate change in Alaska. *Climatic Change*, 120(3), pp. 557–567.

[35] Laidler, G. J., Ford, J. D., Gough, W. A., Ikummaq, T., Gagnon, A. S., Kowal, S., Qrunnut, K. and Irngaut, C., 2009. Travelling and hunting in a changing Arctic: Assessing Inuit vulnerability to sea ice change in Igloolik, Nunavut. *Climatic Change*, 94(3-4), pp. 363–397.

[36] Laidler, G. J., 2006. Inuit and scientific perspectives on the relationship between sea ice and climate change: The ideal complement?. *Climatic Change*, 78(2-4), pp. 407–444.

[37] Johnson, N., Alessa, L., Behe, C., Danielsen, F., Gearheard, S., Gofman-Wallingford, V., Kliskey, A., Krümmel, E. M., Lynch, A., Mustonen, T. and Pulsifer, P., 2015. The contributions of community-based monitoring and traditional knowledge to Arctic observing networks: Reflections on the state of the field. *Arctic*, 68, pp. 1–12.

[38] Pulsifer, P. L., Laidler, G. J., Taylor, D. R. and Hayes, A., 2011. Towards an Indigenist data management program: Reflections on experiences developing an atlas of sea ice knowledge and use. *The Canadian Geographer/Le Géographe canadien*, 55(1), pp. 108–124.

[39] Robinson, C. J. and Wallington, T. J., 2012. Boundary work: Engaging knowledge systems in co-management of feral animals on Indigenous lands. *Ecology and Society*, 17(2), p. 16.

http://dx.doi.org/10.5772/64214

[40] AHDR. 2004. Arctic Human Development Report. Stefansson Arctic Institute, Akureyri, Iceland. 235 pp.

[41] Larsen, J. N., Anisimov, O.A., Constable, A., Hollowed, A. B., Maynard, N., Prestrud, P., Prowse, T. D. and Stone, J. M. R. 2014. Polar regions. In: Climate Change 2014: Impacts, Adaptation, and Vulnerability. Part B: Regional Aspects. Contribution of Working Group II to the Fifth Assessment Report of the Intergovernmental Panel on Climate Change, V. R.Barros, C. B. Field, D. J. Dokken, M. D. Mastrandrea, K. J. Mach, T. E. Bilir, M. Chatterjee, K. L. Ebi, Y. O. Estrada, R. C. Genova, B. Girma, E. S. Kissel, A. N. Levy, S. MacCracken, P. R. Mastrandrea, and L. L. White (Eds.). Cambridge University Press, Cambridge, United Kingdom and New York, NY, USA. pp. 1567–1612.

[42] Oktay, J. S., 2012. Grounded Theory. Oxford University Press, New York, NY. 192 pp.

[43] Gearheard, S., Aipellee, G. and O'Keefe, K., 2010. The Igliniit Project: Combining Inuit knowledge and geomatics engineering to develop a new observation tool for hunters. In: Krupnik, I et al. (Eds.), SIKU: Knowing Our Ice. Springer, Netherlands. p. 181–202.

[44] Eicken, H. and Salganek, M. (eds.), 2010. Field Techniques for Sea-ice Research. University of Alaska Press, Alaska.

[45] Gearheard, S., Aporta, C., Aipellee, G. and O'Keefe, K., 2011. The Igliniit project: Inuit hunters document life on the trail to map and monitor arctic change. *The Canadian Geographer/Le Géographe canadien*, 55(1), pp. 42–55.

[46] Laidler, G. J., Ford, J. D., Gough, W. A., Ikummaq, T., Gagnon, A. S., Kowal, S., Qrunnut, K. and Irngaut, C., 2009. Travelling and hunting in a changing Arctic: Assessing Inuit vulnerability to sea ice change in Igloolik, Nunavut. *Climatic Change*, 94(3-4), pp. 363–397.

[47] Laidler, G. J., Elee, P., Ikummaq, T., Joamie, E. and Aporta, C., 2010. Mapping Inuit sea ice knowledge, use, and change in Nunavut, Canada (Cape Dorset, Igloolik, Pangnitung). In: Krupnik, I et al. (Eds.), SIKU: Knowing Our Ice. Springer, Netherlands. p. 45–80.

[48] Tremblay, M., Furgal, C., Lafortune, V., Larrivée, C., Savard, J. P., Barrett, M., Annanack, T., Enish, N., Tookalook, P. and Etidloie, B., 2006. Communities and ice: Bringing together traditional and scientific knowledge. *Climate Change*, 10, pp. 123–138.

[49] Isogai, A., McCarthy, D. D., Gardner, H. L., Karagatzides, J. D., Vandenberg, S., Barbeau, C., Charania, N., Edwards, V., Cowan, D. and Tsuji, L. J., 2013. Examining the potential use of the collaborative-geomatics informatics tool to foster intergenerational transfer of knowledge in a remote first nation community. *The Australian Journal of Indigenous Education*, 42(01), pp. 44–57.

[50] Cameron, E. S., 2012. Securing Indigenous politics: A critique of the vulnerability and adaptation approach to the human dimensions of climate change in the Canadian Arctic. *Global Environmental Change*, 22(1), pp. 103–114.

[51] Fienup-Riordan, A., 2014. Linking local and global: Yup'ik elders working together with one mind. *Polar Geography*, 37(1), pp. 92–109.

[52] Bennett, T. D. and Lantz, T. C., 2014. Participatory photomapping: A method for documenting, contextualizing, and sharing indigenous observations of environmental conditions. *Polar Geography*, 37(1), pp. 28–47.

[53] Pulsifer, P., Gearheard, S., Huntington, H. P., Parsons, M. A., McNeave, C. and McCann, H. S., 2012. The role of data management in engaging communities in Arctic research: Overview of the Exchange for Local Observations and Knowledge of the Arctic (ELOKA). *Polar Geography*, 35(3-4), pp. 271–290.

[54] Bell, T., Briggs, R., Bachmayer, R. and Li, S., 2014. Augmenting Inuit knowledge for safe sea-ice travel—The SmartICE information system. In: Oceans-St. John's Conference Proceedings, Sept 14–19, 2014, St. John's, Newfoundland, Canada. p. 1–9.

[55] Druckenmiller, M. L., Eicken, H., George, J. C. and Brower, L., 2010. Assessing the shorefast ice: Iñupiat whaling trails off Barrow, Alaska. In: Krupnik, I et al. (Eds.), SIKU: Knowing Our Ice. Springer, Netherlands. p. 203–228.

[56] Eicken, H., Kaufman, M., Krupnik, I., Pulsifer, P., Apangalook, L., Apangalook, P., Weyapuk Jr, W. and Leavitt, J., 2014. A framework and database for community sea ice observations in a changing Arctic: An Alaskan prototype for multiple users. *Polar Geography*, 37(1), pp. 5–27.

[57] Laidler, G. J., Elee, P., Ikummaq, T., Joamie, E. and Aporta, C., 2010. Mapping Inuit sea ice knowledge, use, and change in Nunavut, Canada (Cape Dorset, Igloolik, Pangnirtung). In: Krupnik, I et al. (Eds.), SIKU: Knowing Our Ice. Springer, Netherland. p. 45–80.

[58] Ford, J. D., Gough, W. A., Laidler, G. J., Macdonald, J., Irngaut, C. and Qrunnut, K., 2009. Sea ice, climate change, and community vulnerability in northern Foxe Basin, Canada. *Climate Research*, 38(2), p. 137.

[59] Tedesco, M., 2015. Remote Sensing of the Cryosphere. John Wiley & Sons, New York. 432 pp.

[60] Norton, D. W. and Gaylord, A. G., 2004. Drift velocities of ice floes in Alaska's northern Chukchi Sea flaw zone: Determinants of success by spring subsistence whalers in 2000 and 2001. *Arctic*, 57, pp. 347–362.

[61] Kapsch, M. L., Eicken, H. and Robards, M., 2010. Sea ice distribution and ice use by indigenous walrus hunters on St. Lawrence Island, Alaska. In: Krupnik, I et al. (Eds.), SIKU: Krupnik, I et al. (Eds.), Knowing Our Ice. Springer, Netherlands. pp. 115–144.

http://dx.doi.org/10.5772/64214

[62] Laidler, G. J., Hirose, T., Kapfer, M., Ikummaq, T., Joamie, E. and Elee, P., 2011. Evaluating the Floe Edge Service: How well can SAR imagery address Inuit community concerns around sea ice change and travel safety?. *The Canadian Geographer/Le Géographe canadien*, 55(1), pp. 91–107.

[63] Fraser, R. H., Olthof, I., Maloley, M., Fernandes, R., Prevost, C., van der Sluijs, J., Kokelj, S., Lantz, T. and Tunnicliffe, J., 2015. UAV photogrammetry for mapping and monitoring of Northern Permafrost Landscapes. *ISPRS-International Archives of the Photogrammetry, Remote Sensing and Spatial Information Sciences*, 1, p. 361.

[64] Lee, O., Eicken, H., Kling, G. and Lee, C., 2015. A framework for prioritization, design and coordination of arctic long-term observing networks: A perspective from the US search program. *Arctic*, 68(5), pp. 76–88.

[65] Mahoney, A., Gearheard, S., Oshima, T. and Qillaq, T., 2009. Sea ice thickness measurements from a community-based observing network. *Bulletin of the American Meteorological Society*, 90(3), p. 370.

[66] Fidel, M., Kliskey, A., Alessa, L. and Sutton, O. O. P., 2014. Walrus harvest locations reflect adaptation: A contribution from a community-based observation network in the Bering Sea. *Polar Geography*, 37(1), pp. 48–68.

[67] Maynard, N. G., Oskal, A., Turi, J. M., Mathiesen, S. D., Eira, I. M. G., Yurchak, B., Etylin, V. and Gebelein, J., 2010. Impacts of arctic climate and land use changes on reindeer pastoralism: Indigenous knowledge and remote sensing. In: Gutman, G. and Reissell, A. (Eds.), Eurasian Arctic Land Cover and Land Use in a Changing Climate. Springer, Netherlands. pp. 177–205.

[68] Gardner-Youden, H. L., Barbeau, C., McCarthy, D. D., Edwards, V., Cowan, D. and Tsuji, L. J., 2011. Indigenous mapping technologies: The past, present and future of the collaborative geomatics web-based tool. *Knowledge Management for Development Journal*, 7(3), pp. 340–353.

[69] Pulsifer, P., Yarney, L., Godøy, Ø., Friddell, J., Vincent, W., DeBruin, T. and Parsons, M., 2013. Data management for Arctic observing. Arctic Observing Summit, White Paper.

[70] Pulsifer, P. L., Huntington, H. P. and Pecl, G. T., 2014. Introduction: Local and traditional knowledge and data management in the Arctic. *Polar Geography*, 37(1), p. 1.

Chapter 9

GIS Applications in Agronomy

Suarau O. Oshunsanya and OrevaOghene Aliku

Additional information is available at the end of the chapter

http://dx.doi.org/10.5772/64528

Abstract

Agronomy is a branch of agriculture that deals with soil and crop. Soil varies in space and is responsible for variation in the growth and yield of crops on the field. This variation in the yields of crops planted and monitored on the same parcel of land under the same environmental conditions has been a great concern to farmers. Spatial variations of soil nutrients status, as caused by topography, soil texture and management practices, have been observed across the fields. Hence, the need to separate the field into site specific management units using geographical information systems (GIS) for effective soil and crop management in order to obtain optimum productivity. Over the years, field sizes, farming direction, locations of fences, rotations and fertility programmes have changed the nutritional status of the farms. Consequently, the productivity of the soil has equally been affected. In spite of these factors, conventional agriculture treats an entire field uniformly with respect to the application of fertiliser, pesticides, soil amendments and other chemical application. The use of GIS will help farmers to overcome over- or under-applications of fertiliser and other agrochemical applications. The potential of GIS application in agronomy is obviously large. However, the GIS user community in the field of agronomy is rather small compared to other business sectors. To advance the use of GIS in agronomic studies, this Chapter in book tends to explore the applications of GIS to some fields in agronomy.

Keywords: spatial variability, soil properties, site-specific management, crop yields, ArcGIS

1. Introduction

Agronomy, an aspect of agriculture, is a spatial activity that represents the backbone of the economy of many nations. This is the result of its noticeable contribution to the employment of labour and the gross domestic product of most developing countries. However, as land is

a finite resource, the increase in food production in order to meet an affluent population becomes one of the major issues faced by many developing countries in the world. Hence, the improvement in agronomic practices is inevitable to ensure wise land-use planning and proper management of available resources for Crop cultivation.

With the growing interest in placing site-specific information in a spatial and long-term perspective [1], precision in agronomic practices would require a technology that can calculate spatial and temporal variations in crop growth with a time scale appropriate for management decisions [2]. Today, advances have been made towards extraordinary digital systems for utilization in soil fertility examination, soil survey and land-use planning, crop production and yield monitoring. Computer programmes, such as geographical information system (GIS), contribute to the speed and efficiency of overall agronomic planning processes [3].

According to [1], most process-based agronomic models examine temporal variations using point data from specific sites, while GIS facilitates storage, manipulations, analysis and visualization of data. They further stated that the interaction of both spatial and temporal issues can be best handled through interfacing agronomic models with geographical information system (GIS).

2. What is geographical information system (GIS)?

A geographical information system (GIS) is a thematic mapping system, which allows for the production of maps based on themes such as soils or hydrology [4]. Geographical information systems are a special class of information systems that keep track of events, activities and things and also of where these events, activities or things happen or exist [5].

GIS is a part of a suite of technologies that enhance precision in agronomic practices. The system requires preliminary basic information that is relevant to the particular project discipline. The importation of information into a GIS would require time and attention, mainly because this information will provide the basic knowledge of the territory and on the individual parameters, and it is difficult to modify in a second time [6]. According to [6], all the information in a GIS can be linked and processed simultaneously, obtaining a syntactical expression of the changes induced in the system by the variation of a parameter. The GIS allows the updating of geographical information and their relative attributes, producing a fast adaptation to the real conditions and obtaining answers in near real time [6]. In [7], the authors reported that GIS techniques have been used for farm-related assessments at national and regional scales for many years. Geographical information systems have been in existence for about three decades, but only in the last 10 years, these applications have widely been used for agronomic and natural resource management [8]. The GIS is a dynamic product rather than a static product, Making it easy to update, edit, and reproduce maps [4]. According to [9], geographical information systems allow for the visualization of information in new ways that reveal relationships, patterns and trends that are not visible with other popular systems. Geographical information systems provide valuable support to handle out voluminous data that are generated through conventional and spatial format and for the integration of these

http://dx.doi.org/10.5772/64528

data sets [10, 11]. The GIS technique uses a digital map that allows the users to view, update, query, analyse and manipulate the spatial and tabular data either alone or together, within few minutes. Unlike paper maps, GIS can prepare and manage large collection of agronomic and land resource data necessary for crop production [12].

2.1. Importance of GIS to agronomy

Agronomic activities are spatial and the need to place site-specific information in a spatial and long-term perspective would require special models that can be used to calculate spatial variation in crop growth and monitor variations in trend with a time scale appropriate for guiding decisions. GIS could play a significant role in agronomy at several levels due to the fact that it can be used to study the nutrient status of individual fields to arrive at specific requirements for external application of nutrients [12]. According to [13], the use of GIS in precision agronomic practices helps to manage the information intensive environment in crop production by combining site-specific (within field) management with computer software modelling for analyses and interpretation of varying inputs and outputs. As opposed to farmers' typical manual adjustment, GIS helps farmers to manage with-in field variable rate application, which results from spatial variation in crop yields within a field [14]. Hence, GIS enhances the assessment and understanding of variations in a field crop. According to [14], GIS can be used to assemble many layers of information such as soil nutrients, elevation, moisture content and topography to produce a map to show which factors influence crop yield. In [14], it was Also reported that the yield can then be estimated or used for future reference and the economic inputs and outputs can be calculated based on anticipated yield. This will have a huge potential for saving costs spent on over applied fertilisers that otherwise could have been used on another field.

3. Applications of GIS in agronomy

According to [1], applications of GIS have grown from primarily hydrological applications in the mid-1980s to the current wide range of applications in agronomy and natural resource management research. Examples of GIS applications in agronomy and natural resource management research include: atmospheric modelling [15], climate change, sensitivity and/or variability studies [16–18], characterization and zonation [19, 20], hydrology, water quality, water pollution [21, 22], soil science [8, 23] and spatial yield calculation—regional, global [24, 25] and precision farming (spatial yield calculation) [26, 27]. Several studies have been reported on the application of GIS on cultivation practices of various crops [10, 28–31]. In [12], the authors reported The application of GIS to fertility management of Soils planted to tea where digitized Maps of the soil pH, potassium, phosphorus and organic matter were prepared using the Arc MAP software. According to [12], it would be beneficial for tea growers in those locations for calculating fertiliser requirements. In [12], it was reported that measures may be required to reduce to a desired level the pH of fields having pH > 5.5. In [32], a geodatabase was developed using GIS mapping. This was to provide soil quality monitoring based on data of agrochemical soil survey in order to monitor land cover/soil quality changes between

periods of soil survey. In the work of [32], ArcGIS was employed for mapping soil quality and it was reported that soil data can easily be handled and analysed using ArcGIS because they are spatial in nature. It was also reported in [32] that there was no significant changes in humus and easily hydrolysable nitrogen content within the period between the last two soil agrochemical surveys (**Figures 1** and **2**). In [33], a GIS-based decision support system was used to establish potentials and limitations of different soils for crop production, while [34] employed GIS in soil erosion control where the factors and elements affecting erosion were studied by analysing numerical maps of different parts of a basin.

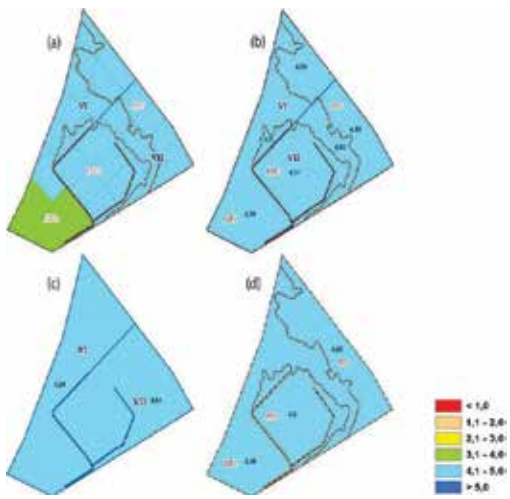

Figure 1. Humus content in the soil: (a) humus content per elementary plots; (b) humus average value per agricultural soil contour per field; (c) average value per field; (d) average value per agricultural soil contours per enterprise (Source: [32]).

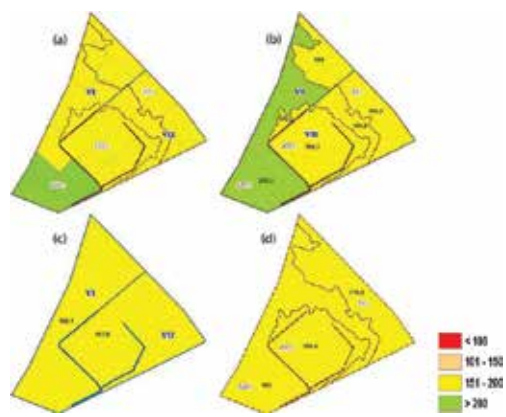

Figure 2. Nitrogen content in the soil: (a) nitrogen content per elementary plots; (b) nitrogen average value per agricultural soil contour per field; (c) average value per field; (d) average value per agricultural soil contours per enterprise (Source: [32]).

http://dx.doi.org/10.5772/64528

3.1. Operational use of GIS in precision farming: regional and local levels

The GIS techniques have been used for farm-related assessments for many years at both national and regional scales, respectively [7]. The combination of these techniques and remotely sensed data have been used to aid the assessments of land capability [35], crop condition and yield [36–38], range condition [39], flood and drought [37, 38], soil erosion [40, 41], soil compaction [42] and climate change impacts [43, 44] on regional levels. Also, attempts have been made by [45, 46] to assess leaching behaviour for regional scale using a combination of the leaching and chemistry examination (LEACHM) models and GIS database.

At the local level, the number and variety of local agricultural GIS applications have dramatically increased during the past 5 years [45]. Most of the applications are targeted at individual farms [47]. For example, [48] utilized the spatial analysis tools in PC ARC/INFO to perform fully automated conservation program determinations, compliance monitoring and farm planning. In [47], it was stated that this particular application is noteworthy both for its substance and because it illustrates how rapidly the computing resources, user interfaces and database functions in desktop GIS have evolved during the past 5 years. Similarly, [49] determined possible pond sites and estimated rainwater-harvesting potential for a 172-ha farm using GIS.

Most of these field- and subfield-scale applications are connected with precision or site-specific farming, Which helps to direct the application of seed, fertiliser, Pesticide and water, within fields in ways that optimize farm returns and minimize chemical inputs and environmental hazards [7, 50]. In [51], the use of GIS in precision farming to generate production-based farming system that can be designed to increase long-term, site-specific and whole-farm production efficiency, productivity and profitability was discussed. In addition, [7, 52] reported that most site-specific farming systems utilize some combinations of Geographical positioning system (GPS) receivers, continuous yield sensors, remote sensing, geostatistics and variable rate treatment applications with GIS. According to [47], the reason for combining these advanced technologies is to collect spatially referenced data, perform spatial analysis, make decisions and apply variable rate treatment.

3.2. GIS applications in agrometeorological operations

Due to the increasing pressure on land and water resources for crop cultivation, land-use management and forecasting (crop, weather, fire, etc.) have become more essential every day. Hence, GIS is an important tool at the disposal of decision makers [6]. For instance, precipitation and solar radiation are meteorological conditions that can be mapped and monitored to directly assist in the agronomic process to provide advice on the occurrence of drought [53]. In [6], it was reported that developed countries use GIS to plan the times and types of agronomic practices, which requires certain information such as soil types, land cover, climatic data and geology, in describing a specific situation in any given location. Each informative layer provides to the operator the possibility to consider its influence on the final outcome [6].

3.3. Operational use of GIS in agroclimatological and agroecological studies

The GIS technology has been shown to synthesize and integrate more data than methods used in the pre-computer era and to shift the design of agroecological and agroclimatological studies towards user-specific classifications [35]. In a study carried out in Zimbabwe, effective rainfall and vegetation for variable interpolation between stations were calculated from rainfall and vegetation data using GIS maps [35]. In addition, seasonal rainfall surfaces were constructed for Zimbabwe using decadal rainfall data while adopting the procedures described by [54]. They also generated surfaces showing mean rainfall and annual rainfall anomalies to describe the main rainfall period for Zimbabwe in terms of rainfall variability. This showed the natural regions experiencing considerable spatial variability in terms of mean and inter-seasonal variability of rainfall (**Figure 3**).

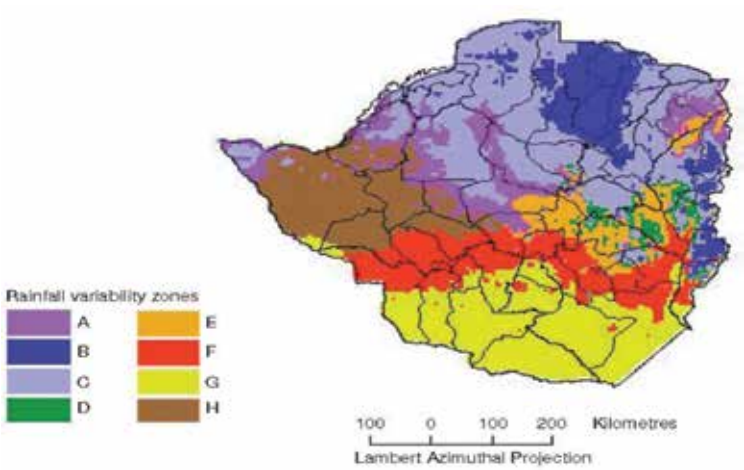

Figure 3. Rainfall variability zones in Zimbabwe (Source: [35]). See Table 4 in Corbett and Carter (1997) for zone descriptions.

3.4. Use of GIS for agronomic characterization and zonation

The GIS techniques have also been used to characterize agroclimatic diversity and to delineate maize-specific adaptation zones [55]. In the report of [55], it was concluded that the emergence of GIS has made it possible to delineate agroclimatic zones with greater precision, especially by allowing many 'layers' of spatially referenced data (including survey data) to be integrated into one digital database.

3.5. GIS application in soil survey studies

According to [47], three approaches have been implemented in an attempt to utilize GIS and/or GPS to improve soil attribute predictions at regional scales. The first approach evaluated the use of GIS and/or GPS to improve traditional soil surveys. For example, Long et al. [56] examined the potential of using GPS methods in soil surveys and found these methods to be

more efficient than traditional methods of mapping and sufficiently accurate to support positioning/navigating in fields and field digitizing of soil boundaries.

The second approach combined geostatistical modelling with soil survey maps to generate improved soil descriptions. In [57], a map that preserved the map unit boundaries and incorporated the spatial variability of the attribute data within the map unit delineations were produced. This was done by combining spatially interpolated (krigged) distributions of measured values with soil map unit delineations within a GIS framework. It was reported by [47] that this approach appeared promising for countries and regions with well-developed soil survey programs.

The third approach neglects the use of traditional soil survey methods and explores the possibilities of integrating GIS, pedology and statistical modelling to improve soil resource inventory [58, 59]. In a study, [60] combined a GIS with an existing soil landscape model to create soil drainage maps. The soil landscape model used multivariate discriminant to predict soil drainage class from parent material, terrain and surface drainage feature variables [61].

3.6. GIS as an agronomic land-use planning tool

Figure 4 is a pictorial view of SPAREC GIS being used for land-use planning [4]. It was stated by Coleman AL and Galbraith JM that soil survey data and geographic information systems (GIS) are important tools in land-use planning. They reported that the map unit interpretive records (MUIR) were used to create interpretation maps, flooding frequency maps and runoff maps after soil data were added to other data layers and images. **Figure 5** shows a flooding frequency map converted from tabular estimates of values in an ArcView GIS. It was explained by [4] that the blue areas are frequently flooded, red areas are occasionally flooded, while the green areas are rarely flooded. They further reported that the soil based-GIS made the decision-making process more accurate, automated and efficient, hence promoting wise land-use planning. In [3] and [62], it was reported that the soil-based GIS is a dynamic product that serves to convert verbal communication into visual communication while preventing information overload. In the Report of [4], it was reported that with the GIS, tabular soil information

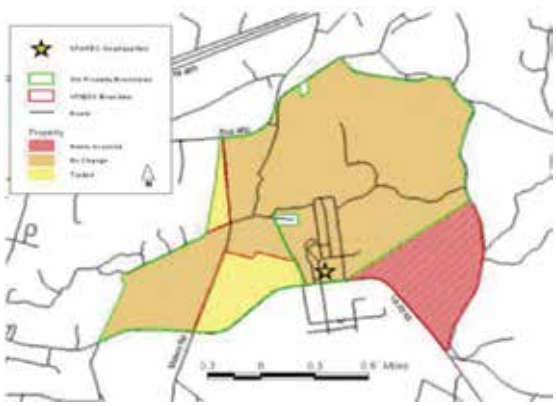

Figure 4. Pictorial view of SPAREC GIS (Source: [4]).

can be georeferenced and easily converted to geographic and interpretive maps, which provides the user with a visual representation of the tabular data. **Figure 6** is an example of an interpretive map showing the ratings for site suitability of local roads and streets, where [4] explained that the green areas represent a slight rating, meaning they are the most suitable, while the yellow areas are rated moderate and the red areas are severe areas having the most serious limitations.

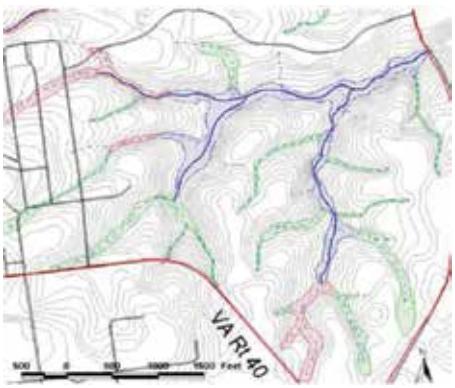

Figure 5. Flooding frequency map (Source: [4]).

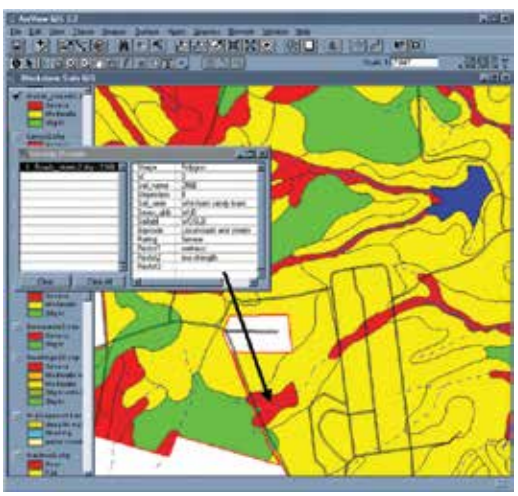

Figure 6. An example of an interpretive map showing ratings for local roads and streets (Source: [4]).

3.7. Operational use of GIS for soil fertility studies

Soil fertility investigations are necessary to confirm soil fertility status [63], which is also necessary as a guide for the fertility management practice to adopt [64, 65]. Several methods

http://dx.doi.org/10.5772/64528

of soil fertility investigation have been employed in confirming the fertility status of soils [66, 67]. In [68], the authors reported that these methods did not ensure the completion of soil fertility investigation within the specified time frame and the required degree of accuracy, as change in soil fertility status over a period of 2 or 3 years makes these methods invalid, thus making it difficult for agronomists to manage soil fertility over large areas. They reported that the application of geospatial technology involving the use of global positioning system (GPS) and geographic information system (GIS) had greatly improved the old traverse techniques.

In the application of space-time evolution of soil fertility data mining based on visualization, a three-dimensional spatial variation of soil nutrient spatial map for soil available phosphorus (**Figure 7**) was produced by [69]. In a study, [70] evaluated the spatial variation of soil organic carbon, soil water content, NO_3–N, PO_4–P (phosphate-phosphorus) and K (potassium) in the 0–15 cm layer of a 3.3 ha field cropped with maize and soya beans. They calculated that as many as 400 randomly selected samples per hectare may be needed to develop an accurate soil NO_3–N map and that an application travelling at 8 km h^{-1} would need to modulate fertiliser rates every 2.25 s to match nitrogen fertiliser rates to soil NO_3–N requirements.

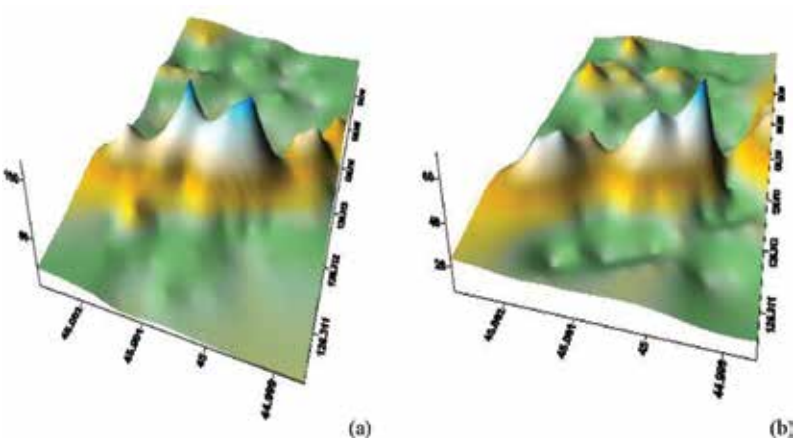

Figure 7. A three-dimensional spatial variability map of available phosphorus for 2003(a) and 2008(b) (Source: [69]).

In [71, 72], the authors reported the use of GIS techniques and remote sensing in forest soil fertility studies. According to [68], GIS could be used to map fertility levels across a farm to serve as basis for the application of farm inputs and also for establishing accurate location of yield data for the production of yield maps for monitoring yield [73, 74]. It was also reported by [68] that periodic review of soil fertility status can be done on digital maps generated with GIS technique (**Figure 8**). According to [12], this is due to the fact that the GIS technique uses a digital map which allows the user to view, update, query, analyse and manipulate spatial and tabular data either alone or together, within a few minutes. In assessing the relative efficiency of GIS map-based soil fertility evaluation in relation to traditional soil testing, [76] reported minor variations in available nitrogen content, no variation in available phosphorus and a large difference in available potassium under the two methods of evaluation (**Table 1**).

They concluded that fertiliser recommendations generated from GIS maps were agronomically as effective as those generated form soil testing (**Table 2**).

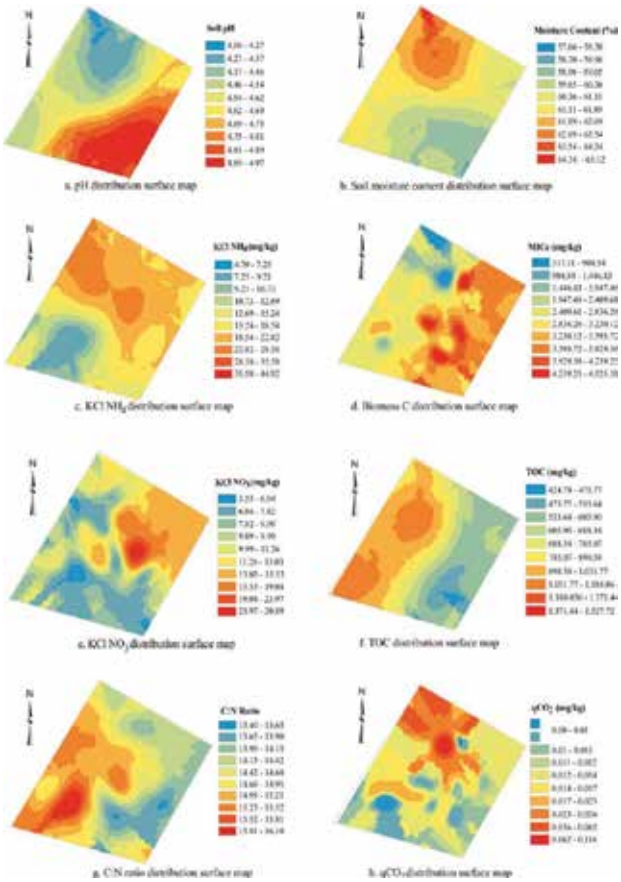

Figure 8. Surface maps showing the distribution of soil fertility indicators (Source: [75]).

Parameter	Low/Slightly Acidic		Medium/Acidic		High/Alkaline	
	Soil test	GIS	Soil test	GIS	Soil test	GIS
Available N (g/kg)	8.9	7.8	11	22	0	0
Available P (mg/kg)	100	100	0	0	0	0
Available K (cmol/kg)	44	33	33	67	22	0
pH	5.6	6.7	4.4	3.3	0	0

Source: [76].

Table 1. Comparison of traditional soil test and GIS method of assessing samples (%) that fall under low, medium and high nutrient availability and pH categories.

Treatment	Rice	Potato	Sesame
Farm	60-30-30	300-200-200	Residual
State	80-40-40	200-150-150	80-40-40
Soil test	Variable	Variable	Variable
GIS	Variable	Variable	Variable

Source: [76].

Table 2. Nutrient rates generated from state, field-specific, soil test-based recommendations and GIS.

3.8. Spatial yield calculation

In [47], it was reported that new GIS data layers developed from models were used with some information in various GIS-based application of existing crop yield models. Several studies Showed that these applications can be used to store and process data for decision making with respect to the factors that influence Crop cultivation and crop yield in a crop production. For example, the climate surfaces can be used as inputs in genotype-sensitive crop models to assess the risks for specific crop varieties [35]. This was illustrated by [36] who used GIS and remote sensing technologies with the SOYGRO [77] physiological soya bean growth model to predict the spatial variability of soya bean yields. In the report of [78], continuous yield sensors with a combination of accurate location information obtained using a GPS with the results of a variable flow rate sensor can provide information about the crop performance for a year that can be used to guide the following year's crop management strategies. According to [36], the examination of spatial patterns of simulated yield improved production estimates and highlighted vulnerable areas during drought.

3.9. Agronomic impact assessment using GIS

The GIS and environmental models have been combined in many projects to evaluate the impacts of modern agriculture [47]. For instance [79], used the EPIC-PST crop growth/chemical movement model [80] interfaced with Earthone GIS to evaluate crop yield and nitrate (NO_3–N) movement to surface and ground waters for four soils and nine cropping systems. In [79], the authors digitized soil maps using GIS and described how the data can be used with model results to compare the predicted changes in crop yields and nitrogen losses on different soils under water quality protection policies that targets specific soils and/or cropping practices.

4. Conclusions

The GIS is an excellent informative tool that enhances visualization and ease of analysis and handling of spatial data. Its digital map allows for the periodic review of soil fertility status as it improves and updates information on crop, soil and the prevailing climatic conditions as they affect agronomic practices, thus greatly enhancing the management of finite resources and accurate land-use planning due to its accurate knowledge base.

The benefits of GIS applications could be better exploited with increase in the level of awareness and understanding of the potential use of GIS and related technologies in the assessment, storage, processing and production of data ranging from site-specific farming systems to global food production and food security issues. The GIS offers the advantage of generating and synthesizing new information cheaply and quickly Over a wide range of areas as well as temporal or historical changes resulting from management practices, thus, aiding the ease in decision-making process.

Author details

Suarau O. Oshunsanya* and OrevaOghene Aliku

*Address all correspondence to: soshunsanya@yahoo.com

Department of Agronomy, University of Ibadan, Ibadan, Nigeria

References

[1] Hartkamp AD, White JW, Hoogenboom G. Interfacing geographic information systems with agronomic modelling. Agronomy Journal. 1999; 91: 761–772.

[2] National Research Council. Precision agriculture in the 21st century. Geospatial and information technologies in crop management. 1997; National Academy Press, Washington, DC.

[3] GeoComm International Corporation. Internet publication. GIS Data Depot. 2000; Available from: http://www.gisdatadepot.com (Assessed: 2015-11-5).

[4] Coleman AL, Galbraith JM. Using GIS as an agricultural land-use planning tool. Virginia agricultural experimental station. Bulletin 00-2. 2000; Available from: http://www.vaes.vt.edu/research/publications/index.html (Assessed: 2015-11-12).

[5] Longley PA, Goodchild MF, Maguire DJ, Rhind DW. Geographic information systems and science, 2nd edition. 2006; Wiley, New York. ISBN 0-470-87001-X paperback.

[6] Basso B, McVicar TR, Lee B, Yazdanpanah H, Das HP. Remote sensing and GIS applications in agro meteorology. Guide to Agricultural Meteorological Practices. 2005; Commission for Agricultural Meteorology, Geneva, 53 pp.

[7] Usery EL, Pocknee S, Boydell B. Precision farming data management using geographic information systems. Photogrammetric Engineering and Remote Sensing. 1995; 61: 1383–1391.

[8] Burrough PA. Principles of geographical information systems for land resource assessment. 1986; Oxford University Press, New York.

[9] Environmental Systems Research Institute, Inc. Getting to know ArcView GIS. 3rd edition. 1999; ESRI, Redlands, California

[10] Rao BRM. Remote sensing and GIS-Its applications in soil science. Proceedings of National Symposium on Soil Science Research, December 7–9. 2007; Indian Society of soil Science, Kolkata, pp. 25–30.

[11] Vadivelu S. Soils of coastal ecosystem in the southern states and their problems and potentials for land use planning. Proceedings of National Symposium on Soil Science Research, December 7–9. 2007; Indian Society of Soil Science, Kolkata, pp. 31–35.

[12] Senthurpandian VK, Jayaganesh S, Srinivas S, Palani N, Muraleedharan N. Application of geographic information system to fertility management of tea soils of Anamallais. Asian Journal of Earth Sciences. 2010; 3: 136–141.

[13] Melakeberhan H. Embracing the emerging precision agriculture technologies for site-specific management of yield-limiting factors. Journal of Nematology. 2002; 34(3) :185–188.

[14] Bullock DS, Lowenberg-DeBoer J, Swinton SM. Adding value to spatially managed inputs by understanding site-specific yield response. Agricultural Economics: The Journal of the International Association of Agricultural Economists. 2002; 27: 233–245.

[15] Lee TJ, Pielke RA, Kittel TGF, Weaver JF. Atmospheric modelling and its spatial representation of land surface characteristics. In: M. F. Goodchild et al. (eds) Environmental modelling with GIS. 1993; Oxford University Press, New York, pp. 108–122.

[16] Rosenzweig C. Crop response to climate change in the southern Great Plains: A simulation study. Professional Geography. 1990; 42: 20–37.

[17] Wei Y, Hoogenboom G, McClendon RW, Gresham DD. Impact of global climate change on crop production at a farm level. Paper. 1994; ASAE, St. Joseph, MI, 94-3523.

[18] Beinroth FH, Jones JW, Knapp EB, Papajorgji P, Luijten J. Evaluation of land resources using crop models and a GIS. In: G. Y. Tsuji et al. (eds) Understanding options for agricultural production. 1998; Kluwer Academic Publication, Dordrecht, Netherlands, pp. 293–311.

[19] Aggarwal PK. Uncertainties in crop, soil and weather inputs used in growth models: Implications for simulated outputs and their application. Agricultural Systems. 1995; 48: 361–384.

[20] Bouman BAM, Wopereis MCS, Riethoven JJ. The use of crop growth models in agro-ecological zonation of rice. SARP Research Proceedings of DLO Research Institute for Agro-Biology and Soil Fertility. 1994; Wageningen Agricultural University and IRRI, Manila, Philippines.

[21] Mamillapalli S, Srinivasan R, Arnold JG, Engel BA. Effect of spatial variability on Basin scale modeling. In: Proceedings of International Conference/Workshop of Integrating GIS and Environmental Modeling, 3rd edition. Santa Fe, NM. 21–25 January. 1996; National Center for Geographic Information and Analysis, Santa Barbara, CA.

[22] Corwin DL, Loague K. Applications of GIS to the modelling of non-point source pollutants in the vadose zone. 1996; SSSA, Madison, WI, SSSA Special Publication No. 48.

[23] Manchanda ML, Kudrat M, Tiwari AK. Soil survey and mapping using remote sensing. Tropical Ecology. 2002; 43(1): 61–74.

[24] Haskett JD, Pachepsky YA, Acock B. Use of the beta distribution for parameterizing variability of soil properties at the regional level for crop yield estimation. Agricultural Systems. 1995; 48: 73–86.

[25] Karthikeyan R, Hoogenboom G, McClendon RW. Regional yield forecasting using crop models and GIS: A conceptual framework. Paper. 1996; ASAE, St. Joseph, MI, 96–5010.

[26] Booltink HWG, Verhagen J. Using decision support systems to optimize barley management on spatially variable soil. In: M. J. Kropff et al. (eds) Applications of systems approaches at the field level. Systems approaches for sustainable agricultural development. 1997; Kluwer Academic Publication, Dordrecht, Netherlands, 6, pp. 219–233.

[27] Hoogenboom G, Lal H, Gresham DD. Spatial yield prediction. Paper. 1993; ASAE, St. Joseph, MI, 93–3550.

[28] Deosthali V, Akmanchi A, Salunke C. Soybena agriculture in India, A spatial analysis. Transactions of the Institute of Indian Geographers. 2005; 27: 13–13.

[29] Rao BRM, Ravishankar T, Dwivedi RS, Thammappa SS, Venkataratnam L, Sharma RC, Das SN. Spectral behaviour of salt affected soils. International Journal of Remote Sensing. 1995; 16: 2125–2136.

[30] Osborne SL, Schepers JS, Francis DD, Schlemmer MR. Detection of phosphorus and nitrogen deficiencies in corn using spectral radiance measurements. Agronomy Journal. 2002; 94: 1215–1221.

[31] Adams ML, Norvell WA, Philpot WD, Peverly JH. Spectral detection of micronutrient deficiency in 'Bragg' Soybean. Agronomy Journal. 2000; 92: 261–268.

[32] Kokhan S, Moskalenko A, Shkvir I. GIS mapping for soil quality evaluation. 2nd International Conference of Informatics and Management Sciences (2013), March 25–29, 2013. ICTIC, Kyiv, Ukraine.

[33] Setia R, Verma V, Sharma P. Soil informatics for evaluating and mapping soil productivity index in an intensively cultivated area of Punjab, India. Journal of Geographic Information System. 2012; 4: 71–76.

[34] Gandomkar R. Using GIS in Soil Erosion Control (Case study: Mousa Abad Basin, Isfahan, Iran). GIS Ostrava, Ostrava, January 25–28, 2009.

[35] Corbett JD, Carter SE. Using GIS to enhance agricultural planning: The example of inter-seasonal rainfall variability in Zimbabwe. Transactions in GIS. 1996; 1: 207–218.

[36] Carbone GJ, Narumalani S, King M. Application of remote sensing and GIS technologies with physiological crop models. Photogrammetric Engineering and Remote Sensing. 1996; 62: 171–179.

[37] Korporal KD, Hillary NM. The Statistics Canada crop condition assessment program. 1993; Statistics Canada, Ottawa.

[38] Wade G, Mueller R, Cook P, Doralswamy P. AVHRR map products for crop condition assessment: A geographic information systems approach. Photogrammetric Engineering and Remote Sensing. 1994; 60: 1145–1150.

[39] Ringrose S, Vanderpost C, Matheson W. The use of integrated remotely sensed and GIS data to determine causes of vegetation cover change in Southern Botswana. Applied Geography. 1996; 16: 225–242.

[40] Desmet, PJJ, Govers G. GIS based simulation of erosion and deposition patterns in an agricultural landscape: A comparison of model results with soil map information. Catena. 1995; 25: 389–401.

[41] Wilson JP, Gallant JC. EROS: A grid-based program for estimating spatially-distributed erosion indices. Computers and Geosciences. 1996; 22: 707–712.

[42] Bober ML, Wood D, McBride RA. Use of digital image analysis and GIS to assess regional soil compaction risk. Photogrammetric Engineering and Remote Sensing. 1996; 62: 1397–1404.

[43] Kern JS. Spatial patterns of soil organic carbon in the contiguous United States. Soil Science Society of America Journal. 1994; 58: 439–455.

[44] Kern JS. Geographic patterns of soil water-holding capacity in the contiguous United States. Soil Science Society of America Journal. 1995; 59: 1126–1133.

[45] Hutson JL, Wagenet RJ. A pragmatic field-scale approach for modelling pesticides. Journal of Environmental Quality. 1993; 2: 494–499.

[46] Petach MC, Wagenet RJ, DeGloria SD. Regional water flow and pesticide leaching using simulations with spatially distributed data. Geoderma. 1991; 48: 245–269.

[47] Wilson JP. Local, national, and global applications of GIS in agriculture. In: P. A. Longley, M. F. Goodchild, D. J. Maguire, and D. W. Rhind (eds) Geographical information systems: Principles, techniques, management, and applications. 1999; Wiley. New York, NY, pp. 981–998.

[48] Ventura S. Conversion of automated geographic data to decision-making information. Photogrammetric Engineering and Remote Sensing. 1991; 56: 511–516.

[49] Vorhauer CF, Hamlett JM. GIS: A tool for siting farm ponds. Journal of Soil and Water Conservation. 1996; 51: 434–438.

[50] Carr PM, Carlson GR, Jacobsen JS, Nielsen GA, Scogley EO. Farming soils, not fields: A strategy for increasing fertilizer profitability. Journal of Production Agriculture. 1991; 4: 57–61.

[51] Liaghat S, Balasundram SK. A review: The role of remote sensing in precision agriculture. American Journal of Agricultural Biological Science. 2010; 5(1): 50–55.

[52] Peterson C. Precision GPS navigation for improving agricultural productivity. GPS World. 1991; 2: 38–44.

[53] McVicar TR, Jupp DLB. The current and potential operational uses of remote sensing to aid decisions on drought exceptional circumstances in Australia: A review. Agricultural Systems. 1998; 57: 399–468.

[54] Hutchinson MF. Stochastic space-time weather models from ground-based data. Agricultural and Forest Meteorology. 1995; 73: 237–264.

[55] Hassan RM. Maize technology development and transfer: A GIS application for research planning in Kenya. 1998; CAB International Wallingford, Oxon OX10 8DE, UK, 256 pp.

[56] Long DS, DeGloria SD, Galbraith JM. Use of the global positioning system in soil survey. Journal of Soil and Water Conservation. 1991; 46: 293–297.

[57] Rogowski AS, Wolf JK. Incorporating variability into soil map unit delineations. Soil Science Society of America Journal. 1994; 58: 163–174.

[58] Gessler PE, Moore ID, McKenzie NJ, Ryan PJ. Soil-landscape modeling and spatial prediction of soil attributes. International Journal of Geographical Information Systems. 1995; 4: 421–432.

[59] Finke PA, Wösten JHM, Kroes JG. Comparing two approaches of characterizing soil map unit behaviour in solute transport. Soil Science Society of America Journal. 1996; 60: 200–205.

[60] Bell JC, Cunningham RL, Havens MW. Soil drainage class probability using a soil-landscape model. Soil Science Society of America Journal. 1994; 58: 464–470.

[61] Bell JC, Cunningham RL, Havens MW. Calibration and validation of a soil-landscape model for predicting soil drainage class. Soil Science Society of America Journal. 1992; 56: 1860–1866.

[62] USGS National Mapping Information. Internet publication. 2000; Available from: http://mapping.usgs.gov (Assessed: 2015-11-5).

[63] Moshki A, Lamersdorf NP. Growth and nutrient status of introduced black locust (Robinia pseudoacacia L.) afforestation in arid and semi-arid areas of Iran. Research Journal of Environmental Science. 2010; 5: 259–268.

[64] Sartori F, Lal R, Ebinger MH, Miller RO. Tree species and wood ash affect soil in Michigan's Upper Peninsula. Plant Soil. 2007; 298(1&2): 125–144.

[65] Ritter E. Development of bioavailable pools of base cations and P after afforestation of volcanic soils on Iceland. Forest Ecological Management. 2009; 257(3): 1129–1135.

[66] Assefa B, Glatzel G. Measuring soil fertility under Hagenia abyssinica (Bruce) J.F. Gmel by the biotest method. International Journal of Agronomy. 2010; Article ID 845087; 5 p. doi:10.1155/2010/845087

[67] Belachew T, Abera Y. Assessment of soil fertility status with depth in wheat growing highlands of Southeast Ethiopia. World Journal of Agricultural Science. 2010; 6(5): 525–531.

[68] Adekayode FO, Akomolafe DT. Creating a soil data base in a reconnaissance soil fertility study of an encroached forest reserve in Northern Nigeria for a reforestation programme. African Journal of Environmental Science and Technology. 2011; 5(9): 748–754.

[69] Dong W, Chen G, Jiang J, Wang G. Research and application of space-time evolution of soil fertility data mining based on visualization. In: D. Li and Y. Chen (eds) (2011) Computer and computing technologies in agriculture, V. Springer, Berlin Heidelberg. 2012; 369: 359–367.

[70] Cahn MD, Hummel JW, Brouer BH. Spatial analysis of soil fertility for site-specific management. Soil Science Society of America Journal. 1994; 58: 1240–1248.

[71] Oza SR, Singh RP, Dadhwal VK, Desai PS. Large area soil moisture estimation and mapping using space-borne multi-frequency passive microwave data. Journal of Indian Society of Remote Sensing. 2006; 34: 343–350.

[72] Bhagat VS. Use of Landsat ETM+ data for detection of potential areas for afforestation. International Journal of Remote Sensing. 2009; 30(10): 2607–2617.

[73] Ziadat FM. Analysing digital terrain attributes to predict soil attributes for a relatively large area. Soil Science Society of America Journal. 2005; 69(5): 1590–1599.

[74] Sudhanshu SP, Hoogenboom G, Paz J. Distinguishing blueberry bushes from mixed vegetation land use using high resolution satellite imagery and geospatial techniques. Computer Electronic Agriculture. 2009; 67(1&2): 51–58.

[75] Nketia KA. Using soil fertility index to evaluate two different sampling schemes in soil fertility mapping: A case study of Hvanneyri, Iceland. United Nation University Land Restoration Training programme, Published Thesis, 2011. pp. 1–45.

[76] Iftikar W, Chattopadhayay GN, Majumdar K, Sulewski GD. Use of village-level soil fertility maps as a fertilizer decision support tool in the red and lateritic soil zone of India. Better Crops. 2010; 94(3): 3.

[77] Wilkerson GG, Jones JW, Boote KJ, Ingram KT, Mishoe JW. Modelling soybean growth for management. Transactions of the American Society of Agricultural Engineers. 1983; 26: 63–73.

[78] Long DS, Carlson GR, DeGloria SD. Quality of field management maps. In: P. C. Robert, R. H. Rust (eds) Site specific management for agricultural systems. 1995; American Society of Agronomy, Madison, pp. 251–271.

[79] Geleta S, Sabbagh GJ, Stone JF, Elliot RL, Mapp HP, Bernado DJ, Watkins KB. Importance of soil and cropping systems in the development of regional water quality policies. Journal of Environmental Quality. 1994; 23: 36–42.

[80] Sabbagh GJ, Geleta S, Elliot RL, Williams JR, Griggs RH. Modification of EPIC to simulate pesticide activities: EPIC-PST. Transactions of the American Society of Agricultural Engineers. 1991; 34: 1683–1692.

Chapter 10

3D GIS Modeling of Soft Geo-Objects: Taking Rainfall, Overland Flow, and Soil Erosion as an Example

Dayong Shen, Kaoru Takara and Yuling Liu

Additional information is available at the end of the chapter

http://dx.doi.org/10.5772/64376

Abstract

In physics, objects can be divided into rigid and soft objects according to the object deformation capacity. Similarly, geo-object can also be classified into rigid geo-objects (e.g., building, urban) and soft geo-objects (e.g., mudflow, water, soil erosion). There are three types of approaches for 3D GIS modeling, i.e., surface-based, volume-based, and hybrids in terms of geometry. These approaches are suitable for representing rigid geo-objects, but they are not suitable to simulate the intrinsic properties of the soft geo-object, i.e., dynamics and deformation. And so far there are few GIS modeling methods for simulation of soft geo-objects. GIS flow elements (FEs) and GIS soft voxels (SVs) were proposed for 3D modeling of soft geo-objects. GIS flow elements can realistically represent the dynamics and stochastics of soft geo-objects, while GIS soft voxels simulate deformation of soft geo-objects. The authors discuss the implementation and computer programming of GIS flow elements and GIS soft voxels in this study. GIS FE and SV have been successfully applied in a case study toward the simulation of the process of rainfall, overland flow, and soil erosion. A software system has been designed and developed, which has the functions of data management, model computation, and 3D simulation.

Keywords: 3D GIS modeling, soft geo-objects, rainfall, overland flow, soil erosion

1. Introduction

Nowadays, severe shortage of water resources, ecological destruction and environmental pollution, global changes, natural disasters, etc., are the key issues of geosciences. Main research objects of these key issues such as water, polluted air, and mudflow are soft geo-objects. Modeling and 3D visualization of soft geo-objects is emerging research area. In

computer graphics, several approaches have been applied for simulation of soft objects, e.g., the particle system approach and the metaball approach [1]. However, the particle system approach and the metaball approach are driven by physical force objects, which are not suitable to simulate geographic process that is driven by more complex geomodeling [2]. Mitasova et al. used densities of particles to sample rainfall excess and sediment transportation of sand and clay. Compared to traditional sampling method, their method showed several advantages [3]. For example, it can be easily extended into arbitrary dimensions, and is fairly straightforward to be implemented in a multiscale framework with data adaptive capabilities. But the method has obvious limitations. Firstly, it cannot accurately represent the dynamic change of sample points' velocity and direction over space and time because all sample points have the same size. Furthermore, the geographic phenomena of soil separation and fusion during the process of soil erosion have not been represented. Soil erosion is a naturally occurring process in land which refers to wearing away of a field's top soil by natural forces of water and wind. How the sediment transports, how the soil separates, and how much soil losses, all these are driven by geomodeling.

2. Methodologies

In GIS existing research studies focus more on rigid objects such as mountains, roads, and buildings, and few methods have been proposed for the modeling and 3D visualization of soft geo-objects. GIS flow elements (FEs) and GIS soft voxels (SVs) were proposed and developed for 3D modeling of soft geo-objects. GIS FEs can realistically represent the dynamics and stochastics of soft geo-objects while GIS SVs can simulate deformation of soft geo-objects.

2.1. GIS FE

A GIS FE is a basic simulation unit and spatially corresponds to a pixel in remotely sensed imagery. It is characterized by the position (i.e., x, y, z coordinates), velocity, and direction of a soft object, but volume is neglected. GIS FE is driven by geomodeling with the objective to simulate the dynamic feature in soft geo-objects. Although a GIS FE is within a pixel, it can take many appearances such as a point, a line segment, or a surface depending on the natural appearance of the soft geo-object. For example, the FE is with line segment shape for rainfall simulation. The velocity and direction of a FE can well reflect the real dynamic change. Besides the above-mentioned fundamental attributes, a FE is able to carry more properties such as color and texture that help distinguish and characterize an object. This provides flexibility for extension.

2.2. GIS SV

A GIS SV is a basic unit for deformation simulation. Similar to FE, a GIS SV is also based on a pixel from remotely sensed imagery and it also features with position, velocity, and direction, which are controlled by geomodeling. But a GIS SV carries volume information. A SV is covered by an isosurface that can well represent volume shape and surface deformation. A

http://dx.doi.org/10.5772/64376

GIS SV has potential to carry more information by adding colors and textures or by modeling its internal structure.

2.3. Calculation of basic parameters

Here the basic parameters include direction, velocity, shape, and volume.

8-neighborhood tracing algorithm is used to calculate the direction of a FE. Eq. (1) is used to compute the velocity of the FE (V) where M_1 is geoscientific model and p_1, p_2, …, p_j are parameters affecting V. Suppose that V is directly proportional to the length of a GIS FE (L), we get (Eq. 2) where L is a proportional coefficient with a value greater than 0. (Eq. 3) is used to control the shape of the GIS SV where g represents isosurface, d is the length of a pixel, h is the average thickness of the soft geo-object, and $r^2 = x^2 + y^2 + z^2$ in which (x, y, z) are 3D coordinates of the critical point of the GIS SV. Eq. (4) calculates the volume Vol of the GIS SV.

$$V = M_1\left(p_1, p_2, \ldots\ldots, p_j\right) \tag{1}$$

$$V = \lambda L \tag{2}$$

$$\boldsymbol{g}(\boldsymbol{r}) = \left(\boldsymbol{r} - \frac{\sqrt{2\boldsymbol{d}^2 + \boldsymbol{h}^2}}{2}\right)^2 \tag{3}$$

$$Vol = d^2 h \tag{4}$$

The following section will introduce the application of using GIS FE and GIS SV theories in modeling and 3D simulation of rainfall, overland flow, and soil erosion.

3. GIS FE-based simulation of rainfall

The objective is to simulate raindrops falling from the sky to the ground surface.

3.1. Raindrop dynamics

Force objects on a raindrop include gravity, air buoyancy, air resistance, wind force, and the kinematic equation for a raindrop in vertical direction is [4]:

$$m\frac{dv}{dt} = mg - F_R - F_B \tag{5}$$

where m represents raindrop mass, v represents raindrop falling velocity, t represents time, g means gravitational acceleration, F_R means air resistance, and F_B means air buoyancy. **Figure 1** shows the force objects of a raindrop.

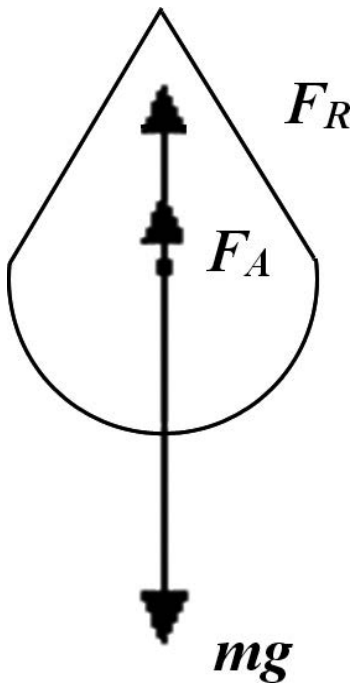

Figure 1. A schematic view of raindrop dynamic analysis.

3.2. Criteria for raindrop GIS FE representation

In this study raindrop GIS FE representation meets artificial rain experiments criteria [5]:

- Raindrop particle size distribution is close to natural rainfall. Natural rainfall raindrop sizes range from near zero to about 7 mm. The median particle size of an erosive rain storm is between 1 and 3 mm. Raindrop diameters normally increase with the increase in rainfall intensity.
- Raindrop impact velocity is close to the natural raindrops. Raindrop impact velocity, from droplet velocity near zero to the maximum raindrop velocity of more than 9 m/s. The landing speed of an ordinary raindrop with a diameter of 2 mm is 6–7 m/s.
- Rainfall intensity is close to the natural rainfall. Natural rainfall intensity from near zero to a few millimeters per minute. In general, low rainfall intensity is not important to soil erosion, and the frequency of high rainfall intensity is very low, so that the importance is limited. Common rainfall intensity of 0.2–2 mm/min is usually the most important rainfall intensity.

http://dx.doi.org/10.5772/64376

- Throughout the study area, raindrop characteristics and strength is fairly uniform.
- The rainfall is continuously simulated in the study area.
- The impact angle of most raindrops is not too much deviated from the vertical line.

3.3. Raindrop GIS FE representation

The representation includes geometry representation and dynamic representation.

Raindrop is considered to have a shape of a combination of a taper and a semisphere with white color and it is transparent. The initial position, x and z are randomly created and y position is on the top of the viewpoint. The velocity and direction are determined based on raindrop dynamics. The raindrop object has its lifespan, which ends when raindrop collides with DEM.

3.4. Programming

The development platforms are Visual Studio C++ and OpenGL.

3.4.1. Define raindrop array

Create raindrops by meeting artificial rain experiment criteria. The raindrop array stores raindrop total number, color, transparency, and coordinates information. 3D coordinates of the start point of rain line are generated with a random function. Coordinates of the end point of the rain line are calculated based on dynamic analysis.

3.4.2. Create animation

Create raindrops animation by meeting artificial rain experiment criteria as well and the pseudo code is as follows:

For *i* from 1 the total number of raindrops

{

Translate the start and end points of the rain line to a new position along *z* axis based on the initial velocity setting

Add an acceleration increment to the initial velocity of the raindrop

If a rain line touches or penetrates DEM, then

{

The life of the rain line is ended

Reinitialize a new rain line and set the initial velocity

}

}

4. GIS FE-based simulation of overland flow

The objective is to simulate the velocity and direction of overland flow.

4.1. Flow streamline dynamics

Saint Venant kinematic equation of unsteady flow of water is used as the governing equation [6]:

$$\Delta M_1 + \Delta M_2 = P_U - P_L + W_x - T \tag{6}$$

or it is written as:

$$V\frac{\partial V}{\partial x} + \frac{\partial V}{\partial t} + g\frac{\partial y}{\partial x} = g\left(i_0 - i_f\right) \tag{7}$$

where P_U and P_L represent pressure on the upstream face and downstream face, respectively; W_x represents the gravity component in water flow direction; T is friction resistance, ΔM_1 and ΔM_2 are local momentum change and transport momentum change, respectively, x is distance in water flow direction, t is time, y is the depth of water, i_0 and i_f are bottom slope and friction slope, respectively. Flow streamline dynamic analysis is shown in **Figure 2**.

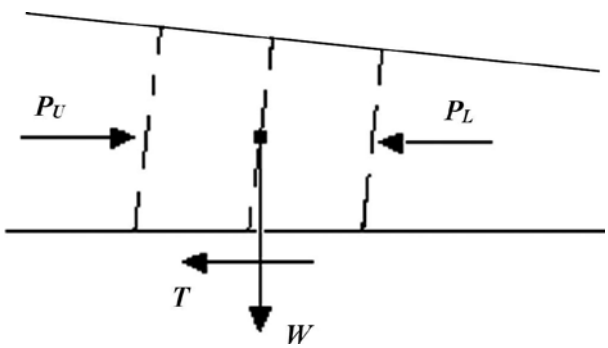

Figure 2. A schematic view of flow streamline dynamic analysis.

4.2. Compute the velocity of overland flow

Overland flow velocity is an equation of discharge per unit width and slope angle [7]:

$$V = Kq^n S^m \tag{8}$$

http://dx.doi.org/10.5772/64376

where *K, m, n* are parameters. Compared to laminar flow and turbulence flow equations, normally the value of *m*/*n* is between that of laminar and turbulent flow. By nonlinear regression analysis, we deduced the equation

$$V = 21.8811 q^{0.4667} S^{0.2510} \tag{9}$$

where *S* and *q* represent the slope angle and the discharge per unit width, respectively. The water discharge was computed using the equation [8]:

$$q = x(I - f)\cos\beta \tag{10}$$

where *x* represents the average slope length from the slope top, β represents the average slope gradient, *I* represents the rainfall intensity, and *f* represents the infiltration rate.

4.3. Compute overland flow direction

Water and sediment discharge computation based on grid DEM is usually determined using single flow path algorithm, i.e., the method of determining the maximum gradient. For a 3 × 3 window, the center cell has eight neighbors. The water and sediment flow direction coding of each cell is based on the digital coding method in Refs. [8, 9]. For example, if the flow direction of water and sediment of a grid unit as the center of the window is due west, i.e., water and sediment in the center of the window flow into the adjacent cell 4, then the flow direction value of the center cell is 4.

In the algorithm, following values are combined for identification of landform structure.

- DEM elevation values, stored in the array ALT[i, j].
- Flow direction values, stored in the array PTR[i, j].
- Flow streamline coordinates, stored in the array FLOWLINE[i, j].

The above arrays have the same size. Each grid unit has a value to identify one of its attributes. In addition, the algorithm uses the following terms:

- Outflow point: if water and sediment flows out of a grid unit, then the unit is called an outflow point.
- Inflow point: if water and sediment flows into a grid unit, then the unit is called an inflow point.
- Flow point: if water and sediment flows from grid cell (i, j) to grid cell (x, y), then (x, y) is a flow point of (i, j).

In fact, in addition to certain points along watershed boundary that only have outflow, other points have both inflow and outflow. Algorithm:

In a 3 × 3 window, gradients from the center cell to its 8-neighborhoods are used to determinate flow directions.

- For cells at the edge of DEM or boundary of the study area, the flow direction of each cell is defined as the direction toward the boundary.
- For any other grid cell, calculate the cell's elevation gradients to its eight neighbors. $EG_{0,i} = Z_0 - Z_i$ (i = 1, 3, 5, or 7) represents the elevation gradient in horizontal or vertical directions, and $EG_{0,i} = Z_0 - Z_i/\text{sqrt}(2)$ (i = 2, 4, 6, or 8) represents the elevation gradient in diagonal directions.
- Determinate the neighboring cell which has the maximum elevation gradient.
- Identification of isolated depression flow direction. Scan the study area using a 3x3 window, and (i, j) is the center cell of the window. Calculate the eight elevation gradients of (i, j). If the maximum gradient value is less than 0, then identify (i, j) as an isolated depression.
- Identification of outflow point flow direction. Scan the study area using a 3×3 window, and (i, j) is the center cell of the window. Calculate the eight elevation gradients of (i, j). If the maximum gradient value is greater than 0, then identify (i, j) as an outflow point.

4.4. Flow streamline GIS FE representation

The representation includes both geometry representation and dynamic representation.

Flow is considered to have a fine cylinder shape with Cambridge blue color and it is transparent. The initial position starts from the intersection point between raindrop and collision plane on DEM. Its velocity and direction is determined based on the analysis of dynamics. The lifetime of the flow streamline ends when it runs into a channel.

5. GIS FE- and SV-based simulation of sediment transport and soil erosion

The objective is to simulate sediment transport and the process of soil erosion by water.

5.1. Sediment particle dynamics

Dynamic analysis of a sediment particle is shown in **Figure 3** [9]. The parameters are W as gravity, P_y as uplift, P_x as traction force, and T as upper-surface friction. In this simulation, only suspended load is considered. The velocity of suspended load in water flow direction is mostly equal to that of flow streamline [10]. Bed load and saltation load will be considered in future work.

Because spatially varied forces acting on flow streamline and sediment particles are too complicated to be precisely represented, we firstly use an 8-neighborhood tracing algorithm to compute the flow direction on hillslopes, then apply the modeling theory of remote sensing information model combined with experimental results to obtain an equation for flow velocity computation on hillslopes to simulate dynamic sediment laden flow in 3D space.

http://dx.doi.org/10.5772/64376

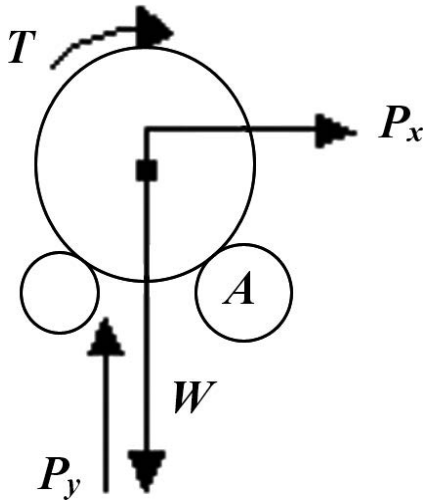

Figure 3. A schematic view of sediment particle dynamic analysis.

5.2. Erosion voxels

We form GIS SVs on a pixel basis and name it erosion voxel to simulate the separation and fusion of soil mass. The erosion voxel combines the attributes not only from geographic pixels, but also from particles and metaballs in computer graphics.

(1) The main characteristics of a pixel-based erosion voxel are described as follows:

- The appearance of an erosion voxel is designed as a circumscribed ellipsoid of a cuboid. The width and length of the cuboid are equal to cell length, and the height of the cuboid represents the averaged thickness of soil loss per unit duration (which depends on specific time, location, and amount of rainfall);
- Represents averaged volume of soil loss per unit duration; therefore, it has statistical meaning;
- Represents the highest precision of geographic image data, and includes soil properties, vegetation coverage, slope, elevation (represented by the elevation of center point of top face of its inscribed cuboid) and other information;
- Once time reaches the specific step of duration, we separate a specific erosion voxel from a specific pixel, and it will run off with water (i.e., erosion voxel separation);
- When the velocity falls to zero, the erosion voxel will subside, and the fusion of erosion voxels will occur;
- When the erosion voxel runs into a channel, its lifetime will be ended.

(2) Quantitative expression of an erosion voxel

An erosion voxel is represented by a circumscribed ellipsoid:

$$\frac{(x-x_0)^2}{\left(\frac{\sqrt{2}}{2}d\right)^2}+\frac{(y-y_0)^2}{\left(\frac{\sqrt{2}}{2}d\right)^2}+\frac{\left(z-z_0+\frac{h}{2}\right)^2}{\left(\frac{\sqrt{2}}{2}h\right)^2}=1 \tag{11}$$

where d represents cell length, h represents averaged thickness of soil loss per unit duration, and (x_0,y_0,z_0-h/2) are the coordinates of the center point of an erosion voxel. The volume of a GIS SV (*Vol*) is computed based on its inscribed cuboid (**Figure 4**).

$$V = d^2h \tag{12}$$

where d is the cell length and h is averaged thickness of soil loss per unit duration.

(3) Elevation

Real surface elevation is represented by the elevation of the center point of the upper surface of the inscribed cuboid of the erosion voxel.

(4) Transport routes

Considering that an erosion voxel only has statistical meaning, we treat its transport routes the same as sediment laden flow [2].

(5) Structure parameters of an erosion voxel

Include center-point coordinates, strength, color, transparency, timer, etc. Other attribute parameters such as soil type, vegetation coverage, and slope angle can be added as needed.

(6) Separation and fusion

Use the basic methods for rendering GIS SVs [11]. Considering that an erosion voxel only has statistical meaning, force analysis to contact surface and volume control are not performed.

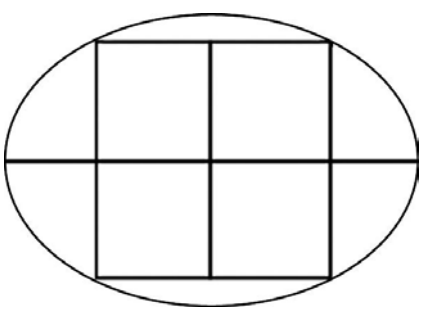

Figure 4. The profile of a GIS SV.

http://dx.doi.org/10.5772/64376

6. Results

Based on the aforementioned technology, including software module design, algorithm design, and pseudo code description, for the implementation of the new methodology, we develop a Modeling and 3D Simulation System for Water Erosion on Hillslopes (M3DSSWEH). The system includes three modules: module of DB management, module of model computation and verification, and module of 3D simulation. The system has been designed and developed based on the platform of Oracle, Visual C++, and OpenGL. It has a user-friendly interface based on human-machine interactive techniques and the advanced module design makes it flexible and easy for function extension.

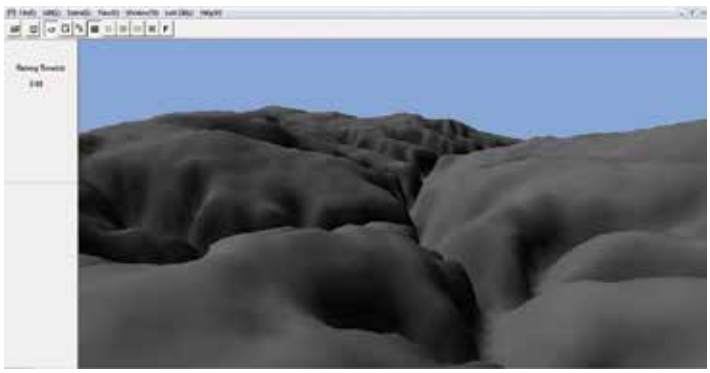

Figure 5. User interface of M3DSSWEH.

- User interface (UI)

The system UI consists of menus, toolbars, floating panels, and viewports (**Figure 5**).

- GIS simulation module

The module simulates rainfall, overland flow, and soil erosion process:

Rainfall simulation in this study references standard artificial rain experiments. Set raindrop intensity and raindrop diameter based on rainfall intensity and pixel size to enhance scientific simulation and further facilitate the simulation of raindrops splash effect.

Overland flow simulation is based on GIS FE, which is represented by a fine cylinder. The height of the cylinder is in direct proportion to the velocity of overland flow; the inclination of the cylinder represents the direction of the movement; the diameter of the cylinder is in direct proportion to the depth of overland flow; and the depth of cylinder color is related to sediment concentration. The deeper the cylinder color is, the greater sediment concentration it represents.

Sediment simulation is also based on GIS FE, which is represented by a sphere. The radius of the sphere is in direct proportion to sediment size, and the color of the sphere is related to soil type.

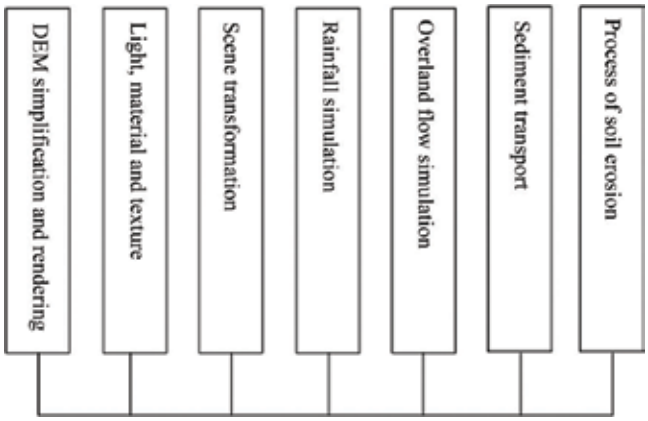

Figure 6. The GIS simulation module of M3DSSWEH.

Soil erosion simulation is based on GIS SV and the rendering of the SVs are using the aforementioned template rendering algorithm (**Figure 6**).

- Data source

As an implementation, the data source is from a research area located between 39°43′37″–39°46′28″N, and 111°7′7″–111°9′14″E, with an area of 3.85 km^2. It is Wufendigou watershed in Inner Mongolia, belonging to China Loess Plateau region. The watershed is characterized by severe water and soil loss and this research will be applicable to improving the understanding of soil erosion in the China Loess Plateau region.

Theory and methodology of GIS FE and GIS SV will be further extended to better serve geoscience in the future.

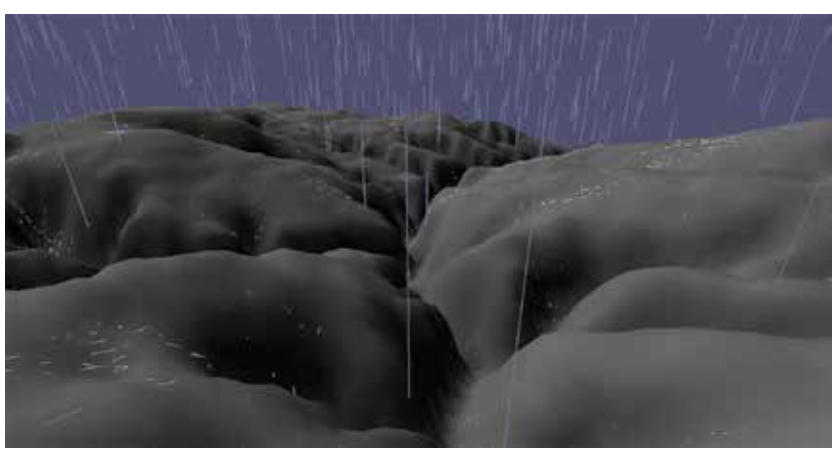

Figure 7. GIS simulation of terrain, light, shadow, rainfall, and overland flow.

http://dx.doi.org/10.5772/64376

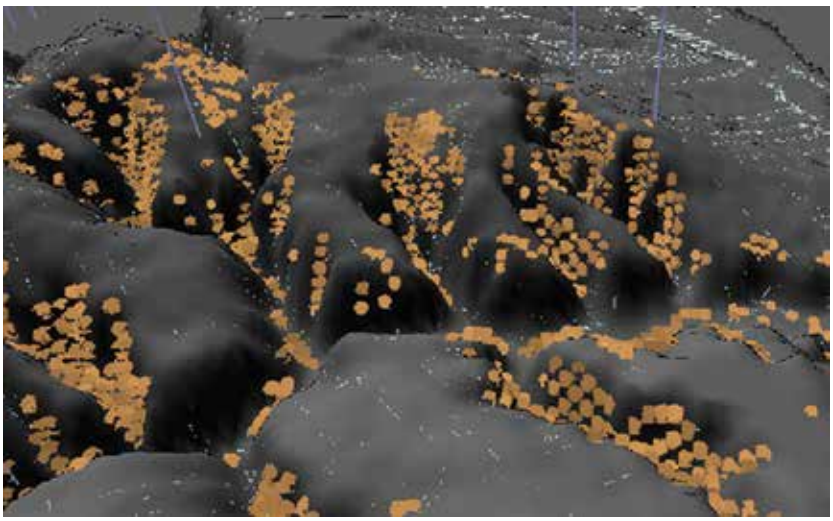

Figure 8. GIS simulation of soil erosion.

- System output (**Figures 7** and **8**)
- System advantages

The system shows rainfall, overland flow, and soil erosion simulation using GIS FEs and GIS SVs, and the results are satisfactory. Compared to traditional GIS models such as TIN, grid, tetrahedral, and octree, it is more convenient, vivid, and efficient to use GIS FE and GIS SV to simulate dynamic soft geo-objects. Combining GIS FE and GIS SV with the traditional GIS models, any geo-object in solid, liquid, or gas phase can be well represented.

- System prospects

7. Conclusions

This paper discusses the implementation and computer programming of GIS FE and GIS SV. Based on a case study in the China Loess Plateau region, we used GIS FE and GIS SV to simulate rainfall, overland flow, and soil erosion, respectively. Implementations show that the spatio-temporal changes of sediment-laden flow can be more intuitively and realistically simulated after GIS flow elements and GIS soft voxels technology are integrated into the system.

Both GIS FE and GIS SV are proposed based on a pixel from remotely sensed imagery that facilitates the data acquisition particularly with the significant use of remote sensing technique in geosciences and its integration with GIS. On the other hand, the pixel level data can be directly used in the calculation without further spatial operation so as to ensure the data accuracy. Moreover, both the GIS FE and GIS SV are driven by reliable geoscientific models. Therefore, GIS FE and GIS SV together can be used as basic units for simulating soft geo-objects

and have the potential for practical use in other research areas such as flood modeling and simulation.

Acknowledgements

Special thanks to Professor Ainai Ma and Professor Shanjun Mao from Peking University, and Professor Hui Lin from the Chinese University of Hong Kong for their help and advice.

Author details

Dayong Shen[1*], Kaoru Takara[2] and Yuling Liu[3]

*Address all correspondence to: dayong_shen@yahoo.com

1 University of Mississippi, Mississippi, USA

2 Kyoto University, Kyoto, Japan

3 University of Maryland, College Park, Maryland, USA

References

[1] Shen D, Ma A, Lin H, Nie H, Mao S, Zhang B, Shi J. A new approach for simulating water erosion on hillslopes. International Journal of Remote Sensing. 2003; 24(14): 2819-2835. DOI:10.1080/0143116031000070418.

[2] Shen D, Takara K, Tachikawa Y, Liu Y. 3D simulation of soft geo-objects. International Journal of Geographical Information Science. 2006; 20(3): 261-271. DOI: 10.1080/13658810500287149.

[3] Mitasova H, Mitas L, Brown WM, Johnston DM. Terrain modelling and soil erosion simulation: applications for evaluation and design of conservation strategies. 2001. Annual Report. Department of Marine, Earth and Atmospheric Sciences (MEAS), North Carolina State University (NCSU) 20 pp.

[4] Xu S. Basic Atmospheric Physics. Beijing: Meteorology Press; 1993 (in Chinese).

[5] Lal R. Erodibility and erosivity. In: Lal R, Editor. Soil Erosion Research Methods. Soil and Water Conservation Society, Ankeny, IA; 1988. p. 141–160.

[6] Rui X. Channel flow and slope flow. In: Yu W, editor. Principles of Hydrology. Beijing: Hydraulic and Electric Press; 1988. p. 83-87 (in Chinese).

http://dx.doi.org/10.5772/64376

[7] Jiang Z, Song W. Test on flow velocities on hillslopes. Bulletin of Northwestern Institute of Soil and Water Conservation, Chinese Academy of Sciences. 1988; 7: 46-52 (in Chinese).

[8] Lu Z. Watershed Geomorphological Systems. Dalian: Dalian Press; 1991. p. 178-180 (in Chinese).

[9] Shen B. Sediment. In: Liang X, editor. Principles of Hydrology. Beijing: Hydraulic and Electric Press; 1992. p. 246-250 (in Chinese).

[10] Sediment Professional Commission. Chinese Water Conservancy Society; 1989. Sediment Manual. (Beijing: China Environmental Science Press), p. 21–200 (in Chinese).

[11] Shen D, Lin H. Erosion voxels. In: Proceedings of the International Advanced Workshop on Virtual Geographic Environments and Geocollaboration; 15-16 December 2003; Hong Kong. (CDROM).

Edited by Pasquale Imperatore and Antonio Pepe

The pervasive relevance of geospatial information and the development of emerging geospatial technologies offer new opportunity for bridging the gap between remote sensing scientific know-how and end users of products and services. Geospatial technology comprises tools and techniques dealing with the use of spatially referenced information, for the description and modeling of spatial and dynamic phenomena related to the Earth's environment. This book addresses environmental and social applications of geospatial technologies, thus also providing a multidisciplinary perspective on emerging geospatial techniques and tools. It consists of ten chapters offering insight into geospatial technology progress and trends. Authors present several application-oriented studies from various parts of the world, including applications in collaborative geomatics, geospatial statistics, GIS, agriculture, and natural hazard monitoring.

ISBN 978-953-51-6674-0

Photo by @spacex / unsplash

IntechOpen